Doctoral programs in:

International Doctorate in Civil and Environmental Engineering

Curriculum: Environment, Resources and Security (cycle XXXIV)

(University of Florence)

and

Doctoral school in Mechanics, Energetics, Civil and Process Engineering

Diploma specialty: Chemical and Environmental Engineering

Doctorate of University of Toulouse

(delivered by National Institute of Applied Sciences - INSA Toulouse)

Insights on the recovery, characterization and valorization of Extracellular Polymeric substances (EPS) from granular sludge applied in innovative wastewater treatment systems

Scientific field ICAR/03

Supervisors

Prof. Lubello Claudio

_____

Prof. Paul Etienne

_____

Co-supervisors

Dr. Lotti Tommaso

_____

Dr. Bessiere Yolaine

_____

Program coordinators

Prof. Solari Luca

_____

Prof. Azzaro-Pantel Catherine

_____

PhD candidate

Pagliaccia Benedetta

_____

2018/2022

Table of contents

List of abbreviations ..... **v**

Summary ..... **ix**

Résumé ..... **xv**

Chapter 1

Introduction **1**

1. From wastewater treatment plants (WWTPs) towards resource recovery facilities (WRRFs) ... 1

2. Granular sludge (GS)-based technologies and their potential for the extraction/recovery of Extracellular Polymeric Substances (EPS) 4

3. The high-diversity of GS-derived extracellular polymeric substances (EPS): the main bottleneck in their fine characterization 7

4. Towards new resource recovery-oriented scenarios exploiting GS-derived EPS-based biomaterials 15

5. Thesis aims and structure 17

Chapter 2

Methodological and mechanical insights on structural extracellular polymeric substances (sEPS)-based hydrogels from aerobic granular sludge (AGS) **21**

Abstract 21

1. Introduction 22

2. Materials and methods 26

2.1 sEPS extraction 26

2.2 Model biopolymers 28

2.3 Hydrogel-forming protocol 28

2.4 Post-gelling mechanical characterization 30

3. Results and discussion 35

3.1 Hydrogel-formation of sEPS versus model biopolymers 35

3.2 Compression studies 41

3.2.1 Stress-strain response to consecutive compression-decompression cycles 41

3.2.2 Effect of the gelling conditions on the hydrogel stiffness 44

3.3 Oscillatory shear measurements 54
3.4 Outlook and perspectives 61
4. Conclusions 63
Appendix 65

Chapter 3

Towards resource recovery-oriented solutions in agriculture exploiting structural extracellular polymeric substances (sEPS) from aerobic granular sludge (AGS) 70

Abstract 70
1. Introduction 71
2. Materials and methods 76
2.1 sEPS extraction and hydrogel-formation 76
2.2 Gravimetric, colorimetric and elemental analysis 79
2.3 Swelling ability and nutrient release 80
2.4 Biodegradability 82
2.4.1 Experimental set-up 84
2.4.2 Activated sludge preparation 85
2.4.3 Substrate preparation 85
2.4.4 Multiple-OUR experiments 85
2.4.5 Single-OUR experiments 86
2.4.6 COD fractionation 87
3. Results and discussion 88
3.1 sEPS extraction performance 88
3.2 Effect of distinct chemicals on the compositional properties of sEPS and derived hydrogels 90
3.3 Swelling ability of sEPS-based hydrogels 104
3.4 sEPS-based hydrogels as carrier systems for nutrient loading and release 111
3.5 Biodegradability of sEPS and derived hydrogels 116
3.6 Outlook and perspectives 129
4. Conclusions 133

Appendix 136

Chapter 4

Extracellular polymeric substances (EPS) recovered from waste anammox granular sludge as promising biosorbent for the heavy metal removal 140

Abstract 140

1. Introduction 141

2. Materials and methods 145

2.1 EPS extraction and characterization 145

2.2 Equilibrium biosorption studies 146

2.3 Biosorption mechanisms 149

2.4 Composite EPS-activated carbon sorbent media 150

2.4.1 GAC functionalization with AmxGS-derived EPS 150

2.4.2 Metal adsorption studies 151

3. Results and discussion 152

3.1 EPS extraction and characterization 152

3.2 Effect of the initial metal concentration on the biosorption effectiveness 154

3.3 Comparison between extracted EPS and pristine anammox granules 155

3.4 Langmuir and Freundlich adsorption isotherm models 159

3.5 Multi-metal biosorption studies 162

3.6 Biosorption mechanisms 163

3.7 Composite EPS-activated carbon sorbent media 171

3.8 Outlook and perspectives 180

4. Conclusions 184

Appendix 186

Chapter 5

Conclusions and future perspectives 197

References 210

Acknowledgements 241

List of abbreviations

A	area
AC	activated carbon
AD	anaerobic digestion
AGS	aerobic granular sludge
ALE	alginate-like exopolysaccharides
AmxGS	anammox granular sludge
AnGS	anaerobic granular sludge
AOB	ammonia oxidizing bacteria
ASMs	activated sludge models
b	Langmuir constant (in Langmuir adsorption isotherm model)
BCA	bicinchoninic acid (protein assay)
bCOD	biodegradable chemical oxygen demand
B-EPS	bound extracellular polymeric substances
BMP	biochemical methane potential
BOD	biochemical oxygen demand
BSA	bovine serum albumin (protein)
C_0	initial concentration (of metal ions M^{2+})
CAS	conventional activated sludge
C_e	residual equilibrium concentration (of metal ions M^{2+})
CLSM	confocal laser scanning microscopy
COD	chemical oxygen demand
d	diameter
D_F	fractal dimension
DLS	dynamic light scattering
DO	dissolved oxygen concentration
DSC	differential scanning calorimetry
DTG	derivative thermogravimetry
E	Young's modulus
EDS	energy-dispersive X-ray spectroscopy
EPS	extracellular polymeric substances
EWC	equilibrium water content

F/M	substrate to biomass concentration ratio (or food on microrganisms ratio)
F_n	normal force
FT-IR	Fourier transform - infrared (spectroscopy)
G*	complex modulus
G’	storage modulus
G’’	loss modulus
GAC	granular activated carbon
Glu	glucose
Gluc. Acid	glucuronic acid
GS	granular sludge
h	height (or gap width in oscillatory shear experiments)
iCOD	inert COD fraction
ICP-AES	inductively coupled plasma - atomic emission spectroscopy
k_1	pseudo-first-order constant (in pseudo-first-order kinetic model)
k_2	pseudo-second-order constant (in pseudo-second-order kinetic model)
K_{ass}	association constant
K_B	Boltzmann constant
K_f	energy binding constant (in Freundlich adsorption isotherm model)
LB-EPS	loosely-bound extracellular polymeric substances
LVE-region	linear viscoelastic region
m	mass
MRI	magnetic resonance imaging
MS	mass spectrometry
MW	molecular weight
MWCO	molecular weight cut-off
n	Freundlich constant (in Freundlich adsorption isotherm model)
NMR	nuclear magnetic resonance (spectroscopy)
OUR	oxygen uptake rate
pbCOD	particulate biodegradable COD fraction
piCOD	particulate inert COD fraction
PN	proteins
PS	polysaccharides
Q_e	equilibrium adsorption capacity
q_e	equilibrium swelling ratio

Q_m	theoretical maximum adsorption capacity (in Langmuir adsorption isotherm model)
q_t	swelling ratio at time *t*
r	radius
R	Pearson's correlation coefficient
R^2	correlation coefficient
RBCOD	readily biodegradable COD fraction
RHCOD	readily hydrolysable COD fraction
R_L	separation factor
RPD	relative percentage of dehydration
SAPs	superabsorbent polymers
SAXS	small-angle X-ray scattering
sbCOD	soluble biodegradable COD fraction
SEM	scanning electron microscopy
sEPS	structural extracellular polymeric substances
S-EPS	soluble extracellular polymeric substances
siCOD	soluble inert COD fraction
T	temperature
t	time
TB-EPS	tightly-bound extracellular polymeric substances
TEM	transmission electron microscopy
TGA	thermogravimetric analysis
TN	total nitrogen
TOC	total organic carbon
TRLs	technology readiness levels
TS	total solids
TSS	total suspended solids
V	volume
VFA	volatile fatty acids
VMAs	viscosity-modifying agents
V_{ml}	volume of mixed liquor (in the respirometer)
VS	volatile solids
V_s	volume of substrate (added in the respirometer)
VSS	volatile suspended solids

W_0	weight of the 50 °C-dried hydrogel
WAS	waste activated sludge
WC_0	initial water content
$WC_{50\ °C}$	water content upon dehydration at 50 °C
WMUs	water management utilities
WRRFs	water resource recovery factories
W_s	weight of the swollen hydrogel at equilibrium
W_t	weight of the swollen hydrogels at time *t*
WW	wet weight
WWTPs	wastewater treatment plants
x	deflection path (in oscillatory shear experiments)
Y_h	heterotrophic biomass yield
α	initial sorption rate (in Elovich kinetic model)
β	Elovich constant (related to the surface coverage and activation energy)
γ	(shear) amplitude strain
δ	phase angle
ΔDO	consumption of dissolved oxygen
ε	deformation (under compression)
η*	complex viscosity
λ	compression parameter
ρ_C	percolation threshold
ρ_E	entanglement density
σ	normal stress
σ_{true}	true normal stress
τ	shear stress
ω	oscillation frequency

Summary

The urge for more sustainable wastewater treatment solutions based on the well-established concept of "*circular economy*" is progressively paving the way towards new resource recovery-oriented strategies. A paradigm shift has been driven conceiving wastewater treatment plants (WWTPs) as collection points of resources (e.g., nutrient, water, energy, etc.): their redesign from treatment facilities into water resource recovery factories (WRRFs) is considered able to provide multiple opportunities to contribute to a more circular economy-based water sector.

The resource recovery potential is particularly emphasized in the case of granular sludge (GS)-based technologies that were recognized as viable alternative to conventional activated sludge (CAS) systems for a wide range of biological wastewater treatment processes. Biogranulation consists in forcing microrganisms to form granules (i.e., self-aggregated biofilms without the presence of carrier materials) rather than flocs: the compact granular form endows excellent settleability, easier solid/liquid separation, and enhanced biomass retention.

As in conventional biofilms, in granules microorganisms are embedded in a matrix of highly hydrated Extracellular Polymeric Substances (EPS) secreted by bacterial consortia during cell metabolism. The complex and diverse biopolymeric matrix mainly consists of proteins (PN), polysaccharides (PS), uronic acids, lipids, nucleic acids, humic-like substances, etc. EPS contribute to the initial aggregation of microbial cells and are mainly associated with the structural integrity, rheological behaviour, physic-chemical properties, and functional stability of granules. Hence, EPS exert multiple functions within the granular biofilm such as protection, nutrient source, maintenance of a stable structure, and organic substance sorption.

The recovery and conversion of EPS into bio-based commodities is considered an appealing route to enhance the economics and sustainability of wastewater treatment according to a circular economy pattern in waste sludge management. Thanks to their versatile properties, GS-derived EPS can be valorized in multiple industrial/environmental solutions alternatively to synthetic polymers (e.g.,

coating/sizing agents in paper and textile industry, cement curing, biosorption, etc.), thus contributing to a less fossil-fuel dependent manufacturing sector. The development of EPS recovery-oriented solutions is currently hampered by many bottlenecks which can be mainly identified in a still incomplete understanding of various fundamental aspects in terms of both EPS composition/properties and production regulation. Further research effort is therefore demanded to progress towards the sustainable EPS recovery and conversion into value-added biomaterials able to generate a change in the critical status of waste sludge management in WWTPs.

In this perspective, the present thesis mainly aimed to give insights on the recovery, characterization, and valorization of Extracellular Polymeric Substance (EPS) from waste granular sludge of different origin. Particular emphasis was dedicated on potential approaches to move towards the production of EPS-based biomaterials to be valorized in environment-related applications. Particularly, two types of GS were investigated (aerobic granular sludge, AGS, and anammox granular sludge, AmxGS) and distinct resource recovery-oriented scenarios were addressed depending on the nature of the studied microbial aggregates. Various solutions to engineer the most attractive features of these waste-derived biopolymers were hence proposed and all the evaluation criteria and methodologies were consequently adapted: hydrogel-based materials with great potential in sustainable agronomic practises (*AGS-recovered EPS*) and biosorbent media for the treatment of heavy metal-contaminated wastewaters (*AmxGS-recovered EPS*).

More detailed, the thesis structure, methodologies and main findings can be summarized as follows.

Chapter 1 introduces the general background of the thesis. The urge for more sustainable wastewater treatment solutions based on the concepts of "*resource recovery*" and "*circular economy*" was emphasized. The attractiveness of GS-based technologies as viable alternative to conventional activated sludge systems was presented: particularly, their potential in terms of EPS production/recovery was pointed out. The main bottlenecks limiting the large-scale implementation

of EPS-based biomaterials have been comprehensively discussed. Finally, the outlines and main goals of the thesis are presented.

Chapter 2 proposes a comprehensive analysis of the hydrogel-forming ability and resulting post-gelling mechanical properties of structural extracellular polymeric substances (sEPS) extracted from aerobic granular sludge (AGS). The gelling protocols in presence of divalent metal cations (e.g., Ca^{2+}) were adapted with the aim to minimize the polymer consumption and optimize the hydrogel geometry for the analytical investigation. The high-complexity and diversity of AGS-derived sEPS was addressed by evaluating the overall process of hydrogel-formation in comparison with well-known biopolymers (i.e., alginate and k-/ι-carrageenan). The post-gelling mechanical behaviour was evaluated under both compression and shear stress conditions via rheometry. Particularly, sensitive parameters were extrapolated from the observed mechanical profiles (e.g., Young's modulus, *E*, storage modulus, *G'*, loss modulus, *G''*, complex viscosity, η^*) and correlated with the applied gelling conditions to gain insights on the main drivers of the hydrogel-formation processes.
Based on the results emerged from the mechanical characterization, the minimum sEPS (weight) concentration enabling the formation of an extended cross-linked polymeric network was recognized in the range of 2.5 – 5 wt% (for sEPS concentrations lower than 2.5 wt% only weakly interconnected polymeric clusters were probably present). The higher polymer and (ionic) cross-linker concentrations needed for the sEPS hydrogel-formation with respect to the studied reference polymers gave hence a proof-of-principle of the greater complexity and diversity of the sEPS matrix (likely involving also compounds not really contributing to the gelling processes and resulting post-gelling mechanics). Distinct mechanical responses to consecutive compression-decompression cycles were observed among the studied biopolymer-based hydrogels. Particularly, sEPS and ι-carrageenan hydrogels behaved similarly under mechanical stresses: their linear elastic behaviour was preserved along the subsequent loading-unloading cycles, but lower levels of stiffness were achieved compared to alginate and k-carrageenan-based systems. For all the studied biopolymers,

the post-gelling stiffness varied significantly depending on the applied hydrogel-forming conditions, even if the overall mechanical response remained almost unchanged: *E* increased upon increasing the polymer and (ionic) cross-linker concentration and varied based on the (divalent) metal cation used as cross-linking agent. The oscillatory shear measurements confirmed that sEPS were able to form hydrogels with solid-like mechanical properties. From an applicative point of view, the feasibility of forming sEPS-based hydrogels with mechanical properties comparable to other biopolymer-based systems currently applied for commercial purposes was presented, thus suggesting potential resource recovery-oriented solutions able to progress towards a less fossil fuel-dependent manufacturing sector.

Chapter 3 offers a consistent approach to engineer the hydrogel-forming properties of AGS-derived sEPS based on the high qualitative standards imposed by the agronomic sector. Particularly, the influence of various chemicals in the extraction and gelling processes on the quantity/quality of the extractable EPS macromolecules was pointed out, emphasizing the importance to adapt the methodologies on the research objectives. With this regard, extraction and gelling protocols widely discussed in literature were adapted providing chemical reagents containing no sodium or chlorine which are considered phytotoxic in large quantities: K_2CO_3 or $(NH_4)_2CO_3$/HNO_3/KOH (*extraction*) and $Ca(NO_3)_2{\cdot}H_2O$ or $Ca(C_2H_5COO)_2$ (*cross-linking*). The quality/quantity of the extractable EPS macromolecules as well as their overall hydrogel-forming ability did not appear strongly influenced by the distinct chemicals applied. Conversely, more significant differences were observed in terms of compositional analysis (e.g., macronutrients, Na, Cl, heavy metals, etc.). Overall, the obtained sEPS and derived biomaterials (e.g., hydrogels) were consistent with the current environmental legislation in matter of soil improvers and fertilizing products, resulting within the maximum limits imposed in terms of heavy metals (values related to Cr(VI) to be investigated). The great potential of the obtained sEPS hydrogels in agronomy-oriented solutions was emphasized evaluating their swelling ability and nutrient release capacity. Particularly, the behaviour of sEPS-based hydrogels as superabsorbent

polymers (SAPs) able to sorb and hold high quantities of water (up to 16 g H2O per g hydrogel as dry matter) was suggested. Moreover, a preliminary proof-of-principle of the potential application of sEPS hydrogels as carrier systems for nutrient loading and release was given. The biodegradability assessment was preliminarily carried out by adapting respirometric techniques (single- and multiple-OUR experiments): conclusions in terms of organic matter biodegradability were drawn based on the partitioning of the sample Chemical Oxygen Demand (COD) in soluble biodegradable, particulate biodegradable, soluble inert and particulate inert fractions. It has been found that sEPS and derived hydrogels can be utilized as substrate from the microbial communities inhabiting the activated sludge, but their biodegradation was influenced by the chemicals applied in the extraction and gelling processes. Moreover, it has been observed that the readily biodegradable carbonaceous fraction decreased upon hydrogel-formation: the establishment of an extended 3D polymeric network in which the sEPS macromolecules were more confined likely resulted in a decreased substrate accessibility, thus requiring further hydrolytic reactions before their microbial utilization.
Finally, guidelines to progress towards new resource recovery-oriented solutions in agriculture exploiting the versatile properties of AGS-derived sEPS were proposed.

Chapter 4 deals with the feasibility of exploiting EPS extracted from waste anammox granular sludge (AmxGS) in high-performance and cost-effective technologies for the treatment of heavy metal-contaminated wastewater. With this regard, the metal-binding ability of the recovered EPS was addressed in comparison to that of pristine granules in single- and multi-metal biosorption studies mainly to shed light on the biosorption mechanisms of extracted and non-extracted EPS in native biomass. Metal-binding capacities equivalent or higher than conventional and/or unconventional sorbent media were found both for extracted EPS and pristine anammox granules, but distinct biosorption pathways were suggested. These differences could be due to three main reasons: (i) multiple mechanisms participating in the heavy metal biosorption by native granules, in addition to the heavy metal uptake by EPS; (ii) EPS chemical modifications induced by the extraction method

applied; (iii) different polymer chain mobility and binding site availability of extracted EPS in aqueous dispersions and non-extracted EPS in pristine granules. Mechanistic hypothesis on metal biosorption were suggested: as emerged from a detail molecular-level analysis carried out combining various analytical techniques, a multifaceted mechanism based on a combination of electrostatic interaction, ion exchange, complexation and precipitation has been proposed. Particularly, it has been found that AmxGS-extracted EPS behaved like flocculant/complexing agents in presence of high-concentrated heavy metal-contaminated aqueous systems, leading to the spontaneous precipitation of EPS-metal composite aggregate. Finally, a proof-of-principle of the potential application of the extracted EPS in composite sorbent media (e.g., with activated carbon) able to target single and multiple heavy metals simultaneously from contaminated aqueous systems was given, thus suggesting encouraging strategies to enhance the industrial applicability of AmxGS-derived EPS.

Chapter 5 draws the general conclusions and outlooks of the thesis, thus suggesting the next challenges to be addressed in follow up research. The outstanding potential of both AGS- and AmxGS-derived EPS in environment-related applications has been emphasized, thus shedding light on recourse recovery-oriented solutions able to progress towards a more circular economy-based water sector.

Résumé

L'appel à des solutions de traitement des eaux usées plus durables basées sur le concept bien établi d'économie circulaire ouvre progressivement la voie à de nouvelles stratégies axées sur la récupération des ressources. Un changement de paradigme a été conduit vise désormais à concevoir les stations d'épuration des eaux usées comme des points de collecte de ressources (par exemple, nutriments, eau, énergie, etc.): la refonte des installations de traitement en usines de récupération des ressources pourrait de fournir de multiples contributions à un secteur de l'eau basé sur une économie circulaire.

Le potentiel de récupération des ressources est particulièrement mis en évidence dans le cas des technologies à base de boues granulaires qui sont reconnues comme une alternative viable aux systèmes conventionnels de boues activées pour une large gamme de procédés de traitement biologique des eaux usées. La biogranulation consiste à forcer les microorganismes à former des granules (c'est-à-dire des biofilms auto-agrégés sans la présence de matériaux porteurs) plutôt que des flocs: la forme granulaire compacte confère une excellente décantabilité, une séparation solide/liquide plus facile et une meilleure rétention de la biomasse.

Comme dans les biofilms conventionnels, les microorganismes en granulés sont intégrés dans une matrice de substances polymères extracellulaires (EPS) hautement hydratées sécrétées par des consortiums bactériens au cours du métabolisme cellulaire. La matrice biopolymérique est complexe et diversifiée, principalement constituée de protéines (PN), de polysaccharides (PS), d'acides uroniques, de lipides, d'acides nucléiques, de substances humiques, etc. Les EPS contribuent à l'agrégation initiale des cellules microbiennes et sont principalement responsables de la structure, du comportement rhéologique, des propriétés physico-chimiques et de la stabilité fonctionnelle des granules. Par conséquent, les EPS exercent de multiples fonctions dans le biofilm granulaire telles

que la protection des cellules, la source de nutriments, le maintien d'une structure stable et la sorption des substances organiques et minérales.

La récupération et la conversion des EPS en biomatériaux sont considérées comme une voie attrayante pour améliorer l'économie et la durabilité du traitement des eaux usées selon un modèle d'économie circulaire dans la gestion des boues résiduaires. Grâce à leurs propriétés polyvalentes, les EPS dérivés de boues granulaires peuvent être valorisés dans de multiples solutions industrielles et/ou environnementales alternativement aux polymères synthétiques (par exemple, agents de revêtement résistant à l'eau dans l'industrie du papier et du textile, durcissement du ciment, biosorption, etc.), contribuant ainsi à un secteur manufacturier moins dépendant des combustibles fossiles. Le développement de solutions orientées vers la valorisation des EPS est actuellement confronté à de nombreux verrous qui résultent d'une compréhension encore incomplète de divers aspects fondamentaux en termes de composition/propriétés des EPS et d'une mauvaise maitrise des processus de production selon des critères relatifs à l'application sélectionnée. Des efforts de recherche supplémentaires sont donc nécessaires pour progresser vers la récupération et la conversion durables des EPS en biomatériaux à valeur ajoutée capables de générer un changement profitable pour la gestion des boues résiduaires des stations d'épuration.

Dans cette perspective, cette thèse visait principalement à donner un aperçu de la récupération, de la caractérisation et de la valorisation de la substance polymère extracellulaire (EPS) à partir de boues granulaires d'origine différente. Un accent particulier a été mis sur les approches potentielles pour évoluer vers la production de biomatériaux à base d'EPS à valoriser dans des applications liées à l'environnement. En particulier, deux types de boue granulaire ont été étudiés (boues granulaires aérobies, AGS, et boues granulaires anammox, AmxGS) et différents scénarios de récupération ont été abordés en fonction de la nature des agrégats microbiens étudiés. Plusieurs solutions de valorisation ont donc été proposées et tous les critères et les méthodologies d'évaluation ont été adaptés en conséquence: des hydrogels à fort potentiel dans les pratiques agronomiques durables (EPS

récupéré à partir de boue granulaire aérobie) et des matières bio-absorbantes pour le traitement des eaux usées contaminées par des métaux lourds (EPS récupéré à partir de boue granulaire anammox).

La structure de la thèse, les méthodologies et les principaux résultats peuvent être résumés comme suit.

Le **Chapitre 1** présente le contexte général de la thèse. L'urgence de solutions de traitement des eaux usées plus durables basées sur les concepts de "*récupération des ressources*" et d'"*économie circulaire*" a été soulignée. L'attractivité des technologies à base de boue granulaire comme alternative viable aux systèmes conventionnels à boues activées a été présentée. En particulier, leur potentiel en termes de production/récupération de EPS a été mis en évidence. Les principaux goulots d'étranglement limitant la mise en œuvre à grande échelle des biomatériaux à base d'EPS ont été largement discutés. Enfin, les principaux objectifs et la structure de la thèse sont présentés.

Le **Chapitre 2** propose une analyse complète de la capacité de gélification des substances polymères extracellulaires structurelles (sEPS) extraites de boues granulaires aérobies (AGS) et une caractérisation mécanique détaillée des hydrogels résultants. Les protocoles de gélification en présence de cations métalliques divalents M^{2+} (par exemple Ca^{2+}) ont été adaptés avec l'objectif de de minimiser la consommation de polymère et d'optimiser la géométrie de l'hydrogel pour l'analyse rhéologique. La grande complexité et la diversité des sEPS dérivés d'AGS ont été abordées en évaluant le processus global de formation d'hydrogel par rapport à des biopolymères bien connus (alginate et k-/ι-carraghénane). Le comportement mécanique post-gélification a été évalué dans des conditions de contraintes de compression et de cisaillement par rhéométrie. En particulier, plusieurs paramètres ont été extrapolés à partir des profils mécaniques observés (par exemple, le module de Young, E, le module de stockage, G', le module de perte, G'', la viscosité complexe, η^*) et corrélés avec les conditions de gélification appliquées pour obtenir des informations sur les principaux moteurs des processus de formation d'hydrogel. Sur la base des résultats de la caractérisation mécanique, la concentration minimale (en masse) de sEPS permettant la formation d'un réseau

tridimensionnel étendu a été reconnue dans la plage de 2.5 à 5 wt% (pour les concentrations de sEPS inférieures à 2.5 wt%, seuls des clusters polymères faiblement interconnectés étaient probablement présents). Les concentrations plus élevées de polymère et de réticulant ionique M^{2+} nécessaires pour former des hydrogels à base de sEPS par rapport aux polymères de référence étudiés ont donc fourni une preuve d'une plus grande complexité et diversité de la composition de sEPS (incluant probablement aussi des molécules qui ne contribuent pas vraiment à la gélification et à la mécanique des hydrogels dérivés). Des réponses mécaniques distinctes aux cycles de compression-décompression consécutifs ont été observées parmi les hydrogels à base de biopolymères étudiés. En particulier, les hydrogels à base de sEPS et de ι-carraghénane se sont comportés de manière similaire sous des contraintes mécaniques. Leur comportement élastique linéaire a été préservé tout au long des cycles de chargement-déchargement, mais des niveaux de rigidité inférieurs ont été atteints par rapport aux systèmes à base d'alginate et de k-carraghénane. Pour tous les biopolymères étudiés, la rigidité des hydrogels variait significativement en fonction des conditions de gélification appliquées, même si la réponse mécanique globale restait presque inchangée. Le module de Young *E* augmentait avec l'accroissement des concentrations de polymère et d'agent de réticulation M^{2+} et variait en fonction du cation métallique M^{2+} utilisé. Les mesures réalisées en régime oscillatoire (contrainte de cisaillement) ont confirmé que les sEPS étaient capables de former des hydrogels avec des propriétés mécaniques solides. D'un point de vue applicatif, cette étude a démontré la possibilité de former des hydrogels à base de sEPS ayant des propriétés mécaniques comparables à d'autres systèmes à base de biopolymères actuellement appliqués à des fins commerciales, suggérant ainsi des solutions potentielles orientées vers la récupération de ressources capables d'évoluer vers un secteur manufacturier moins dépendant des combustibles fossiles.

Le **Chapitre 3** propose une approche robuste pour obtenir des biomatériaux à base des sEPS récupérés à partir de boues granulaires aérobies (AGS) répondant aux normes de qualité requises par le secteur agronomique. En particulier, l'influence de divers produits chimiques dans les processus

d'extraction et de gélification sur la quantité/qualité des macromolécules des sEPS extractibles a été soulignée, en mettant en évidence l'importance d'adapter les méthodologies aux objectifs de recherche. A cet égard, des protocoles d'extraction et de gélification largement discutés dans la littérature ont été modifiés en utilisant des réactifs chimiques ne contenant ni sodium ni chlore (qui sont considérés comme phytotoxiques en grande quantité): K_2CO_3 or $(NH_4)_2CO_3/HNO_3/KOH$ (*extraction*) and $Ca(NO_3)_2{\cdot}H_2O$ or $Ca(C_2H_5COO)_2$ (*gélification*). La qualité/quantité des macromolécules de sEPS extraites ainsi que leur capacité à former des hydrogels ne semblent pas être fortement influencées par les différents produits chimiques appliqués. Au contraire, des différences plus significatives ont été observées en termes de composition élémentaire (macronutriments, Na, Cl, métaux lourds, etc.). Dans l'ensemble, les sEPS obtenus et les biomatériaux dérivés (hydrogels) étaient conformes à la législation environnementale en vigueur en matière d'amendements des sols et de produits fertilisants, résultant dans les limites maximales imposées en termes de métaux lourds (valeurs liées au Cr (VI) à étudier). Le grand potentiel des hydrogels à base de sEPS dans les applications agronomiques a été mis en évidence. En particulier, la capacité de ces hydrogels à assimiler et retenir de grandes quantités d'eau (jusqu'à 16 g H2O par g d'hydrogel sur matière sèche) a été démontrée, suggérant un comportement similaire aux polymères superabsorbants (SAPs). En outre, une preuve de principe a été fournie concernant l'application potentielle d'hydrogels à base de sEPS en tant que systèmes pour la libération de nutriments dans un milieu environnant. La respirométrie a été utilisée pour obtenir des informations sur la biodégradation des sEPS et des hydrogels dérivés: des conclusions en termes de biodégradabilité de la substance organique ont été tirées sur la base du fractionnement de la demande chimique en oxygène (DCO) en composants solubles biodégradables, particulaires biodégradables, solubles inertes et particulaires inertes. Il a été constaté que les sEPS et les hydrogels dérivés peuvent être utilisés comme substrats par les communautés microbiennes habitant les boues activées, mais leur biodégradation a été influencée par les produits chimiques appliqués dans les processus d'extraction et de gélification. De plus, il a été observé que la fraction organique facilement biodégradable diminuait avec la formation de l'hydrogel:

la création d'un réseau polymérique 3D dans lequel les macromolécules de sEPS étaient plus confinées conduisait probablement à une diminution de l'accessibilité au substrat. Enfin, des lignes directrices pour progresser vers de nouvelles solutions axées sur la récupération des ressources dans l'agriculture exploitant les propriétés polyvalentes des sEPS dérivés d'AGS ont été proposées.

Le **Chapitre 4** traite de la possibilité d'utiliser les EPS récupérés à partir de boues granulaires anammox (AmxGS) pour le traitement des eaux usées contaminées par des métaux lourds. À cet égard, la capacité d'adsorption des métaux par les EPS a été comparée à celle des granules d'origine. Des capacités d'élimination des métaux équivalentes ou supérieures à celles des matériaux adsorbants conventionnels et/ou non conventionnels ont été trouvées, mais des mécanismes de bioabsorption distinctes ont été suggérées pour les EPS et les granules natifs. Ces différences pourraient être dues à trois raisons principales: (i) plusieurs mécanismes impliqués dans la bioabsorption des métaux lourds par les granulés natifs; (ii) des modifications chimiques des EPS induites par la méthode d'extraction appliquée; (iii) une mobilité différente des chaînes polymères et une disponibilité différente du site de liaison des EPS extraits en dispersions aqueuses et des EPS non extraits en granules. Des hypothèses mécanistiques pour la bioadsorption des métaux ont été proposées: en combinant diverses techniques analytiques, un processus complexe basé sur une combinaison d'interaction électrostatique, d'échange d'ions, de complexation et de précipitation a été suggéré. En particulier, il a été constaté que les EPS agissaient comme des agents floculants/complexants en présence de systèmes aqueux ayant de fortes concentrations de métaux lourds, provoquant la précipitation spontanée d'agrégats composites (contenant EPS et métaux). Enfin, une preuve de principe a été fournie concernant l'application potentielle des EPS dans des matériaux adsorbants composites (par exemple avec du charbon actif) à haute performance de purification, suggérant ainsi des stratégies pour augmenter l'applicabilité industrielle de ces biopolymères.

Le **Chapitre 5** résume les conclusions générales et les perspectives de la thèse, suggérant ainsi les prochains défis à relever dans les recherches futures. Le potentiel exceptionnel des EPS récupérés à

partir de boues granulaires (AGS et AmxGS) dans les applications liées à l'environnement a été souligné, mettant en évidence des solutions orientées vers la récupération des ressources capables d'évoluer vers un secteur de l'eau basé sur une économie circulaire.

Chapter 1

Introduction

1. From wastewater treatment plants (WWTPs) towards resource recovery facilities (WRRFs)

The urge for a more sustainable development, including a more circular use of resources, together with the high energy demand and large environmental footprint of the current treatment plant design, have driven a paradigm shift within the scientific community regarding the wastewater treatment solutions. New practices should be developed to cope with population growth and improving standards of living, which are pushing our use of natural resources towards limits beyond sustainability: the current ‘‘*linear*’’ approach to urban water management, which is sometimes called the *take, make, waste* approach in the sustainability literature when applied more broadly to natural resource use, is becoming increasingly unsustainable (Daigger, 2009). Within academia, it seems to be clear since the last decades that more sustainable wastewater treatment practices should not be based on the concepts established in the early 20th century (Kehrein et al., 2020). The research effort has been therefore gradually shifted from the protection of the aquatic environment (i.e., pollutant removal and water quality control) towards the energy/resource recovery (Feng et al., 2021). More circular resource flows could be established recognising wastewater as a resource rather than a waste stream (Guest et al., 2009; Ma et al., 2013; Van Loosdrecht and Brdjanovic, 2014), thus making the water sector able to contribute to national and European sustainable development goals (Kehrein et al., 2020). Given that wastewater treatment plants (WWTPs) also represent collection points for a variety of resources, namely water, energy, nutrients and other products, their redesign from treatment facilities into water resource recoveries facilities (WRRFs) provides multiple possibilities to contribute to a more circular economy (Kehrein et al., 2020). This conceptual transformation might allow the perceived impact of wastewater treatment on communities to become net positive (Beck et al., 2008).

Despite the urge for the establishment of a more circular economy-based water sector has been progressively emphasized, the broad implementation of full-scale resource recovery technologies in the wastewater sector is still limited (Stanchev et al., 2017). The application of resource recovery-oriented processes can be difficult because changing the current wastewater handling system implies costs, creates operational distractions, and consumes resources (Daigger, 2009). In addition to technical uncertainties (e.g., which techniques among the growing range of available technical options are most useful, how to combine them according to an integrated resource-oriented approach, etc.) various non-technological bottlenecks could hinder the successful implementation of such technologies into WWTPs. The transfer of scientific insights to decision-makers in water management utilities (WMUs) is an important requirement to make progress in developing resource-oriented wastewater management strategies: there is a need for WMUs to strategically plan the transition from wastewater treatment plants towards resource recovery factories and it is possible only if decision-makers at WMUs have a clear understanding of the available and emerging technologies (Kehrein et al., 2020). Another source of uncertainty can be found into the market potential and competition against the recovered resources (Van Der Hoek et al., 2016). Kerein et al. (2020) calculated the market supply potentials of water, energy, fertilizer, and other products recoverable from municipal WWTPs in the Netherlands or Flanders, showing that part of the market could be successfully covered by wastewater-derived resources (e.g., up to 20 % for water and about 14% for nitrogen and phosphorus supply). Regardless of the technical and non-technical limitations described, the research effort remains focalized on the search for new sustainable, cost-effective, and high-performance strategies which help to conceive and valorize wastewater as a resource stream to be recovered and exploited in multiple sectors.

As known, in biological wastewater treatment, microorganisms use pollutants as substrates and gain energy for growth from their transformation into harmless products (Lotti et al., 2019b). The biomass hence produced, the so-called excess sludge, represents the main waste product in WWTPs, whose processing cost accounts for nearly half of the total operational capital (de Valk et al., 2019): a circular

economy approach in its management could be driven by the multiple opportunities to recover energy and/or other resources (like nutrients, biopolymers, etc.). Together with environmental concerns, biopolymers produced from renewable resources are getting emerging interest, representing the focus of intensive research efforts (Kreyenschulte et al., 2014). Indeed, the global polymer production annually exceeds 300 million tons, consuming approximately 6% of fossil oil produced, and it is anticipated to increase up to 20% in the coming decades (Payne et al., 2019). Since the middle years of the 20th century, the petroleum-derived chemistry, refinery, and engineering processes have been the basis of the polymer industry (Morales et al., 2021), accounting for about 99% in 2015 (Payne et al., 2019), but surely the polymer production based on depleting fossil fuel reserves has become unsustainable (Rabnawaz et al., 2017). Therefore, the urgent transition from a petroleum-based to a bio-based economy has marked the beginning of the current century, shifting the type of carbon resources from fossil to natural and renewable ones (Morales et al., 2021). The biopolymer industry utilizing alternative feedstocks like biomass has emerged as promising strategy to deal with such concern (Zhu et al., 2016). Microbial polymers include intracellular and extracellular polymers. With respect to limited intracellular polymers (e.g., polyhydroxyalkanolates – PHA, polyphosphate, glycogen) (Feng et al., 2020), extracellular polymeric substances (EPS) have drawn emerging commercial interest as potential alternative to conventional synthetic polymers. EPS are high-molecular-weight mixtures of polymers secreted by bacterial consortia during cell metabolism, also including products of cellular lysis and hydrolysis of macromolecules (Sheng et al., 2010). EPS form a complex and diverse biopolymeric matrix mainly consisting of proteins (PN), exopolysaccharides (PS), DNA, lipids, glycoproteins, S-layer proteins, and humic-like substances (Seviour et al., 2019). Unlike other natural sources, EPS can be extracted from a large variety of bacterial biomass and hold great attractiveness being bio-based and biodegradable; moreover, EPS are characterized by highly production rate and easier extraction procedure than oil-based synthesizing polymers (Feng et al., 2021). Thanks to their versatile properties, EPS have been already studied as promising bio-based products in multiple fields such as sizing/coating agents in paper and textile industry (Kim et al.,

2020; Lin et al., 2015), cement curing in construction material sector (Karakas et al., 2020) and biosorbent media in wastewater treatment systems (Guibaud et al., 2012; Li et al., 2017a); moreover, further environmental and industrial applications might be discovered upon improvement of their mechanistic and compositional understanding. Overall, the EPS recovery/valorization attributes value-added to waste sludge, reducing the amount of residues to be handled and so promoting a perspective shift from WWTPs to WRRFs. The environmental and economical sustainability of wastewater treatment would be hence enhanced (Lin et al., 2015), thus leading to resource recovery-oriented solutions able to progress towards a more circular economy-based water sector (Seviour et al., 2019; van Leeuwen et al., 2018).

2. Granular sludge (GS)-based technologies and their potential for the extraction/recovery of Extracellular Polymeric Substances (EPS)

In the field of wastewater treatment, biofilm technologies are based on the use of biofilms grown on a support (i.e., moving- and fixed-bed bioreactors) or self-aggregating biofilms (i.e., granular sludge) (Lotti et al., 2019b). Biofilm-based processes are replacing conventional activated sludge systems (CAS) for a wide range of biological wastewater treatment processes thanks to the lower plant footprint, due to the higher conversion rates and easier solid/liquid separation (Van Loosdrecht and Brdjanovic, 2014), and relevant savings in terms of operational costs, because of the reduced energy consumption for oxygen supply and internal recirculation flows (Bengtsson et al., 2018; Lackner et al., 2014). Particularly, granular sludge (GS) technologies are getting increasingly attention in the last decades thanks to the unique advantages of efficient biomass retention and more compact reactors than traditional activated sludge systems. In brief, biogranulation consists in forcing microrganisms to form granules (i.e., self-aggregated granular biofilms without the presence of inert carriers) rather than floccular microbial aggregates. GS-based processes have many advantages, including excellent settleability, enhanced biomass withholding, capacity of treating high levels of carbon/nutrient load simultaneously and increased toxicity tolerance (McSwain et al., 2005; Pronk et al., 2015). Different

treatment units can be designed by means of distinct granular biofilms (or granules) that are inhabited by a high-diversity of microbial communities (Nancharaiah and Reddy, 2018).

Aerobic granular sludge (AGS) technology has been established as promising and viable alternative to conventional activated sludge (CAS) systems for biological wastewater treatment (Pronk et al., 2015). AGS is a pseudo-spherical biofilm made of self-aggregated microorganisms, having high density (1.044 – 1.048 g/mL), high settling velocity (25 – 70 mm/h) and the possibility to have a multi-layered structure with different redox potential conditions due to e-donors and e-acceptors radial concentration gradients (Campo et al., 2020). Aerobic granules present a stable ecological structure where anaerobic bacteria are mainly located inside, while the aerobic bacteria are distributed in the outside layer. Indeed, the size of aerobic granules (0.2 – 7 mm; Liu and Tay, 2004) ensures that anoxic conditions are preserved within the granules even when the bulk liquor itself is oxygenated, which facilitates the simultaneous removal of chemical oxygen demand (COD), nitrogen (N) and phosphorus (P) (De Kreuk et al., 2007; Seviour et al., 2009a; Yilmaz et al., 2008).

ANaerobic AMMonium OXidation (anammox) is an established process for the efficient nitrogen removal from wastewater, relying on anammox bacteria to form stable biofilms or granules (Boleij et al., 2018). The process consists of two stages: a first aerobic step of oxidation of about half of the ammonium to nitrite (*partial nitration*) by ammonia oxidizing bacteria (AOB) followed by a second anaerobic step in which anammox bacteria convert the resulting ammonium and nitrite into dinitrogen gas (and ca. 10% of nitrate). If compared to the conventional nitrification/denitrification process, anammox bacteria utilizes nitrite instead of oxygen as electron acceptor to oxidize ammonium, whereas the electron donor is replaced by ammonium over organic matter (Tang et al., 2017). Thanks to these features, the autotrophic biological processes based on the metabolism of anammox bacteria allow removing ammonium from wastewater with significant savings in terms of energy spent for oxygen supply (- 60%) and organic carbon supply (- 100%); in addition, the production of excess sludge is reduced (- 90%) compared to the conventional nitrification/denitrification treatment (Hu et al., 2013; Lotti et al., 2019a). For these reasons, anammox-based technologies are becoming the new

standard for the treatment of nitrogen-rich wastewaters of both municipal and industrial origins (Lackner et al., 2014). Granular systems are characterized by higher biomass concentrations and volumetric conversion rates, if compared to flocculent or biofilm on carriers systems and as a matter of fact treat more than 50% of the total N-load handled with anammox technologies worldwide (Lackner et al., 2014). A spatial distribution of microbial communities has been recognized in anammox granules: AOB in the outer shell consume the dissolved oxygen present in the bulk liquid impeding its penetration in the deeper layers, while anammox bacteria are located in the inner part of granules where they can exert their metabolism under anoxic conditions. Anammox granules appeared like spherical – elliptical self-aggregated biofilms, characterized by reddish coloration (due to the high content of cytochrome-C), average size ranged between 1.5 and 4 mm, high density (1.03 g/mL) and settling velocity (73 – 88 m/h) (Boleij et al., 2018; Feng et al., 2021; Lotti et al., 2019a; Tang et al., 2017).

In addition to AGS and AmxGS-based technologies, anaerobic granular sludge (AnGS) processes have been developed for the anaerobic treatment of industrial effluents (Lim and Kim, 2014). Also AnGS feature a multi-layer structure: a central core of acetoclastic ethanogens is surrounded by a layer of H_2/formate-producing acetogens and H_2/formate-consuming methanogens and by an outside layer of bacteria responsible for the hydrolysis and acidification of carbonaceous pollutants (Feng et al., 2021). Anaerobic granules present a spherical - elliptical shape, black - brown coloration, medium size (2 – 5 mm) and high density (1.004 – 1.065 g/mL) and settling velocity ($\simeq$ 70 m/h) (Gagliano et al., 2020; Pol et al., 2004).

As in conventional biofilms, in granules microorganisms produce a significant amount of highly hydrated extracellular polymeric substances (EPS) to form a polymeric matrix in which they are self-immobilized (Flemming and Wingender, 2010; Seviour et al., 2019, 2012). EPS contribute to the initial aggregation of microbial cells (Flemming and Wingender, 2010) and are mainly associated with the architectural structure, rheological behaviour and functional stability of granules, thus influencing the physic-chemical properties of the biomass catalyzing the biological purification

process. Particularly, various important functions concerning EPS have been demonstrated, such as a protective barrier against detrimental environment, maintenance of a stable structure, settling properties, surface charge, protection against dehydration, nutrient source, and organic substance sorption capacity (Seviour et al., 2019; Sheng et al., 2010). It has been reported that the (extractable) EPS content accounted for about 25% of VSS (VSS: volatile suspended solids) in AGS (Felz et al., 2016), 40-59% of VSS (Feng et al., 2019; Lotti et al., 2019a; Ni et al., 2010) in AmxGS and up to 29% of VSS (D'Abzac et al., 2010) in AnGS. With this regard, significative EPS recovery potentials might be anticipated, thus making the production of EPS-based materials a viable alternative for a more efficient waste sludge management. As calculated, the sEPS potential production from AGS accounts for about 58 g/KgCOD removed and it is anticipated to achieve 85 kton in the coming decade in the Netherlands (Pronk et al., 2015; van Leeuwen et al., 2018). A higher content of EPS can be extracted/recovered from AmxGS (Feng et al., 2019; Lotti et al., 2019a) compared to other granules (up to 40 wt% of the organics originally present in the biomass): considering the growth yield of anammox bacteria (0.11 gVS/gNH4-N removed, Lotti et al., 2014), the extraction potential of EPS accounts for more than 40 gEPS per kgNH4-N removed from wastewater. Considering an ammonium-nitrogen load of an average size full-scale anammox granular sludge installation on the order of 3 ton-N/d (Lackner et al., 2014), it could be anticipated that about 125 kg/d of EPS dry weight might be extracted from the excess sludge of this size of installation (Lotti et al., 2019a). Given that currently more than 1000 full-scale anaerobic reactors exist worldwide (Lim and Kim, 2014), large quantities of EPS are also expected from AnGS, thus greatly expanding the great potential towards resource recovery (Feng et al., 2021).

3. The high-diversity of GS-derived extracellular polymeric substances (EPS): the main bottleneck in their fine characterization

As previously mentioned, EPS are secreted by microrganisms during the cell metabolism and their accumulation helps to bridge bacterial cells and other particles into aggregates (Feng et al., 2021).

Consequently, the high-diversity of microbial communities inhabiting the aggregates would reflect the high-diversity in terms of quality/quantity of GS-derived EPS contents. Well-established and emerging classification criteria are currently available. One of the most adopted methods is based on a distribution criterion, according to which EPS can be divided into *bound* EPS (B-EPS) and *soluble* EPS (S-EPS). B-EPS represent the fraction of EPS closely bound with the cells and can be further sub-classified as loosely-bound (LB-EPS) and tightly-bound (TB-EPS) (Raszka et al., 2006; Su et al., 2013). Based on their nature, EPS may be classified as *capsular* and *slime* (More et al., 2012; Raszka et al., 2006). Moreover, emerging classification criteria have been based on physical, chemical and/or structural features such as electrical charge (*anionic*, *cationic* EPS), physic-chemical properties (*acidic*, *alkaline*, *polar* EPS), etc. (Pronk et al., 2017). Recently, the concept of *structural EPS* extractable from both AGS and AmxGS has been comprehensively discussed within the dedicated scientific community. Structural EPS (sEPS) could be considered as the fraction of total EPS strongly involved in the structural integrity of granules: indeed, both AGS- and AmxGS-derived EPS have been demonstrated to endow hydrogel-formation properties and this ability is considered as well-linked with the physical strength of GS (Boleij et al., 2019; Felz et al., 2016; Lin et al., 2018; Lotti et al., 2019b).

The broad molecular weight (MW) distribution, typically from a low (< 3 kDa) to a large (> 235 kDa) MW, would reflect the complexity and high diversity of macromolecules forming the biopolymeric matrix (Boleij et al., 2019; Feng et al., 2019). Even if multiple compounds have been usually detected in EPS (e.g., PS, PN, (phosho)lipids, glycoconjugates, humic acids, nucleic acids, etc., Felz et al., 2019; Flemming and Wingender, 2010), total PN (up to 60 wt%) and total PS (40 – 95 wt%) have been recognized in most studies as the major constituents in the extractable extracellular biopolymers (Dubé and Guiot, 2019; More et al., 2014a), with PN-like compounds dominant with respect to PS (Feng et al., 2019; Lotti et al., 2019a; McSwain et al., 2005). Intense research effort has been recently focused on appreciating new EPS contents, with particular attention to PN, PS and polymers with specific functions. Glycoproteins with a heterogeneous O-glycan structure (Boleij et al., 2018) as well

as amyloid-like substances (Lotti et al., 2019b) have been found in AmxGS-derived EPS. Glycosylated amyloid-like PN have been extracted from AGS (Lin et al., 2018); moreover aromatic PN-like and tryptophan PN-like substances have been found more abundant in the AGS/AnGS matrices (Zhu et al., 2015). Monosaccharides including some neutral sugars (glucose, galactose, mannose etc.), glucuronic acids, galacturonic acids, amino sugars (galactosamine and glucosamine) have been detected in AGS-derived EPS (Felz et al., 2019a). Moreover, siliac acids and glycosaminoglycans (GAGs)-like biopolymers have been found in both AmxGS- and AGS-derived EPS products (Boleij et al., 2020; de Graaff et al., 2019; Felz et al., 2020b). Two exopolysaccharides have been recognized as crucial gel-forming constituents in AGS: alginate-like exopolysaccharides (ALE) (Lin et al., 2010; Schambeck et al., 2020) and Granulan (Seviour et al., 2010). Both granulan and ALE display hydrogel-forming properties, but they are completely distinct. Granulan has been reported as a complex heteropolysaccharide with a repeat sequence of α-galactose, β-mannose, β-glucosamine, N-acetyl-β-galactosamine and 2-acetoamido-2-deoxy-α-galactopyranuronic acid, having a disaccharide branch of β-galactose and β -glucuronic acid attached to 2-acetoamido-2-deoxy-α-galactopyranuronic acid. It is able to undergo sol-gel transition at pH 9.0 – 12.00 and therefore exist in a strong gel state at pH < 9 (Seviour et al., 2012, 2010, 2009b). Conversely, alginate-like exopolysaccharides were isolated from granules treating a mix of abattoir and domestic wastewater (and/or acetate-fed synthetic influents) and form hydrogels in presence of divalent metal cation aqueous solutions (e.g., $CaCl_2$) at pH 4.5 (Lin et al., 2010; Schambeck et al., 2020). Chemical and functional similarities have been recognized for ALE and alginate: indeed, both are alkaline extracted, form stable hydrogels with calcium ions, precipitate as a gel at acidic pH and are rich in carboxyl groups (Draget et al., 1994; Felz et al., 2020a; Lin et al., 2010). However, follow up research demonstrated sEPS to be much more complex than alginate: while alginate is a linear polysaccharide composed of alternating guluronic and mannuronic acid units, sEPS are a complex mixture and mainly composed of proteins, neutral sugars, amino sugars, uronic acids and polyphenolic compounds (Felz et al., 2019a). With this regard, to give a ubiquitous definition, currently it is usually referred to

sEPS as the fraction of total EPS enabling the gelling properties and hence considered to be strongly involved in the mechanical strength of aerobic granules (Felz et al., 2016). Indeed, a quite different chemistry in the hydrogel-formation has been observed for sEPS versus alginate by Felz et al. (2020a) who studied the impact of various metal cations on the biopolymer post-gelling stiffness. Particularly, it has been found that sEPS favour Zn^{2+} and transition metals over alkaline earth metals to form stiffer hydrogels; conversely, enhanced mechanical properties could be achieved for alginate hydrogels formed in presence of alkaline earth metals. Overall, it has been observed that gelling processes with metal ions able to complex with carboxyl groups give weaker gels for sEPS than for alginate. With this regard, it should be considered that not only the abundance of functional groups able to interact with metal ions (e.g., Ca^{2+}) during the hydrogel-formation processes, but also their availability due to the polymer chain arrangement can affect the post-gelling mechanical properties: alginate presents a large amount of available carboxyl groups distributed on a linear polysaccharide chain; conversely, sEPS consist of proteins and a much higher diversity of sugar monomers than alginate (Felz et al., 2019a). Different structural patterns have been found for dried sEPS and alginate hydrogels: more detailed, the inhomogeneous structures of dried sEPS hydrogels could be due to the high complexity of their composition and the various molecular interactions. Moreover, sEPS hydrogels feature a greater biochemical stability towards dissolution by the cheating agent EDTA with respect to alginate (Felz et al., 2020a). Reasonably the high complexity of the sEPS constitutes could reflect the occurrence of gelling mechanisms potentially ascribed to both ionic cross-linking and interactive reactions of multiple functional groups in sEPS (Felz et al., 2020a).

As previously mentioned, also AmxGS-derived EPS have been reported to endow gel-forming properties. The main differences between AGS- and AmxGS-derived sEPS hydrogels can be found in the functional components and mechanisms involved in the gelling processes. Particularly, EPS extracted from AmxGS are able to form hydrogels with solid-like mechanical properties, without any additional chemical cross-linker (e.g., metal cations) (Lotti et al., 2019b) which is instead needed for AGS-derived sEPS (Felz et al., 2016): for high EPS concentrations (above 17% w/v EPS) an extended

3D network is formed conferring to the material high mechanical and water retention properties. Functional amyloid fibrils have been recognized as potential key component of the complex hydrogel network representing the structural units of the 3D network formed in concentrated EPS dispersions (Lotti et al., 2019b).

Despite the key findings described above, the identity of the EPS from biofilm-based systems is still poorly understood. As highlighted by Seviour et al. (2019), structural and functional assignment of key biofilm EPS is confounded by their compositional complexity and interactions as well as by the challenges in processing and isolating the EPS components. Unless methods are developed to extract the whole spectrum of biofilm EPS, the understanding on EPS will be distorted by solubility (being biofilms and many of the EPS poorly soluble in aqueous systems) and characterization biases. The chemical and mechanical extraction methods developed are often only partially or marginally effective, thus resulting in the characterization of EPS that are not important for the biofilm structure (Felz et al., 2016), especially in the case of stratified and dense aggregates like fixed biofilms or granular sludge.

A key aspect to be considered dealing with biofilm-derived EPS is hence the effect of the extraction method on the quality/quantity of the recoverable EPS macromolecules. In light of the high diversity and complexity of the EPS matrix described above, the application of various methods might result in significative differences in terms of quantitative and qualitative properties (e.g., extraction yield, biochemical composition, functional groups, etc.). Overall, the architecture of each protocol is almost the same, including sample preparation, extraction, purification (optional), enrichment and recovery (Feng et al., 2021). Despite these structural similarities, different approaches can be implemented and integrated in the EPS extraction processes:

- *Physical methods*: they include treatments like centrifugation (Liu and Fang, 2002), sonication (Dubé and Guiot, 2019), blending (Gehr and Henry, 1983), heating (Felz et al., 2016; Feng et al., 2019). The application of physical forces (e.g., centrifugal force, impulsive pressure, shear stress, molecule vibrations, etc.) able to disrupt and dissolve polymers from the extracellular matrix

allows to softly extract a small amount of EPS but with a guarantee of cell integrity (Feng et al., 2021);

- *Chemical methods*: they provide the use of chelating agents like EDTA (Liu and Fang, 2002), cation exchange resins (CER) (Dignac et al., 1998), alkaline reagents like NaOH or Na_2CO_3 (Lin et al., 2010; Seviour et al., 2010), acid reagents like H_2SO_4, HCl or CH_3COOH (Feng et al., 2019; Pronk et al., 2017), organic solvents such as chloroform or methanol (Lin et al., 2010; Seviour et al., 2012, 2010) or aldehydic reagents (Felz et al., 2016; Liu and Fang, 2002) to solubilise polymeric matrix. These methods are usually considered the most effective being able to extract higher amount of EPS (Sheng et al., 2010);
- *Biological methods*: they consist in the application of enzymatic treatment (Sesay et al., 2006).

In the perspective to investigate the EPS structure, composition, characteristics, and functions during the water treatment process, the extraction method effectiveness should be addressed based on general targets. Traditional criteria can be summarised as follows: maximization of the EPS extraction yield, no disruption of EPS structure and minimization of cell lysis (Sheng et al., 2010). Moreover, benefits derived from the short time consumption and user-friendly operation units should be considered in the choice of the most appropriate method (Feng et al., 2019). A detailed structural and functional characterization of novel (and relevant) extracellular polymers from biofilm-based systems requires significant quantities of a sufficiently pure compound, which is a common (and often insuperable) obstacle in resolving more precisely the identity of the key EPS components. Indeed, the recovery of a sufficient content of EPS with high degree of purity is crucial to elucidate their structural and functional properties by means of specific analytical techniques. With this regard, EPS can be recovered by solvent/ethanol precipitation (Li et al., 2014), acidic precipitation (Boleij et al., 2019; Lotti et al., 2019a), centrifugal filter device with a membrane (Feng et al., 2019), and purification via dialysis (Felz et al., 2016; Liu and Fang, 2002) or electrophoretic/chromatographic techniques (Seviour et al., 2010). Being aware of analytical challenges of identifying and characterizing functional EPS from biofilm-based systems, the current extraction and spectrophotometric

characterization methods, often prioritizing the integrity of the microbial cells, should be critically assessed with the aim to elucidate the contribution of a broader range of key EPS components (Seviour et al., 2019). A retrospective investigation through microscopic technique (Neu and Lawrence, 2014, Wagner et al., 2009) to understand if the extracted polymers are effectively extracellular should be included in this approach (Seviour et al., 2019).

Conventional analytical techniques (e.g., colorimetric methods) might hence result inappropriate and not specific in appreciating complex EPS components. For instance, PN-glycosylation phenomena commonly happen in biofilms, thus significantly complicating the analytical processes (Feng et al., 2021). Felz et al. (2019) pointed out that the current research in matter of EPS appears largely dependent on analytical colorimetric methods that present significant biases mainly due to the lack of specific standard compounds and the cross-interferences of various EPS compounds in the individual assays. Uncertainties have been found not only in the evaluation of the quality of the GS-derived EPS macromolecules but also in their spatial distribution which appears highly diverse and heterogeneous based on the nature of microbial aggregates. The complexity of the EPS composition, likely resulting from operational conditions, anaerobic or aerobic environment, microbial communities, biological and chemical transformations, etc. (Chen et al., 2010; Zhang et al., 2015), could explain the high heterogeneity in the EPS distribution. Particularly, the relationship between EPS distribution and microorganism distribution is still poorly understood. By means of the available analytical techniques no universal conclusions have been drawn (Feng et al., 2021). Furthermore, based on the commonly applied analytical techniques, it is currently not possible to track the production of specific EPS components over time and/or attribute them to the specific host organism in mixed species biofilm communities; additionally, tools to effectively manipulate EPS quantity or composition are not available (Seviour et al., 2019). Metabolic labelling approaches might be useful for this purpose (Liang et al., 2017), but the limitations due to a still incomplete understanding of the biofilm-derived EPS make these methodologies considerably difficult to be implemented (Seviour et al., 2019). Considering that biofilm composition, structure and functionality strictly depend on EPS,

the lack of specificity of analytical methods for the EPS characterization could limit the biofilm research progress. Consequently, it appears clear within the scientific community that multidisciplinary approaches and analysis (e.g., cross-referencing between model biofilms and full-scale biofilm systems) should be synergically integrated to gain insights on the functional, compositional and physical-chemical properties of biofilm-derived EPS. Particularly, intense research effort should be devoted on improving and developing more advanced analytical methods able to shed light on the identity of the key EPS components (e.g., functional description of isolated EPS with *in situ* techniques like FT-IR imaging, Raman microscopy, magnetic resonance imaging MRI, but also confocal laser scanning microscopy CLSM, mass spectrometry MS imaging, combined to nuclear magnetic resonance NMR analysis, genomics, proteomics and glycomics, etc.) (Seviour et al., 2019). A deeper knowledge of the EPS matrix could therefore lead to a greater understanding of the biofilm processes, thus allowing to improve the stability performance of GS technologies, and support the development of EPS valorization pathways (Felz et al., 2019; Seviour et al., 2019).

The optimization of the EPS extraction/recovery methods is relevant not only to progress towards a deeper understanding of the key extracellular polymers, but also to enhance the industrial applicability of the recovered EPS-based biomaterials. Even if research effort has been focalized on the optimization of the extraction processes based on the research purposes in terms of EPS analytical investigations, the existing methods have never considered in terms of viability of the extractable biopolymers as raw biomaterials for specific practical applications (Feng et al., 2021). The implementation of resource recovery-oriented strategies based on the use of these waste-derived biopolymers cannot exclude this aspect that should be deeply assessed in order to promote the development of EPS-based products with reasonable market-value. Enhanced criteria in the evaluation of the extraction method effectiveness should be therefore implemented considering the different chemical, functional and structural properties required for the recovered EPS-based biomaterials based on the specific application sector selected. In this sense, not only the approach

used (e.g., physical, chemical, and/or biological methods) but also the operational conditions and/or the chemicals applied should be critically evaluated.

4. Towards new resource recovery-oriented scenarios exploiting GS-derived EPS-based biomaterials

The outstanding and versatile properties of GS-derived EPS can be exploited in multiple industry- and environment-related applications. EPS-based hydrogels from both AmxGS and AGS can be used as raw biomaterial for the industrial paper coating with the aim to increase the properties of water-proof capacity and grease resistance (Lin et al., 2015; Lotti et al., 2019b). Given the hydrophilic properties and the similarities with alginate, AGS-derived EPS has been applied to improve the curing of cement with befits with respect to conventional additives due to the eco-friendly and cost-effective nature of the EPS-based materials (Karakas et al., 2020). AGS-based EPS have been also proven to be suitable as bio-based flame retardant materials for flax fabrics (Kim et al., 2020). Numerous studies document the capability of GS-derived EPS to bind heavy metal ions (Ni^{2+}, Pb^{2+}, Cd^{2+}) (Guibaud et al., 2012; Li et al., 2017a) as well as organic and/or dye pollutants (Wei et al., 2015), thus suggesting their potential application as biosorbent materials for a variety of water treatments. Moreover, the effectiveness of using AnGS-based EPS for the cation exchange membrane (CEM) fabrication has been recently reported (Sudmalis et al., 2020).

To be noticed that the growing commercial interest for biopolymer-based hydrogels which feature the unique advantages of biocompatibility, biodegradability, non-toxicity, and relative low-cost (Lima-Tenório et al., 2015) could open new valorization scenarios for the GS-derived gelling EPS. With this regard, it should be considered that the application of hydrogel-based materials in miscellaneous sectors is driven by many fundamental properties (e.g., mechanical behaviour, physical-chemical features, biodegradability, chemical resistance and durability, biological stability, etc.) whose level of priority appears strictly dependent on the final use of the designed bioproducts. For instance, the development of EPS-based biomaterials with high effectiveness in agriculture-

related applications (e.g., soil conditioning) imposes high qualitative standards (e.g., absence of phytotoxic elements, low levels of heavy metals, etc.) and capacity to adsorb and hold significant water quantities. Polymer-related applications in agriculture should also feature high degradation rates (avoiding soil contamination due to the production of non-biodegradable residues) as well as long-term functionality and stability (Milani et al., 2017). In the case of hydrogel-based materials to be applied in the construction sector (e.g., additive to improve the concrete durability) an adequate chemical resistance (for instance against chemical attacks by acids, chlorine, sulphate) has been emphasized as crucial in addition to great water-binding properties (Afridi et al., 2019). Regardless of the specific industrial solution, the mechanical behaviour of hydrogels has long been recognised as fundamentally important: given that a substantial fraction of hydrogel-based materials consists of water, a limiting factor in their widespread adoption might be found in their poor mechanical properties, especially if compared with traditional engineering materials (Oyen, 2014). By way of example, the production of stiff (and stable) biopolymer-based hydrogels is crucial when they are applied in water treatment systems, to ensure an effective post-treatment separation, in agriculture and/or biomedical applications, if used as carrier systems for delivery and controlled-release of drugs and/or agrochemicals, respectively, to protect the encapsulated components by the mechanical deformation.

In summary, even if it seems to be clear that the EPS recovery and conversion into added-value bioproducts gives a new perspective on a less fossil fuel-dependent economy, further research effort should be dedicated to better design and manage future biorefinery implementation, especially in enhancing the quantity/quality of the recovered biomaterials. As emphasized in the above presented dissertation, additional work is expected to be focused on a better understanding of the EPS fine structure, physic-chemical and functional properties as well as on the optimization of the extraction/recovery processes based on the specific applicative goals. Moreover, the environmental and economic impacts of the overall process of EPS production/valorization should be addressed, paying attention to the market supply/demand potential.

5. Thesis aims and structure

The present thesis has been developed starting from the described holdups with the aim to progress towards the feasible conversion of GS-derived EPS into value-added biomaterials to be applied in multiple sectors. The work mainly aimed to give insights on the EPS recovery, characterization, and valorization, thus shedding light on integrated approaches to engineer some attractive properties of these waste-derived biopolymers. Additionally, this analysis was employed to show how the whole EPS production and valorization chain should be critically assessed based on the targeted application sector. The versatile properties of GS-derived EPS have been addressed to illustrate the wide range of potential industrial and/or environmental solutions which could guide the broader implementation of resource recovery facilities. Two types of GS have been investigated (i.e., AGS and AmxGS) and distinct valorization scenarios have been addressed as a function of the nature of the microbial aggregates. Particularly, the affinity of EPS for metal cations, enabled by the abundance of (acidic) functional groups able to interact with metals (e.g., carboxyl, hydroxyl, phosphoric and amine groups, etc., Felz et al., 2020a; Guibaud et al., 2012; Li et al., 2017; Li et al., 2020; Wei et al., 2016, 2019), has been exploited to develop and characterize bio-based commodities suitable in multiple sectors such as hydrogel-based materials with great potential for agriculture-related applications (*AGS-recovered EPS*) and biosorbent media for the treatment of heavy metal-contaminated wastewaters (*AmxGS-recovered EPS*).

Concerning the AGS-derived EPS, the focus of this thesis was hence on the structural EPS (sEPS), the fraction of total EPS considered to be strongly involved in the structural integrity of granules (Felz et al., 2016), and particularly on their hydrogel-forming ability. The aim was to strengthen the knowledge on these complex biopolymers to move towards the feasible conversion into value-added biomaterials (e.g., hydrogels) with outstanding properties in various fields (e.g., agriculture). With this regard, the scheme proposed has been based on the following fundamentals:

i. Comprehensive analysis of the sEPS hydrogel-forming ability and post-gelling mechanics with the aim to progress towards a stronger awareness of this class of waste-derived biopolymers, emphasizing various methodologic aspects (e.g., optimization of the gelling methods) as key tools to strengthen the outcome of the analytical investigation;

ii. Regulation of the sEPS extraction and hydrogel-forming processes based on the specific applicative purposes;

iii. Definition of macro-classes of properties to be synergically investigated as general criteria to lead towards the production of sEPS-based hydrogels in line with the requests of the specific application sector.

With reference to point (i), **Chapter 2** mainly aims to give insights on AGS-derived sEPS hydrogels, proposing a detailed focus on their mechanical properties. Rheometry has been used to characterize the sEPS post-gelling mechanical behaviour under both compression and shear stress conditions. Taking advantage of robust and material-saving gelling protocols (optimized based on the mechanical characterization goals), the high complexity of AGS-derived sEPS has been approached evaluating the overall process of hydrogel-formation in comparison with well-known biopolymers (i.e., alginate and k-/ι-carrageenan). Particularly, sensitive parameters have been extrapolated from the observed mechanical profiles (e.g., Young's modulus, *E*, storage modulus, *G'*, loss modulus, *G''*, complex viscosity, η^*) and correlated with the applied hydrogel-forming conditions (e.g., polymer concentration and ionic cross-linker concentration and nature) to shed light on the mechanics of the obtained sEPS hydrogels and draw speculative conclusions about the gelling processes.

With reference to points (ii) and (iii), in **Chapter 3** the influence of the whole process of sEPS recovery/valorization on the quantity/quality of the extractable EPS macromolecules and on the properties of the derived biomaterials (i.e., hydrogels) has been emphasized: particularly, agriculture has been studied as target sector and all the evaluation criteria has been consequently adapted. With this regard, various chemicals have been tested in both extraction and hydrogel-forming protocols with the aim to obtain sEPS-based biomaterials consistent with the current environmental legislation

that imposes high qualitative standard for the agronomic sector. In addition to the mechanical behaviour described in **Chapter 2**, various properties have been recognized as pivotal in developing sustainable agro-practices exploiting sEPS-based hydrogels and therefore deeply addressed (e.g., elemental composition, physical-chemical characteristics like swelling-deswelling capacity, nutrient loading and release capacity and biodegrability). Particularly, the potential behaviour of sEPS-based hydrogels as superabsorbent polymers (SAPs) able to sorb and hold high quantities of water has been evaluated. Moreover, a proof-of-principle of the feasible application sEPS hydrogels as carrier systems for nutrient loading and release is given.

The choice to focus on the hydrogel-forming ability of AGS-derived sEPS instead of AmxGS-derived EPS can be motivated as follows. With respect to AmxGS-derived EPS, it has been proved that sEPS from AGS are able to form stable hydrogels at lower weight concentrations (Felz et al., 2016): this would allow to obtain biopolymer-based hydrogels with high-water content that result particularly appealing in the agriculture sector.

Concerning the potential valorization of AmxGS-derived EPS, the focus of **Chapter 4** is therefore aimed to demonstrate the feasibility of exploiting them in high-performance and cost-effective technologies for the treatment of heavy metal-contaminated wastewater. With this regard, the metal-binding ability of the extracted EPS has been described based on the results emerged from single- and multi-metal biosorption studies and interpreting the observed profiles by means of theoretical models. The comparison with pristine granules in terms of biosorption effectiveness and pathways has been introduced mainly to shed light on the biosorption mechanisms of the extracted and non-extracted EPS in native biomass. A mechanistic hypothesis for metal biosorption has been proposed based on the results emerged from a detail molecular-level analysis performed by combining various analytical techniques. A proof-of-principle of the feasible application of the extracted EPS in composite sorbent media (e.g., with activated carbon) has been given with the aim to suggest strategies able to enhance the industrial applicability of AmxGS-derived EPS.

Chapter 5 summarizes the main results reported in each chapter and draws general conclusions about the attractiveness in implementing resource recovery-oriented solutions based on the production of GS-derived EPS-based biomaterials. Moreover, the next challenges to be addressed in follow up research have been suggested.

Chapter 2

Methodological and mechanical insights on structural extracellular polymeric substances (sEPS)-based hydrogels from aerobic granular sludge (AGS)

Abstract

This chapter proposes a comprehensive analysis of the hydrogel-forming ability and post-gelling mechanical properties of structural extracellular polymeric substances (sEPS) extracted from aerobic granular sludge (AGS). Methodologic insights to overcome practical and theoretical concerns often addressed by researchers working on this field (e.g., scarcity of material, complexity of the biopolymeric matrix, etc.) were given. Taking advantage of material-saving and optimized gelling methods, the comparison between AGS-extracted sEPS and well-known biopolymers (i.e., alginate and k-/ι-carrageenan) was implemented to strengthen the outcome of the mechanical characterization. The dependence of the post-gelling mechanics on the applied gelling conditions (i.e., polymer concentration and ionic cross-linker concentration and nature) was hence established: the mechanical response to consecutive compression-decompression cycles was evaluated and the Young's modulus *E* was studied as sensitive parameter to gain insights on the main drivers of the hydrogel-formation processes.

While alginate and k-/ι-carrageenan underwent sol-gel transition for all the investigated conditions (1 – 5 wt% polymer content; 0.001 – 0.1 M Ca^{2+} concentration), the establishment of an extended 3D network occurred for sEPS concentrations higher than 2.5 wt% (and $Ca^{2+} \geq 0.1$ M): higher driving forces were hence required to enable the formation of stable and stiff sEPS hydrogels, thus giving a proof-of-principle of the higher complexity and diversity of the extracellular biopolymeric matrix.

With respect to alginate and k-carrageenan-based systems, sEPS and ι-carrageenan hydrogels behaved similarly one subjected to consecutive compression-decompression cycles, deforming elastically for all the applied range of deformations ($\varepsilon \leq 20\%$). For all the studied biopolymers, the Young's modulus *E* (and hence the post-gelling stiffness) varied significantly based on the applied gelling conditions, even if the overall mechanical response remained almost unchanged: *E* increased upon increasing the polymer and (ionic) cross-linker concentration and varied based on the (divalent) metal cation used as cross-linking agent.

The mechanical response under shear stress conditions was also addressed: the solid-like behaviour of (1 – 10 wt%) sEPS-based hydrogels was hence confirmed in oscillatory shear experiments.

Overall, this study demonstrated that AGS-derived sEPS can form hydrogel-like materials with high-water content (up to 97.5 - 99 wt%) and versatile mechanical properties: level of stiffness and elasticity (*E* up to about 20 kPa under the tested conditions) comparable to other biopolymer-based systems currently applied for commercial purposes (e.g., ι-carrageenan-based materials) could be achieved, thus suggesting the promising development of sEPS-based biomaterials in resource recovery-oriented solutions.

1. Introduction

Aerobic sludge granulation emerged in the last decade as novel biotechnology for a wide range of biological wastewater treatment processes. This technology forces microorganisms to form granular sludge rather than floccular sludge. The compact granular form provides better settling property, more effective sludge-effluent separation, and higher biomass retention. These advantages allow running wastewater treatment plants (WWTPs) that require up to 30% less energy input, 75% less space occupation combined with significant lower investment costs (Lin et al., 2015). As in conventional biofilms, in aerobic granular sludge (AGS) microorganisms produce a significant amount of highly hydrated extracellular polymeric substances (EPS) to form a hydrogel matrix in which they are self-immobilized (Flemming and Wingender, 2010; Seviour et al., 2019, 2012). EPS are a complex

mixture of polysaccharides, proteins, nucleic acids, (phospho)lipids, humic substances, etc. (Flemming et al., 2007; Flemming and Wingender, 2010) and represent a key element for shape, structure, strength, filterability and settling behaviour of the microbial aggregates. The EPS recovery and conversion into bio-based commodities is getting increasing attention as appealing route to enhance the environmental and economic sustainability of wastewater treatment (Lin et al., 2015). Indeed, the excess sludge is considered the main waste product in WWTPs and its processing costs account for nearly half of the total operational capital (de Valk et al., 2019): the recovery of biopolymers like EPS as new cost-effective and high-performance bio-based materials with reasonable market-value would promote a circular economy framework in waste sludge management, thus contributing to a perspective shift from WWTPs to water resource recovery facilities (WRRFs) (Lin et al., 2010; Sam and Dulekgurgen, 2016; Van Loosdrecht and Brdjanovic, 2014). Thanks to their versatile properties, EPS have been already studied as promising bio-based products in multiple fields, like water-proof coating in paper industry (Lin et al., 2015), flame retardant agents (Kim et al., 2020), cement curing (Karakas et al., 2020) and biosorbent media (Guibaud et al., 2012; Li et al., 2017); moreover, further applicative scenarios might be opened upon improvement of their mechanistic and compositional understanding.

Aerobic granules contains EPS which endow gel-forming properties: particularly, these AGS-derived EPS have the ability to form stable hydrogels with calcium ions after extraction and they are previously denominated in literature as alginate-like exopolysaccharides or ALE (Lin et al., 2010) due to the chemical and functional similarities with alginate. However, the higher complexity of sEPS with respect to alginate has been proved by follow up research (Felz et al., 2020a). These EPS are considered to be strongly involved in the structural integrity of aerobic granules (Felz et al., 2016), and hence they are currently referred to as *structural EPS* (sEPS). The molecular-level understanding of the sEPS hydrogel-forming processes is still incomplete and further research effort is therefore demanded to progress from the characterization towards the broader implementation of sEPS hydrogel-based materials in environment- and/or industry-related applications. To be noticed that the

high complexity of sEPS makes challenging a comprehensive analysis of their gelling mechanisms: consequently, the development of a sensitive and accurate methodologic approach could become a crucial point to be evaluated. Another concern often addressed by researchers in this field is the low availability of raw material for the sEPS characterization studies: working with laboratory- and/or pilot-scale reactors for the AGS cultivation, the amount of extractable sEPS (up to about 25 wt% of the organics originally present in the granules; Felz et al., 2016) might become a limiting aspect for a comprehensive study.

In this perspective, the present work mainly aimed to give insights on the hydrogel-forming ability and resulting post-gelling mechanics of AGS-derived sEPS, emphasizing methodologic aspects along the entire research line. With this regard, the scheme proposed provided the development of a material-saving, reproducible and robust hydrogel-forming protocol easily adaptable on various biopolymers combined to rheological studies for the post-gelling mechanical characterization. As mentioned in **Chapter 1**, the focus on the mechanical properties is a fundamental prerequisite in evaluating existing and/or potential application fields for biopolymer-based hydrogels (Oyen, 2014), thus becoming one of the most emphasized goals of this study.

The sEPS hydrogel-formation and post-gelling mechanics was addressed in comparison with well-known biopolymers: this approach was implemented with the aim to strengthen the investigation in matter of sEPS through indirect observations and provide a consistent positioning into the literature context in terms of gelling biopolymers. Below, a brief dissertation concerning the polymers selected as *"models"* in this study: alginate and k-/ι-carrageenan.

Alginate is a linear polysaccharide commercially extracted from brown algae (*Phaeophyceae*) that contains varying amounts of 1,4-linked β-D-mannuronic acid and α-L-guluronic acid residues, which are arranged in a block-wise manner along the backbone (Lee and Mooney, 2012; Lee and Yuk, 2007). Particularly, it consists of homopolymeric blocks of either β-mannuronic acid (MM) or α-guluronic acid (GG), or heteropolymeric blocks of alternating β-mannuronic and α-guluronic acid (MG). An associative gel-forming mechanism has been validated for alginate according the so-

called “egg-box” model: GG blocks in series are buckled and form cavities into which divalent cations (especially Ca^{2+}) fit, and act as ionic bridges to guluronic acids in other alginate chains, thus enabling cross-links to form (Christensen et al., 1990; Seviour et al., 2012).

Carrageenan is a polysaccharide extracted from red seaweeds (*Rodophyceae*). Chemically, it is a linear polymer composed by galactose residues: D-galactose and 3,6-anhydro-D-galactose connected by α-1,3 and β-1,4-glycosidic linkage. It can be classified into three main types: kappa (k), iota (ι) and lambda (λ), depending on the number and position of sulphate groups (Kozlowska et al., 2018). Both k- and ι-carrageenan can be solubilized in aqueous dispersions with heating (at about 65 °C) and their sol–gel transition occur upon cooling and/or addition of counter ions such as Na^+, K^+ and Ca^{2+}. Conversely, λ-carrageenan does not show gelation, likely due to its high degree of sulphate substitution (Thrimawithana et al., 2010). K-/ι-carrageenan feature the capability to form thermo-reversible hydrogels. The conformation of κ- and ι-carrageenan chains in aqueous solution changes from a random coil to a helix structure below a critical temperature (T_c) (Rochas and Rinaudo, 1982): the helices have a tendency to associate causing aggregation and gelation of carrageenan below T_c (Nu and Viet, 2019).

The choose of alginate and k-/ι-carrageenan as reference polymers was driven by different reasons. Indeed, all the studied biopolymers (including sEPS) are able to form (ionically cross-linked) hydrogels in presence of metal ions; however, their gelling processes are enabled by distinct functional groups and mechanisms. As already discussed in literature (Felz et al., 2020a), alginate can be considered an appropriate reference for a deeper understanding of the sEPS hydrogel-forming processes and post-gelling properties thanks to the functional and chemical differences/similarities that might be found with respect to sEPS: for this reason, it was included as starting point for the investigation. Additionally, a broader comparative analysis extended to polysaccharides with other gelling mechanisms and acidic groups (e.g., carrageenan) was provided to emphasize the potential role of various components in the sEPS hydrogel-formation and gain insights on the dependence of the post-gelling mechanics on the polymer compositional properties. Particularly, the presence of

sulphate groups in AGS-derived sEPS has been reported in literature (Felz et al., 2020a), thus making k-/ι-carrageenan adequate candidates for this purpose.

The post-gelling mechanical response of both sEPS and reference polymers to various hydrogel-forming conditions (e.g., polymer concentrations and ionic cross-linker concentration and nature) was therefore assessed. More detailed, the stress-strain response to consecutive compression-decompression cycles was addressed for each biopolymer-based system, varying the above-mentioned gelling conditions. The Young's modulus *E* has been evaluated for each tested condition and studied as sensible parameter to point out the functional and mechanical similarities/differences among the studied systems. Further mechanical insights on sEPS-based hydrogels were given by oscillatory shear measurements carried out by varying the sEPS concentration in the studied systems. Particularly, sensitive parameters have been extrapolated from the observed mechanical profiles (e.g., storage modulus, *G'*, loss modulus, *G''*, complex viscosity, η^*) and correlated with the applied hydrogel-forming conditions (e.g., sEPS concentration) not only to shed light on the hydrogel mechanics but also to gather information (at speculative level) on the gelling processes.

Overall, the present contribution proposes a comprehensive analysis on the post-gelling mechanics of sEPS extracted from AGS: this would represent a prerequisite in studying potential valorization strategies for these waste-derived biopolymers, thus paving the way towards the development of sEPS-based products to be applied in multiple fields thanks to their versatile mechanical features.

2. Materials and methods

2.1 sEPS extraction

Structural EPS (sEPS) were extracted from aerobic granules cultivated in two distinct pilot-scale sequencing batch reactors (SBR), R1 and R2, respectively, whose characteristics are detailed described in *Appendix* (**Paragraph A.1**). For convenience, sEPS from reactor R1 are termed $sEPS_A$ while sEPS from reactor R2 are termed $sEPS_B$. Giving insights on the rector operation units and performance and resulting effect on the sEPS production and properties was not the object of the

present study: the comparison has been mainly added to validate the developed methodologies on sEPS from different microbial aggregates.

The extraction protocol was adapted from Schambeck et al. (2020). In brief, a known amount of dried granules was incubated in 0.2 M Na_2CO_3 (32 mL of solvent for each 0.2 g of dried granules; 300 rpm, 30 min) and then homogenized with ultraturrax (Janke & Kunkel from IKA-Labortechnik) at a speed of 13500 rpm for 3 cycles of 1 minute separated by 45 seconds of resting phases. Then disrupted granules were then heated for 60 min in a water bath at 80°C. After centrifugation (22000xg, 15 minutes, 4 °C), the supernatant, consisting of EPS, was collected. Structural EPS (sEPS) were hence recovered via acidic precipitation by adding 1 M HCl to the (alkaline) EPS dispersion until pH 2.0 ± 0.2 was achieved (Lin et al., 2010). After centrifugation (22000xg, 15 minutes, 4 °C), the pellet of sEPS was collected, re-solubilized in 0. 1 M NaOH, dialyzed for 36 hours (3.5 kDa molecular weight cut off, MWCO) against distilled water, frieze-dried and finally analysed for their Volatile Solids (VS) content. The frieze-dried $sEPS_A$ were dissolved in 0.05 NaOH while $sEPS_B$ needed stronger alkaline conditions for the re-solubilization (0.1– 0.2 M NaOH). The obtained sEPS dispersions at various weight concentrations (1 – 10 wt% sEPS) were applied in the hydrogel-forming experiments. The extracted sEPS were analyzed through colorimetric assays for the evaluation of proteins, humic acids, uronic acids, and neutral sugars. Particularly, proteins (as Bovine Serum Albumin, BSA, equivalent) and humic acids were estimated according to the modified Lowry method (Frolund et al., 1995), while uronic acids and neutral sugars were determined by means of the double anthrone method (Rondel et al., 2013) as glucuronic acid (Gluc. Acid) and glucose (Glu) equivalents, respectively. The extracted sEPS were also analyzed by Fourier Transform-Infrared (FT-IR) spectroscopy using a BioRad FTS-40 spectrometer (4 cm^{-1} resolution, 64 scans, spectral range 2000 – 400 cm^{-1}, DTGS detector).

2.2 Model biopolymers

The hydrogel-forming ability and post-gelling mechanical behaviour of sEPS were compared to those of well-characterized biopolymers chosen as "*reference models*": alginate and k-/ι-carrageenan. With this regard, an alginic acid from brown algae (*Macrocystis pyrifera*) pursuit from Sigma-Aldrich approximately composed by 61% mannuronic acid (M) and 39% guluronic acid (G) (M/G ≃ 1.56) was dissolved in 0.1 M NaOH with concentrations ranging between 1 and 5 wt% to be then applied in the hydrogel-forming experiments. Conversely, commercial k- and ι-carrageenan (from Sigma-Aldrich) were dissolved in 0.01 M NaOH with heating at about 65 °C with concentrations ranging between 1 and 5 wt%; the heated k-/ι-carrageenan dispersions were then subjected to hydrogel-formation upon cooling at room temperature.

2.3 Hydrogel-forming protocol

Limitations due to the low material supply are addressed by many researchers working with AGS from laboratory- and/or pilot-scale reactors. Combining minimized polymer consumption and high accuracy in the characterization studies is therefore challenging. A material-saving hydrogel-forming protocol, characterized by reproducibility, sensitivity and minimized polymer consumption, was therefore adapted from Felz et al. (2020a). The biopolymer-based hydrogels were obtained via ionic cross-linking in presence of different divalent metal cations (i.e., Ca^{2+}, Cu^{2+}, Ni^{2+}, Mg^{2+}) controlling the cross-linking kinetics by means of the use of dialysis membranes (3.5 kDa MWCO). The hydrogel geometry was controlled by forcing the sol-gel transition in a fixed cylindrical shape: to this aim, hollow cylindrical supports in polylactic acid (PLA) were designed and developed with a 3-D printer (UPBOX Tiertime) (**Figure 1**). The hollow plastic cylinders were filled with the polymeric solution, covered on both sides through dialysis membranes and kept under stirring in glass beakers containing 200 mL of cross-linker solution ($[M^{2+}]$ ranging between 0.001 and 1 M) for 36 hours of dialysis. Four sequences of dialysis of about 9 h each were provided, by replacing the cross-linker solution for three times. The metal cation diffusion into the polymeric solution via dialysis allowed slowing and

controlling the effective polymer chain cross-linking kinetics, with benefits on the post-gelling homogeneity and reproducibility.

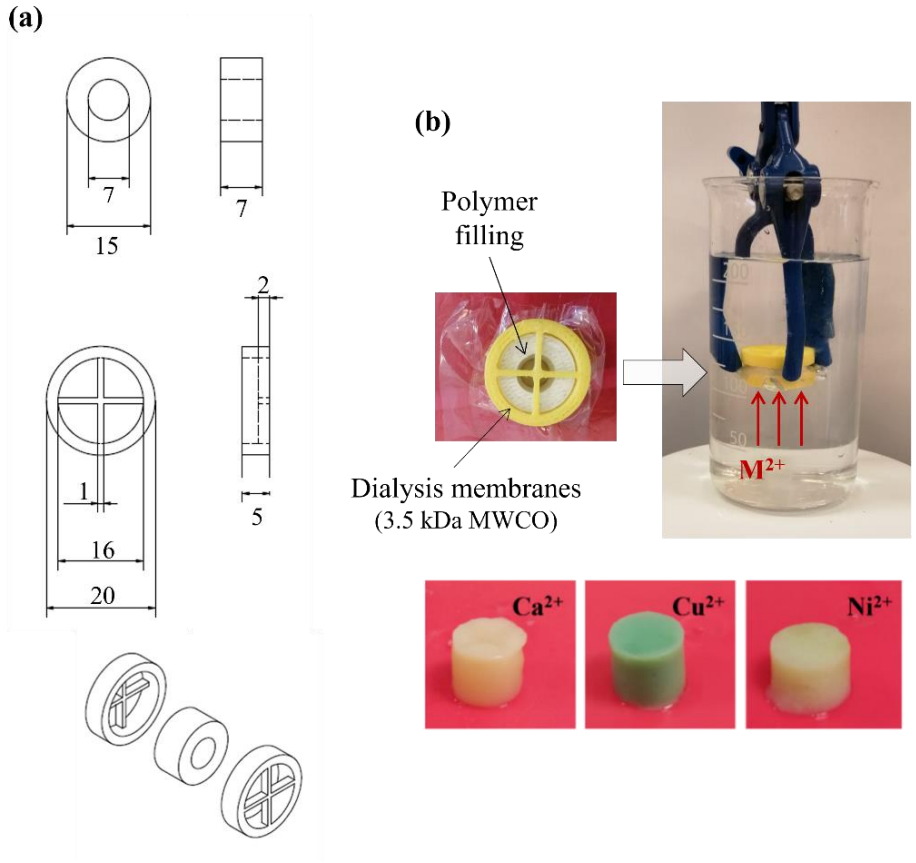

Figure 1 – Hollow cylindrical supports in polylactic acid (PLA) developed to minimize the polymer consumption and control the hydrogel-geometry (**a**) and hydrogel-forming protocols applied to obtain hydrogel cylinders (**b**) to be tested via rheometry. All the dimensions are expressed in millimeters.

Preliminary miniaturization studies were carried out on 2.5 wt% alginate hydrogels obtained in presence of 0.1 M Ca^{2+} as ionic cross-linker: acting on the design of the cylindrical supports described above (5 < height, h < 10 mm; 5 < diameter, d < 10 mm with various h/d ratios), the hydrogel geometry was optimized based on the level of accuracy required by the mechanical characterization via rheometry (**Table 1**). More detailed, the described geometry was studied for improving the accuracy of compression-decompression experiments. Heights and/or diameters lower than 5 mm made difficult the manipulation of the polymeric hydrogel system during its preparation and recovery as well as compromised the accuracy of the rheological measurements (data not shown). High h/d ratios resulted in slower gelling kinetics and therefore greater post-gelling mechanical properties and

homogeneity. Based on these preliminary observations, the geometry of the hollow cylindrical supports was fixed to 7 mm of heigh and diameter (h/d = 1 mm/mm): a polymer saving of about 33 % wt was obtained compared to studies in literature reporting similar hydrogels (Felz et al., 2020a) and the reproducibility of the tests were ensured by intensive dedicated preliminary studies.

Table 1 – Influence of the geometry of alginate hydrogels (2.5 wt% alginate; 0.1 M Ca^{2+}) on the mechanical characterization via rheometry. Young's moduli are expressed as average values ± standard deviation (n. 3 test replications). The level of accuracy is indicated on a qualitative scale based on the noisy of the rheological measurements: +++ is high accuracy, ++ is medium accuracy, + is low accuracy, - is very low accuracy (measure too noisy to be representative).

Geometry			Young's modulus (kPa)	Accuracy of rheological measurements
h (mm)	d (mm)	h/d (-)		
7	7	1.00	36.8 ± 1.4	+++
5.5	6.5	0.85	24.6 ± 2.7	-
5.5	7.5	0.73	30.7 ± 2.9	+
5.5	8.5	0.65	22.6 ± 2.0	++

Oscillatory shear experiments required a quite different geometry compared to compression studies: in this case, hydrogel disks of about 20 mm of diameter and 2 mm of thickness were used to ensure high-accuracy measurements.

To gain of a proof-of-principle of the potential hydrogel-forming behaviour of mixed protein-polysaccharide systems like sEPS, composite BSA (Bovine Serum Albumin protein)-alginate hydrogels (1 wt% alginate + 1 wt% BSA, 1 g BSA/g Alginate) were prepared adapting the above-described protocols via ionic cross-linking in presence of Ca^{2+} (0.1 M) and studied in comparison with pure alginate hydrogels (1 wt% alginate).

2.4 Post-gelling mechanical characterization

The post-gelling mechanical response under different hydrogel-forming conditions (i.e., polymer concentration and ionic cross-linker concentration and nature) was evaluated for all the selected

biopolymers. Various rheological measurements were combined to gain insights on the mechanics of the studied biopolymer-based systems: particularly, sensitive parameters were extrapolated from the mechanical profiles observed under both compression (e.g., Young's modulus, E) and shear stress conditions (e.g., storage modulus, *G'*, loss modulus, *G''*, complex viscosity, η^*) and correlated to the applied gelling conditions to shed light on the main drivers of the hydrogel-formation.

Biopolymer-based hydrogels formed by varying the sEPS concentration and (ionic) cross-linker concentration and nature (**Table A.1** in *Appendix*) were studied under (uniaxial) compression conditions. The hydrogels cylinders were subjected to consecutive compression-decompressions cycles (fixed compression-decompression duration: 2+2 min each), increasing the maximum deformation achieved in the loading step from 4 to 20%. These mechanical tests were performed in triplicate with a strain-controlled rheometer (Mars III, Thermo Scientific), using a parallel-plate geometry at room temperature. **Figure 2** schematically represents the apparatus used in these tests and the geometry of the compressed and decompressed biopolymer hydrogel cylinders.

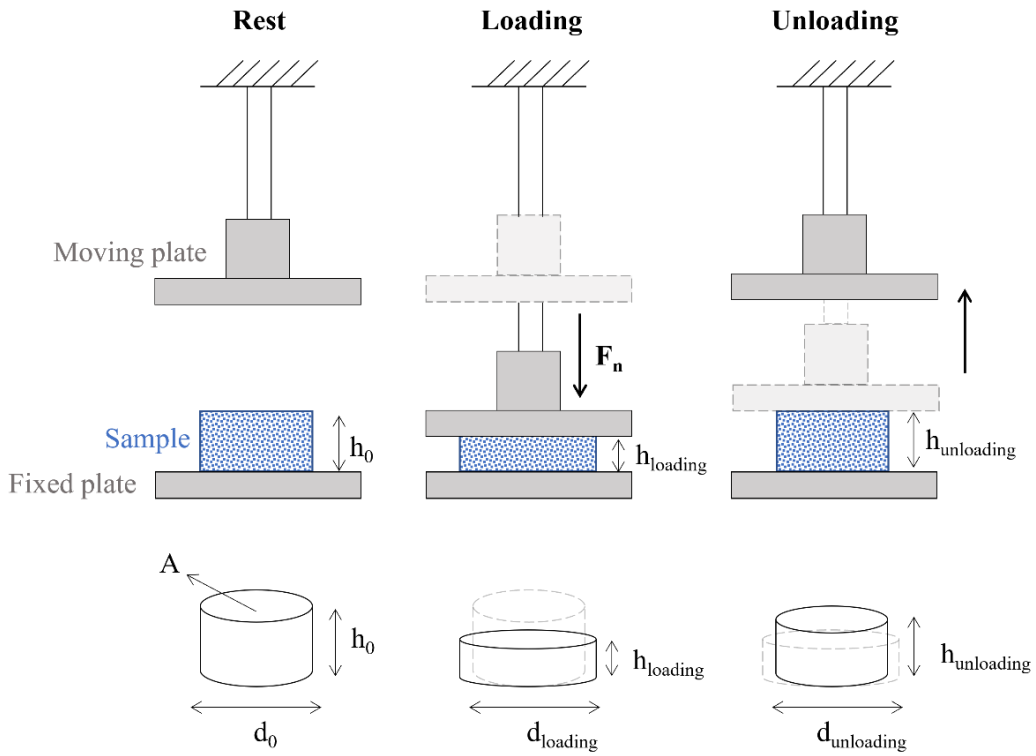

Figure 2 – Scheme of the apparatus used for the compression-decompression experiments and geometry of the deformed biopolymer-based hydrogels. Considering as negligible the sample extension in the plane normal to the loading direction: $d_{loading} = d_{unloading} = d_0$.

Load and displacement data, represented by normal force F_n [Pa] and deformed height of the sample h [mm], were collected during the experiments and the related stress σ [Pa] and deformation ε [%] were calculated according to the following equations (Eqs. 1 – 2):

$$\sigma = \frac{F_n}{\pi \cdot r^2} \tag{1}$$

$$\varepsilon = \frac{h_0 - h}{h_0} \cdot 100 \tag{2}$$

where h_0 and h [mm] are the original and deformed height of the hydrogel cylinder, respectively, while $\pi \cdot r^2$ [mm^2] is its cross-section area (in which r [mm] is the sample radius).

True stress σ_{true} [Pa] and compression parameter λ [-] were also calculated as follows (Eqs. 3 – 4):

$$\sigma_{true} = \frac{F_n}{\pi \cdot r^2} \cdot \lambda \tag{3}$$

$$\lambda = \frac{h}{h_0} \tag{4}$$

If compared to stress σ, true stress σ_{true} allowed normalizing data for the slight differences in terms of initial height of the samples over consecutive compression-decompression cycles. For convenience, stress was defined positive. The effect of the biaxial extension of the sample in the plane normal to the loading direction was assumed as negligible, as observed in preliminary studies (data not shown). For each tested condition, the Young's modulus (E, Pa) was obtained from the linear regression of the $\sigma - \varepsilon$ data in the linear elasticity domain of the material (in which the Hooke's law is objected, i.e., $\sigma = E \cdot \varepsilon$). For each loading-unloading cycle in the elastic region, a value of Young's modulus was obtained and an average value for each sample was calculated as the mean on all the applied compression-decompression cycles in the linear elasticity domain. The elastic region for the calculation of the Young's modulus was assumed to be the range of deformations over the consecutive compression-decompression cycles for which the $\sigma - \varepsilon$ relation was kept linear (i.e., sample was able to recover the original state upon reduction of the mechanical load at a certain decompression rate).

In other words, deformations recoverable in 2 minutes upon reduction of the mechanical load were assumed as elastic. The Young's modulus allowed to compare samples in terms of hydrogel stiffness, and it was therefore studied as sensitive parameter to assess the effect of various gelling conditions on the post-gelling mechanics of the studied biopolymer-based systems. All tests were performed in triplicate (i.e., on 3 distinct hydrogel cylinders formed under the same conditions) and the results (e.g., Young's modulus *E*) were expressed as average values ± standard deviations.

The hysteresis (Pa=J/m^3), representing the energy dissipated during a loading-unloading cycle, was calculated approximating the area enclosed in the hysteresis loop (i.e., between loading and unloading curves, respectively) with the trapezoidal rule (**Figure 3**) as follows (Eqs. 5 – 7).

$$E_{hystersis} = A_{Load} - A_{Unload} \tag{5}$$

where:

$$A_{Load} = \sum_{i=1}^{n} (\lambda_i - \lambda_{i+1}) \cdot \sigma_{true\ i} + (\sigma_{true\ i+1} - \sigma_{true\ i}) \cdot (\lambda_i - \lambda_{i+1})/2 \tag{6}$$

$$A_{Unload} = \sum_{j=1}^{n} (\lambda_{j+1} - \lambda_j) \cdot \sigma_{true\ j+1} + (\sigma_{true\ j} - \sigma_{true\ j+1}) \cdot (\lambda_{j+1} - \lambda_j)/2 \tag{7}$$

with:

i = 1, ..., n: data acquisition along the compression cycle (i.e., load)

j = 1, ..., n: data acquisition along the decompression cycle (i.e., unload)

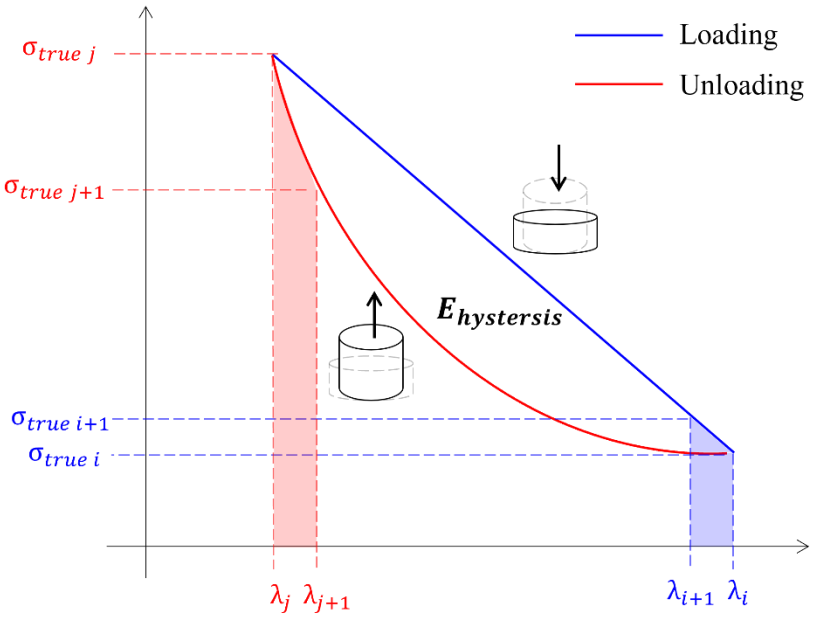

Figure 3 – Approximation of hysteresis energy through trapezoidal role.

To gather further information on their mechanical behaviour, sEPS-based systems with increasing polymer concentration (1 – 10 wt% sEPS) obtained in presence of 0.5 M Ca^{2+} were also subjected to oscillatory shear measurements. Since the mechanical similarities between the studied sEPS, only the results related to $sEPS_B$ are reported. These experiments were performed by using a plate-plate geometry (20 mm diameter, 400 µm gap) on a Discovery Hybrid Rheometer (Disc.HR-3, TA Instruments) working in controlled shear stress mode. The sample was loaded between the plates at a known gap h and the upper plate oscillated back and forth at a given stress and frequency ω. Working in a controlled-stress mode, an oscillating torque was applied to the upper plate and the resultant angular displacement was measured from which the (shear) strain was calculated (**Figure 4**). The (shear) stress τ [Pa] and strain γ [%] can be defined as follows (Eqs. 8 – 9):

$$\tau = \frac{F}{A} \tag{8}$$

$$\gamma = \frac{x}{h} \cdot 100 \tag{9}$$

where F is the shear force assumed to slide laterally on the face of area A, and x is the related deflection path, as highlighted in **Figure 4**.

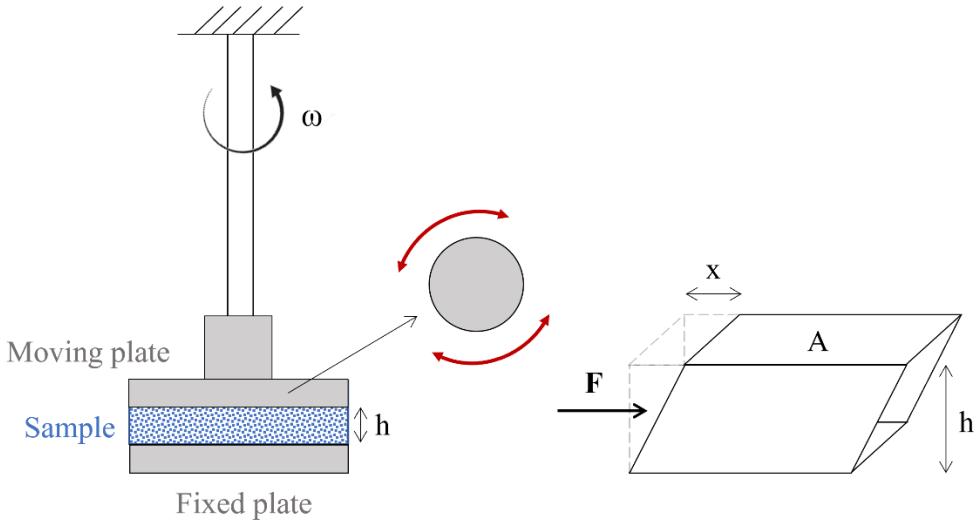

Figure 4 – Scheme of the apparatus used for the oscillatory shear measurements and related geometry of the deformed biopolymer-based hydrogels.

For each tested condition (1 – 10 wt% sEPS), the linear viscoelastic (LVE) region of deformations (in which stress and strain are proportional) was determined through amplitude sweep tests. In these experiments, the amplitude of the applied shear stress was varied while the oscillation frequency was kept constant and equal to 1 Hz. The storage modulus *G'* and loss modulus *G"* (representing the energy stored and dissipated upon deformation, and therefore the elastic and viscous contribution, respectively, to the overall sample stiffness) was therefore addressed in the LVE-region. The storage modulus *G'* and the loss modulus *G"* were then measured through frequency sweep experiments carried out by varying the oscillation frequency ω in the range 0.01 – 100 Hz at a constant (shear) strain amplitude (γ = 0.4%). All these experiments were performed at a constant temperature of 25.00 ± 0.01°C. The complex viscosity ($|\eta^*|$) was calculated as follows (Eq. 10):

$$|\eta *| = \sqrt{\frac{G'^2(\omega) + G''^2(\omega)}{\omega^2}} \quad (10)$$

More details on the theory of the descibed oscillatory shear experiments are given in *Appendix* (**Paragraph A.2**).

3. Results and discussion

3.1 Hydrogel-formation of sEPS versus model biopolymers

Insights on the nature of the macromolecules consisting of the here studied AGS-derived sEPS (i.e., $sEPS_A$ and $sEPS_B$) could be pivotal to shed light on their hydrogel-forming behaviour. With this regard, the results emerged from the biochemical characterization carried out by means of colorimetric assays were given in **Figure 5**. The major difference between $sEPS_A$ and $sEPS_B$ was found in the relative content of proteins and uronic acids, while comparable quantities of humic acids and neutral sugars were estimated. Particularly, similar amounts of proteins, humic acids and uronic acids were found for $sEPS_A$ (about 30.5, 3.82 and 32.4 wt% of the organic matter, respectively). Conversely, the quantity of uronic acids was much higher in $sEPS_B$ (ca. 64.4 wt% of the organics), thus being predominant with respect to proteins and humic acids ($\simeq$ 0.237 g $BSA_{equivalent}$/g Gluc.

$Acid_{equivalent}$ and 0.479 g Humic Acids/g Gluc. $Acid_{equivalent}$). Both in $sEPS_A$ and $sEPS_B$, neutral sugars were estimated in lower amounts compared to the other components (49.72 ± 8.06 and 49.64 ± 6.59 g $Glu_{equivalent}$/g VS; VS: Volatile Solids).

The results emerged from the biochemical characterization partially agreed with literature: while the protein content was similar to that estimated in other studies (Felz et al., 2019a; Schambeck et al., 2020), the evaluation of neural and uronic sugars appeared significantly different. Particularly, uronic acids were estimated in larger quantities with respect to the available literature data (Felz et al., 2019a; Schambeck et al., 2020) especially in the case of $sEPS_B$. To be noticed that the nature of the extractable sEPS macromolecules was likely dependent on the origin and properties of AGS (e.g., physical-chemical features, microbial populations, characteristics of the treated wastewater, operational strategies, sludge retention time, environmental conditions, etc.): biochemical differences for the recovered sEPS are therefore expected. Moreover, as emphasized by Felz et al. (2019), colorimetric methods suffer from interference towards various substances present in sEPS, thus leading to uncertainties in the effective estimation of the target compounds, which result strictly dependent on the method and standard applied.

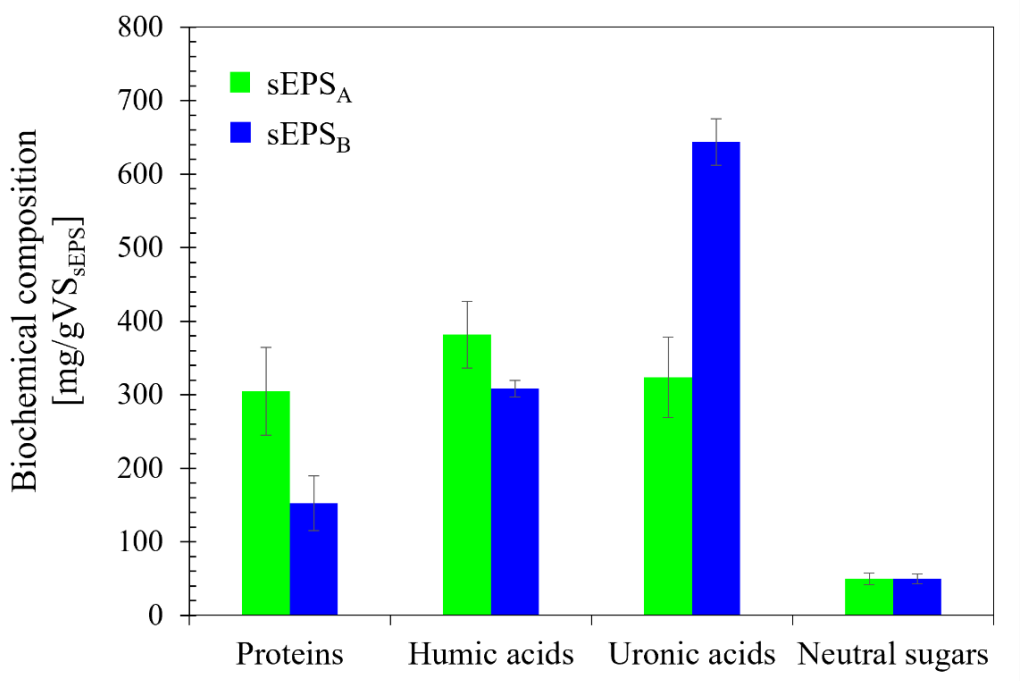

Figure 5 – Content of proteins, humic acids, uronic acids, and neutral sugars in $sEPS_A$ and $sEPS_B$ estimated through colorimetric assays as BSA, Humic Acid, Glucuronic Acid and Glucose equivalents, respectively. Data = average values ± standard deviations (n. 3 sample replication).

Despite the above-described differences in terms of biochemical components, similar FT-IR spectra were obtained for the studied AGS-derived sEPS. By way of example, the FT-IR spectrum of $sEPS_B$ is reported in **Figure 6**. The peak assignment agreed with literature data (Karakas et al., 2020; Lin et al., 2010). The strong broad band detected at 3287 cm^{-1} and the weaker ones at around 2931 cm^{-1} can be assigned to stretching vibrations of O-H and C-H, respectively, associated with hydrocarbons. The peak at 1645 cm^{-1} was attributed to C=O stretching vibrations associated with proteins (amide-I region), while the peak at 1539 cm^{-1} was assigned to N-H bending and C-N stretching vibrations in -CO-NH of proteins (amide-II region). The region at 1500−1300 cm^{-1} is related to carboxylic group and hydrocarbon-like compounds. Accordingly, the peak at 1453 cm^{-1} was assigned to C-H bending (methylene group) and that at 1401 cm^{-1} to C=O symmetrical stretching of $-COO^-$ groups. The region at 1200-900 cm^{-1} could be associated with the polysaccharides and nucleic acids present in the sEPS extracts. More detailed, the peak at 1060 cm^{-1} might be assigned to the C-O-C ring vibrations and C-OH stretches of polysaccharides.

As arisen from literature data (Karakas et al., 2020; Lin et al., 2010), chemical and functional similarities between sodium alginate and sEPS from AGS treating municipal sewage could be found looking at the results emerging from the FT-IR spectroscopy characterization; however, AGS-derived sEPS have been demonstrated much more complicated with respect to pure alginate (Felz et al., 2020a). To be pointed out is the peak assignment related to the fingerprint (or anomeric) region of carbohydrates (950-750 cm^{-1}). Leal et al. (2008) addressed peaks at 902 and 823 cm^{-1} in the secondary derivative spectrum of alginic acids from brown seaweeds as attributed to the C1-H deformation of α-L-guluronic acid residues and deformation vibration of β-D-mannopyranuronic acid residues, respectively, similarly to what observed by Lin et al. (2010) for AGS-derived EPS which they characterized as alginate-like exopolysaccharides (ALE). Even if in this study it was not possible to resolve the organic functional groups at the fingerprint region, we can reasonably extend

these considerations to our AGS-derived sEPS given the correspondence of the detected FT-IR spectra with literature data. To be noticed that in the 1700-1200 cm^{-1} region, mainly associated with the presence of proteins, the spectra of sodium alginate and sEPS appeared different: the high content of proteinaceous compounds of sEPS compared to alginate might explain these differences.

More significative chemical differences might be found between sEPS and k-/ι-carrageenan. Indeed, k-/ι-carrageenan present FT-IR spectra typical of sulphonated polysaccharides from red seaweeds with the characteristic broad band of sulphate esters (S=O) between 1210 to 1260 cm^{-1} and the strong ones at 930 cm^{-1} assigned to 3,6-anhydro-galactose residues (Gómez-Ordóñez et al., 2011).

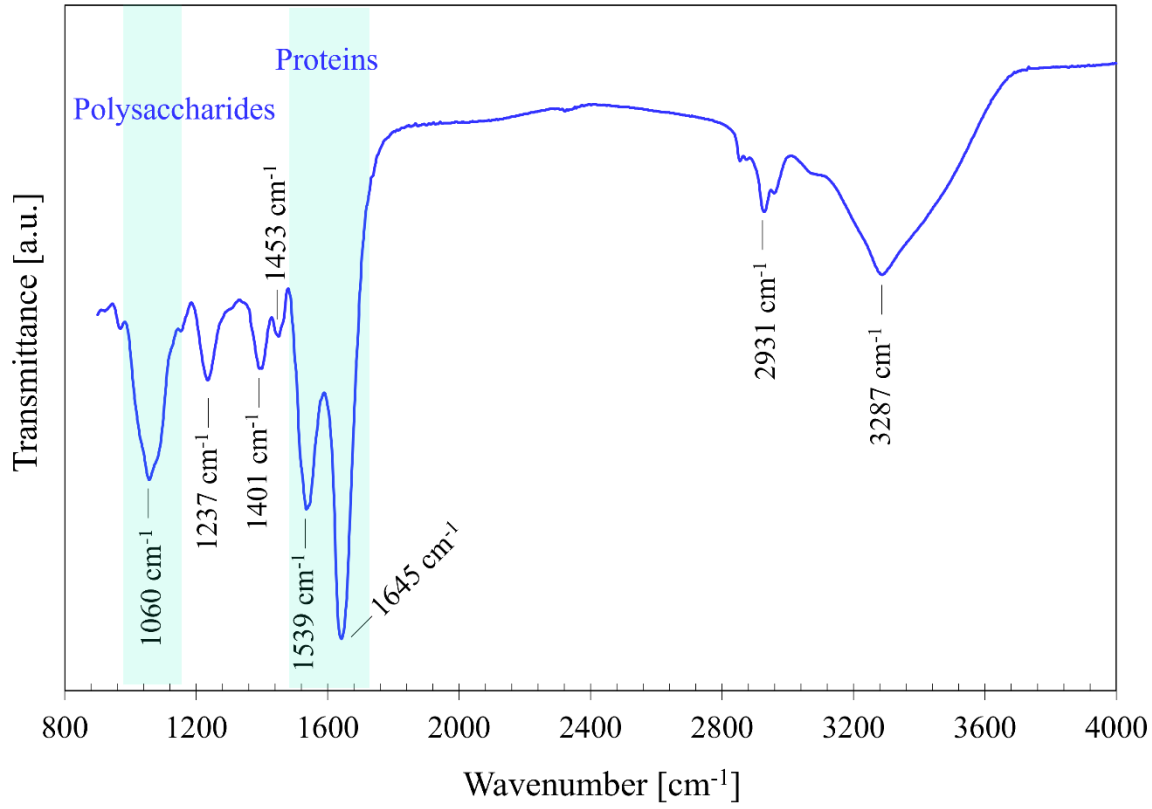

Figure 6 – FT-IR spectrum of AGS-derived $sEPS_B$.

All the studied biopolymers (i.e., sEPS, alginate, and k-/ι-carrageenan) were able to form hydrogels in presence of divalent metal cations M^{2+}. Hydrogels are classified are gels able to reversibly sorb and exude water and/or biological fluids (i.e., swell, and de-swell). Swelling requires the existence of hydrophilic groups within the polymeric network, conditions common to all the studied

biopolymers. The ability to form hydrogels via ionic cross-linking is instead driven by the abundance of (acidic) functionals groups (e.g., carboxyl and sulphate-half ester groups for alginate and k-/ι-carrageenan, respectively) able to interact with metal cations during the cross-linking reaction, thus leading to the formation of an extended 3D network. The outcome emerged from FT-IR spectroscopy demonstrated that sEPS contained various functional groups (e.g., carboxyl, hydroxyl, amino groups, etc.) representing potential metal-binding sites, thus suggesting the presence of multiple of functional components likely involved in the hydrogel-formation processes. Despite these similarities, the distinct biopolymer nature (emphasized by the above-described chemical and functional differences) resulted in a different response to various hydrogel-forming conditions. Particularly, the hydrogel-formation appeared differently influenced by polymer concentration and (ionic) cross-linker concentration and nature. The effect of polymer and (ionic) cross-linker concentrations was addressed for biopolymer-based hydrogels formed in presence of Ca^{2+}. **Figure 7** illustrates a conceptual phase diagram related to $sEPS_A$ which covers the range of 1 – 10 wt% sEPS content and 0.05 – 1 M Ca^{2+} concentration: the green area represents the region in which stable sEPS hydrogels with measurable mechanical properties were obtained (i.e., the formation of an extended cross-linked polymeric network occurred). Regardless of the origin of the microbial aggregate (i.e., AGS from R1 and R2), sEPS were able to form stable and stiff hydrogels at concentrations higher than 2.5 wt% in presence of high calcium concentrations (at least 0.1 M). To be noticed that at 2.5 wt%, hydrogels obtained with $sEPS_B$ were not sufficiently stiff to be tested via rheometry under compression conditions regardless of the Ca^{2+} concentration.

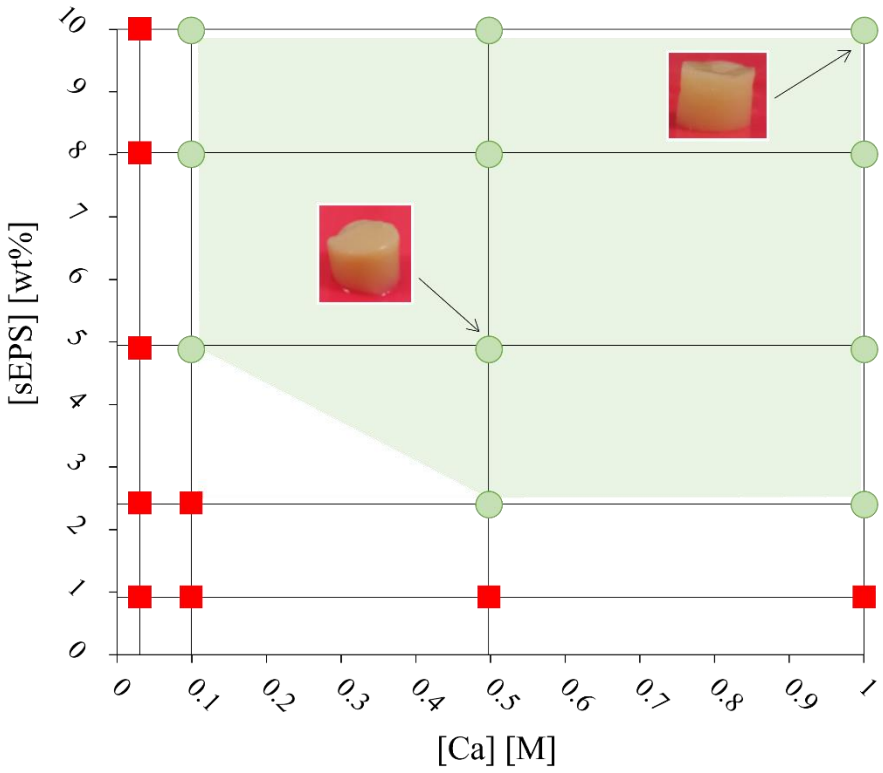

Figure 7 – Conceptual phase diagram of $sEPS_A$ hydrogels formed in presence of increasing Ca^{2+} concentrations.

The comparison with "*model*" biopolymers (i.e., alginate and k-/ι-carrageenan) disclosed that the sEPS hydrogel-formation was allowed by higher driving forces (e.g., Ca^{2+} concentrations) and polymer concentrations. Indeed, alginate was able to form stable hydrogels under all the tested conditions ($[Ca^{2+}] \geq 0.01$ M; [Alginate] ≥ 1 wt%). The k-/ι-carrageenan hydrogel-formation occurred for all the tested range of polymer concentrations ([k-/ι-carrageenan] ≥ 1 wt%) and did not appear strictly dependent on the Ca^{2+} concentration adopted: indeed, k-/ι-carrageenan dispersions underwent sol-gel transition upon cooling without adding (external) divalent metal ions (i.e., $[Ca^{2+}]$ = 0 M). The presence of Na^+ ions in the pristine aqueous dispersions (stable at high temperatures, T ≥ 65 °C) which are able to ionically bound to sulphate groups of the carrageenan units might favour polymer aggregation and therefore gelation upon cooling (Thrimawithana et al., 2010).

These qualitative observations gave a preliminary proof-of-principle of the higher diversity and complexity characterizing the sEPS matrix with respect to the studied model biopolymers: AGS-

extracted sEPS might contain compounds not effectively participating in the gelling processes, thus making higher driving forces necessary to lead to the formation of stable hydrogels (with measurable mechanical properties). The dependence of the gelation on the applied conditions (e.g., polymer concentration and ionic cross-linker concentration and nature) has been confirmed and more detailed discussed based on the results emerged from the rheological characterization (under both compression and shear stress conditions), as described in the following paragraphs.

3.2 Compression studies

3.2.1 Stress-strain response to consecutive compression-decompression cycles

The stress-strain response to consecutive compression-decompression cycles disclosed mechanical differences among the tested biopolymer-based hydrogels. However, the overall mechanical behaviour seemed to be preserved over the wide range of hydrogel-forming conditions applied. By way of example, **Figure 8** plots the true stress σ_{true} against the compression parameter λ over the consecutive loading-unloading cycles applied on 5 wt% alginate, k-/ι-carrageenan and sEPS hydrogels formed in presence of 0.1 M Ca^{2+}. Regardless of the origin of the microbial aggregates (i.e., AGS from R1 and R2), sEPS hydrogels deformed elastically for all the applied range of deformations (up to 20%) over the consecutive compression-decompression cycles, as confirmed by the linearity and overlapping of loading curves (**Figure 8a**). Even if characterized by significative differences in terms of hydrogel-forming mechanisms and biochemical composition, ι-carrageenan hydrogels behaved similarly to sEPS hydrogels (**Figure 8b**). Conversely, for k-carrageenan and alginate hydrogels the linear elastic behaviour seemed to be maintained over the first loading - unloading cycles up to a maximum deformation $\varepsilon = 10 – 15\%$ (**Figure 8c**, **8d**): increasing the number of compression-decompression cycles, and therefore the maximum level of deformation achieved in the loading step above $\varepsilon = 10 – 15$ %, the σ_{true} - λ plots exhibited a stress plateau to then increase with a higher slope, thus suggesting the occurrence of many non-reversible deformations in the cross-linked polymeric network. In this case, the decompression rate might be not slow enough to

equilibrate the stresses in the hydrogel structure, leaving a residual deformation not recoverable at the end of the unloading phase (Banerjee and Ganguly, 2019). Moreover, for alginate and k-carrageenan hydrogels the loading and unloading curves did not match. This type of behaviour, referred to hysteresis, is common in viscoelastic materials and it is the result of energy dissipation, fluid diffusion and polymer molecular realignment during loading (Ahearne et al., 2009). The hysteresis, and therefore the energy dissipated during a loading-unloading cycle, increased as a function of the maximum deformation achieved in the loading step over the consecutive compression-decompression cycles but also upon increasing the polymer concentration (**Figure 9**).

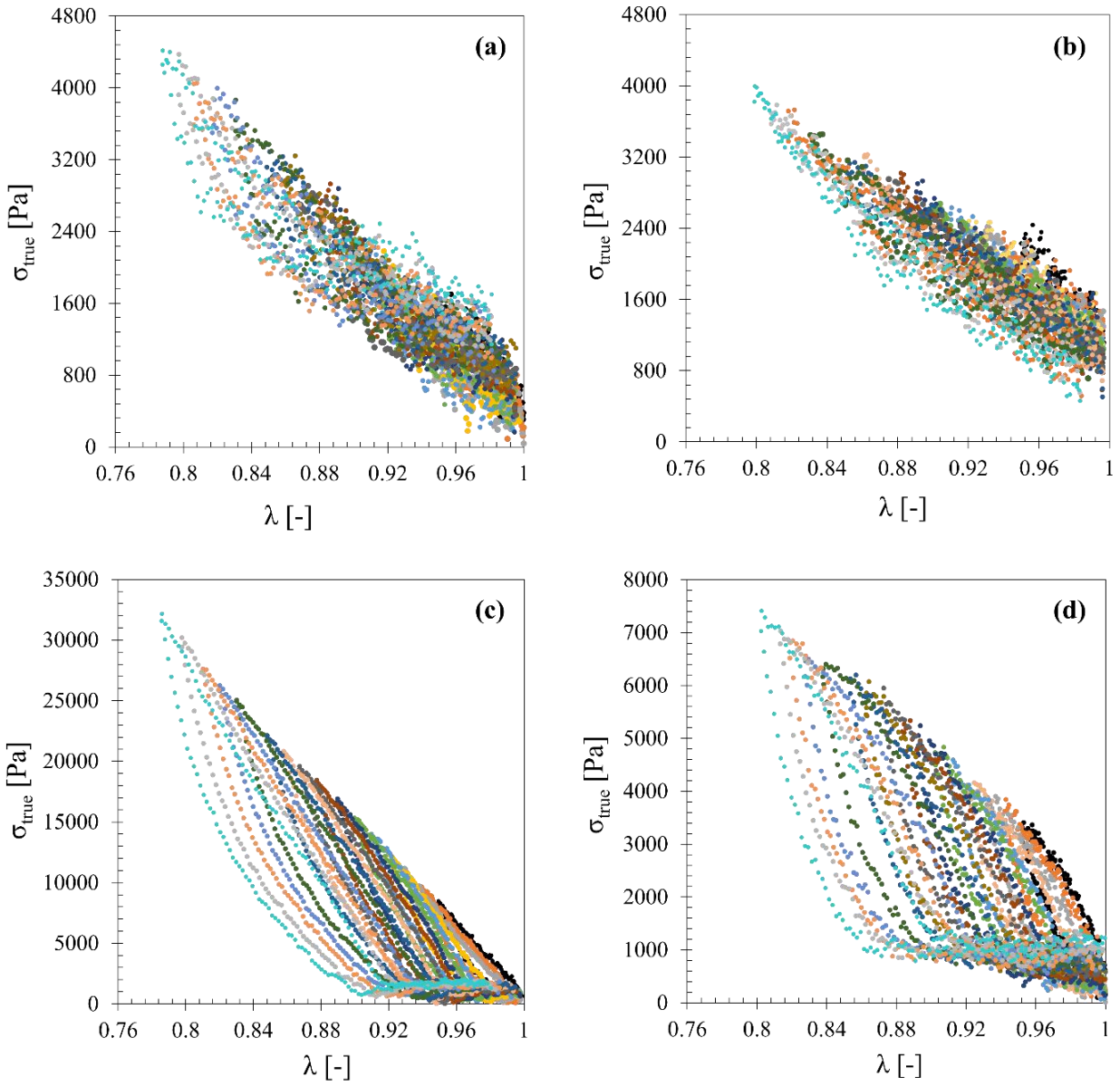

Figure 8 – Stress-strain plots related to consecutive compression-decompression cycles on 5% (w/v) $sEPS_A$ (**a**), ι-carrageenan (**b**), k-carrageenan (**c**), and alginate (**d**) hydrogels obtained in presence of 0.1 M Ca^{2+} as ionic cross-linker. Each loading-unloading cycle is represented in a different colour.

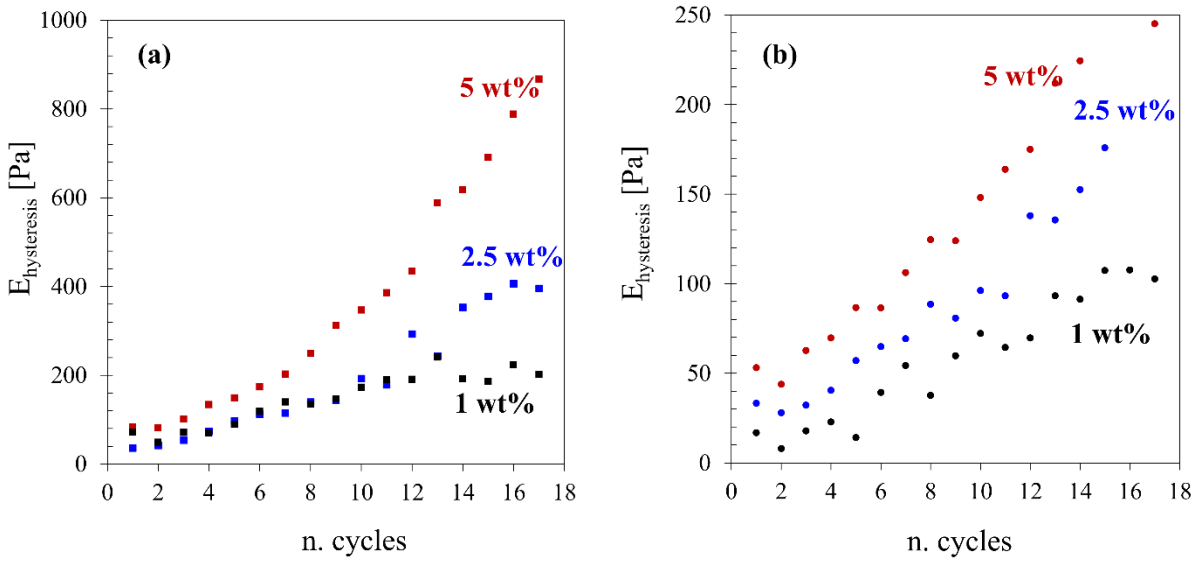

Figure 9 – Hysteresis [Pa] observed for k-carrageenan (**a**) and alginate (**b**) hydrogels (0.1 M Ca^{2+} as ionic cross-linker) over the consecutive compression-decompression cycles at various polymer concentrations.

To interpret the observed mechanical profiles, a schematic representation of the hydrogel structure in given in **Figure 10**. A hydrogel consists of a network of polymeric chains swollen in aqueous solution: the network endows the elastic and plastic features while the aqueous phase provides the viscous properties. Water in the hydrogel might be classified into bound and free water. Free water does not interact with the polymeric chains, and it is assumed to fill the space within the network (**Figure 10a**): consequently, it is able to be redistributed when the hydrogel is deformed. When a strain is applied to the hydrogel (e.g., the hydrogel is compressed), fluid is pushed through the pores in the polymeric network and the polymer chains are realigned. As the strain is increased, the ability of fluid to pass through pores is reduced and the polymer chains stiffen (Ahearne et al., 2009), thus increasing the energy dissipation and therefore the hysteresis (**Figure 10b**). The same behaviour might be evidenced upon increasing the polymer concentration (i.e., the cross-linking density) which might decrease the network "porosity". With respect to alginate and k-carrageenan, sEPS and ι-carrageenan hydrogels featured more significative linear elastic properties for a broader range of deformations (i.e., they were able to recover the deformation upon reduction of the mechanical load):

this behaviour could be influenced by the greater ability of (free) water to be redistributed in the space within the network upon compression.

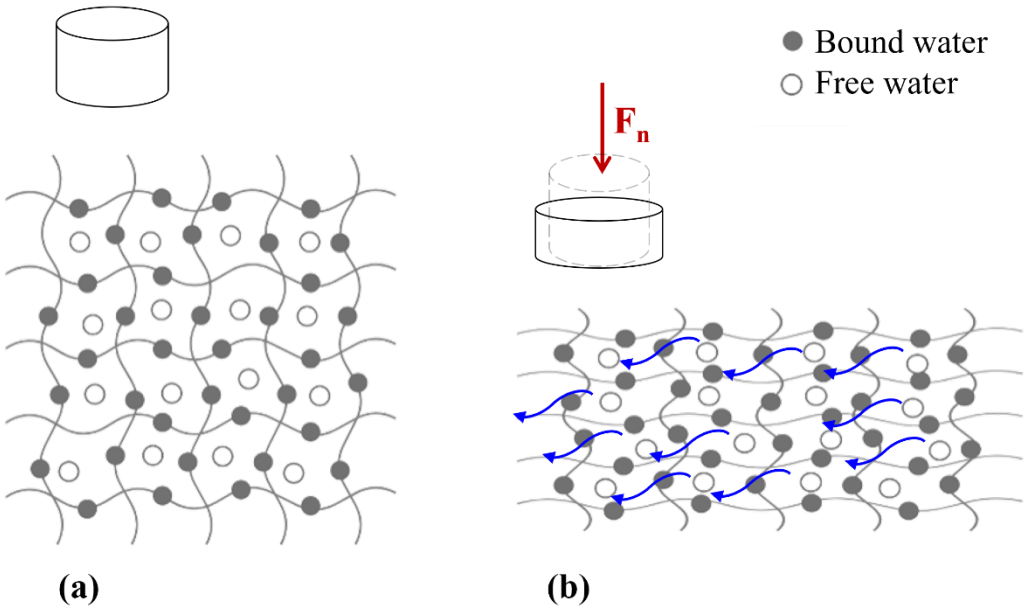

Figure 10 – Schematic representation of a hydrogel at reast (**a**) and under compression (**b**). A hydrogel consists of a network of polymeric chains swollen in aqueous solution. When a strain is applied (e.g., the hydrogel is compressed), fluid (i.e., free water able to be redistributed in the space within the network) is pushed through the pores in the network and the polymer chains are realigned. Increasing the applied deformation, the ability of fluid to pass through pores is reduced and the polymer chains stiffen.

3.2.2 Effect of the gelling conditions on the hydrogel stiffness

The Young's modulus *E* (and therefore the hydrogel stiffness) appeared significantly affected by polymer concentration and (ionic) cross-linker concentration and nature, thus proving to be an eligible parameter to give insights on the hydrogel-formation processes and resulting post-gelling mechanical and functional properties. A detail dissertation is given below.

Effect of polymer concentration

Despite the distinct hydrogel-forming mechanism and biopolymer nature, the Young's moduli (and hence the post-gelling stiffness) increased linearly with the polymer concentration in the tested range (**Figure 11**), likely due to the increasing polymer chain density and entanglement (Kuo and Ma, 2001). Based on the origin of the microbial aggregate (i.e., AGS from R1 and R2), sEPS hydrogels

formed in presence of 1 M Ca^{2+} evidenced different stiffness at the same polymer content (wt% sEPS): indeed, the Young's modulus of $sEPS_A$ hydrogels increased from about 2.9 to 15.7 kPa upon increasing the polymer concentration from 2.5 to 10 wt%, while $sEPS_B$ presented lower levels of post-gelling stiffness in all the investigated range of polymer concentrations. Moreover, the values of Young's modulus were significantly different among the tested biopolymers: k-carrageenan was able to form the stiffest hydrogels in presence of Ca^{2+} as ionic cross-linker, followed by alginate, ι-carrageenan, and sEPS. Particularly, at 5 wt% polymer concentration the measured values of *E* were the following: 168.8 ± 10.8 kPa for k-carrageenan, 60.0 ± 0.6 kPa for alginate, 19.5 ± 2.2 kPa for ι-carrageenan, 6.2 ± 0.7 kPa for $sEPS_A$ and 3.9 ± 0.2 kPa for $sEPS_B$.

For all the tested biopolymer-based hydrogels, the observed Young's moduli appeared significantly lowered compared to traditional engineering materials and/or synthetic polymers likely due to the high-water content (ranging between 90 and 97.5 % wt). Indeed, as previously explained, the elastic/plastic properties of hydrogel-like systems are given by the polymeric network, while the aqueous phase provides the viscous features thus not greatly contributing to the post-gelling stiffness.

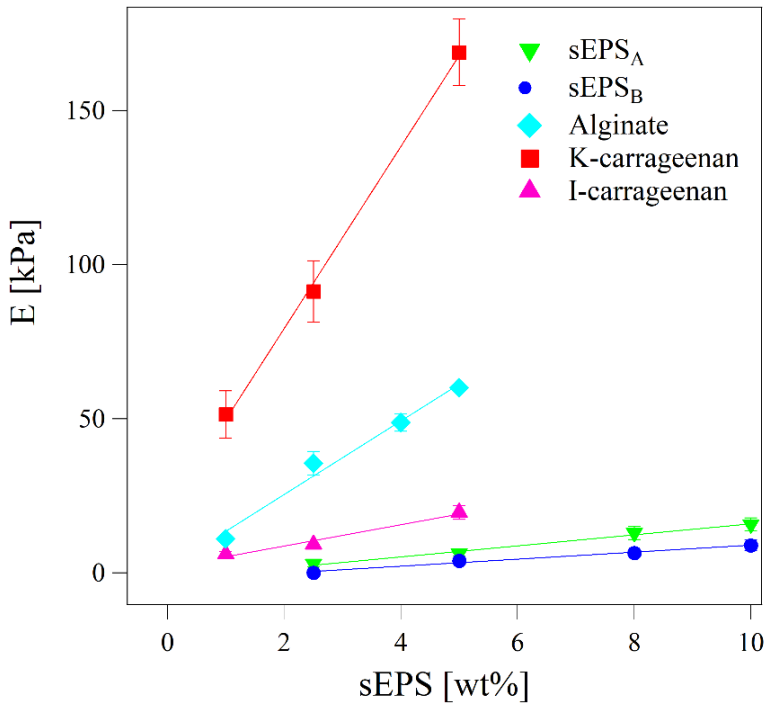

Figure 11 – Effect of polymer concentration on k-/ι-carrageenan, alginate, and structural EPS post-gelling stiffness. [Ca^{2+}] = 0.1 and 1M, for model biopolymers and sEPS, respectively. Data = average value ± standard deviation (n. 3 sample replications).

Effect of (ionic) cross-linker concentration

As previously introduced, stable sEPS hydrogels (with measurable mechanical properties) were not obtained in presence of Ca^{2+} concentration lower than 0.1 M, even increasing the sEPS content up to 10 wt%; conversely, alginate was able to undergo sol-gel transition for all the studied range of (ionic) cross-linker concentrations. The dependence of the post-gelling stiffness on the applied driving force was therefore established and studied in terms of E – Ca^{2+} concentration relationship both for alginate and sEPS. The effect of the (ionic) cross-linker content on the k-/ι-carrageenan post-gelling mechanics were not assessed: their ability to undergo sol-gel transition without addition of divalent metal cation makes this dependence less significative compared to the other studied biopolymer-based systems.

Figure 12 depicts the Young's moduli of sEPS and alginate hydrogels obtained in presence of increasing concentrations of Ca^{2+} as (ionic) cross-linker. The post-gelling stiffness increased upon increasing Ca^{2+} concentration up to a threshold limit, above which different post-gelling mechanical responses were observed among the tested biopolymers. Increasing Ca^{2+} concentrations could likely promote higher cross-linking densities, thus leading to increasing E values (Kuo and Ma, 2001). Moreover, higher Ca^{2+} concentrations in the cross-linker solution would result in higher gradients between the core of the biopolymer-based system and the outside aqueous medium, thus favouring the Ca^{2+} ion diffusion into the polymeric matrix and hence formation of an extended three-dimensional cross-linked polymeric network.

The effect of an increased Ca^{2+} concentration was negligible above 0.05 M and 0.5 M for alginate and $sEPS_A$ hydrogels, respectively, corresponding to 0.37 mol Ca/g Alginate and 1.16 mol Ca/g sEPS, which means that the saturation of the available Ca^{2+}-binding sites was probably achieved under these conditions. Conversely, while for the lowest Ca^{2+} concentrations $sEPS_A$ and $sEPS_B$ presented comparable post-gelling stiffness, at 1 M Ca^{2+} concentration the Young's modulus of

$sEPS_B$ hydrogels appeared 40 – 50% lower compared to that of $sEPS_A$ hydrogels: this might be due to the formation of precipitates within the polymers (e.g., $NaCO_3$ and/or $CaCO_3$) favoured by the stronger alkaline (pH ≃ 10.5 – 11.5) conditions of the original $sEPS_B$ dispersions, which could form a layer on the polymer surface hindering the (ionic) cross-linker diffusion inside the sEPS matrix. Particularly, $Ca(OH)_2$ precipitation was observed for pH between 8 and 12 and it increased linearly with the pH value (data not shown). The evaluation of the Ca^{2+} concentration as driving force could be hence dependent on the pH and resulting presence of insoluble $Ca(OH)_2$. Considering the distinct pH conditions of the pristine sEPS dispersions, the Ca^{2+} diffusion as well as the initial amount of $Ca(OH)_2$ (part of which could be potentially solubilized during dialysis) are expected to be different. Another potential explanation is that an excessive calcium concentration (> 0.5 M in the case of $sEPS_B$ and in general depending on the available Ca^{2+}-binding sites for instance in terms of *R* value equal to $2[Ca^{2+}]/[COO^-]$) might promote too fast ion diffusion kinetics thus resulting in inhomogeneous cross-linking processes, which decreases the post-gelling stiffness and elasticity. Indeed, with reference to alginate, it has been found that high Ca^{2+} concentrations promote the formation of mono-complexes and egg-box dimers, generating a dense and elastic hydrogel structure with increased strength and stiffness. However, excessive Ca^{2+} concentrations could lead to heterogeneous binding with alginate and thus inhibit the formation of complete-symmetrical egg-box dimers, promoting the cross-linking between and within the alginate molecules (Cao et al., 2020, Farrés et al., 2013). Moreover, excessive Ca^{2+} could produce the collapse of gel network by crosslinking with MG blocks, which decreases the gel thermodynamic stability (Donati et al., 2009).

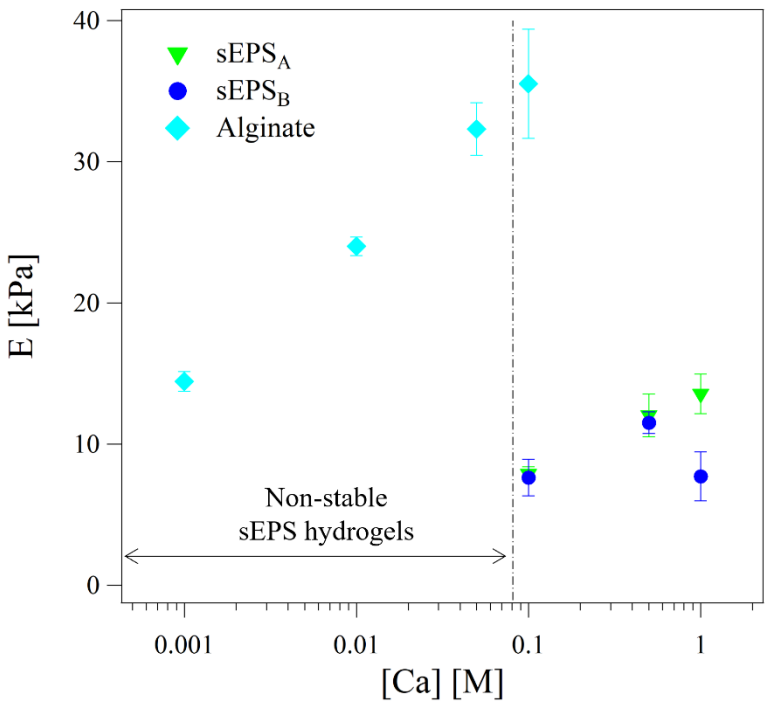

Figure 12 – Effect of Ca^{2+} concentration (as ionic cross-linker) on the sEPS and alginate post-gelling stiffness. [sEPS] = 8 wt%; [Alginate] = 2.5 wt%. Experimental data = mean ± SD (n. 3 sample replications). X-axis is represented in log-scale for a clearer visualization. Data = average value ± standard deviation (n. 3 sample replications).

In summary, higher diving forces (e.g., Ca^{2+} concentrations) were needed to enable the polymer chain cross-linking of AGS-extracted sEPS thus leading to the formation of stable hydrogels with measurable mechanical properties. Moreover, regardless of the origin of the microbial aggregates (AGS from R1 and R2), sEPS formed weaker hydrogels than alginate. As previously remarked, whit respect to alginate (i.e., a linear polysaccharide composed of alternating guluronic and mannuronic acid units), sEPS are a complex mixture of proteins, neutral sugars, amino sugars, uronic acids and humic compounds (Felz et al., 2019a) and it is reasonable to speculate that not all these components are directly involved in the hydrogel-formation. In addition, some compounds could negatively interfere with the gelling macromolecules in the sEPS extracts, thus hindering the polymer chain cross-linking. For example, it has been reported that the decreased gel-forming ability of ι-carrageenan compared to k-carrageenan, resulting in softer hydrogels upon cross-linking, is likely due to the higher content of sulphate residues: since the sulphate residues are bulky and repulse each other electrostatically, they hinder the formation of double or single helixes of carrageenan molecules and inhibit their subsequent aggregation, thus compromising the gelation (Watase and

Nishinari, 1987). Previous research suggested the presence of sulphate groups in EPS (Felz et al., 2020b): these groups could have a role in the hydrogel-formation processes acting as binding sites during the cross-linking reaction; on the other side, an excessive sulphate content could hinder the polymer chain cross-linking, similarly to ι-carrageenan macromolecules.

Overall, the exact fraction of hydrogel-forming macromolecules in the sEPS extracts appeared unknown and therefore the concentration of gelling sEPS may be significantly overestimated. There is no consensus in literature about the role of polysaccharides and proteins in the gelling properties of microbial aggregates (Schambeck et al., 2020). Proteins should have an important role in bonding EPS due to their high affinity for cations (Zhu et al., 2015). Although the protein hydrophobicity is believed to be helpful for the gel-formation (Li et al., 2014), some studies consider polysaccharides or types of glycosides (e.g. proteoglycans) as key macromolecules responsible for the EPS gelling ability, observing post-gelling mechanical properties independent from the protein content (Seviour et al., 2009b). Schambeck et al. (2020) reported that peptide and peptidoglycans bonds may not play a role on gel-forming properties of sEPS, while uronic carbohydrates containing mannuronic acids are key molecules involved in the sEPS gel-formation and hydrogel cohesion.

In the framework of this study, indirect observations based on composite alginate-BSA hydrogels agreed these evidences. Alginate (1 wt%) and alginate-BSA composite hydrogels (1 wt% alginate + 1 wt% BSA; 1 g BSA/g Alginate) presented similar Young's moduli (E = 14.4 ± 0.6 kPa versus 13.9 ± 1.1 kPa, respectively), thus proving the negligible influence of BSA on the alginate post-gelling stiffness. Alginate-BSA composites might simulate the gel-forming ability and post-gelling mechanical behaviour of mixed polysaccharide-protein gelling systems like sEPS. Surely, this hypothesis consists in a strong simplification of the sEPS matrix and biochemical composition which is much more complicated and heterogenous. However, these results could indirectly suggest (at speculative level) which macromolecules endows the main functional and mechanical features of hydrogels. Being aware of the speculative nature of this hypothesis, which should be experimentally validated, the sEPS post-gelling mechanical properties could not be significantly enhanced by the

presence of protein-like substances. A key point which remains to be clarified is hence the role of proteins (and other compounds) during the cross-linking reaction as well as the level of purity of the sEPS macromolecules in order to avoid a potential overevaluation of the effective sEPS gelling macromolecules. Interestingly, the higher content of uronic acids of $sEPS_B$ with respect to $sEPS_A$ did not result in stiffer hydrogels: even if uronic sugars are considered strongly involved in the hydrogel cohesion, it is not only their content, but also their type to govern the sEPS hydrogel elasticity (Schambeck et al., 2020). Particularly, mannuronic acids form weaker hydrogels (Hay et al., 2013) and have been suggested to be present in higher contents in sEPS extracted from AGS fed with VFA-rich wastewaters (Schambeck et al., 2020).

Effect of (ionic) cross-linker nature

The hydrogel stiffness was significantly affected by the type of metal cation used as (ionic) cross-linker (e.g., Mg^{2+}, Ni^{2+}, Ca^{2+}, Cu^{2+}), as summarized in **Figure 13**. However, the overall stress-strain response to consecutive compression-decompression cycles was preserved over the tested metal ions (data not shown). The dependence of the post-gelling stiffness on the nature of the (ionic) cross-linker suggested that the polymer affinity towards the tested metals influenced the hydrogel mechanics, thus reflecting the participation of distinct functional groups during the cross-linking reaction. Particularly, the alginate post-gelling stiffness increased in the following order: $Ni^{2+} << Ca^{2+} < Cu^{2+}$ (**Figure 13a**). However, alginate was not able to form stable hydrogels in presence of Mg^{2+}: literature generally reports that alginate gelation via Mg^{2+}-driven cross-linking does not occur due to the lack of strong polymer–ion interactions; in addition, many researchers described Mg^{2+} ions as diffusively bound, if compared to strongly site-bounded ions like Ca^{2+} (Donati et al., 2009). Despite the origin of the microbial aggregates (AGS from R1 and R2) and resulting differences in terms of biochemical composition (**Figure 5**), $sEPS_A$ and $sEPS_B$ featured comparable selectivity in interacting with (divalent) metal cations during the cross-linking reaction ($Mg^{2+} < Ni^{2+} \sim Ca^{2+} < Cu^{2+}$, **Figure 13a**), thus resulting in hydrogels with similar Young's moduli except for Mg^{2+}. Indeed, $sEPS_B$ were not able to form stable hydrogels in presence of Mg^{2+} similarly to alginate. The ability of amino acids and

phosphate to bind with Mg^{2+} could enable the $sEPS_A$ hydrogel-formation in presence of Mg^{2+} (Felz et al., 2020a). Conversely, a potential reduced content of these functional groups in $sEPS_B$ could explain its inability to undergo sol-gel transition in presence of Mg^{2+}; however, the lack of a detail assessment of the compositional properties of the here studied AGS-extracted sEPS allowed to draw only speculative conclusions on such concern. Another aspect to be considered is the affinity of the extractable sEPS macromolecules for metals naturally present in AGS, including a wide range of alkali, alkaline earth, and heavy metals (e.g., Ca, Cu, Ni, Zn, Mg, etc.): these metals could be more efficiently used by the extracted sEPS as (ionic) cross-linker, thus leading to greater post-gelling mechanical properties. In comparison with alginate, sEPS seemed to show higher affinity for Ni^{2+}, resulting in greater post-gelling mechanical stiffness: this could be linked to the affinity of humic- and protein-like substances for Ni^{2+} (Li et al., 2017a). Both alginate and sEPS formed stiff but heterogeneous hydrogels in presence of Cu^{2+}, likely due to the their great affinity for complex formation with this metal (Felz et al., 2020a; Lee and Mooney, 2012; Ouwerx et al., 1998). Moreover, too fast gelation kinetic driven by the high polymer affinity for the (ionic) cross-linker could result in inhomogeneous structures.

Comparing alginate and sEPS to k-/ι-carrageenan hydrogels, more significative differences were pointed out as result of the distinct functional components and mechanisms involved in the hydrogel-formation. As previously explained, k-/ι-carrageenan dispersions (in 0.01M NaOH) could undergo sol-gel transition upon cooling without addition of (external) divalent ions. However, the post-gelling stiffness was improved by adding (external) divalent metal ions in the following order (**Figure 13b**): $Ca^{2+} < Cu^{2+} < Mg^{2+} \sim Ni^{2+}$ for k-carrageenan and $Ca^{2+} \sim Mg^{2+} < Cu^{2+} < Ni^{2+}$ for ι-carrageenan. Indeed, small monovalent ions like Na^{+} are only able to bond ionically to the sulphate groups reducing their efficacy in controlling the flexibility of disaccharide units of carrageenan. Conversely, divalent cations are able to form intra-molecular bridges between the sulphate groups of adjacent anhydro-D-galactose and D-galactose residues of carrageenan; upon cooling, the quaternary structure forms due to intermolecular M^{2+} bridging (Thrimawithana et al., 2010).

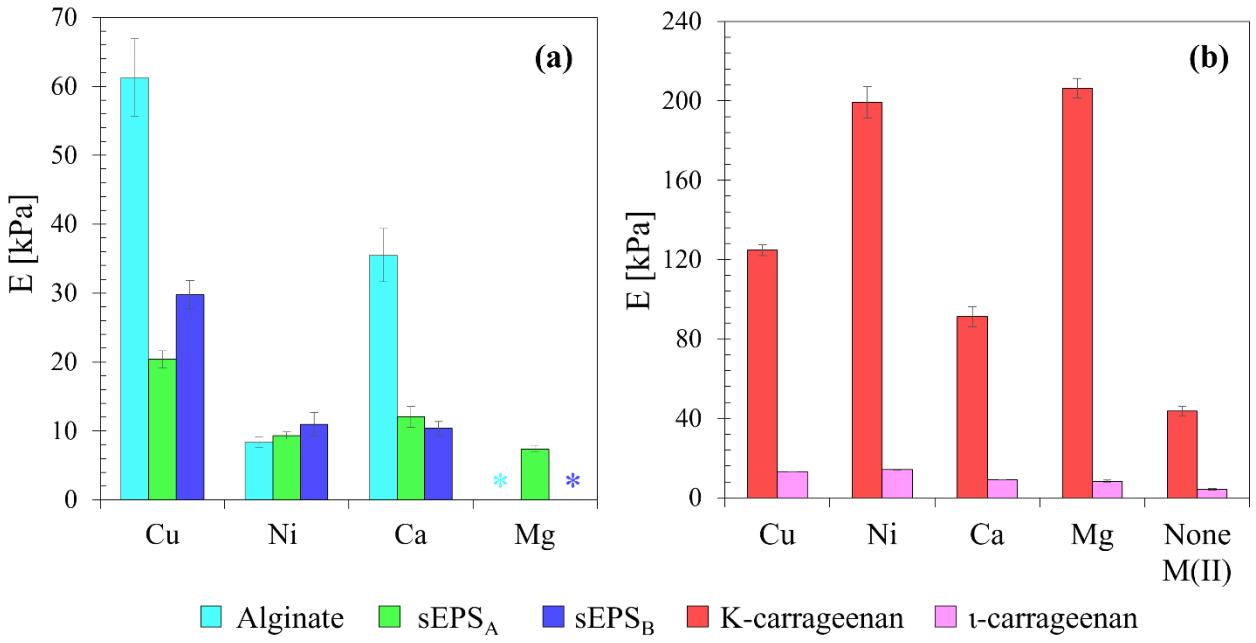

Figure 13 – Effect of various divalent metal cations as (ionic) cross-linker on the post-gelling stiffness of alginate, sEPS **(a)** and k-/ι-carrageenan **(b)**. [M^{2+}] = 0.1 and 0.5 M, for model biopolymers and sEPS, respectively. [Model biopolymers] = 2.5 wt%; [sEPS] = 8 wt%. Data = average value ± standard deviation (n. 3 sample replications).

Overall, these results evidenced that the hydrogel-formation could be site-specific: various levels of post-gelling stiffness might be obtained based on the polymer affinity towards the metals used as (ionic) cross-linker, thus reflecting the participation of specific binding sites during the cross-linking reaction. The polymer affinity towards metal cations is affected by type and availability of binding sites and polymer conformation (i.e., polymeric chain arrangement). By way of example, the comparison between sEPS and alginate, characterized by more significative chemical and functional similarities compared to k-/ι-carrageenan, was highlighted. Alginate interacts with metal ions via its carboxyl groups, distributed on linear polysaccharide chains, easily accessible during the hydrogel-formation processes. Conversely, as previously remarked, sEPS are characterized by a more complex structure and biochemical composition which suggests the participation of multiple functional groups (and hence various and heterogenous binding sites) during the cross-linking reaction, as already reported by Felz et al. (2020a). Moreover, the extraction protocol applied could provide modifications of the polymer chain arrangement and binding site availability, thus affecting the resulting hydrogel-forming ability and post-gelling mechanics.

To gain insights on the nature of the polymer-metal interaction, the correlation between hydrogel stiffness and chemical properties of the (ionic) cross-linker was addressed, pointing out some differences in the chemistry of the sEPS and alginate hydrogel-formation, in agreement with literature data (Felz et al., 2020a). Alginate favoured alkaline earth metals and Cu^{2+} to form stiffer hydrogels: the selectivity for alkaline earth metal ions depends on the M/G ratio in the alginate backbone, especially in terms of G-block content involved in the hydrogel-formation (Lee and Mooney, 2012). The alginate post-gelling stiffness was directly related to intrinsic chemical properties of the (ionic) cross-linker, and in metal affinity for alginate (or logarithm of the association constant for alginate, $LogK_{ass}$) and ionic radius (**Figure A.2a** in *Appendix*) in agreement with literature data (Ouwerx et al., 1998). Values corresponding to Cu^{2+} did not respect these linear correlations, likely due to the heterogenous structure of hydrogels formed in presence of Cu^{2+} (Felz et al., 2020a; Lee and Mooney, 2012; Ouwerx et al., 1998). Even if clear (linear) correlations between post-gelling stiffness and metal properties were not detected for sEPS, an overall preference for transition metals with increasing atomic number was highlighted (**Figure A.2b** in *Appendix*). Overall, this trend agreed literature data (Felz et al., 2020a), thus suggesting that the sEPS hydrogel-formation could be driven by similar mechanisms and chemical functions regardless of the origin of the microbial aggregates. In the case of Mg^{2+}, the cross-linking effectiveness would appear more dependent on the sEPS compositional properties. However, despite these evidenced, elucidating the sEPS post-gelling mechanical properties as a function of their origin is not an easy issue to be addressed due to the broad range of variables involved. For instance, it has been found that the origin of the microbial aggregate as well as the nature of the extractable sEPS macromolecules can influence the elasticity of the resulting hydrogels (Schambeck et al., 2020). In the context of the present study, enough elements were not available to shed light on these aspects, which in any case did not the constitute the research goals. The comparison between $sEPS_A$ and $sEPS_B$ has been mainly added to give a proof-of-principle of the applicability of the above-described methodologic approach to distinct AGS-derived sEPS. Further work is hence encouraged to gain insights on the influence of the AGS origin and characteristics (e.g.,

physical-chemical features, microbial populations, characteristics of the treated wastewater, operational strategies, sludge retention time, environmental conditions, etc.) on the sEPS production and properties: this assessment could be pivotal in designing the actual implementation of the EPS recovery/valorization processes.

Overall, the comparison with well-known biopolymers has proved to be a powerful tool to strengthen the results of the rheological characterization, but all the emerged considerations have to be interpreted according to their speculative nature. Dedicated techniques able to shed on the hydrogel structure and cross-linking processes (e.g., imaging techniques such as SEM, TEM and confocal laser scanning microscopy CLSM, FT-IR, DSC, small-angle X-ray scattering SAXS, etc.) could be implemented to validate the here proposed hypothesis. The methodologic approach proposed in this chapter allowed to emphasize the dependence of the post-gelling mechanics on the applied hydrogel-forming conditions in terms of polymer concentration and (ionic) concentration and nature and it could be hence seen as starting point for further analytical investigations.

3.3 Oscillatory shear measurements

Further mechanical insights on sEPS-based hydrogels have been inferred from the oscillatory shear measurements carried out by varying the sEPS concentration (1 – 10 wt% sEPS). To assess the viscoelastic properties of a certain material the measurements should be carried out in the linear viscoelastic (LVE)-region. For all the investigated sEPS-based systems (1 -10 wt% sEPS) the LVE-region was hence determined through amplitude sweep tests. **Figure 14** shows the trend of the storage modulus G' and loss modulus G'' as a function of the amplitude strain γ for all the studied sEPS-based systems at increasing polymer content (1 – 10 wt% sEPS). In the LVE-region G' and G'' appeared almost invariant (up to a γ value of about 1%); moreover, G' resulted higher than G'' thus suggesting that all the samples behaved like viscoelastic solids. As the strain was increased, G' started to decrease, thus indicating the occurrence of a yield point (and therefore the end of the LVE-region) due to the structural breakdown of the polymeric network (i.e., non-linear behaviour). At higher

strain, crossover of the *G'* and *G''* profiles were observed: above this point (termed flow point), *G''* exceeded *G'*, thus evidencing a sample behavior as liquid-like systems.

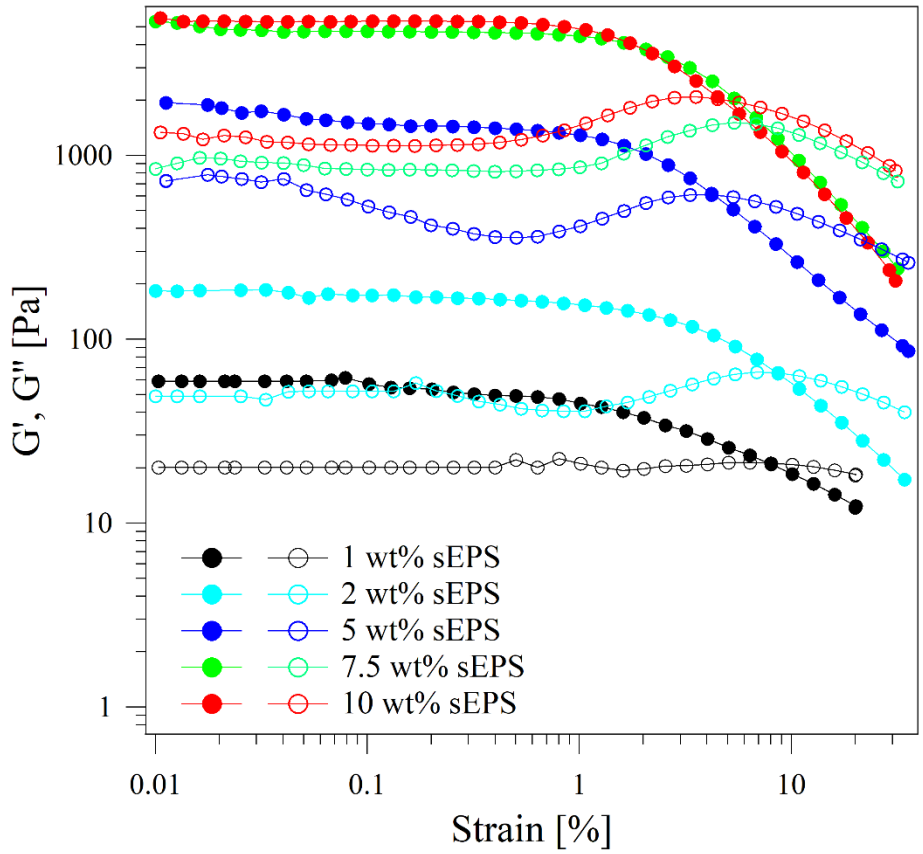

Figure 14 – Strain dependence of storage modulus *G'* (full markers) and loss modulus *G''* (empty markers) for sEPS-based systems with increasing polymer content (1 – 10 wt% sEPS) determined through amplitude sweep experiments.

An amplitude strain $\gamma = 0.4\%$ within the LVE-region was chosen for frequency sweep (i.e., frequency-dependent) experiments. **Figure 15** depicts the dependence of storage modulus G', loss modulus G'' and complex viscosity η^* on the oscillation frequency ω for all the investigated sEPS-based systems (from 1 to 10 wt% sEPS). The storage modulus *G'* appeared always larger than the loss modulus *G''* and no crossover between the G' and G'' profiles was observed within the investigated range of frequencies. In compliance with this trend, complex viscosity decreased in all the studied range of frequencies. This behavior (i.e., $G' > G''$) is typical of systems presenting an infinite relaxation time τ. Being gels classified as fluids characterized by a solid-like behaviour (i.e., τ value that tends to infinite) (Almdal et al., 1993), the trend observed suggested the gel-like nature of the studied sEPS-based systems. These results agreed with literature data: Schambeck et al. (2020) reported for 2.3

wt% sEPS hydrogels from AGS fed with VFA-rich synthetic influents the same solid-like behaviour ($G' > G''$) with values of the storage modulus G' slightly lower compared to those observed in this study.

Furthermore, the storage modulus G' did not significantly depend on frequency (in the studied frequency range) but it appeared strictly affected by the sEPS concentration: G' values increased from about 50 Pa up to 5000 Pa upon increasing the sEPS concentration from 1 to 10 wt%, while the overall rheological behavior remained almost the same, indicating that while the main relaxation mechanism was unchanged upon increasing the EPS concentration, the timescale of the process changed. As reported in literature, the storage modulus results to be proportional to the entanglement density ρ_E: $G' = \rho_E \cdot K_B \cdot T$, where K_B is the Boltzmann constant and T (K) is the temperature (Gottlieb et al., 1981; Mackintosh et al., 1995): consequently, considering that G' increased upon increasing the sEPS concentration in the studied sEPS-based hydrogel systems, an increase of ρ_E with the sEPS content might be speculated, thus suggesting a higher complexity of the sample structure and an increased strength of the three-dimensional cross-linked polymeric network thus formed.

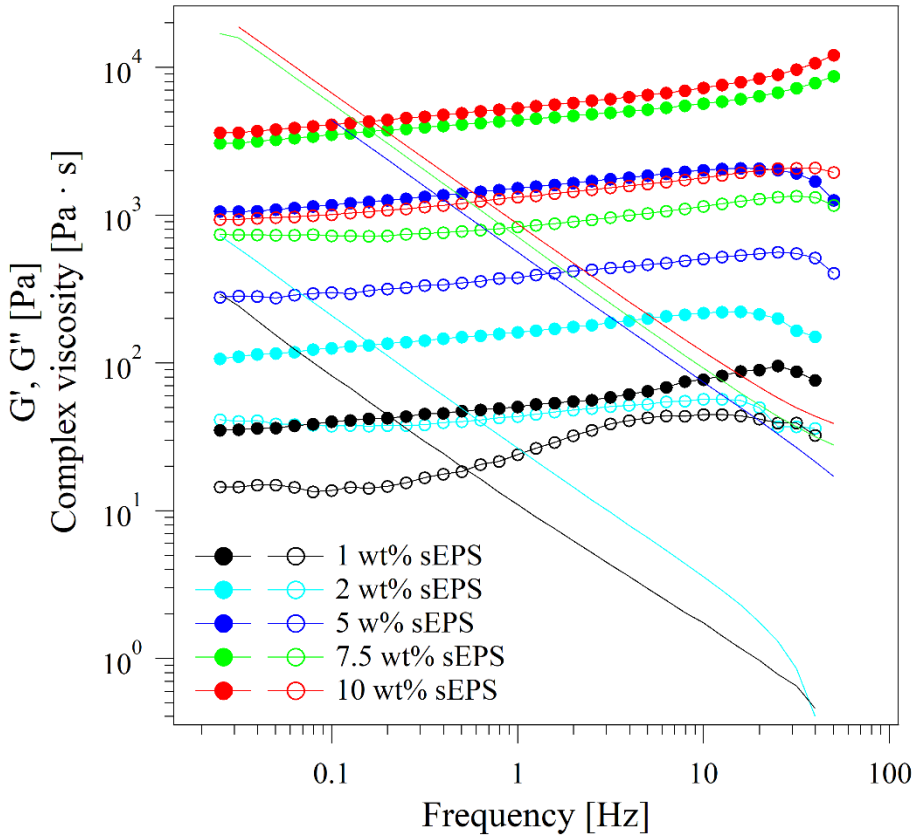

Figure 15 – Dependence of storage modulus *G'* (full markers), loss modulus *G''* (empty markers) and complex viscosity η^* (continuous lines) on the oscillation frequency for sEPS-based systems at increasing concentrations (1 -10 wt% sEPS).

The complex viscosity η^* (**Figure 16**), extrapolated from the frequency sweep curves at a oscillation frequency ω = 1 Hz, is nearly constant (in the order of 0.5 – 1 Pa · s) up to 2.5 wt% sEPS concentration and then significantly increased up to 870 Pa · s at 10 wt% sEPS concentration: this could indicate the occurrence of a concentration threshold between 2.5 and 5 wt% sEPS which defines the formation of an extended three-dimensional hydrogel network. However, the mechanical profiles reported above evidenced a gel-like behavior ($G' > G''$ in the LVE-region for all the applied range of oscillation frequencies) even at the lowest sEPS concentrations (< 2.5 wt% sEPS). It can be speculated that for sEPS concentrations lower than 2.5 wt% only weakly interconnected polymeric clusters were present, while a strong increase in the cross-linking density which led to the formation of an extended network can be observed upon increasing the sEPS above this concentration threshold.

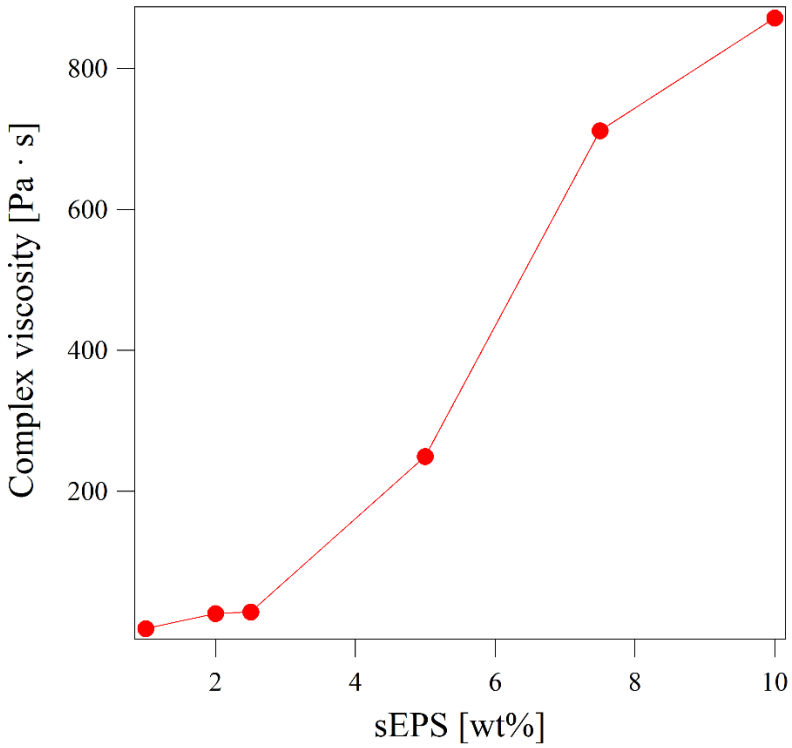

Figure 16 – Dependence of complex viscosity η^* (at ω = 1 Hz) on sEPS concentration.

The dependence of the storage modulus G' on the weight fraction of the gelling agent Φ has been largely discussed in literature and mainly described by a power-law function ($G' = a \cdot \Phi^n$) (Ueno et al., 2008, Guenet 2000). In the present work, the relationship between the storage modulus G' and the sEPS (weight) concentration was established: the power-law function satisfactorily fitted the experimental data (R^2 = 0.975) (**Figure 17**). Particularly, the exponent value $n \simeq 2$ could be consistent with the percolation model to describe the hydrogel-forming mechanisms. This model (Stauffer, 1976, 1985; de Gennes, 1976) relies upon a critical phenomenon of connectivity. If p is the fraction of connected objects, a so-called percolation threshold p_c can be defined: below p_c only clusters are present, whereas above p_c an infinite network is formed (Guenet 2000). **Figure 18** schematically figures out the so-called site percolation process in a square lattice, in which each intersection between two lines represents a site. If two neighboring sites are filled, a bond between them is established, thus producing clusters of size s with frequency n_s. The percolation threshold, p_c, can be therefore defined as the critical value of p at which the formation of a cluster occurs, which means that $s_{av} \rightarrow \infty$ where s_{av} represents the average cluster size (i.e., the number of sites forming the cluster itself)

(Zallen et al., 1983). Interestingly, alginate gelation is generally described through a percolation model (Funami et al., 2009): similar hydrogel-forming mechanisms might be hence promoted in presence of Ca^{2+} for AGS-derived sEPS and alginate, despite their chemical differences.

Further hypothesis (at speculative level) on the hydrogel structure could be suggested from the rheological data interpretation. The simulation of the *G'* – sEPS concentration data via power-law function, and in particular the value of the exponent *n*, might be used to estimate the fractal dimension D_F. Indeed, for solid-like systems like cross-linked polymeric network (i.e., hydrogels), the Jones and Marquès theory (Jones and Marquès, 1990) describes the relation between the elastic modulus G' and the network volume fraction *C* as follows: $G' \propto C^{\frac{3+D_F}{3-D_F}}$. Assuming that *C* could be approximated with the sEPS weight fraction (wt%) (Lotti et al., 2019b), it could be possible to estimate $D_F \simeq 1$ suggesting that the network might be constituted by interconnected straight fibrils. Surely, this data treatment only allows to draw speculative conclusions that should be confirmed by dedicated techniques: for instance, in order to gather information on the structural units constituting the 3D network, measurements of Small Angle X-ray Scattering (SAXS), supported by sample observation by Transmission Electron Microscopy (TEM), could be implemented. Being aware to the hypothesis weakness not confirmed by experimental validation, these results might suggest differences in the 3D structure of sEPS hydrogels of different origin. Indeed, AmxGS-derived EPS hydrogels evidenced a fractal dimension D_F equal to 2.50 indicating a polymeric network probably constituted by interconnected branched fibrillar units (Lotti et al., 2019b). The main differences of EPS-based hydrogels from AGS and AmxGS could be found in the functional components and mechanisms involved in the hydrogel-formation: indeed, it has been proved that AmxGS-extracted EPS formed hydrogels with solid-like mechanical properties at higher concentrations (above 17% w/v) without metal cation addition (Lotti et al., 2019b) which is instead necessary for AGS-derived sEPS. The sludge origin, and hence the microbial communities populating the bioaggregates, seemed therefore to affect the EPS hydrogel structure and mechanics. Conversely, a fractal dimension of about 1 has

been reported for alginate hydrogels formed in presence of Ca^{2+} (i.e., gels constituted by a connected network of rod-like fibrils) (Hernández et al., 2010), thus suggesting a certain similarity with the structure of AGS-derived sEPS hydrogels.

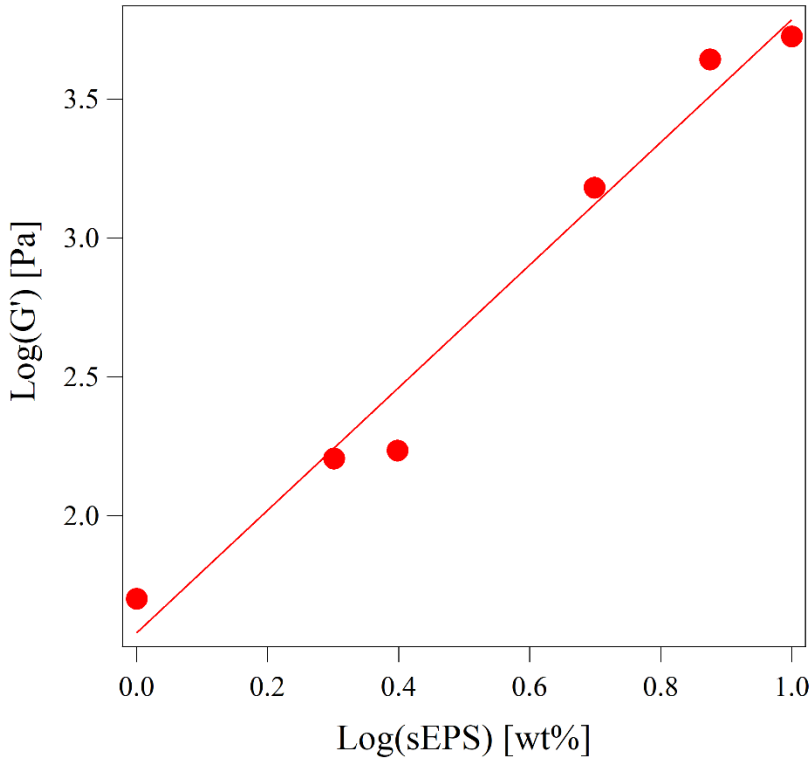

Figure 17 – Dependence of the logarithm of the storage modulus Log(*G'*) on the logarithm of the sEPS (weight) concentration Log(sEPS) and related linear fitting: Log(*G'*) = Log(a) + n · Log(sEPS). The best fitting parameters are Log(a) = 1.58 and *n* = 2.2 (R^2 = 0.975).

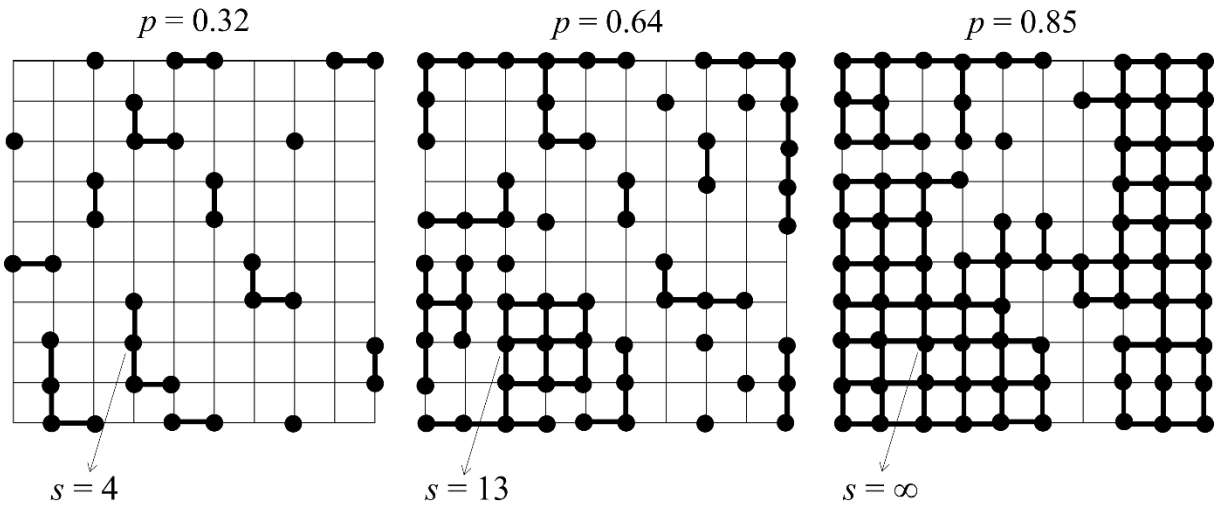

Figure 18 – Scheme of the site percolation process. Various cluster sizes (*s*) and three different fractions of filled sites *p* are represented.

3.4 Outlook and perspectives

A comprehensive analysis of the main drivers of hydrogel-formation of AGS-derived sEPS was given in comparison with well-known biopolymers, thus providing guidelines to approach the complexity of the sEPS matrix and related gelling processes. The results emerged can also indicate appealing applicative potentials. The dependence of the sEPS post-gelling mechanics on the applied hydrogel-forming conditions (e.g., polymer concentration and ionic cross-linker concentration and nature) could be exploited to develop waste-derived bioproducts to be valorized in multiple fields. AGS-extracted sEPS can be used to form hydrogel-like materials with high-water content (up to 98.5-99 wt%) and versatile mechanical properties: indeed, level of stiffness (*E* up to about 20 kPa under the tested conditions) comparable to other biopolymer-based systems currently applied for commercial purposes (e.g., ι-carrageenan hydrogels) could be achieved, thus suggesting the opportunity to develop sEPS-based bioproducts with remarkable market-value. Even if a broader implementation might be limited in sectors related to direct human contact/consumption, like in production of thickeners and gelation agents in food industry, and drug-delivery systems in medical applications (Karakas et al., 2020), a wide range of potential uses common to other biopolymer-based systems (e.g., alginate, ι-carrageenan) could be explored like soil and water bioremediation technologies, biochemistry and biotechnology industry, agriculture. Moreover, the interesting rheological features of sEPS-based systems could also suggest their potential application as viscosity-modifying agents (VMAs): they could be studied as alternative to natural polymers (including microbial polysaccharides such as welan gum, diutan gum, and guar gum, cellulose, and starch) currently applied as VMAs in developing advanced cement-based materials with adapted rheology (Bessaies-Bey et al., 2022).

A robust strategy to engineer the hydrogel-forming capability of AGS-derived sEPS might be therefore found in a comprehensive analysis of their most peculiar properties: various chemical and

functional features should be synergically assessed and optimized based on the type of application pathway chosen. Typical properties of growing interest dealing with biopolymer-based hydrogels are biochemical composition, mechanical properties, water-holding capacity, biodegradability, whose level of priority is strictly dependent on the fate of the designed bio-based materials. The agronomic sector is particularly interesting for biopolymer-based systems like sEPS hydrogels thanks to their unique properties (e.g., high-water content and holding ability, softness, biocompatibility, etc.). However, the use of sEPS-based systems in agriculture would result strictly related to all the above cited chemical and functional characteristics. The required mechanical properties depend on the specific application area: to the best of our knowledge, the use of hydrogels in nursery and/or horticulture sector (e.g., as substrates for cutting and/or micropropagation) would require a medium level of stiffness, while hydrogel-like systems applied as carriers for delivery and controlled-release of agrochemicals (e.g., nutrients, phytostimulants, etc.) should be more performing from a mechanical point of view having to protect the encapsulated components by potential deformations. With reference to the sEPS here studied, these levels of mechanical properties could be achieved for hydrogels containing around 2.5 – 5 wt% sEPS in the first case ($E \simeq 3$ kPa) and around 5 – 10 wt% sEPS in the second one ($E \simeq 11$ kPa). It should be pointed out that the origin of the microbial aggregates (e.g., type of wastewater to be treated, reactor operative conditions, etc.) as well as the sEPS extraction protocol applied could affect the sEPS post-gelling mechanics. The same level of stiffness could be reached at different polymer content and (ionic) cross-linker concentration and nature as result of the different level of purity of the sEPS gelling macromolecules and related abundance and availability of binding sites. In this perspective, these results might be seen as proof-of-principle of the feasibility of forming hydrogels with various mechanical properties acting on the hydrogel-formation processes, thus paving the way towards appealing routes of valorization in compliance with a circular economy approach in waste sludge management. Follow up research should be hence dedicated to develop extraction and gelling processes with high-effectiveness both in terms of quality/quantity of the extractable EPS macromolecules and post-gelling mechanics.

Despite the hydrogel mechanics, also its biochemical composition is fundamental dealing with environment-related potential applications. This study demonstrated the feasibility of forming sEPS hydrogels by means of different metal ions M^{2+} as cross-linker agent (e.g., Ca^{2+}, Ni^{2+}, Cu^{2+}, Mg^{2+}), thus resulting in various levels of stiffness and an almost unchanged overall mechanical behavior (for instance in terms of stress-strain response under compression). The choice of the ionic cross-linker should be therefore subordinated to the level of quality and mechanics demanded by the desired application field. Moreover, the ionic cross-linker source (i.e., the metal salt used to prepare the aqueous medium) should be carefully addressed. In this work, MCl_2 synthetic aqueous solutions were used as ionic cross-linker M^{2+} source: Cl^- ions could diffuse from the aqueous phase into the polymeric matrix together with M^{2+}, thus becoming part of the final hydrogel composition. In agronomy-oriented applications, an excessive chlorine content should be avoided being phytotoxic for plant growth: consequently, Cl^- should be replaced as counterion of M^{2+} in developing sEPS-based hydrogels to be valorized in agriculture. These aspects define the outlines of the **Chapter 2** of the present thesis.

4. Conclusions

This work shed light on the hydrogel-forming ability and post-gelling mechanics of AGS-extracted sEPS: the key role of various methodologic aspects (e.g., polymer consumption, hydrogel geometry, etc.) was emphasized leading to the development of material-saving and reproducible gelling methods able to improve the robustness of the rheological analysis. The comparison with well-known biopolymers (i.e., alginate and k-/ι-carrageenan) has proved to be a useful tool to strengthen the outcome of rheology. The main findings can be summarized as follows.

i. As result of the higher complexity and diversity of the extracellular biopolymeric matrix, higher driving forces (sEPS concentrations $\geq$ 2.5 wt%, $Ca^{2+} \geq$ 0.1 M) were required to allow the establishment of an extended three-dimensional polymeric network, and hence the formation of stiff sEPS hydrogels, with respect to the studied model biopolymers.

ii. As evidenced in compression-decompression studies, levels of elasticity and stiffness (*E* up to about 20 kPa under the tested conditions) comparable to other biopolymer-based systems currently applied for commercial purposes (e.g., ι-carrageenan) were observed for the studied sEPS hydrogels, thus suggesting the promising development of sEPS-based biomaterials towards the broader implementation of WRRFs.

iii. Hydrogels-based materials with distinct levels of stiffness and an almost unchanged mechanical behaviour might be formed by varying sEPS concentration and (ionic) cross-linker concentration and nature, thus expanding the potential range of viable applications. Furthermore, a distinct dependence of the post-gelling stiffness on the nature of the metal cation used in the gelling processes was observed among the studied biopolymers, thus suggesting the involvement of distinct functional groups during the hydrogel-formation.

iv. The ability of AGS-derived sEPS to form hydrogel-like materials with high-water content and solid-like mechanical properties was confirmed by the frequency dependence of *G'*, *G''* and η^* in oscillatory shear experiments.

Appendix

A.1 Origin of aerobic granular sludge (AGS) used as raw material for the sEPS extraction

R1 – $sEPS_A$

Structural EPS_A were extracted from granules cultivated in a 17 L bubble column sequencing batch reactor (SBR – R1) fed by a synthetic influent composed of VFAs (1/3, acetate and propionate), peptone (1/12) and glucose (7/12). The COD/N ratio was of 21.6 mg COD/mg N, and therefore no nitrification could take place. The SBR cycle was composed of 30 min anaerobic feeding, 30 min additional anaerobic time, 110 min aeration and 5 min settling followed by withdrawal. At the end of the reactor operation, the granules were then freeze-dried and stored at room temperature to be then used for the $sEPS_A$ extraction.

R2 - $sEPS_B$

Structural EPS_B were extracted from granules cultivated in a sequencing batch reactor (SBR – R2) fed with a simple synthetic wastewater composed of equal COD fractions of acetate and propionate. The SBR cycle consisted of 90 min anaerobic phase, 240 min aerobic phase, settling (with a critical settling velocity varying between 1.7 to 5.1 m/h) and finally a phase where the removal of excess sludge was done (Layer et al., 2019). The granules were then freeze-dried and stored at room temperature to be then used for the $sEPS_B$ extraction.

Table A.1 – Hydrogel-forming conditions investigated through rheological measurements (i.e., compression-decompression experiments) for all the studied biopolymer-based hydrogels.

	Effect of biopolymer concentration		
	Polymer concentration [wt%]	Ionic cross-linker type	Ionic cross-linker concentration [M]
$sEPS_A$	2.5, 5, 8, 10	Ca^{2+}	1
$sEPS_B$	2.5, 5, 8, 10	Ca^{2+}	1
Alginate	1, 2.5, 4, 5	Ca^{2+}	0.1
K-carrageenan	1, 2.5, 5	Ca^{2+}	0.1
I-carrageenan	1, 2.5, 5	Ca^{2+}	0.1
	Effect of (ionic) cross-linker concentration		
	Polymer concentration [wt%]	Ionic cross-linker type	Ionic cross-linker concentration [M]
$sEPS_A$	8	Ca^{2+}	0.5
$sEPS_B$	8	Ca^{2+}	0.5
Alginate	2.5	Ca^{2+}	0.1
K-carrageenan	-	-	-
I-carrageenan	-	-	-
	Effect of (ionic) cross-linker nature		
	Polymer concentration [wt%]	Ionic cross-linker	Ionic cross-linker concentration [M]
$sEPS_A$	8	Ca^{2+}, Mg^{2+}, Cu^{2+}, Ni^{2+}	0.5
$sEPS_B$	8	Ca^{2+}, Mg^{2+}, Cu^{2+}, Ni^{2+}	0.5
Alginate	2.5	Ca^{2+}, Mg^{2+}, Cu^{2+}, Ni^{2+}	0.1
K-carrageenan	2.5	Ca^{2+}, Mg^{2+}, Cu^{2+}, Ni^{2+}	0.1
I-carrageenan	2.5	Ca^{2+}, Mg^{2+}, Cu^{2+}, Ni^{2+}	0.1

A.2 Oscillatory shear measurements: theoretical fundamentals

In an oscillatory shear experiment carried out through a stress-controlled rheometer the sample is loaded between two plates (a fixed lower plate and a moving upper plate) at a known gap *h* and the upper plate oscillates back and forth at a given stress τ and frequency ω: the resulting (shear) strain γ is measured from the torque extended by the upper plate.

This oscillatory shear stress profile applied on the sample can be represented as a sinusoidal wave $\tau(t)$ with the stress plotted on the y-axis and time on the x-axis (Eq. A.1).

$$\tau(t) = \tau_0 \sin(\omega \cdot t) \tag{A.1}$$

If the investigated sample behaves like a viscoelastic material, it will respond to the applied stress with a (shear) strain also sinusoidal $\gamma(t)$, out of phase by an angle δ with respect to the applied stress, whose value depends on the characteristics of the studied material (Eq. A.2).

$$\gamma(t) = \gamma_0 \sin(\omega \cdot t + \delta) \tag{A.2}$$

The phase angle δ (or phase shift) describes the viscous and elastic characteristics of the sample. For a purely elastic material, δ is equal to 0°, while a purely viscous material shows a δ value equal to 90°. Consequently, for viscoelastic materials featuring both viscous and elastic properties (dissipating and storing energy) $0 < \delta < 90$ °C.

The ratio between the applied stress and the measured strain gives the complex modulus G^* (Eq. A.3), which gives an indication of the material stiffness.

$$G^* = \tau_0/\gamma_0 \tag{A.3}$$

It has been demonstrated that the phase shift δ can be used to quantify the elastic and viscous contribution to G^* by using trigonometry (Goodwin et al., 2000), as shown by the vector diagram in **Figure A.1a**. The in-phase or elastic component of G^* represents the energy stored upon deformation, and hence it is termed storage modulus *G'*. Conversely, the viscous contribution to G^* (out-of-phase

component), the so-called loss modulus *G''*, represents the energy dissipated upon deformation. *G'* and *G''* and can be calculated as follows (Eqs. A.4 and A.5, respectively):

$$G' = G^* \cos(\delta) \tag{A.4}$$

$$G'' = G^* \sin(\delta) \tag{A.5}$$

According to this notation, $\tan(\delta)$ can be represented as follows (Eqs. A.6):

$$\tan(\delta) = G''/G' \tag{A.6}$$

Alternatively, *G** can be mathematically represented by means of a complex number notation as follows (Eq. A.7):

$$G^* = G' + iG'' \tag{A.7}$$

where *G'* and *G''* are the real and imaginary parts, respectively, of the complex modulus *G** (**Figure A.1b**).

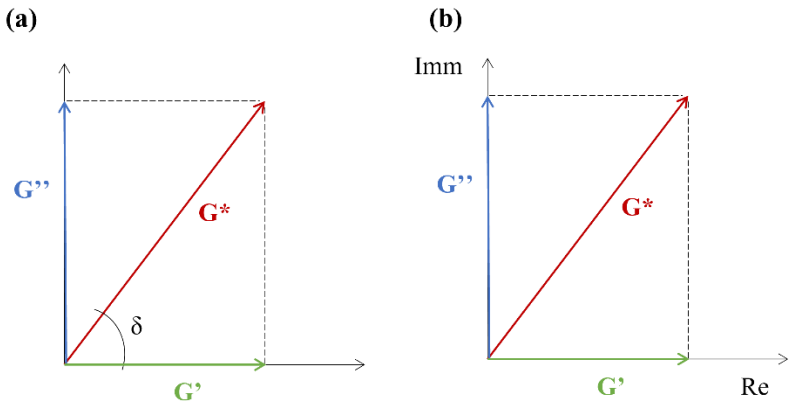

Figure A.1 – Alternative representation of complex viscosity *G** and its elastic and viscous components *G'* and *G''* (storage and loss modulus, respectively).

For more details refer to (Barnes 2000, Macosko 1994).

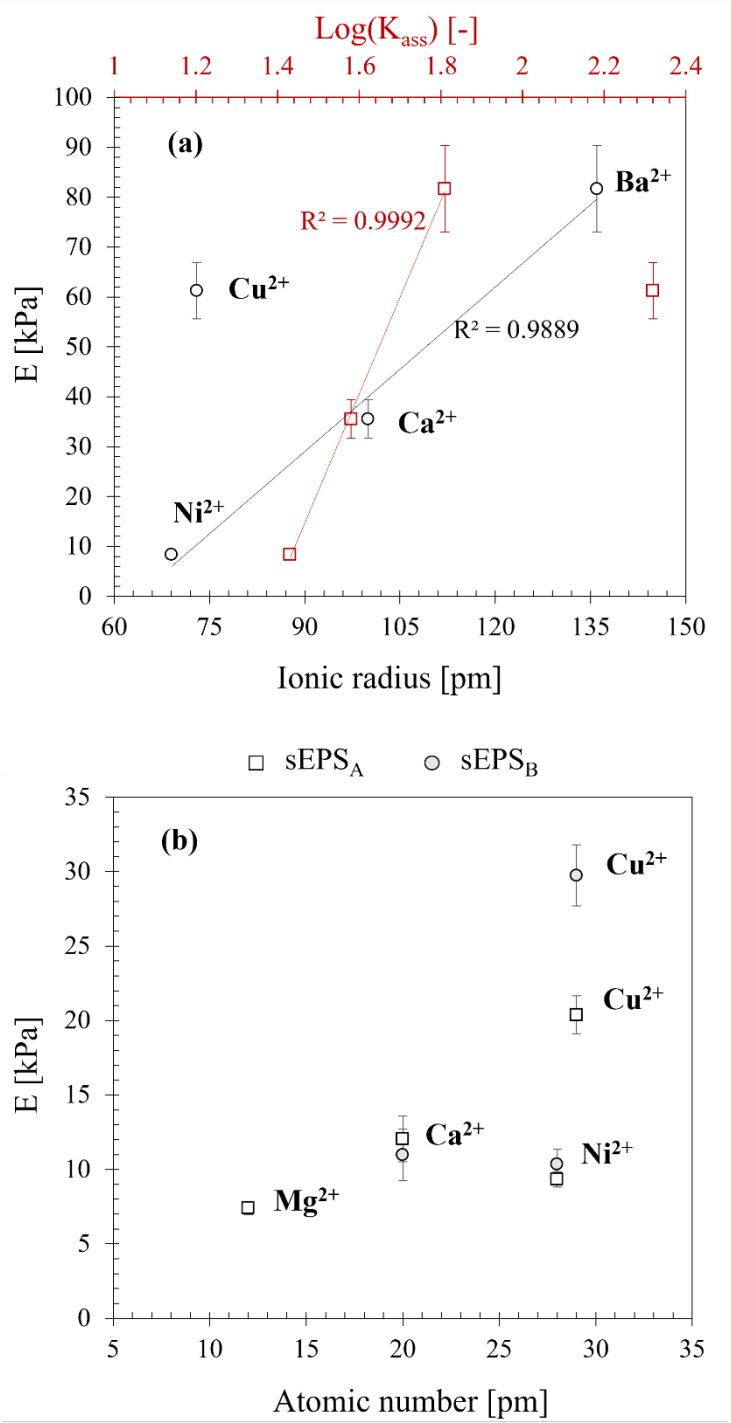

Figure A.2 – Dependence of the Young's modulus of 2.5 wt% alginate hydrogels **(a)** and 8 wt% sEPS hydrogels **(b)** on the chemical properties of the metal cation used as (ionic) cross-linker. Values of Log(K_{ass}) (i.e., constant affinity of metal for alginate) refer to (Ouwerx et al., 1998). Data = average value ± standard deviation (n. 3 replicates).

Chapter 3

Towards resource recovery-oriented solutions in agriculture exploiting structural extracellular polymeric substances (sEPS) from aerobic granular sludge (AGS)

Abstract

This chapter offers a synergic approach to engineer the hydrogel-forming properties of structural extracellular polymeric substances (sEPS) from aerobic granular sludge (AGS) based on the high qualitative standard imposed by the agronomic sector. Particularly, the aim was to emphasize the impact of the overall process of sEPS extraction/valorization on the quality/quantity of the recoverable macromolecules, pointing out the impact of the chemicals applied on some agriculture-related properties (e.g., composition, swelling ability, nutrient release capacity, biodegradability). More detailed, experimental protocols widely discussed in literature for the sEPS extraction and hydrogel-formation were adapted by using chemical reagents not containing sodium and chlorine considered as phytotoxic in large quantities: K_2CO_3 or $(NH_4)_2CO_3$/HNO_3/KOH (*extraction*) and $Ca(NO_3)_2{\cdot}H_2O$ or $Ca(C_2H_5COO)_2$ (*cross-linking*).

It has been found that the extraction yield and the nature of recovered macromolecules as well as the overall sEPS hydrogel-forming ability were not strongly affected by the distinct chemicals applied, while more significant differences were observed in terms of elemental composition. Particularly, the sEPS and derived hydrogels obtained according to the here developed agriculture-oriented protocols resulted conform with the current environmental legislation in matter of soil improvers and fertilizing products in terms of inorganic pollutant content (e.g., heavy metals, to be verified the Cr(VI) levels). The capability of sEPS-based hydrogels to reversibly sorb and desorb water was assessed through swelling experiments, evincing a great water-holding ability especially using $CaNO_3{\cdot}4H_2O$ as (ionic) cross-linking agent (up to 16 $gH_2O/gTS_{Hydrogel}$). Nutrient-loaded hydrogels were obtained upon

swelling in nutrient-enriched aqueous solutions, suggesting their potential applications in sustainable agro-practices as carrier for the delivery/controlled-release of agrochemicals in soil.

The biodegradability assessment carried out through respirometric techniques revealed that the biodegradation of sEPS and hydrogels varied based on the extraction and gelling processes applied (in terms of chemicals used). Despite the protocols implemented, the readily biodegradable organic matter was reduced upon hydrogel-formation: a potential explanation might be that the formation of an extended 3D polymeric network in which the sEPS macromolecules were more confined likely resulted in a decreased substrate accessibility, thus requiring further hydrolytic reactions before their microbial utilization.

Overall, this contribution gives guidelines to progress towards new resource recovery-oriented solutions in agriculture exploiting the versatile properties of AGS-derived sEPS according to a circular economy pattern in waste sludge management.

1. Introduction

Global polymer production annually exceeds 300 million tons, consuming approximately 6% of the fossil oil produced, and it is anticipated to rise to 20% in the coming three decades (Payne et al., 2019). Since the middle years of the 20th century, the petroleum-derived chemistry, refinery, and engineering processes have been the basis of the polymer industry (Morales et al., 2021), accounting for about 99% in 2015 (Payne et al., 2019): the increasing environmental pressure towards more eco-friendly technologies and industrial solutions made unsustainable the polymer production based on depleting fossil fuel reserves (Rabnawaz et al., 2017). Therefore, the urgent transition from a petroleum-based to a bio-based economy has marked the beginning of the current century, shifting the type of carbon resources from fossil to natural and renewable ones (Morales et al., 2021). The biopolymer industry utilizing alternative feedstocks like biomass has emerged as promising strategy to deal with such concern (Zhu et al., 2016).

Polymer-based materials of great interest for scientists working in miscellaneous fields are hydrogels. Hydrogels can be described as three-dimensionally cross-linked polymeric networks containing many hydrophilic groups that endow huge absorption of water molecules within their porous structure without being dissolved (Kalinoski and Shi, 2019). Owing to their outstanding properties as well as the wide variety of substrates and forms in which they can be prepared, hydrogels have been commercially applied in multiple fields such as personal hygiene, agriculture, and biomedicine (e.g., drug delivery, tissue engineering, etc.): as a matter of fact, their global market represented in 2016 a total of $15.6 billion, and it is anticipated to achieve a total $22.3 billion in 2022 (Morales et al., 2021). The commercial interest in biopolymer-based hydrogels (e.g., produced from starch, carboxymethylcellulose, alginate, carrageenan, and chitosan) for environment-related applications has strongly grown in the last decade thanks to their unique properties such as biocompatibility, biodegradability, non-toxicity, and relative low-cost (Lima-Tenório et al., 2015). Particularly, biopolymer-based materials like hydrogels are gaining increasingly attention in agriculture. Indeed, the main growing, harvesting, and processing practices in agriculture were achieved through the exploitation of natural resources (e.g., water and soil) combined with the excessive use of agrochemicals: the high demand for fresh water, increasing manufacturing costs of agrochemicals as well as heightened awareness of the ecological adversities of conventional agro-practises have therefore shed light on the urge for more sustainable technologies (Milani et al., 2017). The major application fields biopolymer-based might be identified as follows:

i. Superabsorbent polymer (SAPs) for soil conditioning;
ii. Delivery systems for controlled-release of agrochemicals (e.g., nutrients, phytostimulants);
iii. Soil and water bioremediation (e.g., for the metal removal).

Hydrogel-based systems currently applied as soil conditioners are from the poly(acrylic acid)/polyacrylamide types: these materials are non-renewable, contain potentially toxic monomers (e.g., acrylamide), and are biodegradable only to a limited extent (Passauer et al., 2015). In common agricultural and garden soils, degradation rates of polyacrylate-based SAPs range between 0.2 −

0.82% within 11 − 14 weeks as a function of the cross-linking degree, soil type, and temperature range (Stahl et al., 2000; Wilske et al., 2014). Owing to these advantages, polyacrylate-based hydrogels are becoming unacceptable from an ecological point of view, thus driving the research efforts towards more sustainable solutions. Biopolymers (i.e., natural polymers produced by plants, animals, and microorganisms, which present biodegradability as their main advantage, Morales et al., 2021; Nakajima et al., 2017), have proved to be an eco-friendly alternative for sustainable agro-practices. Particularly, hydrogels based on chemically modified and cross-linked polysaccharides (e.g., starch, cellulose, chitosan, pectin, or alginates) can be successfully applied alternatively to conventional acrylate/acrylamide-based systems: their degradation rates in soil and/or compost range between 25 − 95% within 4 − 14 weeks depending on the polysaccharide nature, cross-linking degree, incubation temperature, and soil/compost type (Passauer et al., 2015).

The microbial extracellular polymeric substances (EPS), and particularly structural EPS (sEPS) from granular sludge (GS) which endow hydrogel-forming properties (Felz et al., 2016; Lin et al., 2010; Lotti et al., 2019b; Seviour et al., 2012), might be promising candidates to progress towards more sustainable agro-practices. Indeed, they are bio-based (and particularly waste-derived) and can be potentially produced in high quantities (with recovery potentials anticipated to achieve up to 58 g/kg COD removed and 40 g/kg NH_4-N removed for aerobic granular sludge (AGS)- and anammox granular sludge (AmxGS)-based processes, respectively) by means of more easily extraction procedures with respect to fossil oil-based synthesized polymers (Feng et al., 2021). Hence, the EPS recovery and conversion into value-added biomaterials for environment- and/or industry-related applications gives a new perspective on a less fossil fuel-dependent manufacturing sector, contributing to a more circular economy-based water sector.

As widely reported in literature (Felz et al., 2016; Feng et al., 2019; Sheng et al., 2010), the EPS composition and characterization largely depend on the extraction method applied: distinct extraction and recovery processes might reflect differences in terms of both *quantity* (extraction yield, EPS components, etc.) and *quality* (biochemical composition, functional groups, etc.) of the extractable

EPS macromolecules (Feng et al., 2021). Physical, chemical, and biological processes could be applied in the EPS extraction/recovery, as detailed described in **Chapter 1**: the specific research goals should lead to the choice of the most appropriate approach, searching for a balance between extraction yield and intrinsic features. Among the feasible protocols, chemical methods are usually considered more effective and appear to yield a relatively higher EPS content (Sheng et al., 2010). The effect of various chemical agents (both in the phases of alkaline solubilization and acidic precipitation) on the quality/quantity of the extractable EPS macromolecules deserves a dedicated focus. Indeed, this aspect is crucial to engineer the conversion of EPS into value-added bioproducts according to the qualitative standard imposed by the specific applicative sector. With the aim to valorize AGS-derived sEPS as hydrogel-based materials, similar considerations might be done for the (ionic) cross-linker source used in the gelling processes, which can compromise the quality of the resulting biomaterials. The use of various chemical reagents in both extraction and gelling protocols might be therefore seen as potential tool to set and control the qualitative properties of sEPS-based biomaterials depending on the application field selected. The choice of the chemicals to be used in the overall process of sEPS recovery/valorization might be hence considered as application-dependent, thus becoming part of the design phase. By way of example, the use of biopolymer-based hydrogels in agriculture imposes a certain level of quality (e.g., low levels of heavy metals and toxic elements like Na and Cl, high content of nutrients like K, N, and P, etc.) and therefore the reagents mainly reported in literature for the sEPS-based hydrogel production, i.e., NaOH, Na_2CO_3, HCl (*extraction*) and $CaCl_2$ (*cross-linking*) (Felz et al 2016), could be not appropriate.

In this perspective, the first goal of the present contribution was to understand the effectiveness in adapting the overall process of EPS recovery/valorization by means of various chemicals able to improve the quality of the derived biomaterials (e.g., hydrogels) based on the specific environmental or industrial solution selected. Particularly, sEPS-based hydrogels from AGS have been produced and studied based on the high qualitative standard imposed by the agronomic sector. With this regard, the sEPS extraction and hydrogel-forming protocols proposed by Felz et al. (2016) have been studied

as reference methods and slightly modified maintaining the overall structure but providing more "*green*" and eco-friendly chemicals like $K_2CO_3/(NH_4)_2CO_3$–HNO_3–KOH (*extraction*) and $CaNO_3 \cdot 4H_2O/Ca(C_2H_5COO)_2$ (*cross-linking*). The influence of the distinct chemicals on the overall properties of the obtained sEPS and derived hydrogels was hence addressed. Particularly, the potential of AGS-derived sEPS biomaterials (e.g., hydrogels) in developing sustainable agronomic practices has been emphasized based on a comprehensive analysis of the following aspects:

i. *Composition*: a complete overview of the sEPS and hydrogel composition has been proposed, highlighting the influence of the extraction and gelling processes on the overall quality of the resulting biomaterials. A particular focus has been dedicated on the content of nutrients and inorganic pollutants (e.g., heavy metals) with reference to the current legislation in matter of soil improvers and fertilizing products;
ii. *Swelling capacity and nutrient release*: the ability of sEPS-based hydrogels to reversible sorb and desorb water (e.g., swell and de-swell in aqueous phase) has been assessed to shed light on their potential behaviour as SAPs. Moreover, sEPS hydrogels swollen in nutrient-enriched aqueous solutions (KNO_3) have been study for their nutrient release ability;
iii. *Biodegradability*: respirometric techniques have been adapted on both sEPS and derived hydrogels to give a preliminary assessment of their microbial degradation under distinct extraction and gelling conditions;

With reference to point (iii), it should be considered that this proof-of-concept investigation was carried out to emphasize the crucial role of the overall sEPS extraction/valorization processes on the potential biodegradation of the derived bioproducts (e.g., hydrogels), taking advantage of time-saving and well-established experimental protocols. Indeed, polymer biodegradability in soil is a comprehensive research area since the huge amount of variables to be considered (e.g., soil type, polymer nature, temperature range, cross-linking density, etc.) that make challenging the identification of standard methods. Many regulations in matter of microbial soil respiration (e.g., UNI EN ISO 16072:2002) might be adapted for this purpose, but the identification of the reference

conditions to be tested (e.g., soil type, temperature, etc.) is not an easy issue to be addressed. In this context, the outcome of this analysis is therefore helpful to gain a preliminary assessment able to shed light on the key factors influencing the biodegradation of sEPS-based materials (e.g., hydrogels), thus leading to a more aware design of the experiments to be carried out in soil. In line with the focus proposed in this chapter, the goal was not to obtain absolute values of biodegradability (which would not be representative of the sample behaviour in soil) but highlight the impact of the whole process of sEPS extraction and hydrogel-formation (including the chemicals applied) on the microbial utilization of the final products. Additionally, this investigation might be helpful in designing sEPS-based materials (e.g., bio-based flocculants) destinated to other environment- and/or industry-related applications (e.g., wastewater treatment sector).

Overall, this chapter gave insights on a potential approach to engineer the hydrogel-forming ability of AGS-derived sEPS in compliance with the qualitative standard imposed by the target sector, thus shedding light on the impact of the overall production process on the AGS-derived sEPS valorization effectiveness. General guidelines to progress towards the promising valorization of sEPS-based hydrogels in agriculture have been drawn, empathizing the urge for more dedicated approaches in investigating/exploiting the interesting properties of these waste-derived biopolymers.

2. Materials and methods

2.1 sEPS extraction and hydrogel-formation

sEPS were extracted from waste AGS coming from a full-scale reactor treating municipal wastewater, adapting the thermo-chemical method reported by Felz et al. (2016). After sampling and sieving, granules were stored at -20°C until use. AGS was then centrifuged (4000xg, 4°C, 20 min): granules were collected in the pellets for the extraction and the supernatant was discarded. The wet weigh of granules (WW, g) was measured as weight of the granules taken directly from the pellet. In brief, the sEPS extraction process provided a first step of alkaline solubilization (0.5% w/v Na_2CO_3) under heated and stirred conditions (1 hour, 80 °C, 400 rpm) followed solid-liquid separation (4000xg, 4°C,

20 min): the supernatant (containing EPS) was collected and subjected to acidic precipitation (1 M HCl, pH 2.2 ± 0.05). With respect to the reference method, the (acidic) sEPS suspension was subjected to consecutive centrifuges (10000xg, 4 °C, 5 min) in order to increase the sEPS (weight) concentration in the acidic pellets (in terms of percentage total solids on wet weight ratio, TS/WW [wt%]) before their re-suspension (0.5 M NaOH, pH 8.5). The extraction yield was calculated with respect the organics originally present in the granules [gVS_{sEPS}/gVS_{AGS}].

The sEPS hydrogel-forming protocol described in **Chapter 2** was adjusted on the specific research goals of the present contribution. The method structure (*dialysis + controlled geometry*) adapted from Felz et al. (2020a, 2016) was preserved, thus obtaining hydrogels with enhanced homogeneity. Briefly, the sEPS dispersion was dialyzed (3.5 kDa MWCO, 24 hours) against the (ionic) cross-linker aqueous solution (0.225 M $CaCl_2$): indeed, the Ca^{2+} ions diffusion into the polymeric solution through dialysis membranes has been proved to control the gelling kinetics thus resulting in improved post-gelling homogeneity and reproducibility. Various hydrogel geometries were used as a function of the specific research goals. An example is given in **Figure 1**, showing a particular type of support developed via 3-D printing able to force the sol-gel transition in a disc-like shape (5.2 cm of diameter, D, and 1.0 cm of thickness, H; H/D = 0.192 cm/cm). For the physic-chemical characterization studies hydrogels were produced in cylinder-like geometry (D = 0.8 cm, H = 1.2 cm; H/D = 1.5 cm/cm).

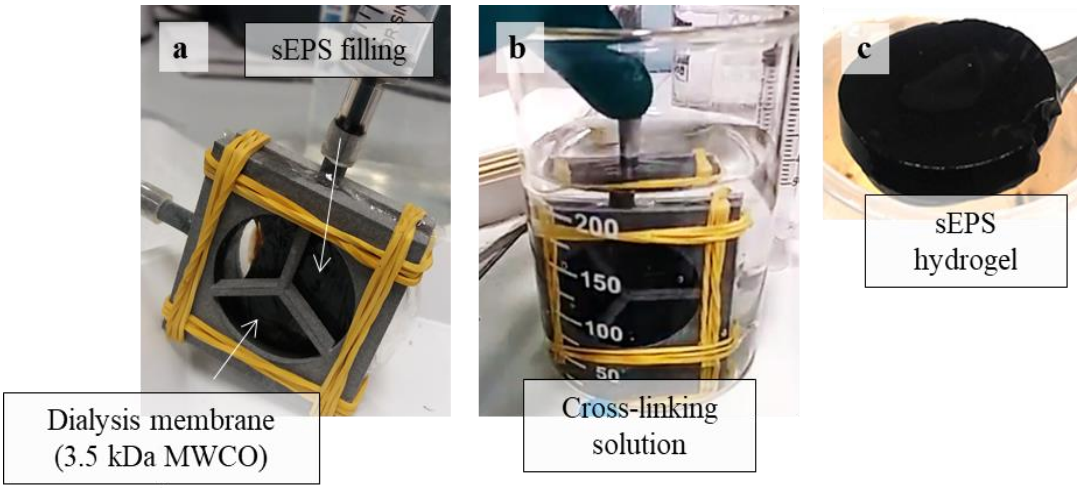

Figure 1 – sEPS hydrogel-forming protocol. The sEPS dispersion was transferred into specific supports covered through dialysis membranes **(a)** to be then dialyzed against the cross-linker solution **(b)**: the sol-gel transition was therefore forced into fixed geometries **(c)**, thus resulting in hydrogels with improved homogeneity.

With the aim to valorize the sEPS-based hydrogels in agriculture, the above-described extraction and gelling methods were adapted by means of more appropriate chemicals (**Figure 2**), potentially able to promote the inclusion of nutrients (N and K) into the sEPS polymeric network. In brief, for the alkaline extraction Na_2CO_3 was replaced with K_2CO_3 (protocol "*Agro 1*") and $(NH_4)_2CO_3$ (protocol "*Argo 2*"), for the acidic precipitation HNO_3 instead of HCl was used, while the sEPS (acidic) pellets were resuspended by adding KOH rather than NaOH. Concerning the gel-formation processes, two different calcium sources were tested as alternative to calcium chloride: $Ca(NO_3)_2{\cdot}H_2O$ (protocols "*Agro 1a*" and "*Agro 2a*") and $Ca(C_2H_5COO)_2$ (protocols "*Agro 1b*" and "*Agro 2b*").

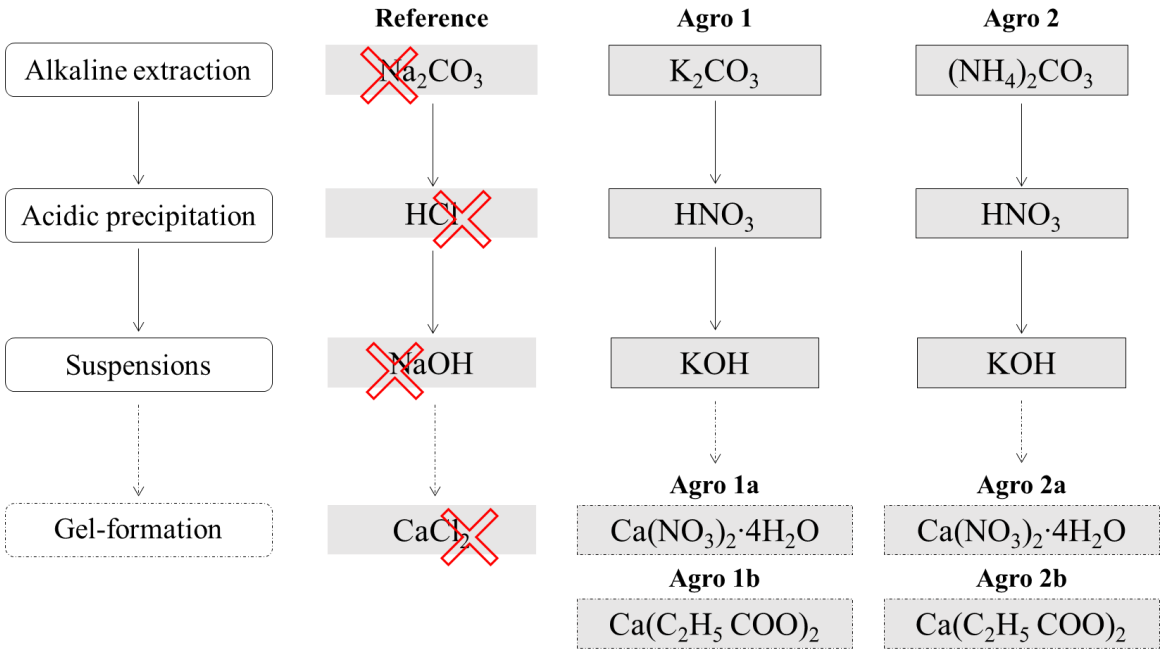

Figure 2 – Schematic representation of the adaptation of the sEPS extraction and gel-forming protocols proposed for agronomic applications.

2.2 Gravimetric, colorimetric and elemental analysis

Total Solids (TS, g) and Volatile Solids (VS, g) were addresses for AGS, sEPS and derived hydrogels. For the wet weight (WW, g) measurement, sEPS hydrogels were beforehand pressed with adsorbing paper sheets to remove the excess water. For the TS quantification, AGS, sEPS extracts and derived hydrogels were weighted on a digital balance after 24 hours at 105 °C. Moreover, the further weight loss of 105 °C-dried samples subjected to increasing temperatures (up to 215 °C) was measured to address the potential existence of residual moisture not removable below 105 °C. The ash content (Ash, g) was determined by weighting the dried samples after 2 hours at 560 °C. The Volatile Solids (VS, g) were therefore calculated as the weight difference between TS and Ash. The measurements were carried out in triplicate and the results are expressed as average values ± standard deviation. Total solids on wet weight ratios (TS/WW, wt%) and volatile solids on total solids ratios (VS/TS, wt%) were therefore calculated for each sample.

The influence of distinct chemicals in the extraction/gelling processes on the compositional properties of AGS-extracted sEPS and derived hydrogels was demonstrated combining various techniques.

Elemental analysis and Total Organic Carbon (TOC) of AGS/sEPS/hydrogels were performed in triplicate with a CHN-S Analyzer (FLASH 1112 EA/Soil Thermo).

The analysis of various inorganic components (e.g., metals and non-metals) contained in AGS/sEPS/hydrogels were carried out in triplicate by a Varian 720-ES Inductively Coupled Plasma - Atomic Emission Spectrometer (ICP-AES) equipped with a pneumatic nebulizer and a cyclonic spray chamber and by ion chromatography.

The amount of proteins (PN) and polysaccharides (PS) in the extracted sEPS was estimated through colorimetric assays to address the effect of distinct extraction protocols (in terms of chemicals applied) on the quality/quantity of the recoverable sEPS macromolecules. Particularly, the PN content was measured as BSA (Bovine Serum Albumin) equivalent using the BCA (Bicinchoninic Acid) assay (Smith et al., 1985), while the PS content was evaluated with the anthrone sulphuric acid method (Dreywood, 1946) using d-glucose as standard.

2.3 Swelling ability and nutrient release

The ability of hydrogels to reversible sorb and desorb water (i.e., swell and de-swell in aqueous solutions) might pave the way towards interesting scenarios in multiple fields, first of all the agronomic application. With this regard, sEPS hydrogels were therefore subjected to consecutive dehydration – rehydration studies to address their swelling behaviour. As suggested by literature (Wang et al., 2018), the hydrogel dehydration was carried out at 50 °C and monitored as weight loss over time with a Moisture Analyzer (MJ33 Mettler Toledo). The relative percentage of dehydration (RPD, %) was calculated as follows (Eq. 1):

$$RPD = \frac{WC_0 - WC_{50\,^\circ C}}{WC_0} \cdot 100\% \quad (1)$$

where WC_0 [g] and $WC_{50\,^\circ C}$ [g] represent the initial water content and the residual water content upon dehydration at 50 °C, respectively. Known the sEPS dry matter content in hydrogels ($TS_{Hydrogel}$, g), WC_0 was calculated as weight difference between the hydrogel wet weight (WW, g) and $TS_{Hydrogel}$.

Conversely, $WC_{50\ °C}$ was calculated as weight difference between the weight of the 50 °C-dried hydrogels and $TS_{Hydrogel}$.

The swelling ability of 50 °C-dried sEPS hydrogels was assessed both in ultrapure water and nutrient-enriched surrounding medium (i.e., 0.2 M KNO_3 aqueous solution) using gravimetric analysis. To follow the swelling kinetics, sEPS hydrogels (dried at 50 °C) were transferred into 150 mL of ultrapure water/KNO_3 solution and sampled at scheduled time intervals. The swollen hydrogels were gently pressed with adsorbing paper sheets to remove excess water and then weighted on a digital balance. The swelling ratio (q_t, g/g) was therefore calculated over time as follows (Eq. 2):

$$q_t = \frac{W_t - W_0}{W_0} \tag{2}$$

where W_0 [g] is the weight of the 50°C-dried sample and W_t [g] is the weight of the swollen sample at time t. The equilibrium water content (EWC, %) of the swollen hydrogels was calculated as follow (Eq. 3):

$$EWC = \frac{W_s - W_0}{W_s} \cdot 100\% \tag{3}$$

where W_s [g] is the weight of the swollen sample at equilibrium. Pseudo-first-order, pseudo-second-order and Elovich models were used to simulate the experimental kinetic data (Eqs. 4, 5, and 6, respectively):

$$q_t = q_e \cdot (1 - e^{-k_1 \cdot t}) \tag{4}$$

$$q_t = \frac{k_2 \cdot q_e^2 \cdot t}{1 + k_2 \cdot q_e \cdot t} \tag{5}$$

$$q_t = \frac{1}{\beta} \cdot ln\,(\alpha \cdot \beta \cdot t + 1) \tag{6}$$

where k_1 [min^{-1}] and k_2 [min^{-1}] are the pseudo-first- and pseudo-second-order constants, respectively; in Elovich model α [min^{-1}] represents the initial sorption rate while β [g/g] is a constant related to the surface coverage and activation energy for chemical adsorption (Zhou et al., 2014).

The fitting goodness was evaluated with the Pearson's correlation coefficient as follows (Eq. 7):

$$R = \frac{\sum_{i=1}^{n}(z_i - z_m)(w_i - w_m)}{\sqrt{\sum_{i=1}^{n}(z_i - z_m)^2 \sum_{i=1}^{n}(w_i - w_m)^2}} \quad (7)$$

where z_i and z_m are the observed values and their average value, respectively, while w_i and w_m are the predicted values and their average value, respectively.

The sEPS hydrogels swollen in KNO_3 were placed in ultrapure water (20 mL) to monitor the potential K release over time. At scheduled time intervals (0.5, 1, 3, 6, 8 hours), 10 mL solution aliquots were removed and filtered through a 0.45 mm membrane filter (Whatman). An equivalent volume (10 mL) of ultrapure water was added to the solution in order to keep the hydrogels immersed in a volume of 20 mL (and maintain a significative driving force for all the sampling period). The released amount of K^+ at each time interval was determined by analysing the (filtrated) bulk samples through ion chromatography.

2.4 Biodegradability

As previously introduced, respirometric techniques have been implemented to gather information on the biodegradation of sEPS and derived hydrogels under distinct extraction and gelling conditions in terms of chemicals applied. The aim was to emphasize the impact of the whole process of sEPS production/valorization on the microbial utilization of the final biomaterials. Indeed, respirometry is a technique widely adopted for wastewater characterization which allows to easily adapt time-saving and well-established protocols on the here studied sEPS-based systems. Proposals for the characterization of the biodegradable carbonaceous substrate fractions are available in literature depending on both Chemical Oxygen Demand (COD) biodegradability and removal kinetics (Ziglio et al., 2001). With this regard, two main fractions can be identified:

i. *soluble biodegradable COD* (**sbCOD**), composed from a readily biodegradable fraction (RBCOD), which is the fraction ready to be assimilated through the cellular membrane and the fraction easily hydrolyzed (RHCOD) (Henze, 1992);

ii. slowly biodegradable COD assimilated to the *particulate biodegradable COD* (**pbCOD**), whose metabolization is delayed from the necessary enzymatic hydrolysis (Henze, 1992). This fraction includes large molecules with relatively complex structures that, before utilization, need to be broken down into small molecules by several extracellular enzymatic hydrolytic steps inside the microorganism flocs (Borzooei et al., 2021).

The inert carbonaceous substrate fractions can be assimilated to the non-biodegradable or inert COD (iCOD) and classified as soluble inert COD (**siCOD**) and particulate inert COD (**piCOD**).

To be considered that in the framework of the Activated Sludge Models (ASMs), distinct notations have been implemented for the various carbonaceous fractions; moreover, the degree of required COD fractionation depends on the type of process to be designed/simulated and on the ASM to be used (Borzooei et al., 2021). For instance, in ASM1, the carbon substrates present in wastewater are characterized according to their solubility, biodegradability, viability, and biodegradation rates (Vanrolleghem et al., 2003). The total COD is divided into three major fractions: biodegradable, non-biodegradable (biologically inert) COD, and active biomass. The biodegradable COD is distinguished in readily biodegradable (S_s) and particulate slowly biodegradable or hydrolysable (X_s) COD. The unbiodegradable COD is classified as soluble unbiodegradable (S_i) and particulate unbiodegradable (X_i) COD. Finally, the fractions related to active biomass are heterotrophic (X_{BH}) and autotrophic (X_{BA}), accounting for 10 – 20% of total organic matter in municipal wastewater, which are under continuous alternation due to the decay and growth processes (Gumpta et al., 2018). Due to the lack of reliable and easy methods to quantify these fractions, X_{BH} can be lumped into the Xs as a common practice that may not considerably affect the modeling results if the heterotrophic yield coefficient (Y_H) is increased by 10% (Borzooei et al., 2021; Henze et al., 2000). In ASM2d (Henze et al., 2000) the variables are organized according to particle size, organic/inorganic properties and degradability and distinct notations have been implemented: for instance, the former X_S in ASM1 becomes XC_B in ASM2d (including also colloidal particles) (Corominas et al., 2010).

For convenience, in the framework of this analysis we refer to the COD partitioning in terms of soluble biodegradable, particulate biodegradable, soluble inert and particulate inert COD fractions (sbCOD, pbCOD, siCOD and piCOD, respectively). The biodegradable substrate fractions of sEPS and derived hydrogels were addressed by the so-called *multiple-* and *single-OUR method* (OUR: *Oxygen Uptake Rate*) (Borzooei et al., 2021; Ekama et al., 1986; Ziglio et al., 2001). Particularly, the multiple-OUR method was used to evaluate the biodegradable organic fraction (or biodegradable COD, bCOD) of both sEPS and derived hydrogels. The single-OUR method was instead adapted on both types of substrates to address their readily biodegradable fractions (or soluble biodegradable COD, sbCOD): to this aim, these experiments were carried out on 0.1 µm-filtered samples (i.e., assuming as soluble the fraction with particle size < 0.1 µm). All the operative conditions applied in the respirometric measurements are summarized in *Appendix* (**Table A.1**). More details are presented below.

2.4.1 Experimental set-up

The respirometric batch tests were performed in a respirometer equipped with a removable reactor having an internal volume of approximately 2L (internal diameter = 112 mm, external diameter = 135 mm, height = 200mm) (**Figure A.1** in *Appendix*). The reactor is made of DURAN® glass and has an external jacket where water from a thermostatic bath circulates in order to maintain a constant temperature during the tests. The reactor is closed with a plastic ABS cover where Hamilton® dissolved oxygen (DO) and pH probes were housed. Each probe has its temperature sensor. The activated sludge inside the reactor was mixed through a HEIDOLPH RZR 2021 mixer and pH during the tests was controlled with the automatic dosage of NaOH and HCl. Regarding the signals acquisition and the control system, digital DO, pH and temperature signals were sent via ModBUS protocol to a PC. A dedicated software installed in the PC was used to manage data elaboration and to send automatic commands to actuators (peristaltic pumps, solenoid valves, air blowers, etc.).

2.4.2 Activated sludge preparation

For these experiments, activated sludge was sampled at the San Colombano WWTP (Florence, Italy). Total and Volatile Suspended Solids (TSS, VSS) were determined according to standard methods (APHA, 2005). Sludge was aerated overnight until the endogenous respiration was achieved; about 0.533 g/L of nitropyridine was added before the respirometric tests to inhibit nitrification. The activated sludge was then diluted with the effluent collected from the same WWTP in order to have a biomass VSS concentration in the reactor of about 2 gVSS/L.

2.4.3 Substrate preparation

Before the COD quantification and respirometric measurements, sEPS hydrogels were physically suspended in aqueous phase by using a mechanical potter while sEPS were directly used as aqueous dispersions. Both substrates (i.e., sEPS and derived hydrogels) were diluted with ultrapure water in order to have an equivalent COD concentration of 1.8 g/L. The COD of the studied substrates was evaluated through colorimetric methods by means of commercial kits (Hack LCK 614). For the soluble COD (sCOD) assessment, the samples were beforehand filtered through 0.1 µm nylon filters and syringe. The volume of substrate (V_s) to be added in the reactor was calculated based on the pre-selected initial substrate to biomass concentrations ratio (F/M = 0.025 and 0.003 in multiple- and single-OUR tests, respectively).

2.4.4 Multiple-OUR experiments

This method is based on the continuous monitoring of the OUR measured via general mass balance for DO concentration over the liquid phase (Borzooei et al., 2021). The reactor was filled with 1.4 L of activated sludge pre-treated according to what described in *Paragraph 2.4.2.* A known volume of the substrate (V_s) was added to the reactor during one of the aeration cycles. After the addition of the substrate maintaining the pre-selected initial substrate to biomass concentrations ratio (F/M = 0.025), OUR was continuously monitored. Generally, the initial peak of the respirogram occurs immediately after the sample addition due to the utilization of the readily biodegradable COD, which is followed

by a shoulder made by consumption of slowly biodegradable COD needing hydrolysis to be processed. The total amount of oxygen consumed *ΔDO* [mg/L] at the expense of bCOD can be estimated integrating the surfaces under the respirogram as follows (Eq. 8):

$$\Delta DO = \int_0^{t_f} OUR\,(t) \cdot dt \tag{8}$$

where $t = [0, t_f]$ is the time interval for the definite integral between the time of the initial endogenous state before feeding the sample and the second endogenous state after complete utilization of organic matter. The integral was approximated through the trapezoidal method by averaging the left and right Riemann sums, thus estimating the net area under the exogenous respirogram (i.e., subtracted from the endogenous contribution). The bCOD [mg/L] of the studied substrates was finally evaluated according to Eq. 9:

$$bCOD = \frac{\Delta DO}{1 - Y_h} \cdot \frac{V_{ml} + V_s}{V_s} \tag{9}$$

Where Y_h is the heterotrophic biomass yield which is assumed to be equal to 0.67 as proposed by Henze et al. (2000) for municipal wastewater, V_{ml} and V_s are the volume of mixed liquor and substrate added in the respirometer, respectively. Overall, the ratio $(V_{ml} + V_s)/V_s$ takes into account the dilution factor of the substrate bCOD in the reactor.

2.4.5 Single-OUR experiments

The method is based on estimating the variations of respiration rates due to the utilization of RBCOD and RHCOD (together accounting for the soluble biodegradable COD, sbCOD) (Borzooei et al., 2021). With this regard, the reactor was filled was filled with 1.4 L of activated sludge pre-treated according to what described in *Paragraph 2.4.2*. Firstly, the sludge was aerated until DO_{sat} (ca. 7.5 mgO_2/L) was achieved. The aeration was then stopped, and the endogenous respiration rate was acquired by means of continuous monitoring of DO profile before the substrate addition. At this point, a known volume of the 0.1 µm-filtered sample (V_s) was fed into the reactor maintaining the pre-selected initial substrate to biomass concentrations ratio (F/M = 0.003 $gCOD/gCOD_x$), thus resulting

in a temporary increase of the respiration rate due to the utilization of the readily biodegradable substrate fractions. The exogenous respiration was considered finished when the DO profile recovered the original endogenous respiration rates: the oxygen consumption *ΔDO* [mg/L] linked to the utilization of sbCOD was therefore graphically obtained. The change in endogenous/exogenous/endogenous respiration rates was estimated from the slopes of the related sections of DO profile. The substrate sbCOD [mg/L] was finally calculated similarly to bCOD in multiple-OUR method as follows (Eq. 10):

$$sbCOD = \frac{\Delta DO}{1 - Y_h} \cdot \frac{V_{ml} + V_s}{V_s} \quad (10)$$

2.4.6 COD fractionation

Combining the results of multiple- and single-OUR experiments and the soluble COD (sCOD) assessment (as $\%\,^{sCOD}/_{COD}$), the total COD was fractionated as schematically depicted in **Figure 3**. Firstly, COD was distinguished into biodegradable (**bCOD**) and non-biodegradable (**iCOD**) COD. Particularly, the bCOD (as percentage fraction of the total COD, $\%\,^{bCOD}/_{COD}$) was experimentally addressed from multiple-OUR experiments performed on "pristine" samples and iCOD (as $\%\,^{iCOD}/_{COD}$) was calculated as $100\% - \%\,^{bCOD}/_{COD}$.

Both bCOD and iCOD was then dived into soluble and particulate fractions: soluble biodegradable (**sbCOD**, assimilated to the readily biodegradable COD), particulate biodegradable (**pbCOD**, assimilated to the slowly biodegradable COD), soluble inert (**siCOD**) and particulate inert (**piCOD**) COD. More detailed, the sbCOD (as percentage fraction of the soluble COD, $\%\,^{sbCOD}/_{sCOD}$) was determined by single-OUR experiments carried out on 0.1 µm-filtered samples and then normalized with respect to 100% of total COD ($\%\,^{sbCOD}/_{COD}$). The other fractions have been hence calculated (as percentage fractions with respect to 100% of total COD) as follows:

- $pbCOD = \%\,^{bCOD}/_{COD} - \%\,^{sbCOD}/_{COD}$
- $siCOD = \%\,^{sCOD}/_{COD} - \%\,^{sbCOD}/_{COD}$

- $piCOD = \%^{iCOD}/_{COD} - \%^{siCOD}/_{COD}$

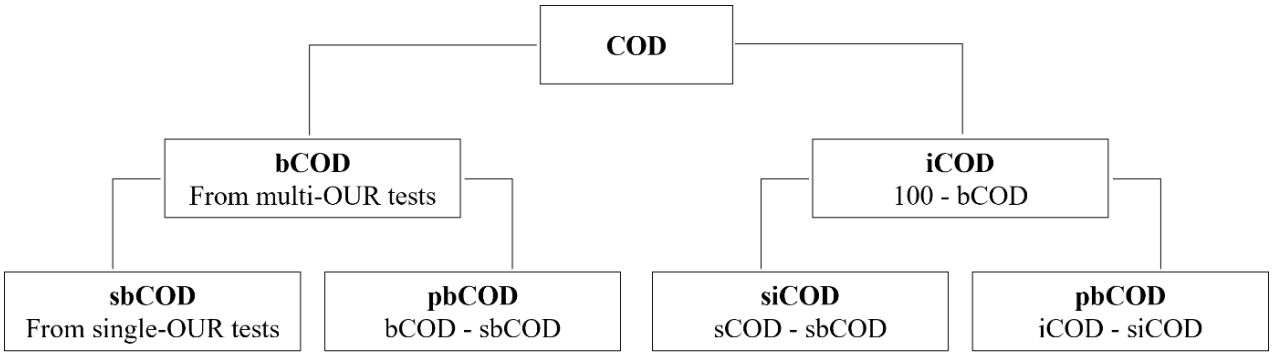

Figure 3 – COD fractionation in soluble biodegradable COD (sbCOD), particulate biodegradable COD (pbCOD), soluble non-biodegradable (or inert) COD (siCOD), particulate non-biodegradable (or inert) COD (piCOD) for all the studied substrates (i.e., sEPS and related hydrogels). Each fraction is expressed as percentage with respect to 100% of total COD.

3. Results and discussion

3.1 sEPS extraction performance

Table 1 evidences the influence of distinct chemicals used in the extraction process on the quantity/quality of the extractable sEPS macromolecules. The modified protocols "*Agro 1*" and "*Agro 2*" were able to extract an amount of sEPS (as volatile solids, VS) of about 20% of the organics originally present in the granules, thus showing extraction yields slightly lower compared to the values obtained with reference method (Felz et al., 2016) of about 23%. The volatile on total solid ratios of sEPS were comparable among the tested protocols and in agreement with literature data. The obtained sEPS were mainly composed by proteins (PN) with a lower content of polysaccharides (PS) (PN/PS ratios in the range 3.47 – 4.58 g/g, depending on the chemical reagents used in the extraction phase). Particularly, the agronomy-oriented protocols favored the extraction of a higher PS content with respect to the reference method. Regardless of the protocol applied, the PN content appeared noticeable high, and probably overestimated thus not allowing a proper mass balance. As emphasized by Felz et al. (2019), colorimetric methods suffer from interference towards various substances present in sEPS, thus leading to uncertainties in the exact assessment of the target compounds: for instance, BCA assay for PS evaluation is particularly susceptible to humic acid, gallic acid and

glucosamine. To shed light on the potential error involved in the PN estimation through colorimetric assays, the comparison with the Kjeldahl method, still recognized as the official method for protein determination in complex materials such as food (Latimer, 2016), was introduced. Being aware on the critical assumptions made both in the result analysis and conversion factor (N-content in protein of 16%, absence of non-proteinaceous N such as nucleic acids, free amino acids, etc.) (Lotti et al., 2019a), it was highlighted that the results emerged from the colorimetric measurements were not so far to those obtained with the Kjeldahl method using a conversion factor of 6.25 gPN/gTN (i.e., 573.8, 676.6 and 798.4 mgPN/gVS_{sEPS} for protocols "*Reference*", "*Agro 1*" and "*Agro 2*", respectively). Overall, despite the above-described analytical uncertainties, the AGS-derived sEPS here studied appeared more reach in proteinaceous and polysaccharidic materials compared to what observed in literature (Felz et al., 2019; Lin et al., 2010). In this sense, it should be considered that the origin of the microbial aggregates (e.g., type of wastewater treated, microbial consortia, operation units, sludge retention time, etc.) can affect the quality of the extractable sEPS macromolecules.

Table 1 – Physic-chemical characterization of sEPS extracted according to different protocols. Reference studies are *(Felz et al., 2016), **(Lin et al., 2010), ***(Felz et al., 2019a).

		This study			**Reference studies**
		Reference	*Agro 1*	*Agro 2*	
VS/TS	**[gVS_{sEPS}/gTS_{sEPS}]**	0.875 ± 0.013	0.842 ± 0.010	0.878 ± 0.003	0.870*
Extraction yield	**[gVS_{sEPS}/gVS_{AGS}]**	0.231 ± 0.014	0.206 ± 0.009	0.192 ± 0.010	0.200 ± 0.010* 0.160 ± 0.004**
$PN_{as\ BSA\ equivalent}$	**[$mgPN_{BSA}/gVS_{sEPS}$]**	888	894	903	381 ± 5***
$PS_{as\ glucose\ equivalent}$	**[$mgPS_{Glu}/gVS_{sEPS}$]**	194	258	233	138.0 ± 2.5*** 122.5 **
PN/PS	**[gPN_{BSA}/gPS_{Glu}]**	4.58	3.47	3.88	-
TN	**[$mgTN/gVS_{sEPS}$]**	92	109	128	-
PN/TN	**[gPN_{BSA}/gTN]**	7.52	5.90	7.07	-

3.2 Effect of distinct chemicals on the compositional properties of sEPS and derived hydrogels

The overall sEPS hydrogel-forming ability did not appear significantly affected by the chemicals used in extraction and gelling processes. Indeed, the sEPS hydrogel-formation presented the same dependence on the calcium and polymer concentrations used, regardless of the protocols applied. By way of example, **Figure 4** illustrates a conceptual phase diagram covering the range of 0.25 – 1 wt% sEPS concentration and 0.01 – 0.225 M Ca^{+} concentration for sEPS hydrogels formed in presence of $Ca(NO_3)_2 \cdot 4H_2O$ as cross-linking agent and using protocol "*Agro 1*" for the extraction process (i.e., $K_2CO_3/HNO_3/KOH$). The grey area represents the region in which sEPS hydrogels can be obtained; conversely, the combinations in terms of sEPS – Ca^{2+} concentrations in the white area (highlighted with red squares) did not allow the formation of stable sEPS hydrogels (with measurable mechanical properties). As clearly noticeable, sEPS were able to form hydrogels in presence of a high calcium content (e.g., 0.225 M) starting from 0.5 wt% sEPS concentration. For lower sEPS concentrations an increase in viscosity was observed upon increasing the calcium concentration, but stable hydrogels were not formed. Increasing the sEPS concentration up to 1 wt%, sEPS hydrogels can be obtained also for lower calcium concentrations (from 0.01 to 0.225 M). In summary, lightly cross-linked sEPS hydrogels with high-water content (up to 99.5 wt%) can be formed in presence of various calcium concentrations, thus opening promising scenarios in multiple application sectors. To be noticed that the here presented sEPS were able to form stable hydrogels at lower concentrations compared to those described in **Chapter 2**. These differences could be explained looking at the origin of the starting microbial aggregates. In comparison to sEPS extracted from granules cultivated in pilot-scale reactor fed by synthetic influents (**Chapter 2**), the AGS used in this study came from a full-scale reactor treating a municipal wastewater. The influent nature but also the operative conditions of the treatment unit could therefore affect the quality/quantity of the extractable sEPS macromolecules and resulting hydrogel-forming ability.

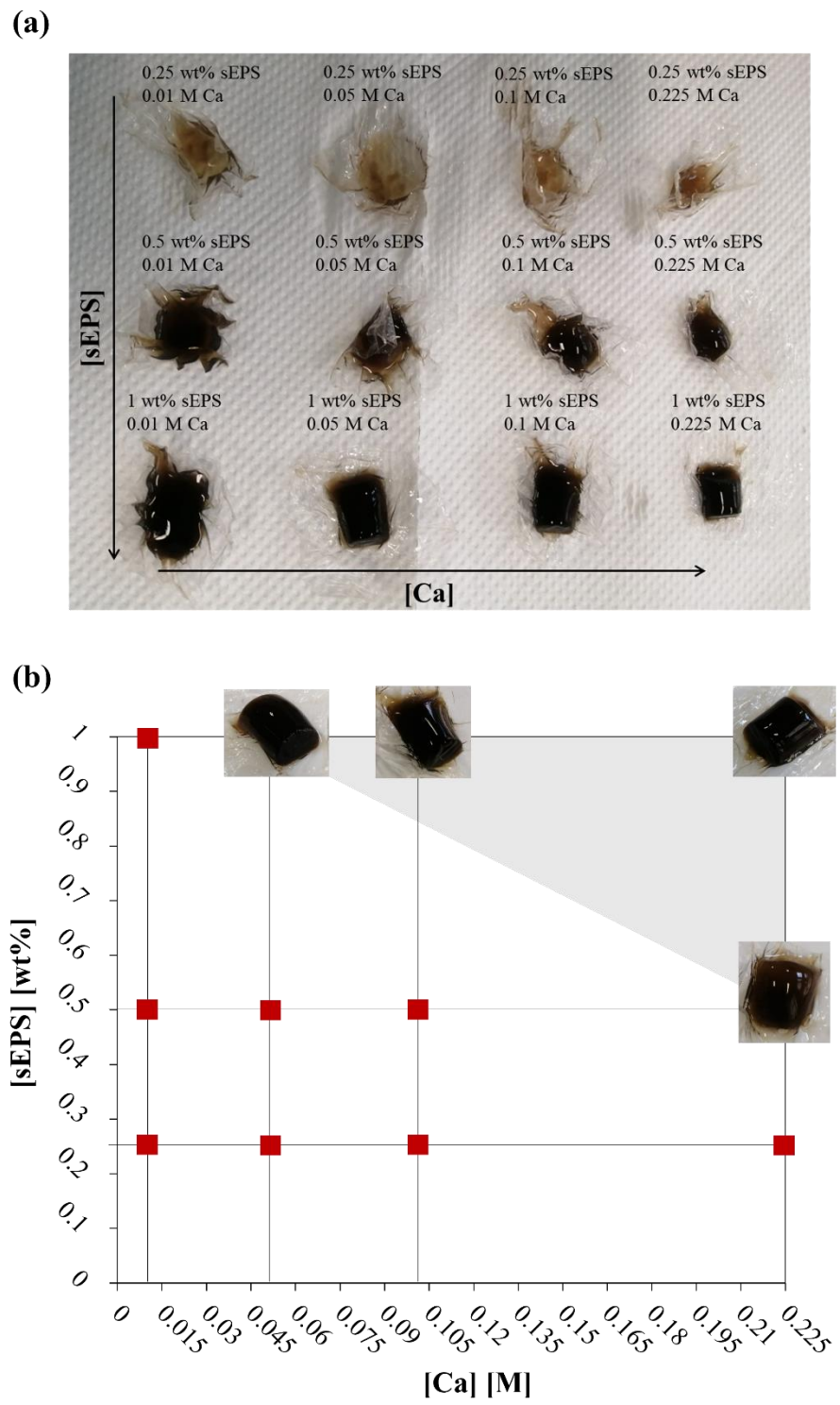

Figure 4 – sEPS after the cross-linking reaction in presence of increasing calcium concentrations (**a**) and corresponding conceptual phase diagram (**b**) in the case of protocol "*Agro 1a*". The grey region represents the conditions (i.e., sEPS and calcium concentrations) enabling the sEPS gel-formation, while the red squares the conditions for which stable hydrogels were not formed.

As depicted in **Figure 5**, 105 °C-dried sEPS and derived hydrogels presented a further weight loss once subjected to temperature increases up to 215 °C. Each point of the graphs in **Figure 5** was

obtained keeping the sample at a certain temperature until the maximum dehydration state was achieved, which means that further weight loss over time was not observed (mass variations lower than 0.0001% · h^{-1}). Examples of dehydration kinetics are given in *Appendix* (**Figure A.2**).

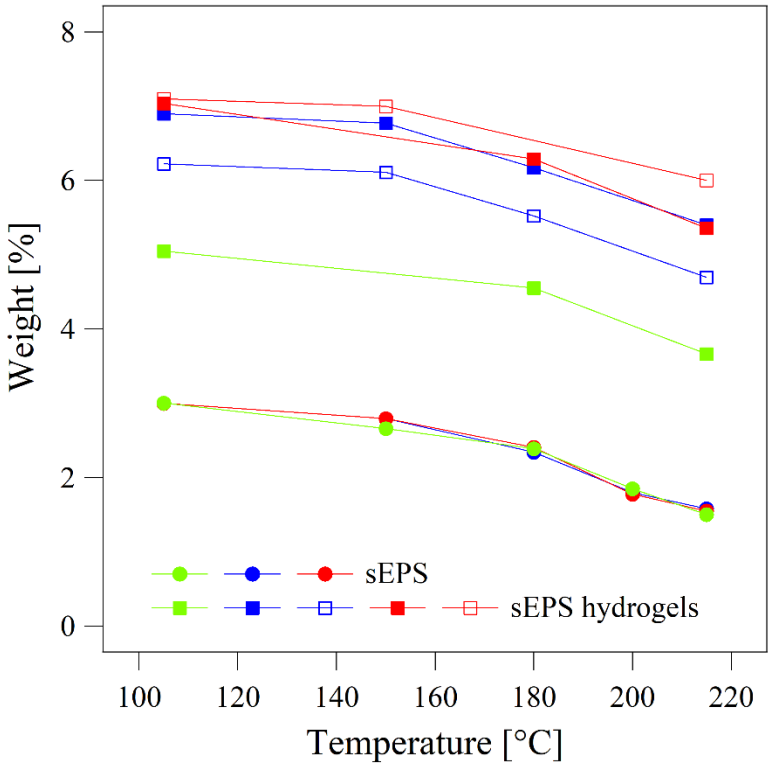

Figure 5 – Thermogravimetric analysis of sEPS dispersion and derived hydrogels. Weight [%] on the Y-axis is calculated with respect to the initial sample wet weight. Particularly, green markers refer to sEPS and resulting hydrogels prepared according to reference methods. Conversely, blue markers and lines indicate sEPS extracted with protocol "*Agro 1*" (i.e., K_2CO_3, HNO_3, KOH) and derived hydrogels obtained upon cross-linking with $Ca(NO_3)_2{\cdot}H_2O$ (full markers) and $Ca(C_2H_5COO)_2$ (empty markers). Red markers and represent sEPS extracted with protocol "*Agro 2*" (i.e., $(NH_4)_2CO_3$, HNO_3, KOH) and derived hydrogels obtained upon cross-linking with $Ca(NO_3)_2{\cdot}H_2O$ (full markers) and $Ca(C_2H_5COO)_2$ (empty markers).

The mass loss above 105 °C could be not ascribed to emissions of volatile fractions (organic matter) but to evaporation of residual moisture and/or weakly bound water. Indeed, literature data suggest three main stages occurring during the thermal decomposition are: (i) dehydration related to the elimination of external residual moisture below 200 – 250 °C; (ii) volatilization of the organic matter (up to 450 – 550 °C), and (iii) decomposition of the mineral fraction for higher temperatures (Li et al., 2019; Reguieg et al., 2020; Wang et al., 2018). The temperature bounders of each region depends on the type of sample treated; moreover, using the thermogravimetric (TG) analysis, the range of

temperatures for each stage of decomposition would be slightly different at different heating rates due to the so-called thermal lag (Li et al., 2019). Particularly, a higher devolatilization temperature (≃ 220 °C), and more in general a higher thermal stability, has been reported for granular sludge with respect to floccular sludge (Li et al., 2019): reasonably, a similar thermal response might be expected for the GS-extracted EPS whose water-retention ability is considered to prevent granules from desiccation (Seviour et al., 2019). Moreover, Wang et al. (2018) observed that the thermal decomposition process of alginate gel beads begins around 200 °C due to the removal of surface bound water and continues to 257 °C, while mass loss due to volatile emission occurred at 600 °C. Based on differential thermogravimetric (DTG) analysis (and identification of pseudo-components through DTG signal deconvolution), distinct temperatures are reported in literature for the thermal degradation of the various organic fractions present in sewage sludge and/or other types of biomass (e.g., macro- and microalgae); particularly, the interpretation of pseudo-components in sludge varies from study to study. Alvarez et al. (2015) observed that decomposition of carbohydrates, proteins and lipids in sewage sludge occur at around 300 °C, in the range 360 – 525 °C and at 255 °C, respectively. Li et al. (2010) reported the peak decomposition temperature of sodium alginate at around 230 °C. Other studies suggested the decomposition of some proteins in the range between 220 and 385 °C (degradation peaks were in the range of 285 – 301 °C) (Dandurand et al., 2014), while lipids mostly degraded in the temperature range of 270 –580 °C (peak at around 400 °C) (Muniz et al., 2015).

The above-mentioned literature reports suggest therefore that at temperatures below 220 °C the observed mass loss can be reasonably attributed to water/moisture evaporation. In this study the temperature upper limit for dehydration experiments was thus set at 215 °C. The mass loss observed for 105 °C-dried sEPS samples upon temperature increase up to 215 °C was higher with respect to hydrogels: particularly, about 2.6 wt% for sEPS and 1.1 – 1.6 wt% for hydrogels (with reference to the initial sample wet weight), depending on the chemicals used in the extraction and gelling processes. Based on this preliminarily thermogravimetric assessment, the extent of external residual moisture and surface bond water (not removable at 105 °C) decreased upon formation of the extended

three-dimensional cross-linked polymeric network. On the other hand, these results could preliminarily suggest that higher energy is needed to thermally decompose the macromolecules (e.g., polysaccharides) that are strongly cross-linked with Ca^{2+} in the three-dimensional network of hydrogels. Further work is encouraged to better elucidate these aspects: thermogravimetric (TG)/differential thermogravimetric (DTG) analysis and differential scanning calorimetry (DSC) are currently ongoing to shed light on the thermal behavior of both sEPS and derived hydrogels and to characterize their water populations. These techniques might be integrated with other analysis (e.g., FT-IR, PN/PS assessment after thermal treatment, etc.) to better understand the behaviour of each organic fraction during the thermal decomposition processes of both sEPS and derived hydrogels.

The results presented below in terms of elemental composition have been hence calculated with reference to the effective dry matter of sEPS and derived hydrogels (i.e., determined upon sample dehydration at 215 °C). **Figure 6** illustrates the elemental compositions (in terms of weight percentages, wt%) of sEPS extracted according to different protocols (i.e., distinct extraction agents). Despite the chemicals used in the extraction process, carbon, nitrogen, and hydrogen represented the predominant elements in the sEPS compositions, representing together about 64.9, 57.8, and 57.4 wt% for protocols using $CaCl_2$, K_2CO_3, and $(NH_4)_2CO_3$, respectively. The sodium content ($\simeq$ 1.8 wt% in sEPS extracted according to the reference method) was significantly reduced replacing Na_2CO_3 as alkaline reagent in the extraction phase (0.2 and 0.1 wt% using K_2CO_3 and $(NH_4)_2CO_3$, respectively); at the same time, the sEPS potassium content was increased by applying the modified extraction protocols (up to 11.2 wt% using K_2CO_3 during the alkaline solubilization) compared to the reference method (about 0.01 wt%). The remaining fraction of sEPS was mainly composed by oxygen, alkali and alkaline metals, and lower concentrations of heavy metals (e.g., Pb, Cu, Ni, Zn, Cr, etc.).

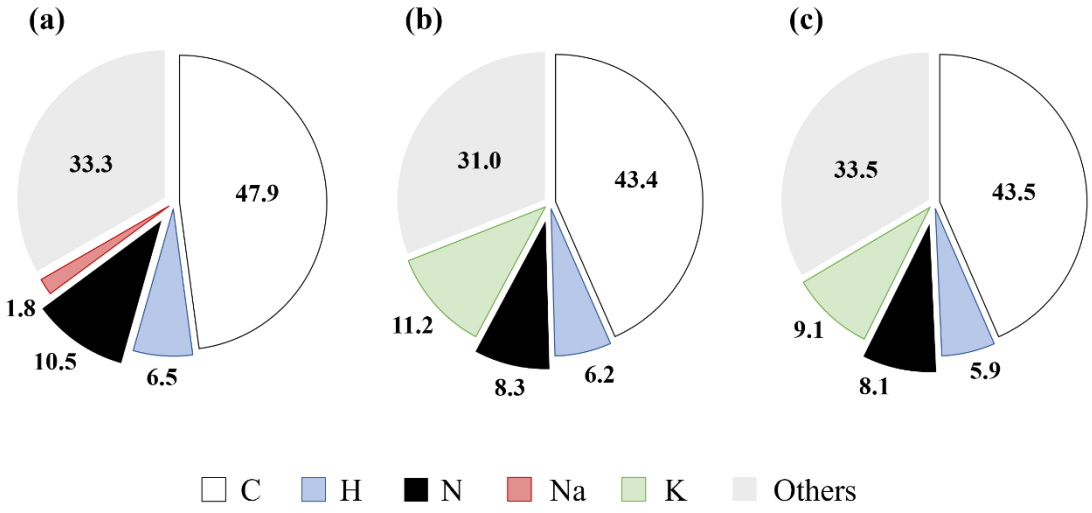

Figure 6 – Elemental composition of sEPS extracted according to different protocols (i.e., distinct chemical reagents): "*Reference*" **(a),** "*Agro 1*" **(b),** "*Agro 2*" **(c)**.

The calcium source used during the hydrogel-formation, i.e., $CaCl_2$, $Ca(NO_3)\cdot 4H_2O$ or $Ca(C_2H_5COO)_2$, affected the post-gelling elemental composition (**Figure 7**). Carbon, nitrogen, hydrogen, and calcium represented together 42.8, 30.0, 39.0, 28.0 and 32.7 wt% for sEPS hydrogels obtained with protocols "*Reference*", "*Agro 1a"*, "*Agro 1b"*, "*Agro 2a"*, "*Agro 2b"*. Both for sEPS and derived hydrogels, carbon was mostly organic (85.4 – 99.8 % of total carbon). The weight percentages of calcium ranged between 4 and 15 wt%, based on the calcium source adopted in the hydrogel-formation. sEPS hydrogels formed in presence of calcium propionate (i.e., protocols "*Agro 1b*" and "*Agro 2b*") evidenced a higher carbon content likely due to the diffusion of $C_2H_5COO^-$ ions into the polymeric matrix during the gel-formation. Conversely, the use of calcium nitrate as cross-linking agent (i.e., protocols "*Agro 1a*" and "*Agro 2a*") provided a higher nitrogen content in the resulting hydrogels as result of the NO_3^- ion diffusion into the three-dimensional polymeric network during the cross-linking reaction. Significant differences in terms of post-gelling elemental compositions were not detected among sEPS hydrogels obtained with the same cross-linker source but different extraction reagents. To be noticed that the chlorine content was significantly reduced by replacing the calcium source used in the hydrogel-formation processes compared to the reference method: Cl represented about 0.05 wt% in hydrogels formed in presence of $CaCl_2$ while for hydrogels

obtained using $Ca(NO_3)_2 \cdot 4H_2O$ and $Ca(C_2H_5COO)_2$ as cross-linking agent Cl accounted for about 0.01 wt%. This residual Cl content might be ascribed to that originally present in the AGS and not removed through the sEPS extraction and gelling processes.

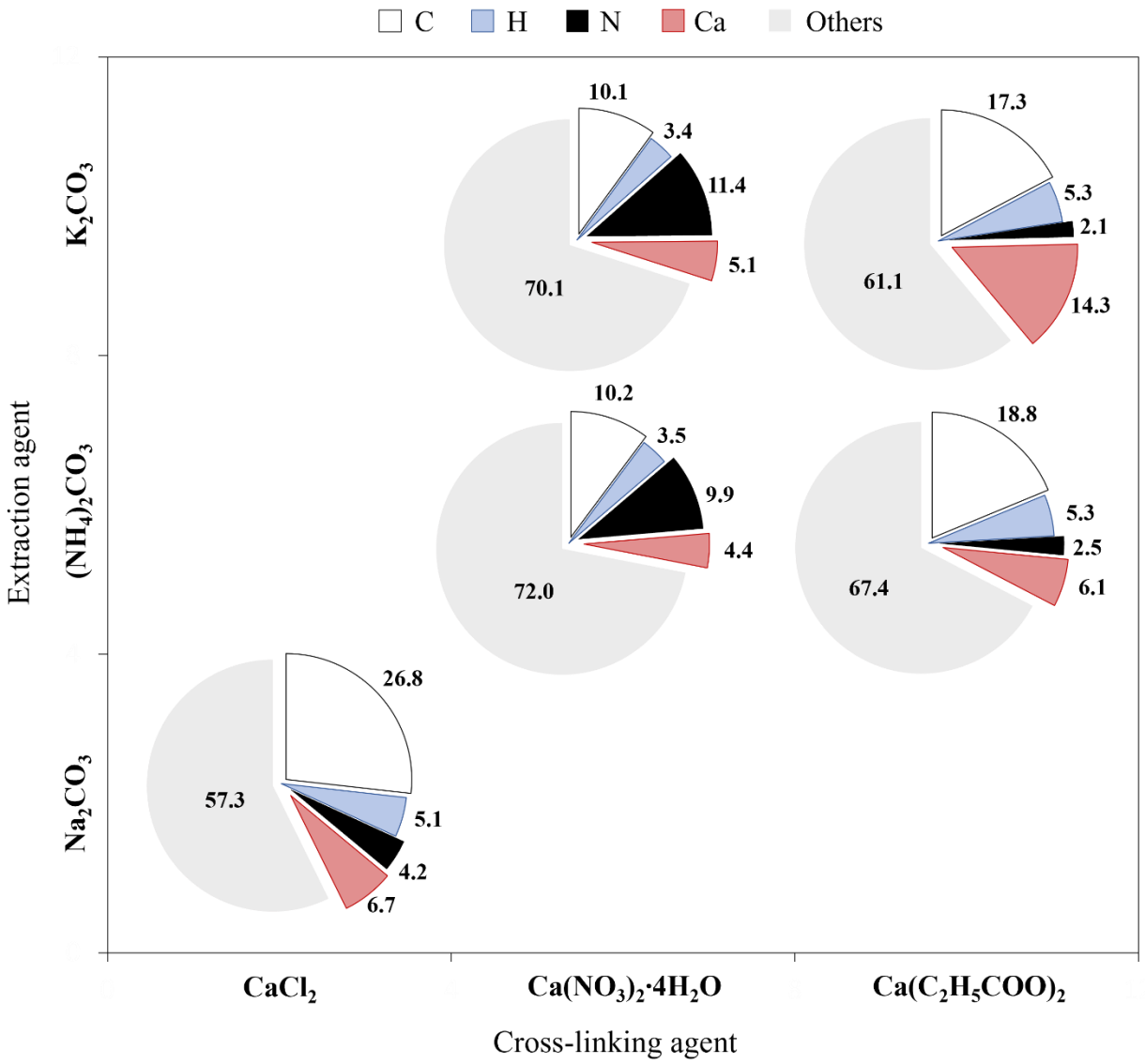

Figure 7 – Elemental composition of sEPS hydrogels obtained according to different extraction and hydrogel-forming protocols (i.e., using different chemical reagents).

The empirical formula reported below summarize the elemental composition of sEPS and sEPS hydrogels obtained according to reference and modified extraction and hydrogel-forming protocols. Heavy metals were not considered because of their low concentrations. The molar ratios are related to C-mol.

Reference

sEPS:

$C_1H_{1.620}N_{0.188}O_{0.461}Ca_{0.0004}Fe_{0.002}K_{0.0001}Mg_{0.0002}Na_{0.020}P_{0.005}S_{0.022}$

sEPS hydrogel:

$C_1H_{2.262}N_{0.134}O_{1.558}Ca_{0.075}Fe_{0.002}K_{0.0004}Mg_{0.0008}Na_{0.006}P_{0.005}S_{0.011}$

Agro 1

sEPS:

$C_1H_{1.702}N_{0.163}O_{0.412}Ca_{0.003}Fe_{0.006}K_{0.079}Mg_{0.001}Na_{0.002}P_{0.017}S_{0.029}$

sEPS hydrogel (Agro 1a):

$C_1H_{4.051}N_{0.972}O_{5.194}Ca_{0.152}Fe_{0.001}K_{0.0002}Mg_{0.0004}Na_{0.003}P_{0.002}S_{0.012}$

sEPS hydrogel (Agro 1b):

$C_1H_{3.636}N_{0.102}O_{2.576}Ca_{0.248}Fe_{0.004}K_{0.007}Mg_{0.0005}Na_{0.001}P_{0.010}S_{0.014}$

Agro 2

sEPS:

$C_1H_{1.604}N_{0.159}O_{0.490}Ca_{0.001}Fe_{0.003}K_{0.065}Mg_{0.0004}Na_{0.001}P_{0.008}S_{0.030}$

sEPS hydrogel (Agro 2a):

$C_1H_{4.118}N_{0.831}O_{5.224}Ca_{0.129}Fe_{0.002}K_{0.0017}Mg_{0.0014}Na_{0.003}P_{0.006}S_{0.017}$

sEPS hydrogel (Agro 2b):

$C_1H_{3.370}N_{0.112}O_{2.625}Ca_{0.098}Fe_{0.002}K_{0.006}Mg_{0.002}Na_{0.004}P_{0.006}S_{0.015}$

The nitrogen on carbon molar ratios were maintained almost constant between sEPS (0.159 – 0.188 molN/C-mol) and hydrogels (0.102 – 0.134 molN/C-mol) and close to literature data (0.139 molN/C-mol; Felz et al., 2019) using $CaCl_2$ and $Ca(C_2H_5COO)_2$ as cross-linking agents. Conversely, in agreement with what explained above, for hydrogels formed in presence of $Ca(NO_3)_2{\cdot}4H_2O$ the carbon on nitrogen molar ratio was higher compared to sEPS dispersions (0.831 – 0.972 molN/C-

mol). Regardless of the extraction and hydrogel-forming protocol applied, the calcium on carbon molar ratio significantly increased from sEPS to hydrogels, thus confirming the inclusion of calcium ions into the three-dimensional polymeric network during the cross-linking reaction (i.e., hydrogel formation). The sulfur on carbon molar ratio significantly decreased in hydrogels compared to sEPS (from 0.022 – 0.030 to 0.011 – 0.017 molS/C-mol). Indeed, sulphur accounted for about 2.8 – 3.4 wt% in sEPS and 0.3 – 0.8 wt% in hydrogels. The sulphur decrease in hydrogels could be associated to humic and fulvic acids releases (Morra et al., 1997), as suggested by the yellow-brown bulk coloration observed during the hydrogel-formation processes especially for high sEPS (weight) concentrations.

The influence of the various chemicals used in the extraction and gelling processes on the quality of the extractable sEPS and derived biomaterials (i.e., hydrogels) is highlighted in **Tables 2**, **3**, and **4**, reporting the elemental analysis and mineral composition (in ppm = mg/kg sEPS dry matter). A particular focus was dedicated to the (weight) concentrations of heavy metals that should be controlled in developing sEPS-based biomaterials to be valorized in agriculture. The current Italian legislation in matter of soil improvers and fertilizing products (D. Lgs. 75/2010) imposes limits in terms of heavy metal concentrations (expressed in ppm = mg/kg dry matter) that have been used in this study to assess the compatibility of the designed sEPS hydrogels with potential agronomic uses. The new European regulation laying down rules on the making available on the market of EU fertilizing products (Regulation (EU) 2019/1009), which will be implemented in Italy within 2022, slightly modifies the concentration limits of contaminants in the (organic) fertilizers/soil improvers: the content of heavy metals of the studied samples was therefore compared to these limits as well.

The origin of AGS (treating real municipal sewage) can explain the presence of various metals in the extracted sEPS. **Table A.2** in *Appendix* reports a detail characterization of the AGS used in this study, with particular attention to its metal content. In the WWTPs, metals can be significantly displaced from the final effluents as result of the partitioning from the liquid (i.e., influent) to the solid phase (i.e., sludge) of the treatment systems. Reasonably, large part of these metals can be adsorbed by the

extracellular biopolymeric matrix and therefore concentrated in the extracted sEPS (up to 5 times compared to pristine biomass, considering an extraction yield of about 20 wt%). The other metals are mainly present in the cells (e.g., adsorbed by granules via intracellular accumulation and/or cell wall sorption) and/or as metal precipitates within the granular biomass: consequently, their concentration in sEPS is lower than in pristine granules (or eventually close to zero). The content of heavy metals in sEPS varied depending on the extraction protocol applied. Particularly, the use of K_2CO_3 as chemical reagent for the EPS alkaline solubilization provided a higher accumulation of heavy metals (e.g., Cu, Ni, Zn) into the sEPS matrix with respect to protocols using Na_2CO_3 and $(NH_4)_2CO_3$. This evidence could suggest that the chemicals applied in the extraction protocol might affect the metal affinity of the extractable macromolecules, thus resulting in extracted sEPS with different qualitative properties. Moreover, different degrees of lysis and associated release of intracellular metals depending on the solvent applied could be potentially promoted.

As emerged from the mass balances (**Tables A.3**, **A.4** and **A.5** in *Appendix*), the mass of various elements (e.g., Na, K, Mg, P) was significantly reduced in hydrogels compared to sEPS dispersions, thus suggesting their potential release during the gelation processes and therefore the occurrence of ion exchange mechanisms in binding Ca upon formation of the extended cross-linked polymeric network. sEPS extracted and subjected to hydrogel-formation according to the reference methods mainly exchanged Na in binding Ca. Conversely, in the case of modified protocols for agronomic objectives, Ca was bound mainly exchanging K ions. The mass of heavy metals (e.g., Cu, Pb, Ni, Zn) did not change significantly during the hydrogel-formation processes, but their concentrations (in terms of $mg/kgTS_{sEPS}$) decreased in hydrogels compared to sEPS. To explain this evidence, it should be noticed that the formation of the cross-linked polymeric network resulted in increased total solid on wet weight ratios [gTS_{sEPS}/gWW_{sEPS}] compared to sEPS dispersions (**Tables 2**, **3**, and **4**): this could produce a dilution of various elements (e.g., metals) together with a reduction of the relative contents of volatile solids [gVS_{sEPS}/gTS_{sEPS}]. Indeed, during the hydrogel-formation processes, calcium ions (but also Cl^-, NO_3^-, $C_2H_5COO^-$, based on the salt used as calcium source) diffused into

the polymeric solution via dialysis: these ions could replace other elements naturally bound to sEPS through ion exchange mechanisms, form complexes with some sEPS functional groups and/or remain as free ions in the aqueous phase filled the space within the network (i.e., free water) thus increasing the relative content of inorganic fraction.

Overall, despite the chemicals applied, both sEPS and derived hydrogels presented relatively low contents of heavy metals which were within the maximum limits imposed by the current Italian and new European regulations in matter of fertilizing products. However, the values of Cr (which refer to total Cr detected by ICP-AES) cannot be compared with the maximum limits imposed by the above-mentioned regulations which are expressed in terms of Cr(VI). The two common oxidation states of Cr present in the environment are Cr(III) and Cr(VI): the relation between Cr(III) and Cr(VI) strongly depends on pH and oxidative properties of the location, but generally Cr(III) is the dominating species (Kotaś and Stasicka, 2000). Cr(VI) might be relevant in the case of industrial wastewaters from textile industry (Cirik et al., 2013). Even if a high content of Cr(VI) is not expected in the studied samples (especially considering the origin of AGS and wastewater treated), specific methods to assess the Cr speciation (Kotaś and Stasicka, 2000) both in sEPS and derived hydrogels might be implemented (e.g., spectrophotometric methods) to verify the overall conformity of the studied systems with the reference regulations.

Table 2 – Elemental composition of sEPS and related sEPS hydrogels obtained according to the reference methods (Felz et al., 2016). The content of nutrients is highlighted in green. The content of heavy metals is highlighted in red and compared to the maximum limits imposed by the current Italian legislation (D. Lgs. 75/2010) and by the European directive to be applied in 2022 (Regulation EU 2019/1009). All the concentrations (including the regulation limits) are expressed in ppm (= mg/kg dry weight where the dry weight, or TS, was evaluated upon sample dehydration at 215 °C).

Element	Unit	sEPS	sEPS hydrogel	D. Lgs. 75/2010	Regulation (EU) 2019/1009
C	**[ppm]**	478811	267688		
C_{org}	**[ppm]**	468617	240780		
H	**[ppm]**	65084	50799		
N	**[ppm]**	104901	41672		
S	**[ppm]**	28107	7607		
Ca	**[ppm]**	681	66776		

Fe	**[ppm]**	4098	2494		
K	**[ppm]**	163	341		
P	**[ppm]**	5547	3410		
Mg	**[ppm]**	146	457		
Mn	**[ppm]**	4.2	6.7		
Pb	**[ppm]**	11.5	3.3	**140**	**120**
Zn	**[ppm]**	96	115	**500**	**800**
Cr	**[ppm]**	6.4	4.5	**0.5** [1]	**2** [1]
Cu	**[ppm]**	173	114	**230**	**300**
Ni	**[ppm]**	9.8	14.7	**100**	**50**
Cd	**[ppm]**	< d. l.	< d. l.	1.5	1.5
Hg	**[ppm]**	< d. l.	< d. l.	1.5	1
Cl	**[ppm]**	8.6	466		
Na	**[ppm]**	18229	3055		
TS/WW	**[wt%]**	0.86 (1.50) [2]	2.01 (2.76) [2]		
VS/TS	**[wt%]**	71.4 (86.3) [2]	65.6 (75.0) [2]		

[1] Legislation limits are related to Cr(VI) while ICP-AES revealed in the studied samples the content of total Cr.
[2] Ratios obtained evaluating TS upon sample dehydration at 105 °C.

Table 3 – Elemental composition of sEPS extracted according to protocol "*Agro 1*" and related sEPS hydrogels formed in presence of $Ca(NO_3)_2 \cdot 4H_2O$ and $Ca(C_2H_5COO)_2$ as calcium sources (i.e., protocol "*Agro 1a*" and "*Agro 1b*", respectively). The content of nutrients is highlighted in green. The content of heavy metals is highlighted in red and compared to the maximum limits imposed by the current Italian legislation (D. Lgs. 75/2010) and by the European directive to be applied in 2022 (Regulation EU 2019/1009). All the concentrations (including the regulation limits) are expressed in ppm (= mg/kg dry weight where the dry weight, or TS, was evaluated upon sample dehydration at 215 °C).

Element	Unit	sEPS	sEPS hydrogel (1a)	sEPS hydrogel (1b)	D. Lgs. 75/2010	Regulation (EU) 2019/1009
C	**[ppm]**	433879	100500	172811		
TOC	**[ppm]**	433499	100383	160313		
H	**[ppm]**	61971	34158	52718		
N	**[ppm]**	82481	113918	20496		
S	**[ppm]**	33918	3333	6411		
Ca	**[ppm]**	3870	50922	142934		
Fe	**[ppm]**	12713	446	2901		
K	**[ppm]**	112110	61	3974		
P	**[ppm]**	18468	609	4222		
Mg	**[ppm]**	870	82	170		
Mn	**[ppm]**	19	1.2	5.6		

Pb	**[ppm]**	29	3.5	9.9	**140**	**120**
Zn	**[ppm]**	148	0.6	9.9	**500**	**800**
Cr	**[ppm]**	18.2	0.8	9.2	**0.5** [1]	**2** [1]
Cu	**[ppm]**	524	20	136	**230**	**300**
Ni	**[ppm]**	35	2.6	13.8	**100**	**50**
Cd	**[ppm]**	< d. l.	< d. l.	< d. l.	1.5	1.5
Hg	**[ppm]**	< d. l.	< d. l.	< d. l.	1.5	1
Cl	**[ppm]**	6.6	136	118		
Na	**[ppm]**	1609	546	330		
TS/WW	**[wt%]**	0.60 (1.53) [2]	4.62 (5.32) [2]	3.52 (4.45) [2]		
VS/TS	**[wt%]**	72.4	67.4 (71.7) [2]	68.4 (75.0) [2]		

[1] Legislation limits are related to Cr(VI) while ICP-AES revealed in the studied samples the content of total Cr.
[2] Ratios obtained evaluating TS upon sample dehydration at 105 °C.

Table 4 – Elemental composition of sEPS extracted according to protocol "*Agro 2*" and related sEPS hydrogels formed in presence of $Ca(NO_3)_2{\cdot}4H_2O$ and $Ca(C_2H_5COO)_2$ as calcium sources (i.e., protocol "*Agro 2a*" and "*Agro 2b*", respectively). The content of nutrients is highlighted in green. The content of heavy metals is highlighted in red and compared to the maximum limits imposed by the current Italian legislation (D. Lgs. 75/2010) and by the European directive to be applied in 2022 (Regulation EU 2019/1009). All the concentrations (including the regulation limits) are expressed in ppm (= mg/kg dry weight where the dry weight, or TS, was evaluated upon sample dehydration at 215 °C).

Element	Unit	sEPS	sEPS hydrogel (2a)	sEPS hydrogel (2b)	D. Lgs. 75/2010	Regulation (EU) 2019/1009
C	**[ppm]**	434474	102164	187641		
TOC	**[ppm]**	434324	101933	160313		
H	**[ppm]**	58472	35306	53057		
N	**[ppm]**	80701	98974	24512		
S	**[ppm]**	34254	4567	7245		
Ca	**[ppm]**	1894	44006	61161		
Fe	**[ppm]**	5298	1059	1821		
K	**[ppm]**	91265	577	3517		
P	**[ppm]**	8601	1518	2846		
Mg	**[ppm]**	389	294	641		
Mn	**[ppm]**	7.4	2.7	6.2		
Pb	**[ppm]**	12.6	3.9	3.3	**140**	**120**
Zn	**[ppm]**	83.4	71.4	32.1	**500**	**800**
Cr	**[ppm]**	9.2	2.5	3.9	**0.5** [1]	**2** [1]
Cu	**[ppm]**	220	44	85	**230**	**300**
Ni	**[ppm]**	22.3	5.4	17.5	**100**	**50**

Cd	**[ppm]**	< d. l.	< d. l.	< d. l.	**1.5**	**1.5**
Hg	**[ppm]**	< d. l.	< d. l.	< d. l.	**1.5**	**1**
Cl	**[ppm]**	5.0	129	181		
Na	**[ppm]**	981	487	1267		
TS/WW	**[wt%]**	0.61 (1.50) [2]	2.19 (3.21) [2]	3.04 (4.41) [2]		
VS/TS	**[wt%]**	76.9 (81.1) [2]	61.8 (67.5) [2]	64.5 (75.6) [2]		

[1] Legislation limits are related to Cr(VI) while ICP-AES revealed in the studied samples the content of total Cr.
[2] Ratios obtained evaluating TS upon sample dehydration at 105 °C.

The successful implementation of sEPS-based practices in agriculture is not only subordinated to a reduced content of heavy metals but also to significant quantities of nutrients: indeed, nutrient deficiency affects the root growth and morphology, leading to much finer roots (Breckle, 1991).

The use of K_2CO_3 or $(NH_4)_2CO_3$, HNO_3 and KOH in the extraction process favored an enrichment in nutrients of sEPS with respect to the reference method: indeed, N, K, P together accounted for 11.1, 21.3, 18.1wt% in sEPS extracted with protocols "*Reference*", "*Agro 1*" and "*Agro 2*", respectively (the minimum limit imposed by the EU Regulation 2019/1009 for $K + P_2O_5 + K_2O$ is 3 wt%). The quality of the extractable sEPS (in terms of elemental composition) might be hence enhanced playing with the chemicals used in the extraction processes: particularly, the solvents here used proved to be a viable option in the case of sEPS-based biomaterials for agronomic purposes. On the other side, the nutrient content (especially in terms of P and K) was significantly reduced upon cross-linking for the reason described above (the sum N + K + P accounted for 4.5, 11.5, 2.9, 10.1 and 3.1 wt% for hydrogels from protocols "*Reference*", "*Agro 1a*", "*Agro 1b*", "*Agro 2a*" and "*Agro 2b*", respectively). Further processes for the nutrient enrichment might be therefore encouraged to ensure the hydrogel effectiveness in agriculture-related applications. Another aspect to be controlled is related to the mutual ratios among various elements, such as macronutrients and micronutrients, whose optimum values depend on the type of designed application. By way of example, in **Table 5** the levels of various macronutrients (e.g., N, K, P, Ca, Mg) broadly adopted in the case of reference substrates for plant growth (Murasnige and Skoog, 1962) have been compared to those of sEPS-based hydrogels obtained with agronomy-oriented protocols. With respect to the *optimum* medium, despite

the quantity of each element, sEPS hydrogels appeared unbalanced: a prevalent content of N and Ca with respect to K, P and Mg was observed. A potential strategy to control the levels of macronutrients (P, K, N, Mg, Ca) in the sEPS hydrogels could be to play with the composition of the (ionic) cross-linker aqueous solution, for instance providing multiple divalent metal ions (e.g., Ca^{2+} and Mg^{2+}) potentially able to simultaneously contribute to the formation of the extended 3D polymeric network. Indeed, as demonstrated in **Chapter 2** and confirmed by literature data (Felz et al., 2020a), various divalent metals can be used as (ionic) cross-linking agents: the polymer affinity towards these metals results in hydrogels with different levels of elasticity. Criteria leading to the choice of the cross-linker aqueous solutions might be therefore found in a balance between mechanical and compositional properties. The occurrence of competition phenomena for the available sEPS active sites among distinct monovalent and/or divalent metal ions simultaneously present in the cross-linker solution could result in a decreased hydrogel-forming ability: these phenomena should be hence addressed looking for the optimum aqueous medium composition which does not compromise the resulting hydrogel mechanics and stability.

Table 5 – Levels of macronutrients in typical substrates for plant growth and in sEPS-based hydrogels obtained with agronomy-oriented protocols.

		Reference medium	**sEPS-based hydrogels**			
		(Murasnige and Skoog, 1962)	*Agro 1a*	*Agro 1b*	*Agro 2a*	*Agro 2b*
N/K	[mol/mol]	3	5214	14.40	478.84	19.46
P/K	[mol/mol]	0.06	12.61	1.34	3.32	1.02
Mg/K	[mol/mol]	0.075	2.16	0.07	0.82	0.29
Ca/K	[mol/mol]	0.170	814.42	35.09	74.40	16.96

3.3 Swelling ability of sEPS-based hydrogels

The dehydration kinetics (50 °C) of sEPS-based hydrogels obtained by means of distinct chemicals in the preparation processes are depicted in **Figure 8**. To be considered that all hydrogels were derived from polymeric dispersions containing about 3 wt% sEPS; the effective sEPS (weight) concentrations

upon cross-linking were the following: 3.6, 5.4, 4.7, 5.1 and 6.0 wt% for protocols "*Reference*", "*Agro 1a*", "*Agro 1b*", "*Agro 2a*", and "*Agro 2b*", respectively. Regardless of the extraction and hydrogel-forming protocol applied, the weight loss over time was kinetically characterized by two parts: an initial step of fast dehydration within 60 – 200 minutes and an asymptotical process towards equilibrium. Hence, a single theoretical model did not allow an accurate simulation of the experimental data: the initial dehydration process was satisfactorily represented by linear regression (R^2 = 0.995 – 0.996).

Despite the chemical reagents used in the extraction phase, sEPS hydrogels formed in presence of $Ca(NO_3)_2 \cdot 4H_2O$ (i.e., protocols "*Agro 1a*" and "*Agro 2a*") featured slower dehydration kinetics compared to those obtained with $Ca(C_2H_5COO)_2$ as cross-linking agent (i.e., protocols "*Agro 1b*" and "*Agro 2b*") and reference method. It should be considered that slight differences in the sample initial (wet) weight and geometry could also affect kinetic aspects. Once achieved the maximum dehydration state, the relative percentage dehydration (RPD) ranged between 96.4 – 98.3% depending on the extraction and hydrogel-forming protocols applied (**Table 6**).

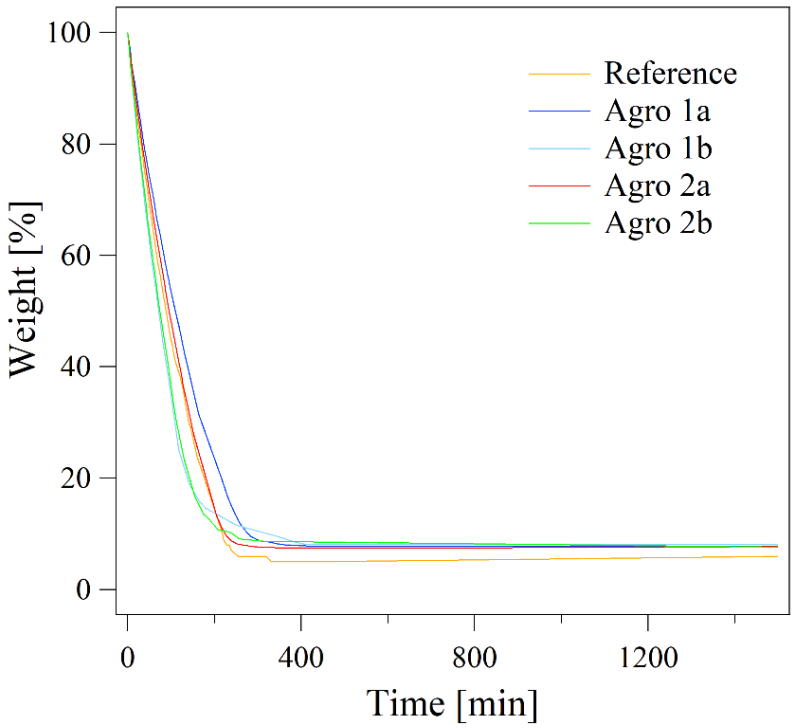

Figure 8 – Dehydration (50 °C) kinetics of sEPS hydrogels obtained according to different protocols.

Table 6 – Results of dehydration studies (at 50 °C) performed on sEPS hydrogels obtained according to different protocols. The initial dehydration rates were interfered from the linear regression of the initial part (with high slope) of the dehydration kinetics in **Figure 8** (related to the initial step of fast dehydration). RPD [%] represents the Relative Percentage Dehydration achieved upon sample dehydration at 50 °C (corresponding to the maximum dehydration state reached at 50 °C).

	RPD [%]	**Initial dehydration rate** [wt% · min^{-1}]
Reference	98.3	0.53
Agro 1a	97.5	0.45
Agro 1b	96.4	0.72
Agro 2a	97.5	0.50
Agro 2b	97.2	0.64

The 50°C-dried sEPS hydrogels were able to partially recover their original structure and geometry upon swelling in ultrapure water (**Figure 9**). More detailed, 50 °C-dried sEPS hydrogels obtained according to protocols "*Reference*", "*Agro 1a*", "*Agro 1b*", "*Agro 2a*", and "*Agro 2b*" recovered about 85.5, 93.3, 85.3, 90.6, and 75.8% of their original weight (i.e., wet weight) once swelling equilibrium was achieved. The dehydration – swelling process was not therefore completely reversible, likely due to partial collapse of the hydrogel structure.

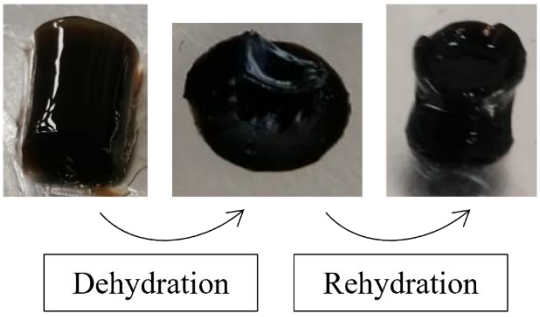

Figure 9 – Appearance of sEPS hydrogels upon dehydration (50 °C) and subsequent rehydration in ultrapure water (i.e., swelling).

Overall, 50°C-dried sEPS hydrogels derived from protocols "*Reference*", "*Agro 1a*", "*Agro 1b*", "*Agro 2a*", and "*Agro 2b*" were able to sorb (and hold) up to 15.58, 15.82, 13.76, 16.25 and 11.35 g H_2O per g $TS_{Hydrogel}$, respectively. Regardless of the extraction agents, the use of $Ca(NO_3)_2{\cdot}4H_2O$ (i.e., protocols "*Agro 1a*" and "*Agro 2a*") instead of $Ca(C_2H_5COO)_2$ (i.e., protocols "*Agro 1b*" and "*Agro 2b*") as calcium source during the cross-linking reaction seemed to promote greater swelling

performance, similar to those observed for the reference method (**Table 7**). In this sense it could be observed that the concentration of elastically effective chains could affect the amount of water taken up by sEPS hydrogels: expansion of the polymer network by osmotic influx of water is indeed resisted by the elastically effective chains. Hence, weakly cross-linked polymers swell to a larger extent than strongly cross-linked polymers (Seviour et al., 2009a). The use of $Ca(C_2H_5COO)_2$ as cross-linking agent favored higher calcium contents in the resulting hydrogels. Reasonably, a larger number of calcium ions diffused into the polymeric matrix, thus participating in the formation of the extended three-dimensional polymeric network. This could result in a higher cross-linking density and therefore reduced swelling performance of the resulting hydrogels compared to those obtained with protocols using $CaCl_2$ and $Ca(NO_3)_2 \cdot 4H_2O$. Moreover, it should be considered that the extraction and cross-linking protocols applied (and hence the chemicals used) could affect various sEPS post-gelling properties like pore volume, complex porosity structure and specific surface area, thus reflecting changes in their water-holding capacity. These considerations are not the object of this dissertation, but they should be assessed in the future for a deeper molecular-level understanding of the swelling behaviour of sEPS-based hydrogels.

To be noticed that the equilibrium water content (EWC) of sEPS-based hydrogels resulted slightly higher compared to that observed for pristine AGS (i.e., 88 – 90% at pH < 9.7, Seviour et al., 2009a). It could be reasonably speculated that the water-holding ability of granules is strongly promoted by the (gelling) extracellular biopolymeric matrix: however, the sEPS extraction and cross-linking with calcium would result in greater water-holding capacity.

Table 7 – Results of swelling studies performed on sEPS hydrogels. The swelling ratios are related to the weight of hydrogel dehydrated at 50 °C. EWC [%] represents the equilibrium water content.

	Equilibrium swelling ratio	**EWC**
	[g/g]	**[wt%]**
Reference	10.62	91.4

Agro 1a	11.00	91.7
Agro 1b	9.54	90.5
Agro 2a	11.07	92.2
Agro 2b	8.93	89.9

An understanding of swelling kinetics is useful to predict the water uptake: to this aim, **Figure 10** shows the experimental swelling kinetics and the related fits via Elovich model related to sEPS hydrogels obtained according to different protocols. Besides the quality of the extracted sEPS and derived hydrogels, similar swelling mechanisms might be postulated. Indeed, based on the statistical indicators reported in **Table 8** that compares the kinetics parameters obtained for the three evaluated theoretical models, the experimental kinetic data was accurately simulated by Elovich model. The Elovich model has been widely applied to describe chemisorption processes being based on a general second-order reaction mechanism for heterogeneous adsorption (Zhou et al., 2014). This model assumes that the solute adsorption rate decreases exponentially as the amount of adsorbed solute increases (Kajjumba et al., 2018). Chemisorption mechanisms on heterogenous surfaces resulting in different kinds of active sites (i.e., with different activation energies) might be therefore speculated to explain the water uptake by 50°C-dried sEPS hydrogels. The increase in swelling ratio was kinetically characterized by two parts: an initial step of fast rehydration within 60 – 90 minutes of contact time (based on the extraction and gel-forming protocol applied) and an asymptotical process towards swelling equilibrium. Reasonably, sEPS hydrogels are rich in hydrophilic groups able to adsorb water molecules, allowing the network to expand. Once swollen, the network behaves like a semi-permeable membrane, regulating the passage of fluid in and out of the network according to osmotic gradient (Blanco et al., 2004; Seviour et al., 2008). Larger is the osmotic pressure difference between the internal structure and the external solution, faster is the water adsorption: for this reason, sEPS hydrogels showed a higher swelling rate in the initial swelling progress. As the swelling continued, more water molecules diffused into the network and progressively decreased the osmotic pressure difference. Consequently to the continuous overcoming of the osmotic pressure inside the

hydrogels, the swelling rate became smaller, and the swelling ability finally achieved the equilibrium (Feng et al., 2016). Quantitative information can be interfered from the Elovich model parameters listed in **Table 8**. The initial sorption rates represented by α values were higher for hydrogels obtained with reference method and using $Ca(NO_3)_2 \cdot 4H_2O$ instead of $Ca(C_2H_5COO)_2$ as calcium source. The lower values of Elovich constant β (related to the adsorbate layer on the adsorbent surface as well as to the activation energy of chemisorption processes, Vieria et al., 2020) for hydrogels formed in presence of $CaCl_2$ and $Ca(NO_3)_2 \cdot 4H_2O$ could suggest more significant water-sEPS interactions, and hence a higher number of chemical bonds between water molecules and sEPS active groups, in the hydrogel network (Zhou et al., 2014).

Interestingly, for alginate gels (formed in presence of Ca^{2+}) a pseudo-second-order model has been reported to well-simulate their swelling kinetics (Wang et al., 2018, Davidovich-Pinhas and Bianco-Peled, 2009): this model assumes that the solute adsorption rate is proportional to the available sites on the adsorbent (i.e., the reaction rate is dependent on the amount of solute on the surface of the adsorbent) (Kajjumba et al., 2018). Differences in the swelling behaviour of sEPS and alginate hydrogels could be hence predicted.

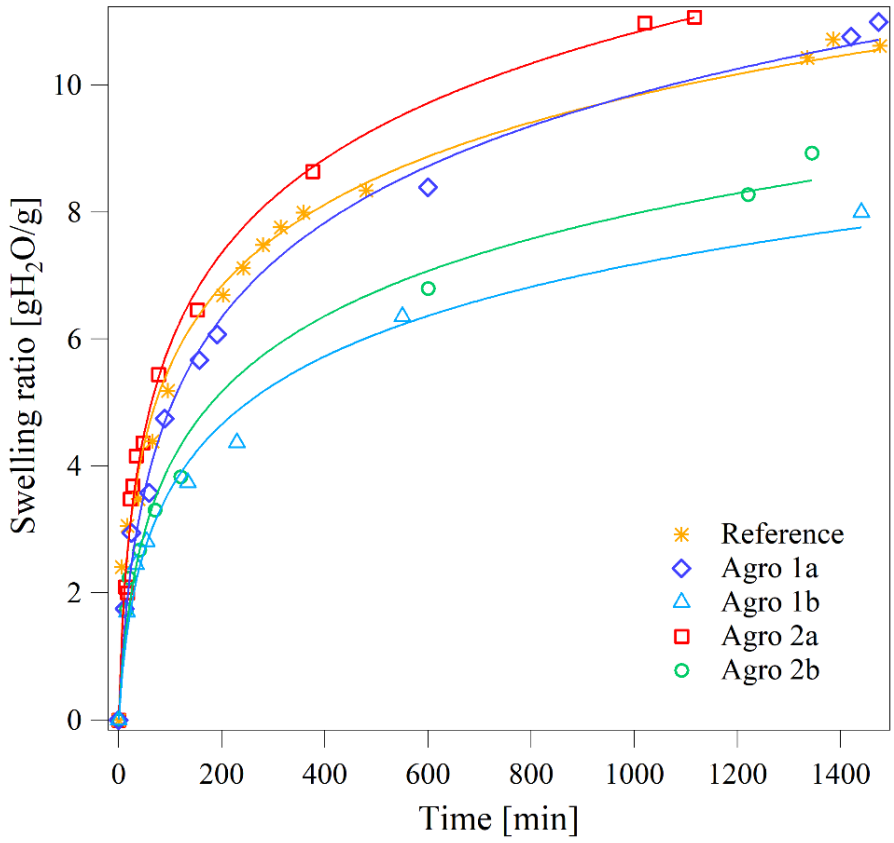

Figure 10 – Experimental swelling kinetics in ultrapure water of sEPS hydrogels obtained according to different protocols and related fits via Elovich model. The swelling ratios are related to the weight of hydrogel dehydrated at 50 °C.

Table 8 – Kinetic model parameters and statistical indicators related to the swelling of 3 wt% sEPS hydrogels in ultrapure water.

	Model	Parameters		R
Reference	Pseudo-first-order	$q_{e=}$ 10.39 g/g	k_1 = 0.006 min^{-1}	0.966
	Pseudo-second-order	q_e = 10.45 g/g	k_2 = 0.001 min^{-1}	0.978
	Elovich	**α = 0.349 min^{-1}**	**β = 0.533 g/g**	**0.993**
Agro 1a	Pseudo-first-order	$q_{e=}$ 10.73 g/g	k_1 = 0.006 min^{-1}	0.966
	Pseudo-second-order	q_e = 11.32 g/g	k_2 = 0.001 min^{-1}	0.978
	Elovich	**α = 0.184 min^{-1}**	**β = 0.452 g/g**	**0.993**
Agro 1b	Pseudo-first-order	$q_{e=}$ 8.65 g/g	k_1 = 0.004 min^{-1}	0.983
	Pseudo-second-order	q_e = 9.56 g/g	k_2 = 0.001 min^{-1}	0.988
	Elovich	**α = 0.107 min^{-1}**	**β = 0.525 g/g**	**0.993**
Agro 2a	Pseudo-first-order	$q_{e=}$ 9.95 g/g	k_1 = 0.012 min^{-1}	0.966
	Pseudo-second-order	q_e = 11.12 g/g	k_2 = 0.001 min^{-1}	0.978
	Elovich	**α = 0.304 min^{-1}**	**β = 0.456 g/g**	**0.993**
Agro 2b	Pseudo-first-order	$q_{e=}$ 8.53 g/g	k_1 = 0.007 min^{-1}	0.983
	Pseudo-second-order	q_e = 9.34 g/g	k_2 = 0.001 min^{-1}	0.988

	Elovich	**$\alpha = 0.152$ min^{-1}**	**$\beta = 0.536$ g/g**	**0.993**

According to the results here presented, sEPS hydrogels behaved like SAPs (*Superabsorbent Polymers*). Indeed, SAP hydrogels can be defined as lightly crosslinked three-dimensional polymer networks, whose property of major interest is the capability of swelling in presence of aqueous or biological fluids (Ullah et al., 2015). The cross-linking density results in an expressive amount of free volume within the polymeric network, which in turn, combined to the presence of an extensive number of hydrophilic groups, can absorb and hold large quantity of water, on the order of 10 to 1000 g/g (Milani et al., 2017; Zohuriaan-Mehr et al., 2010). SAPs are getting emerging interest for agricultural processes, especially if used as soil conditioners (i.e., for improving the water retention of soil matrixes) as alternative to continuous irrigation systems: SAPs are indeed able to swell and hold aqueous solutions, maintaining the humidity of the soil for longer periods. In this perspective, sEPS hydrogels (able to hold more than 10 g/g of water) could be studied as cost-effective and environmentally friendly alternative to more conventional petroleum-based polymers like polyacrylate-based SAPs considered as potentially pollutant for soils due to their low degradation rate (Cannazza et al., 2014; Orts et al., 2000).

3.4 sEPS-based hydrogels as carrier systems for nutrient loading and release

In the previous paragraphs, it was demonstrated that the studied sEPS hydrogels did not present high content of toxic elements (e.g., Na, Cl, heavy metals); moreover, they were able to adsorb and hold significative amount of water behaving like SAP hydrogels. Together these features could suggest their feasible application in agriculture. On the other side, sEPS hydrogels appeared poor in nutrients: for example, large part of potassium was exchanged with calcium during the cross-linking reaction. A strategy to enhance the hydrogel nutrient content might be found in exploiting their ability to swell in aqueous phase: enriching the bulk medium in nutrients, their diffusion/adsorption in the hydrogel could be favoured upon swelling. By way of example, here the results related to the swelling of sEPS hydrogels (containing about 5.2 – 6.0 wt% sEPS) in KNO_3 aqueous solutions are presented.

$Ca(NO_3)_2 \cdot 4H_2O$ was chosen as calcium source in the hydrogel-formation being able to promote higher nitrogen content (up to 11.4 wt%) in the hydrogel matrix, regardless of the chemicals used in the sEPS extraction procedure.

As depicted in **Figure 11**, the swelling kinetic data were well simulated by Elovich model (see statistical indicators in **Table 9**), thus suggesting chemisorption mechanisms on heterogenous surfaces resulting in different kinds of active sites (i.e., with different activation energies). The results agreed those observed in the case of the water uptake over time, thus resulting in similar mechanisms regardless of the bulk medium composition (at least under the tested conditions). However, sEPS hydrogels evidenced swelling performance in K_2NO_3 slightly lower compared to those observed in ultrapure water (equilibrium swelling ratio = 7.44 – 6.83 g H_2O per g 50°C-dried hydrogel; EWC = 88.2 – 87.2% for hydrogels "*Agro 1a*" and "*Agro 1b*", respectively). As interfered from the Elovich model parameters (**Table 9**), decreased initial sorption rates α were observed compared to those evidenced in ultrapure water; moreover, the higher values of constant β suggested lower water-hydrogel interactions. Indeed, the water absorbency decrease of ionic hydrogels in presence of saline solutions is a known phenomenon in literature: this swelling loss, with increases upon increasing the ionic strength of the surrounding medium, can mainly ascribed to a reduced osmotic pressure between the gel and the aqueous phase and/or to an increased cross-linking density due to presence of multivalent metal ion in the swelling solution (Feng et al., 2016; Liu et al., 2011; Mirdarikvande et al., 2014). The hydrogel sensitivity to various surrounding media is therefore expected to be different based on the nature of the monovalent and/or multivalent cations present. For instance, Feng et al. (2016) observed that monovalent metal cations with larger radius (e.g., $K^+ > Na^+$) lead to greater water absorbency by chitosan/yeast hydrogel beads.

Despite the described swelling loss, sEPS hydrogels seemed to favor a greater biochemical stability in KNO_3 aqueous solutions with respect to that evidenced in ultrapure water, as suggested by a qualitative observation (data not shown): the lower osmotic gradient between the bulk medium and

the core of the hydrogel matrix could hinder the (ionic) cross-linker release in aqueous phase, thus preserving the hydrogel structure.

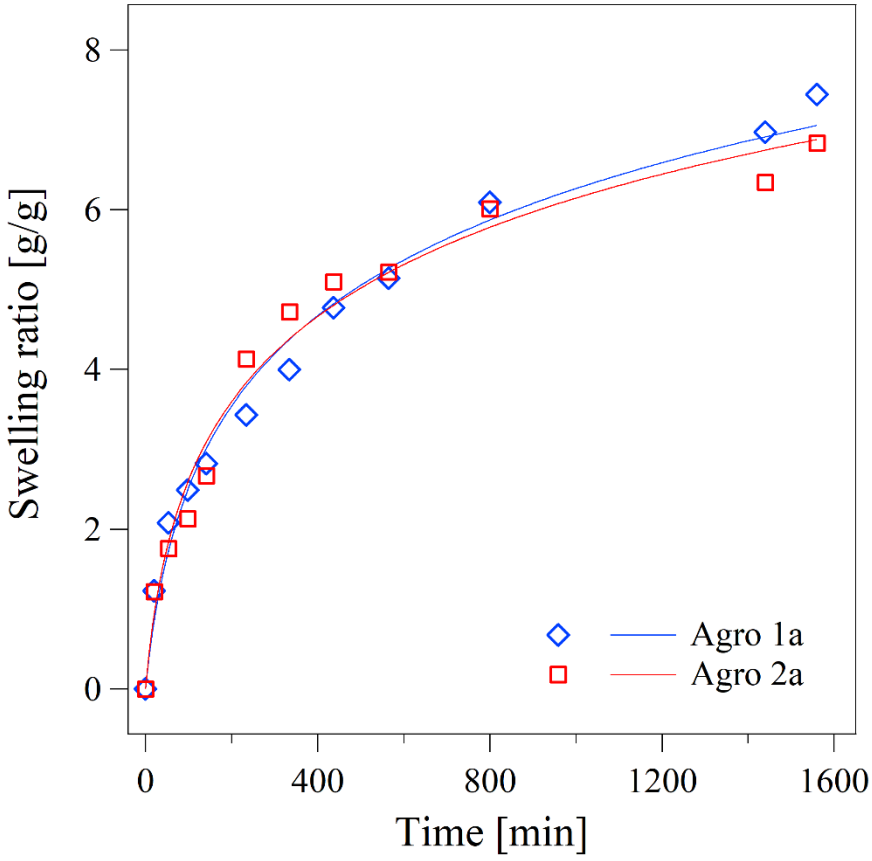

Figure 11 – Experimental swelling kinetics in 2 % (w/v) KNO_3 aqueous solution of sEPS hydrogels obtained according to different protocols and related fits via Elovich model. The swelling ratios are related to the weight of hydrogel dehydrated at 50 °C.

Table 9 – Kinetic model parameters and statistical indicators related to the swelling of 3 wt% sEPS hydrogels in KNO_3 aqueous solutions.

	Model	**Parameters**		**R**
Agro 1a	Pseudo-first-order	$q_{e=}$ 7.03 g/g	k_1 = 0.003 min^{-1}	0.974
	Pseudo-second-order	q_e = 8.22 g/g	k_2 = 0.0004 min^{-1}	0.979
	Elovich	**α = 0.054 min^{-1}**	**β = 0.546 g/g**	**0.987**
Agro 2a	Pseudo-first-order	$q_{e=}$ 9.95 g/g	k_1 = 0.012 min^{-1}	0.966
	Pseudo-second-order	q_e = 11.12 g/g	k_2 = 0.001 min^{-1}	0.978
	Elovich	**α = 0.064 min^{-1}**	**β = 0.456 g/g**	**0.981**

Figure 12 illustrates the expected experimental and theoretical kinetics of nutrient loading (deducted from the swelling kinetics in **Figure 11,** based on critical assumption that each gram of water

adsorbed by the 50 °C-dried sEPS hydrogels had the same initial concentration of 0.2 M KNO_3. Indeed, this hypothesis presents some biases: hydrogels might reasonably have a certain affinity towards nutrients (e.g., potassium) which could lead to a higher uptake with respect to that theoretically speculated; moreover, part of the potassium and nitrate originally present in the hydrogels could be released during the swelling experiments (to equilibrate the osmotic pressure difference with the external bulk medium). Hence, it is not possible to accurately predict the nutrient loading kinetics and equilibrium capacities without implementing a proper mass balance. In this sense, both the hydrogel and the liquid bulk should be analyzed after swelling through analytical techniques (e.g., ICP-AES, ion chromatography, etc.) to shed light on the effective percentage of nutrient loading. Being aware of the limits of above-explained critical assumption, 50 °C-dried sEPS hydrogels would be able to sorb upon swelling in nutrient-loaded aqueous solutions up to 1.350 – 1.472 mmol of $KNO_3/gTS_{Hydrogel}$ (i.e., 52.8 – 57.6 $mgK/gTS_{Hydrogel}$ and 83.7 – 91.3 $mgNO_3/gTS_{Hydrogel}$) depending on the gelling protocol applied. Overall, swelling in nutrient-loaded aqueous solutions could be reasonably suggest as strategy to control the elemental composition of the sEPS-based hydrogels. Playing with the aqueous medium composition, it might be therefore possible to load multiple elements into the hydrogel matrix upon swelling (e.g., Mg, P, etc.) as a function of the specific applicative goals. In this since, the performance stability under distinct ionic strength conditions and the selectivity in presence of elements with different (positive) charges should be investigated to shed light on the feasible application of these processes.

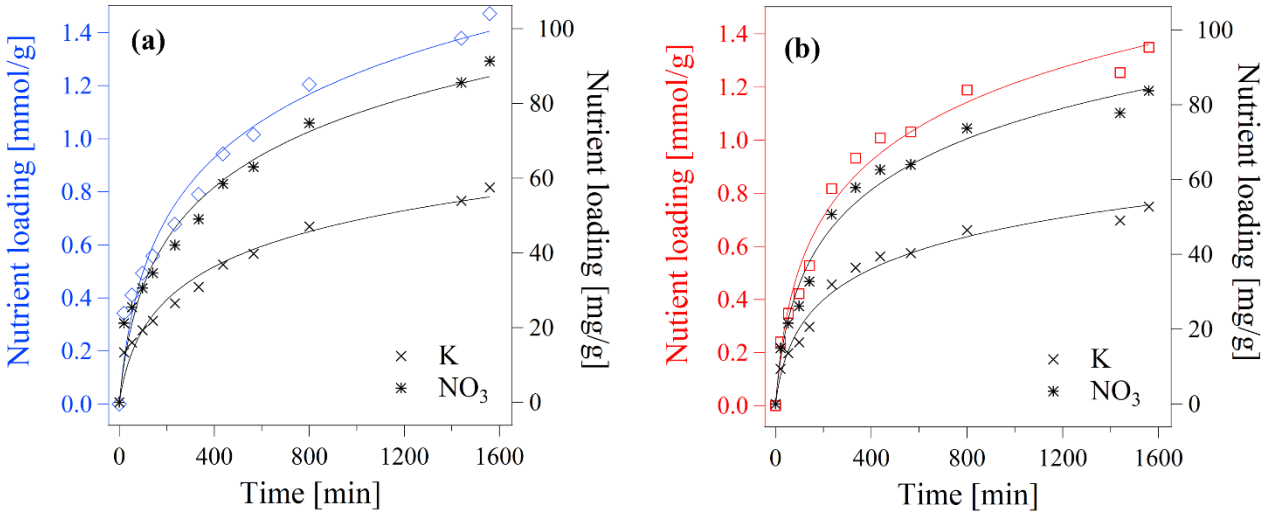

Figure 12 – Expected nutrient loading kinetics upon swelling in 0.2 M KNO_3 of 50°C-dried sEPS hydrogels obtained with protocols "*Agro 1a*" **(a)** and "*Agro 1b*" **(b)**. The nutrient loading is expressed as mmolKNO_3/g$TS_{Hydrogel}$ on the left Y-axis and as mgK^+, NO_3^-/g$TS_{Hydrogel}$ on the right Y-axis.

Once enriched in nutrients, sEPS hydrogels could be more properly applied in agriculture-related applications as soil improvers and/or as coating agent for fertilizing products to control the nutrient release kinetics in soil. A preliminary proof-of-principle of the nutrient (e.g., K) release capacity of (swollen) KNO_3-loaded sEPS is given in **Figure 13**. It might be seen that the K-enriched sEPS hydrogels were able to release in the surrounding medium (i.e., ultrapure water) up to 0.123 – 0.142 mmol K per g $TS_{Hydrogels}$ within one hour of contact time without losing their structural integrity: this amount slightly decreased in the following hours likely due to the partial potassium re-adsorption by the hydrogel itself (**Figure 13a**). Being aware of the critical assumption on the effective loading percentage, the K-enriched sEPS hydrogels would release in the liquid bulk up to 109 – 124% of the potassium loaded in the hydrogels upon swelling in KNO_3 within one hour: the values higher that 100% might be due to (i) underestimation of the loaded K and/or (ii) release of K originally present in the hydrogel. This release percentage decreased down to 91.9 – 111.4% within 8 hours of contact time depending on the extraction/gelling protocol applied (**Figure 13b**).

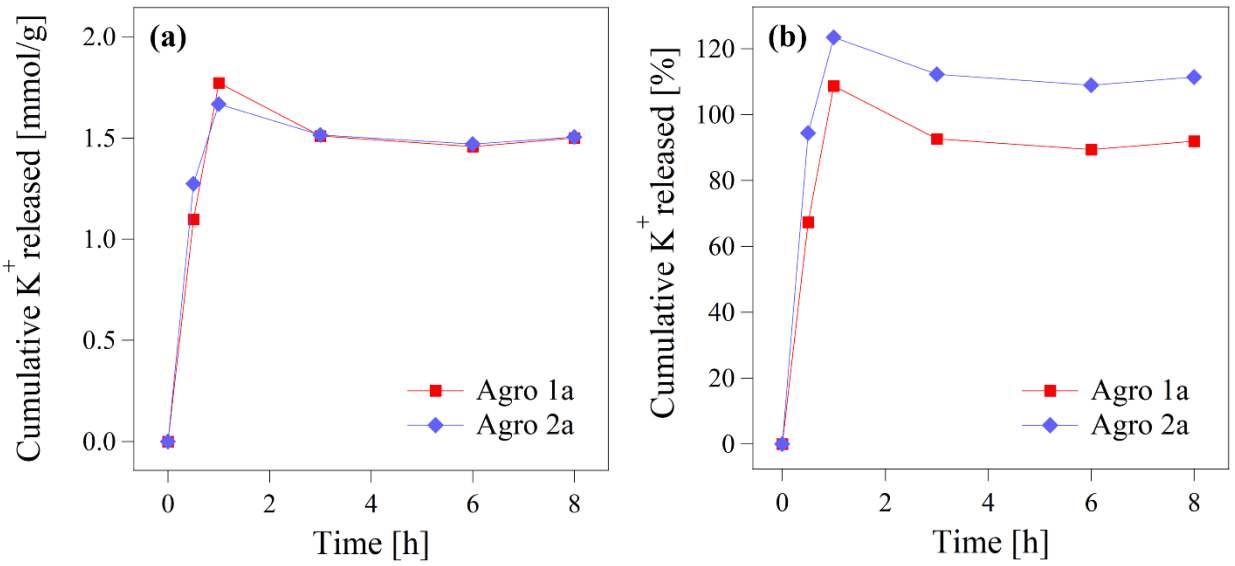

Figure 13 – Cumulative K^+ released in the surrounding medium (i.e., ultrapure water) by (swollen) K-enriched sEPS hydrogels in terms of mmol K per g $TS_{Hydrogel}$ **(a)** and percentage amount of K^+ released with respect to that loaded in the hydrogel upon swelling in KNO_3 **(b)**.

Overall, these results suggested that sEPS hydrogels can be used as carrier systems for nutrient loading and release. The stability performance in soil remains to be investigated: indeed, this research field appears so comprehensive due to the wide range of variables involved such as temperature, soil type, hydrogel physic-chemical properties and hence future work is encouraged to shed light on these aspects. In addition to nutrients, it may be interesting to address the feasibility of loading organic macromolecules (e.g., phytostimulants) in the hydrogels, thus evaluating their viable application as carrier for the delivery/controlled-release of agrochemicals in soil.

3.5 Biodegradability of sEPS and derived hydrogels

The values of total Chemical Oxygen Demand (COD) of the studied substrates (i.e., sEPS and related hydrogels) are reported in **Table 10**. In the case of protocols "*Agro 1*" and "*Agro 2*", $Ca(NO_3)_2 \cdot 4H_2O$ was used as (ionic) cross-linker source for the hydrogel-formation. For the soluble COD assessment, samples (i.e., sEPS dispersions and sEPS hydrogels mechanically disintegrated with potter) were previously filtered at 0.1 µm pore size: the resulting COD partitioning in terms of soluble and particulate fractions (sCOD and pCOD, respectively) is displayed in **Figure 14**. sEPS extracted according to the refence method evidenced a higher sCOD portion compared to those obtained with

the other protocols. With this regard, it could be observed that the chemicals applied during the sEPS extraction/recovery processes might affect the solubility of the carbonaceous fractions of the extractable macromolecules (and more in general their particle size and molecular weight distribution). The relative percentage of sCOD decreased upon cross-linking except for sEPS hydrogels obtained according to protocol "*Agro 1a*": based on the calcium source used as (ionic) cross-linker agent, the solubility of the carbonaceous fractions could be reduced as result of their inclusion into an extended 3D polymeric network. However, it should be highlighted that the measured sCOD could be overestimated, especially in the case of polymeric dispersions, due to the potentially presence of colloidal particles not removable by filtering at 0.1 µm pore size. Generally, soluble constituents are defined as possessing a characteristic dimension less than 1 nm, while colloidal particles are defined as having a characteristic dimension between 1 nm and 1 mm (Hu et al., 2002). To be more precise in the sCOD assessment, the colloidal fraction should be therefore estimated (e.g., by means of clariflocculation experiments and/or physic-chemical techniques like Dynamic Light Scattering, DLS). The sample pre-treatment via filtration also influences the evaluation of the readily biodegradable substrate fractions assimilated to the soluble biodegradable COD (sbCOD). Indeed, the physical separation (e.g., filtration) has been widely reported for determining the rapidly biodegradable COD, with the assumption that this fraction is soluble and consists of small molecules (Spérandio and Paul, 2000). However, this method results highly influenced by the filter pore size and sample pre-treatment. The soluble molecules should reach the inside of the cell by passing through the transmembrane pores. Hence, a typical internal pore diameter for the sCOD assessment should be as small as 0.001 µm (Hu et al., 2002). However, using tiny pore size filters accompanies practical issues, including rapid clogging: 0.45 and 0.1 µm pore size filters are therefore commonly used (Borzooei et al., 2021). In this study, a balance between practical concerns and assessment precision (in terms of sCOD and corresponding sbCOD and siCOD sub-fractions) has been found in the hypothesis according to which the soluble organic matter was considered having particle size lower than 0.1 µm.

Table 10 – Total COD [gCOD/gVS$_{sEPS}$] of sEPS dispersions and hydrogels obtained according to different protocols.

		COD [gCOD/gVS$_{sEPS}$]
Reference	*sEPS*	1.89 ± 0.04
	Hydrogel	0.77 ± 0.00
Agro 1	*sEPS*	1.54 ± 0.08
	Hydrogel	0.39 ± 0.00
Agro 1	*sEPS*	1.99 ± 0.17
	Hydrogel	0.36 ± 0.00

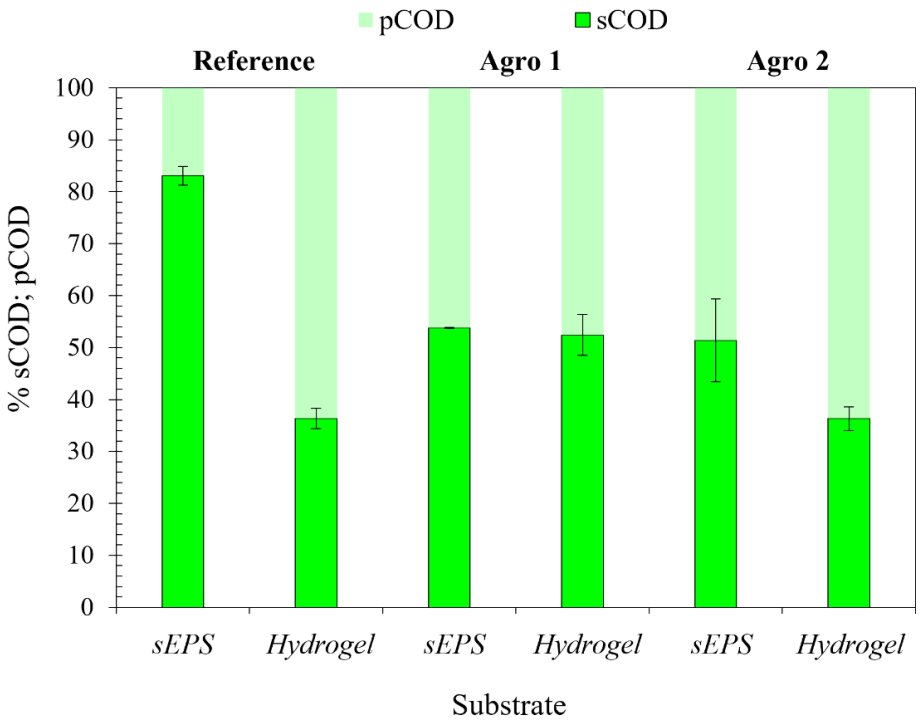

Figure 14 – COD (percentage) fractionation in soluble COD (sCOD) and particulate COD (pCOD) for all the studied substrates (i.e., sEPS and related hydrogels).

Combining the results of respirometric experiments (i.e., multiple- and single-OUR tests) the carbonaceous substrate fractions were characterized in terms of both COD biodegradability and removal kinetics. In the following dissertation, sEPS and derived hydrogels were compared in order to shed light on the effect of the gelling process on the overall sEPS macromolecule biodegradation.

To elucidate the role of the chemicals used in both extraction and hydrogel-forming phases, the reference methods were compared to protocols "*Agro1*".

Multiple-OUR experiments gave a first assessment of the overall biodegradability of the treated substrates. The obtained OUR profiles over time are given in **Figure 15**. To be noticed that the experiments were carried out in series, which means that the biomass concentration in the reactor varied test by test due to the sample addition. Moreover, a foam (likely due to proteins) sometimes formed upon substrate addition and a low content of biomass was loss (remaining attached on the reactor head). These aspects could explain the distinct endogenous OUR values obtained during the different experiments. To be more precise, the exact biomass concentration in the reactor should be calculated before each respirometric test.

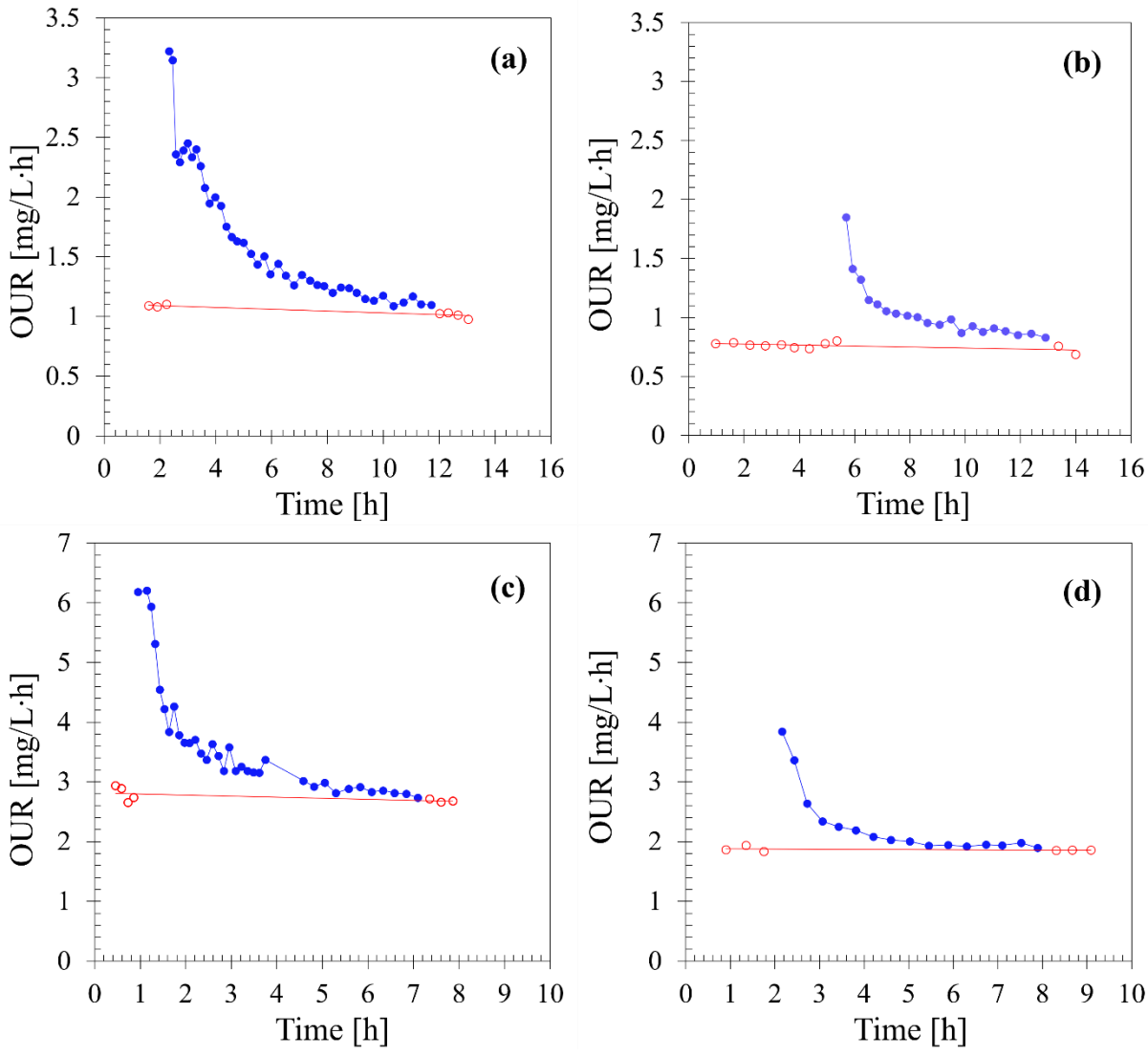

Figure 15 – OUR profiles emerged from multiple-OUR tests performed on pristine substrates: sEPS and hydrogels obtained according to reference methods (**a**, **b**, respectively) and sEPS and derived hydrogels from protocol "*Agro 1*" (**c**, **d**, respectively). The blue markers are related to the exogenous respiration, while the red markers (and corresponding linear regressions) indicated the OUR profile associated with the endogenous respiration.

The relative low F/M ratio selected in these experiments (0.025 $gCOD/gCOD_x$) resulted in the fast utilization of the biodegradable substrate in a period ranging between 1 - 6 hours depending on the sEPS extraction and hydrogel-forming protocols applied. For all the investigated systems, with respect to the endogenous respiration profile, the OUR values notably increased upon substrate addition, depending on the amount of available readily biodegradable fractions, and then decreased due to the utilization of the biodegradable organic matter: after complete depletion of the readily biodegradable substances, the mild decline in OUR values was associated to the utilization of the slowly biodegradable fractions which needed hydrolysis to be processed (pbCOD).

Single-OUR tests were performed on 0.1 µm filtered substrates to address the sbCOD fraction. The obtained DO profiles (**Figure 16**) evidenced a significative increase of their slope upon substrate addition with respect to the endogenous respiration curve. In the case of sEPS dispersions, when the readily biodegradable fractions (RBCOD) were completely depleted, the slop variation before returning to the endogenous respiration profile could be likely to the utilization of the readily hydrolysable fractions (RHCOD) (Borzooei et al., 2021). The complete utilization of sbCOD (i.e., RBCOD + RHCOD) occurred within 30 min. Conversely, in the case of sEPS hydrogels, after utilization of the readily biodegradable fractions (RBCOD), a significant slope variation due to the RHCOD depletion was not appreciated, thus suggesting that the soluble biodegradable COD was mainly constituted by RBCOD that could be utilized within maximum 10 minutes. As visible in **Figure 16** (**b, d**), the slope variation of the DO profile upon substrate addition was not so easily appreciable for hydrogels as in the case of sEPS dispersions, thus giving a preliminary suggestion of their lower sbCOD fraction. However, the low F/M applied (0.025 $gCOD/gCOD_x$) could result in a too fast substrate utilization, thus not allowing to accurately appreciate a significative slope variation of the DO profile with respect to the endogenous respiration. Particularly, the kinetics of endogenous

respiration might be too high with respect to the applied F/M and the degradation kinetics of the sbCOD in question. To better elucidate such concern, these tests could be repeated at higher F/M values, thus improving the measurement precision, and keeping biomass under prolonged starvation before sample dosage in order to better appreciate the extent of both exogenous and endogenous respiration kinetics. To be noticed that the implementation of an accurate method for distinguishing between the oxygen consumption associated with the use of rapidly or slowly biodegradable substrate fractions requires an optimal F/M ratio, greatly dependent on origin and characteristics of the substrate and biomass, which needs to be determined by trial and error (Ekama et al., 1986; Paul and Sperandio, 2000). As previously mentioned, these experiments mainly aimed to give a preliminary assessment of the influence of various factors (i.e., chemicals applied, hydrogel-formation processes) on the overall sEPS biodegradation: further work is currently ongoing to strengthen as much as possible the outcome derivable from these measurements (e.g., optimization of the experimental set-up, biomass pre-treatment and F/M ratio, etc.).

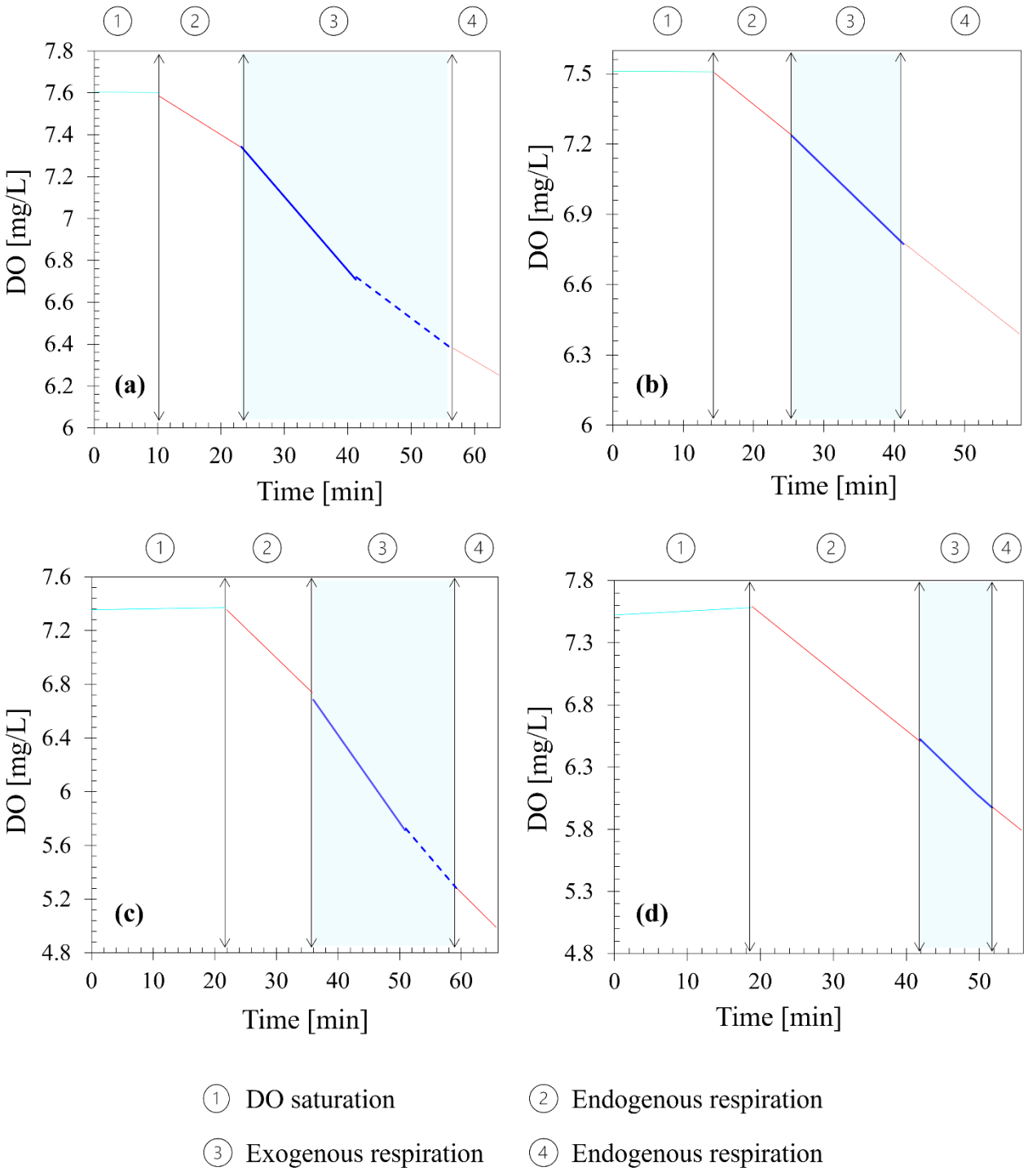

Figure 16 – DO profiles emerged from single-OUR tests performed on 0.1 µm filtered substrates: sEPS and hydrogels obtained according to reference methods (**a**, **b**, respectively) and sEPS and hydrogels from protocol "*Agro 1*" (**c**, **d**, respectively).

The results described above were further analyzed to quantify the COD fractions (i.e., sbCOD, pbCOD, siCOD and piCOD) as percentages with respect to the total COD of the treated substrates (**Figure 17**).

In the case of sEPS dispersions, the biodegradable fraction of the total COD (bCOD) accounted for about 32% regardless of the extraction protocol applied. This would suggest that the overall biodegradability of the recoverable sEPS macromolecules was not significantly affected by the chemicals used in the extraction phase. The hydrogel-formation evidenced an important effect on the COD biodegradability and removal kinetics based on the (ionic) cross-linking agent applied. Concerning the samples obtained according to the reference methods, the bCOD decreased from 31.50 to 13.02% upon hydrogel-formation. The higher chlorine content of hydrogels formed with reference method using of $CaCl_2$ as cross-linking agent (about 5 times higher per gram of dry matter to that observed in sEPS-based hydrogels obtained with agronomy-oriented protocols) could promote an inhibiting effect on the substrate biodegradation. Indeed, it has been reported that high salinity and/or shocks due to high chloride concentrations might have adverse effects on the organic removal efficiency: this appears dependent on the biomass acclimatation and levels of salts involved (Hamoda and Al-Attar, 1995). For instance, Pernetti and Di Palma (2005) observed respiration inhibition for specific salt (NaCl) concentrations ranging between 0.37 and 30.7 g/g_{VSS}. Hence, with the dosage of the hydrogels formed with the reference method, a Cl "shock-load" ($\simeq$ 120 $mgCl^-/L_{mixed\ liquor;}$ $\simeq$ 122 gCl^-/g_{VSS}) was introduced in the reactor with respect to agro-based hydrogels, that could reasonably suggest a more significant adverse effect on the microbial activity.

Conversely, the biodegradability of the sEPS macromolecules seemed to be better preserved upon hydrogel-formation by using $Ca(NO_3)_2{\cdot}4H_2O$ as (ionic) cross-linker source (bCOD = 32.5 and 22.2% for sEPS dispersions and hydrogels, respectively).

Despite the extraction and gelling protocols applied, the bCOD partitioning in terms of sbCOD and piCOD significantly varied upon hydrogel-formation, evidencing a considerable reduction of the readily biodegradable fractions. The bCOD of sEPS extracted according to the reference method was composed by 52.87% of sbCOD which decreased down to 18.48% upon hydrogel-formation. Conversely, in the case of sEPS obtained with protocol "*Agro 1*", the sbCOD accounted for 36.68% of bCOD, thus highlighting the predominance of slowly biodegradable fractions (pbCOD) with

respect to those extractable with the reference method, and decreased to 26.04% of bCOD in the related hydrogels. The cross-linking improved the polymer chain entanglement upon formation of an extended three-dimensional polymeric network in which the biodegradable macromolecules resulted more confined. With this regard, even if the overall biodegradability was not significantly reduced (i.e., the nature of network constituents was the same that in aqueous phase), the accessibility of the substrate carbonaceous fractions might be decreased: consequently, cross-linked sEPS could need to be further processed (into low-molecular weight compounds) via hydrolysis before microbial utilization.

The effect of the chemicals applied in the extraction and gelling processes was considerably highlighted also in terms of inert COD (iCOD) composition. The iCOD of sEPS from reference method mainly consisted of soluble inert fractions (siCOD) which significantly decreased upon hydrogel-formation. Conversely, in the case of protocol "*Agro 1*", the siCOD accounted for about 60% of the non-biodegradable fractions both in sEPS dispersions and hydrogels.

Overall, the described results confirmed that AGS-derived sEPS can be used as substrate from the heterogeneous microbial communities inhabiting the activated sludge. Zhang and Bishop (2003) suggested that the biodegradability of biofilm-derived EPS by activated sludge occurs through a process involving four distinctive phases: (1) instantaneous increase of carbohydrate and protein concentrations in the tested medium upon EPS addition; (2) microbial utilization of the easily biodegradable EPS; (3) microbial production of further soluble EPS, using the slowly biodegradable EPS left from the previously added EPS; (4) consumption of the newly produced EPS by cells until the microbial activity gradually stops.

To the best of our knowledge, the literature concerning the AGS-derived sEPS biodegradability is still scarce; particularly, studies identifying the various sEPS carbonaceous fractions through COD partitioning are currently missing. This lack of knowledge as well as the high-complexity and diversity characterizing the sEPS matrix makes challenging the identification of a target substrate to be used as reference. Comparing the results of COD fractionation to those emerged from literature

data for municipal and/or industrial wastewater and/or other complex substrates widely characterized with these techniques (e.g., landfill leachate, food additives, etc., Mainardis et al., 2021) could be misleading given the high diversity of the considered substrates. Indeed, the biochemical composition of organic matter (both in terms of particle size distribution and macromolecule nature) in municipal and/or industrial wastewater could appear largely different to that of sEPS. Regardless of the origin of the microbial aggregates, the extractable EPS are mainly composed by macromolecular compounds with a large broad molecular weight (MW) distribution, typically from low MW (< 3 kDa) to high MW (> 235 kDa) (Feng et al., 2021). It has been demonstrated that proteins and polysaccharides accounts for the majority of the organics in the microbial EPS (Dubé and Guiot, 2019; More et al., 2014b): particularly, AGS-derived sEPS in this study evidenced a higher content of PN-like substances with respect to PS (PN/PS = 3.88 – 4.58% as a function of the extraction protocol applied). Overall, multiple compounds have been reported as constituents of the complex AGS-derived sEPS matrix: neutral sugars, amino sugars, PN, uronic acids, polyphenolic compounds, glycoconjugates, humic acids, nucleic acids, etc. (Felz et al., 2020b, 2019; Flemming and Wingender, 2010). Consequently, the high-diversity and complexity of the extractable extracellular biopolymeric matrix might be not reflected in wastewater of various origins. For instance, Morgenroth et al. (2002) reported the following typical composition for municipal sewage: 8 - 28% of proteins, 6 -18% of carbohydrates, 10 – 31% of lipids and 22 – 70% of other compounds.

Polymer microbial degradation depends on the extracellular depolymerization followed by cellular uptake and subsequent metabolization (Chróst, 1991). The most effective depolymerization reactions are catalyzed by the process of enzymatic hydrolysis (and only a few through lyase reactions) (Morgenroth et al., 2002). The microbial degradation of polysaccharides entails diverse glycoside hydrolases with different specificities and modes of action (Warren, 1996). Protein hydrolysis by various enzymes (e.g., protease) generates a mixture of free amino acids and oligopeptides. Zhang and Bishop (2003) observed that carbohydrates of biofilm-derived EPS can be used by microrganisms faster than proteins. We can reasonably speculate that neutral sugars could be more easily assimilated

by microbial cells compared to uronic acids and heteropolysaccharides like glycosaminoglycans recently detected in both AGS and derived sEPS (Felz et al., 2020b). However, without specific biological investigations, it is not possible to gain insights on the specific degradation kinetics of the various sEPS macromolecules and so we need to limit to speculative considerations.

In summary, despite the sample filtration at 0.1 µm, large part of the sEPS organic compounds should be processed via enzymatic hydrolysis to be converted into low molecular weight compounds (e.g., peptides, monosaccharides, disaccharides, etc.) before cell uptake and metabolization and it could be therefore assimilated to slowly biodegradable carbonaceous fractions. It's worth to say that the relative rapid multiple-OUR tests could not allow to address the long-term behaviour of complex macromolecules present in AGS-derived sEPS (even if the endogenous respiration seemed to be achieved after substrate depletion), thus underestimating their overall biodegradability. Indeed, as previously explained, the relative low F/M applied in these experiments could result in a too fast substrate utilization thus not allowing to appreciate the microbial utilization of very slowly biodegradable organic compounds (e.g., complex high-molecular weight macromolecules and/or by-products resulting from hydrolysis). Integrating these measurements with long-term carbonaceous BOD test could help to better elucidate such concern. An interesting consideration is that, even if depolymerization into low molecular weight compounds is expected to be crucial in the sEPS microbial utilization, the sbCOD was found to be in the range suggested from literature data for diluted municipal wastewater (10.0 – 41.5% of the total COD, Borzooei et al., 2021) at least for sEPS before (ionic) cross-linking. This would suggest the presence of a class of organic compounds (e.g., neutral sugars) that could be readily assimilated by microrganisms similarly to what happens for municipal sewage.

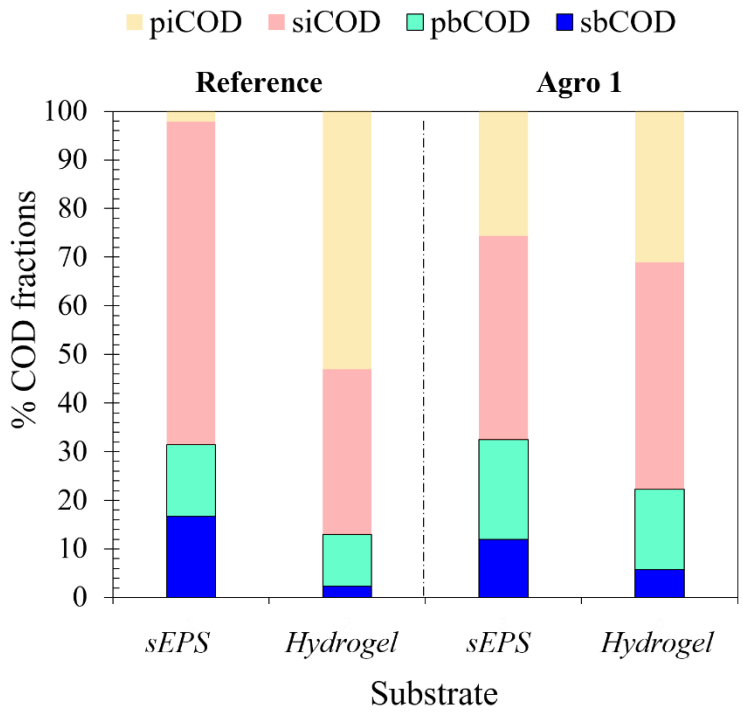

Figure 17 – COD (percentage) fractionation in terms of soluble biodegradable COD (sbCOD), particulate biodegradable COD (pbCOD), soluble inert COD (siCOD) and particulate inert COD (piCOD) for all the studied substrates (i.e., sEPS and related hydrogels).

Selecting agriculture as target sector for the here described sEPS-based biomaterials, the biodegradability assessment plays a crucial role. On one side, an adequate stability of biopolymer-based products in soils is desired providing for a mid-term or long-term functionality of the materials. On the other hand, the protection of soil, ground and/or freshwater resources from contaminant accumulation and/or toxic loads has to be respected in compliance with the stringent normative limits: this makes the biodegradability a crucial aspect in designing biopolymer-based materials for agronomic purposes. Particularly, releases of waste non-biodegradable residues causing soil contamination should be avoided and all the degradation products should be hence included into the natural material cycles (Passauer et al., 2015). Biodegradation in soil involves several key steps that could be reasonably reproposed by using an inoculum of activated sludge: (i) colonization of the polymer surface by microorganisms, (ii) secretion of extracellular microbial enzymes that depolymerize the polymer into low–molecular weight compounds, and (iii) microbial uptake and utilization of these compounds, incorporating polymer carbon into biomass or releasing it as CO_2

(Zumstein et al., 2018). However, the biodegradation processes and kinetics could be highly different as result of the different microbial environment and conditions and hence these results have not to be interpreted as absolute values of biodegradability. In this perspective, the respirometric techniques broadly applied for the wastewater characterization has been chosen in this study (and consequently adapted based on the specific research goals) to give a preliminary assessment of the sEPS microbial utilization under aerobic conditions highlighting the effect of multiple factors (e.g., hydrogel-formation and quality of the target products directly influenced by the chemicals selected in the design phase). With this regard, the results emerged have to be mainly seen according to a comparative approach able to draw speculative conclusions concerning the biodegradation of the treated samples under the tested conditions and the effect of the chemicals used during extraction/recovery protocols. The main findings, supporting the development of sEPS-based biomaterials for sustainable agronomic practices, can be summarized as follows. The formation of an extended 3D polymeric network upon (ionic) cross-linking seemed to kinetically vary the sEPS biodegradable carbonaceous fractions removal, requiring further processes (e.g., hydrolysis) before their microbial utilization. The chemicals used in the sEPS extraction and gelling protocols have proved to be important factors influencing the substrate COD biodegradation: this would remark that the choose of the reagents to be applied during the sEPS-based biomaterial preparation should be driven by criteria strictly connected to the target quality also in terms of biodegradability imposed by the specific application sector. To strengthen the outcome of respirometry, sEPS and derived hydrogels might be compared to well-known gelling biopolymers and/or SAPs (e.g., alginate, cellulose, etc.): the analysis of model polymers would allow to demonstrate the method robustness and validate the conclusions regarding the protective effect of the networked structure upon cross-linking. These experiments are still ongoing.

3.6 Outlook and perspectives

Figure 18 schematically summarizes the approach proposed in the present contribution to progress towards new resource recovery-oriented solutions in agriculture able to contribute to a more circular economy-based wastewater treatment sector: the key actors are the extractable sEPS and their derived biomaterials (e.g., hydrogels). The above-presented dissertation emphasized the importance to address the influence of the overall production/valorization process on the resulting properties of the obtained sEPS-based biomaterials. Particularly, the qualitative standards imposed by the agronomic sector have been selected as general criteria for a comprehensive analysis on AGS-derived sEPS and their potential exploitation. It has been proved that the quality of sEPS and derived bioproducts (e.g., hydrogels) might tuned playing with the chemicals used in the extraction and gelling processes, thus leading to biomaterials in compliance with the increasingly legislative pressure in matter of environment protection. Particularly, the here studied sEPS and derived hydrogels respected the maximum limits in terms of heavy metals imposed by the new European directive (Regulation (EU) 2019/1009) laying down rules on the making available on the market of fertilizing products (to be verified the levels of Cr(VI)). Moreover, the capability of sEPS-based hydrogels to sorb and desorb large amounts of water and/or nutrients behaving like SAPs would suggest their potential application in agriculture for soil conditioning. To be noticed that in Annex II of the above-mentioned European regulation, among the Constituent Material Categories (CMC), there is an item relating to "*polymers other than nutrient polymers*" (CMC 9): "*a fertilizing product can consist of polymers (other than nutrient polymers) whose purpose is to control the water penetration into nutrient particles and thus the release of nutrients (in which case the polymer is commonly referred to as a "coating agent") and/or to increase the water retention capacity or wettability of a fertilizing product*". All the results described above suggested the potential valorization of sEPS and/or derivate biomaterials (e.g., hydrogels) as constituents of fertilizing products according to the item CMC 9 of the Regulation (EU) 2019/1009. The biodegradability and phytotoxicity assessment should be pivotal in follow up research to assess the compatibility of the here studied waste-derived biopolymers with the mentioned

legislation and, in general, to open new resource recovery-oriented solutions for sustainable agro-practices. Particularly, according to the EU regulation, polymers consisting of a fertilizing product should be able to undergo physical and biological decomposition in natural soil conditions and aquatic environments, being ultimately decomposed only into carbon dioxide, biomass, and water. Moreover, they should have at least 90% of the organic carbon converted into carbon dioxide in a maximum period of 48 months after the end of the claimed functionality period of the fertilizing product indicated on the label, and as compared to an appropriate standard in the biodegradation test. Many regulations in matter of microbial soil respiration might be adapted to gather information on the biodegradation in soil of sEPS-based biomaterials (e.g., UNI EN ISO 16072:2002), as reported in literature for hydrogel-like materials (Passauer et al., 2015). Particularly, this International Standard describes the methods to determine the microbial respiration of (aerobic, unsaturated) soils through the evaluation of the O_2 uptake or CO_2 release, either after the addition of a substrate like nutrients, soil improvers, etc. (*substrate-induced respiration*) or without substrate addition (*basal respiration*). Many measuring systems might be implemented: (i) determination of O_2 consumption by static incubation in a pressure-compensation system, (ii) determination of CO_2 release by titration in a static system, (iii) colorimetric determination of CO_2 release in a static system, (iv) determination of CO_2 release using an infrared gas analyzer in a flow-through system, (v) determination of CO_2 release using gas chromatography in a flow-through system and a static system, (vi) determination of soil respiration by pressure measurement in a static system. Each method has its own advantages and disadvantages, that should be critically assessed based on the investigation goals: for instance, the systems for the CO_2 measurement do not distinguish between CO_2 released from microbial activities and CO_2 resulting from abiotic processes (which could be considerable in the case of alkaline soils and/or soils with a high organic matter content). Alternatively, the degradation of SAPs in soil might assessed by monitoring their dry weight loss over time (Ni et al, 2010).

The above-mentioned Regulation (EU) 1009/2019 rule also the phytotoxicity assessment for fertilizing products and bio-stimulants (Annex II, CMC 9). The environmental (e.g., soils, sediments)

and anthropogenic (e.g., compost, sewage sludge) matrix toxicity have been reported to be due to various inorganic (e.g., heavy metals) and organic (e.g., polycyclic aromatic hydrocarbons, PAHs) pollutants present in the matrix itself (Oleszczuk, 2008). While a reduced content of inorganic contaminants was demonstrated in the present study both for sEPS and derived biomaterials (e.g., hydrogels), the potential phytotoxic effect of various macromolecules and organic compounds (e.g., PAHs) remains to be investigated. A preliminary assessment of the sEPS and derived hydrogel phytotoxicity might be performed by means of commercial toxicity bioassay (e.g., Phytotoxkit microbiotest), that measures the decrease (or the absence) of seed germination and root growth after 3 days of exposure of the seeds to the contaminated matrix in comparison to the controls in a reference soil (Oleszczuk, 2008). Similar tests to address the seed germination and root growth on the developed sEPS-based substrates can be performed with reference to various European directives (e.g., UNI EN 16086-1, UNI EN 16086-2).

From an applicative point of view, various solutions might be implemented in agriculture to exploit the outstanding features of sEPS-based hydrogels. The recovered sEPS could be directly applied in soil in the form of aqueous dispersions (eventually enriched in nutrients and/or other agrochemicals): the hydrogel-formation could occur in situ thanks to the metal ions naturally present in soils. On the other hand, the hydrogel-formation could be engineered by means of appropriate chemicals and the resulting products might be homogenously distributed on soil (for instance in the form nutrient-loaded hydrogel beads) and/or used as coating agents for fertilizers to control the nutrients release kinetics. Both these options should be experimentally addressed in follow up research and characterized in terms of treatment effectiveness and economics.

The environmental and economical sustainability of the overall sEPS recovery process has to consider the potential valorization of the residual (i.e., non-extracted) waste AGS. The EPS extraction could improve the sludge treatment efficiency via anaerobic digestion (AD) thanks to the reduction of sludge volumes and the improvement of digestibility and dewaterability of the residual (i.e., non-extracted) sludge (Lotti et al., 2019a). De Sousa et al. (2021) observed that the waste activated sludge

pre-treatment via alkaline solubilization enhanced its biodegradability, improving the bioconversion potentials in full-scale treatment plants: this would suggest that the alkaline EPS extraction might be seen as a waste sludge pre-treatment potentially able to enhance its biodegradability. Moreover, Guo et al. (2020) observed that sEPS in AGS evidence a lower degradation over the AD treatment with respect to sEPS in waste activated sludge (WAS): this would result in a higher residual sEPS fraction in the AGS structure along the entire AD process, which leads to a lower overall biodegradability of AGS compared to WAS: in this sense, the sEPS extraction could enhance the AGS anaerobic digestibility.

The effect of the sEPS extraction on the overall digestibility of the residual waste AGS could be performed through Biochemical Methane Potential (BMP) tests. In this study, it has been demonstrated that the chemicals applied in the extraction phase can affect the overall biodegradability of the recovered sEPS: reasonably the same can happen for the residual (i.e., non-extracted) AGS which can potentially contain large quantities of elements that could compromise its microbial utilization. In this perspective, the choose of the most appropriate chemicals assumes a pivotal role in the overall waste sludge valorization chain (i.e., EPS recovery + anaerobic digestion).

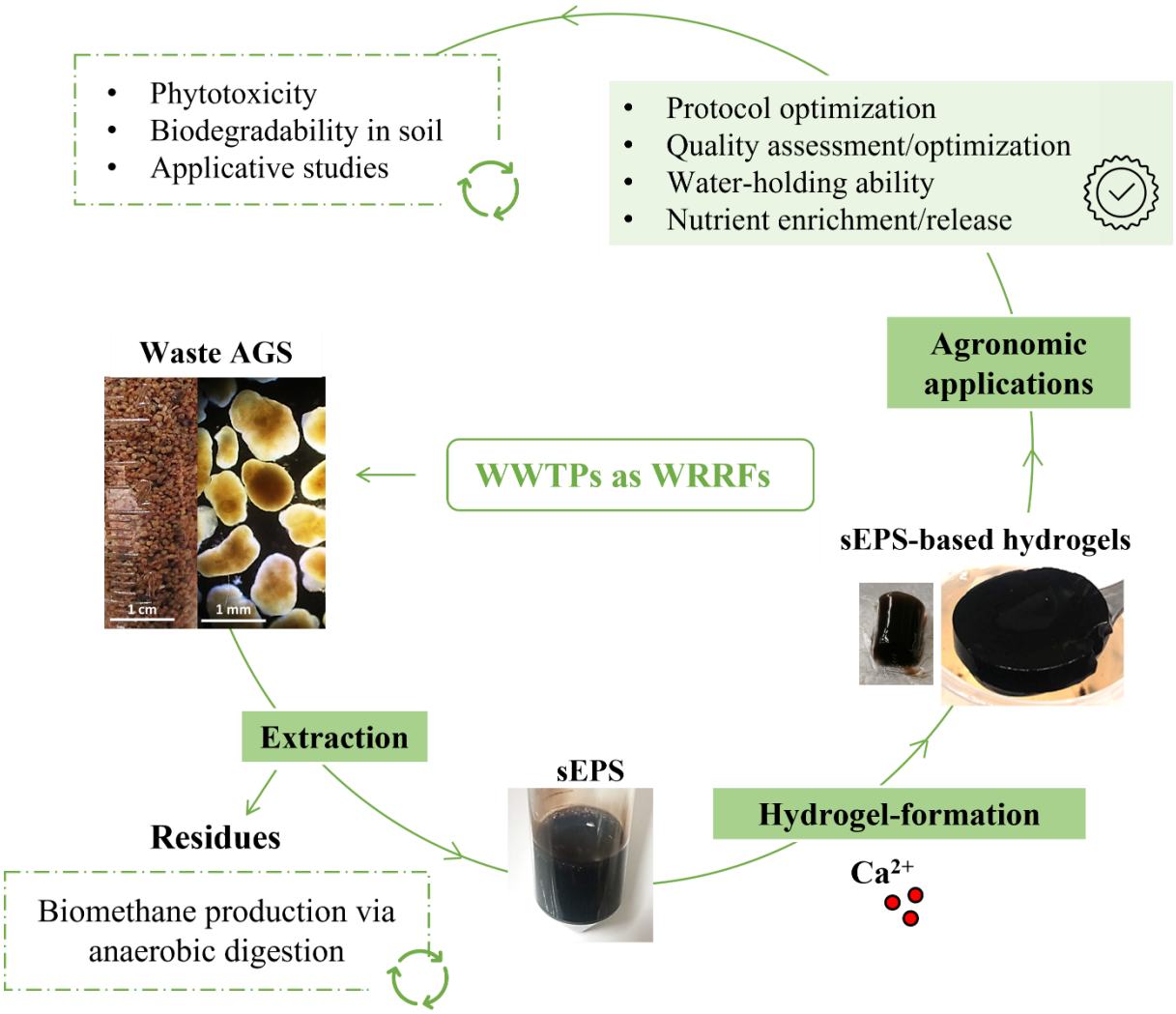

Figure 18 – Scheme of the approach proposed to progress towards new resource recovery-oriented solutions in agriculture able to contribute to a more circular economy-based wastewater treatment sector: the key actors are the extractable sEPS and their derived biomaterials (e.g., hydrogels). Both the aspects already addressed and the objects of follow up research are highlighted.

4. Conclusions

The impact of the whole process of sEPS extraction and hydrogel-formation on the valorization effectiveness in agronomy-oriented solutions was demonstrated in this chapter, emphasizing the key role of the chemicals applied on the agriculture-related properties of the derived biomaterials (e.g., hydrogels).

Overall, the results emerged disclosed that quantity/quality of the extractable sEPS macromolecules as well as their hydrogel-forming ability were not strictly affected by the chemicals used: particularly, the overall extraction yield (0.19 – 0.23 gVS/gVS_{AGS}) and the relative content of PN- and PS-like

substances (PN/PS = 3.88 – 4.58 g/g) were not significantly reduced with respect to literature data. However, the quality of sEPS and derived hydrogels in terms of elemental composition was considerably influenced by the chemicals applied: particularly, the chlorine and sodium contents were decreased by replacing Na_2CO_3/HCl/NaOH (*extraction*) and $CaCl_2$ (*hydrogel-formation*), thus enhancing the biopolymer applicability in sustainable agronomic practices. Overall, both sEPS and derived hydrogels obtained according to agronomy-oriented protocols appeared within the maximum limits in terms of heavy metals imposed by the current environmental legislation in matter of soil improvers and fertilizing products (values related to Cr(VI) remain to be investigated).

Despite the protocols applied, dehydrated sEPS-based hydrogels were able to reversibly swell in both water and nutrient-enriched aqueous solutions (KNO_3). This capability was enhanced by using $CaNO_3 \cdot 4H_2O$ as (ionic) cross-linking agent which resulted in hydrogels able to recover up to 90.6 – 93.3% of their original (wet) weight once rehydrated and sorb up to 16 $gH_2O/gTS_{Hydrogels}$ upon swelling in ultrapure water. The SAP-like behaviour of the obtained sEPS-based hydrogels was hence evidenced, thus suggesting their potential application for soil conditioning. The swelling kinetic data were well simulated by Elovich model, thus suggesting chemisorption mechanisms on heterogenous surfaces resulting in different kinds of active sites (i.e., with different activation energies). Moreover, a proof-of-principle of the nutrient release capacity of nutrient-loaded sEPS hydrogels was given: particularly, the sEPS hydrogels swollen in KNO_3 aqueous solutions have been demonstrated able to release up to 1.7 mmol K per g $TS_{Hydrogel}$ in the aqueous surrounding medium within one hour.

The respirometric assessment proved that the biodegradation of sEPS and derived hydrogels was dependent on the extraction/gelling protocols applied (in terms of chemicals used). Moreover, the readily biodegradable organic matter (assimilated to the sbCOD) was reduced upon hydrogel-formation likely due to the formation of an extended 3D polymeric network in which the sEPS macromolecules were more confined (and hence less accessible), thus making further hydrolytic reactions necessary before microbial utilization.

Overall, the potential of AGS-derived sEPS to progress towards new resource recovery-oriented solutions in agriculture was emphasized in this contribution, thus paving the way for more circular economy-based scenarios in the WWTPs.

Appendix

Table A.1 – Operative conditions applied during the respirometric measurements performed on sEPS and derived hydrogels. The pre-set parameters are highlighted in yellow with respect to those calculated or determined from analysis.

Substrate		**Single-OUR** Pristine samples	**Multiple-OUR** 0.1 µm filtered samples
F/M	**gCOD/gCODx**	**0.003**	**0.025**
Inoculum concentration	gVSS/L	2.00	2.00
Inoculum concentration (as COD equivalent)	gCODx/L	2.86	2.86
VSS/TSS	%	57.4	57.4
Inoculum concentration	gTSS/L	3.48	3.48
Inoculum volume	L	1.40	1.40
Inoculum mass (as COD equivalent)	gCODx	4.01	4.01
Sample concentration (as COD equivalent)	gCOD/L	1.80	1.80
Sample volume	L	0.0074	0.0557

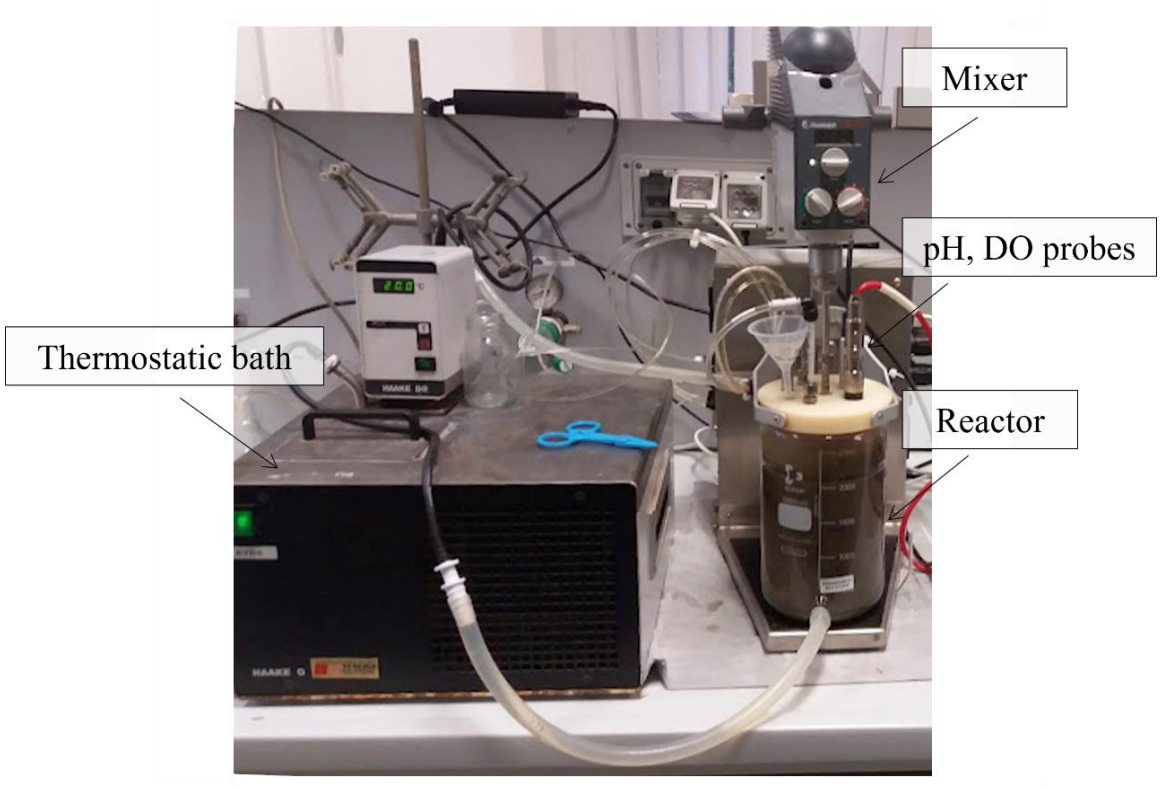

Figure A.1 – Apparatus used for the respirometric experiments carried out on AGS-extracted sEPS and derived hydrogels.

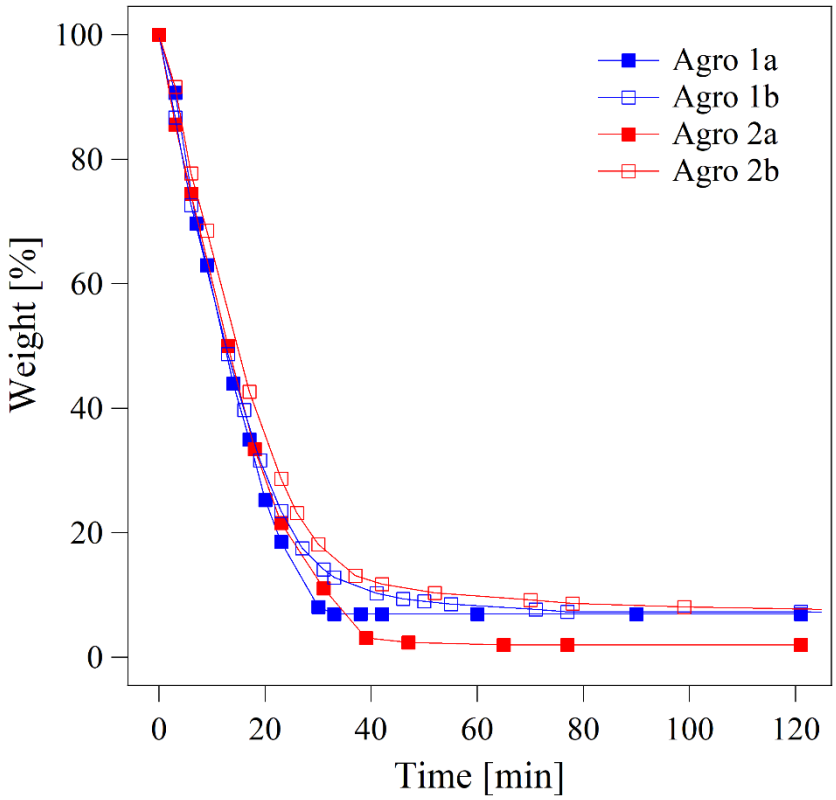

Figure A.2 – Dehydration kinetics (105 °C) of sEPS-based hydrogels obtained with different protocols.

Table A.2 – Elemental analysis and mineral composition of AGS used as raw material for sEPS extraction and gel-formation. All the element (weight) concentrations are expressed as ppm (= mg/kg dry matter or TS).

		AGS
TS/WW	[g/g]	0.109 ± 0.001
VS/TS	[g/g]	0.808 ± 0.005
C	[ppm]	404281
TOC	[ppm]	394909
H	[ppm]	60265
N	[ppm]	68652
Al	[ppm]	5746
Ca	[ppm]	20803
Cd	[ppm]	17.9
Cr	[ppm]	117
Cu	[ppm]	370
Fe	[ppm]	13147
K	[ppm]	1173
Mg	[ppm]	3627
Mn	[ppm]	136
Na	[ppm]	1793
Ni	[ppm]	96

P	[ppm]	12777
Pb	[ppm]	14.8
S	[ppm]	10143
Zn	[ppm]	544

Table A.3 – Mass balance related to various elements between sEPS and derived hydrogels obtained according to reference methods (Felz et al., 2016). The sEPS weight concentration (TS/WW, wt%) was about 0.9 wt% for sEPS (in the form of aqueous suspensions) and 2.0 wt% for hydrogels.

		Reference	
		sEPS	***sEPS hydrogel***
Ca	[µg]	11	1716
Cr	[µg]	0.1	0.1
Cu	[µg]	3	3
Fe	[µg]	65	64
K	[µg]	3	9
Mg	[µg]	2	12
Mn	[µg]	0.1	0.2
Na	[µg]	288	78
Ni	[µg]	0.2	0.4
P	[µg]	88	88
Pb	[µg]	0.2	0.1
Zn	[µg]	2	3

Table A.4 – Mass balance related to various elements between sEPS extracted according to protocol "*Agro 1*" and related hydrogels formed in presence of $Ca(NO_3)_2{\cdot}4H_2O$ and $Ca(C_2H_5COO)_2$ as calcium sources (i.e., protocols "*Agro 1a*" and "*Agro 1b*", respectively). The sEPS weight concentration (TS/WW, wt%) was about 0.6 wt% for sEPS (in the form of aqueous suspensions) and 4.6 and 3.5 wt% for hydrogels formed with protocols "*Agro 1a*" and "*Agro 1b*".

		Agro 1		
		sEPS	***sEPS hydrogel (1a)***	***sEPS hydrogel (1b)***
Ca	[µg]	7	228	362
Cr	[µg]	0.03	0.01	0.02
Cu	[µg]	0.9	0.2	0.4
Fe	[µg]	22	5	9
K	[µg]	195	6	5
Mg	[µg]	2	0.3	2
Mn	[µg]	0.03	0.01	0.02
Na	[µg]	3	0.5	4
Ni	[µg]	0.06	0.02	0.04
P	[µg]	33	7	12

Pb	[µg]	0.05	0.02	0.03
Zn	[µg]	0.3	0.2	0.3

Table A.5 – Mass balance related to various elements between sEPS extracted according to protocol "*Agro 2*" and related hydrogels formed in presence of $Ca(NO_3)_2 \cdot 4H_2O$ and $Ca(C_2H_5COO)_2$ as calcium sources (i.e., protocols "*Agro 2a*" and "*Agro 2b*", respectively). The sEPS weight concentration (TS/WW, wt%) was about 0.6 wt% for sEPS (in the form of aqueous suspensions) and 2.2 and 3.0 wt% for hydrogels formed with protocols "*Agro 2a*" and "*Agro 2b*".

		Agro 2		
		sEPS	***sEPS hydrogel (2a)***	***sEPS hydrogel (2b)***
Ca	[µg]	7	192	270
Cr	[µg]	0.03	0.01	0.01
Cu	[µg]	0.8	0.3	0.2
Fe	[µg]	19	6	5
K	[µg]	327	27	15
Mg	[µg]	1	2	2
Mn	[µg]	0.03	0.02	0.02
Na	[µg]	4	4	1
Ni	[µg]	0.08	0.05	0.04
P	[µg]	31	9	8
Pb	[µg]	0.05	0.02	0.01
Zn	[µg]	0.3	0.3	0.1

Chapter 4

Extracellular polymeric substances (EPS) recovered from waste anammox granular sludge as promising biosorbent for the heavy metal removal

Most of contents of this chapter have been published with slight modifications as: Pagliaccia, B., Carretti, E., Severi, M., Berti, D., Lubello, C., Lotti, T., 2021. *Heavy metal biosorption by Extracellular Polymeric Substances (EPS) recovered from anammox granular sludge*. Journal of Hazardous materials 424, 126661. https://doi.org/10.1016/j.jhazmat.2021.126661

Abstract

This chapter explores the feasibility of exploiting extracellular polymeric substances (EPS) extracted from waste anammox granular sludge (AmxGS) in bio-based technologies for the treatment of heavy metal-contaminated effluents. The metal-binding ability of the AmxGS-derived EPS towards heavy metals commonly found in wastewaters of both municipal and industrial origin (i.e., Pb, Cu, Ni, Zn) was addressed through single- and multi-metal equilibrium biosorption studies and then compared to that of pristine granules mainly to shed light on the adsorption mechanisms of extracted and non-extracted EPS in the native biomass.

AmxGS-extracted EPS evidenced adsorption capacities equivalent or higher than well-established adsorbent media in single-metal biosorption studies (up to 84.9, 52.8, 21.7 and 7.4 mg/gTS_{EPS} for Pb^{2+}, Cu^{2+}, Ni^{2+} and Zn^{2+}, respectively), thus proving to be promising waste-derived biopolymers in the heavy metal removal. Moreover, comparable metal-binding capabilities emerged from single- and multi-metal biosorption experiments: this excluded significant competitions among different heavy metal ions for the available binding sites, thus opening further scenarios in the treatment of complex wastewaters. With respect to pristine anammox granules (adsorbing up to 103.7, 36.1, 48.2 and 49.8 mg/gTS of Pb^{2+}, Cu^{2+}, Ni^{2+}, and Zn^{2+}, respectively), the extracted EPS showed lower adsorption capacities except for copper and distinct adsorption pathways (as postulated based on the

interpretation of the experimental profiles through theoretical models). These differences were ascribed to three main reasons: (i) multiple mechanisms participating in the heavy metal biosorption by native granules, in addition to the heavy metal uptake by EPS; (ii) EPS chemical modifications induced by the extraction method applied; (iii) different polymer chain mobility and binding site availability of extracted EPS in aqueous dispersions and non-extracted EPS in pristine granules.

Combining a series of spectroscopic techniques, mechanistic hypothesis for metal biosorption were proposed: particularly, a multifaceted mechanism based on a combination of electrostatic interaction, ion exchange, complexation, and precipitation was suggested.

The development of EPS-based composite media was reasonably suggested as potential strategy to enhance the industrial applicability of AmxGS-derived EPS. With this regard, a proof-of-principle of the successful exploitation of the extracted EPS in composite sorbent media (e.g., with granular activated carbon, GAC) was given, thus paving the way for appealing scenarios able to progress towards integrated resource recovery-oriented solutions in the wastewater treatment plants (WWTPs).

1. Introduction

Autotrophic biological processes based on the metabolism of anaerobic ammonium oxidizing bacteria (anammox) allow removing ammonium from wastewater with significant savings in terms of energy spent for oxygen supply (- 60%) and organic carbon supply (- 100%); in addition, the production of excess sludge is reduced (- 90%) compared to conventional nitrification/denitrification processes (Hu et al., 2013; Lotti et al., 2019a). For these reasons, anammox-based technologies are becoming the new standard for the treatment of nitrogen-rich wastewaters of municipal and industrial origins (Lackner et al., 2014). Anammox bacteria easily form granules (i.e., self-aggregated biofilms) without the presence of inert carriers. Thanks to these features, anammox granular sludge (AmxGS) systems are characterized by higher biomass concentrations and volumetric conversion rates, if compared to flocculent or biofilm on carriers systems and as a matter of fact treat more than 50% of the total N-

load handled with anammox technologies worldwide (Lackner et al., 2014). Anammox-based process full-scale installations are currently applied in side-stream configurations (e.g., for the treatment of reject waters of anaerobic digestion). Considering the worldwide increasing trend of biogas production (Scarlat et al., 2018), and the effective savings offered by anammox-based technologies in the treatment of digestates (Lackner et al., 2014), the N-load treated in anammox plants, and therefore the excess sludge production, is expected to increase in the future at a similar rate: strategies for the efficient waste anammox granular sludge management are therefore demanded (Feng et al., 2021). As in conventional biofilms, in anammox granules microorganisms are embedded in a matrix of hydrated extracellular polymeric substances (EPS) (Flemming and Wingender, 2010; Seviour et al., 2019, 2012). AmxGS-derived EPS are mostly composed by proteinaceous material (>60%), with a low content (abouut 7%) of carbohydrates (Lotti et al., 2019a). Lotti et al. (2019b) observed the presence of amyloid-like fibrils in AmxGS-derived EPS that possibly have a structural function in biofilms (Flemming et al., 2007; Taglialegna et al., 2017; Lin et al., 2018).

Waste sludge-derived EPS have been already studied for their metal-binding properties (Guibaud et al., 2012; Li et al., 2017b; Wei et al., 2016, 2019), thus suggesting their potential application for metal remediation purposes. Indeed, the EPS matrix contains various functional groups, like carboxyl, phosphoric, amine and hydroxyl groups (Li et al., 2017b) able to interact with cationic species in solution, thus representing potential metal-binding sites. Guibaud et al. (2012) observed that several functional groups (e.g., carboxyl, phosphoric, amine and hydroxyl sites) are involved in Cd^{2+} and Pb^{2+} binding by EPS from anaerobic granular sludge (AnGS). Li et al. (2017) noticed that hydroxyl and amino groups are the key functional groups involved in Ni^{2+} sorption by EPS from both AGS and AnGS. Based on the origin of the microbial aggregates, EPS can display different binding capacities towards metal cations: for instance, it is reported that EPS from AnGS provide a larger contribution to Ni^{2+} biosorption than EPS from aerobic granular sludge (AGS) (Li et al., 2017). However, despite these differences, the high protein content of EPS is generally positively correlated with the adsorption ability towards heavy metal cations: carbonyl and hydroxyl groups located on proteins are

the main binding sites involved in the Pb^{2+}, Cd^{2+}, and Zn^{2+} adsorption by EPS from AGS (Liu et al., 2015). The abundant proteinaceous material of anammox EPS is therefore expected to promote the heavy metal biosorption phenomena: Li et al. (2020) observed that carboxyl groups of proteins of EPS from anammox granules have the fastest response in binding Cu^{2+} compared to polysaccharides and hydrocarbons.

The rapid industrial development and accelerating urbanization resulted in the production of various toxic substances, among which heavy metals have become an issue of great concern, due to their toxicity, non-biodegradability and potential to bioaccumulate in human body and food chain (He and Chen, 2014; L. Wang et al., 2018). Heavy metal contamination exists in aqueous waste streams of many industries, like metal plating facilities, mining operations, and tanneries (Bailey et al., 1999). Heavy metals in wastewaters of industrial origins (e.g., lead, copper, nickel, zinc, cadmium, chromium, etc.) could achieve high concentrations (Heidmann and Calmano, 2010; Sharma et al., 2020; Thomas et al., 2021). Conversely, the heavy metal concentrations found in municipal wastewaters are generally lower (in the order of magnitude of µg/L); however, industrial wastewater discharges into municipal sewers might increase the heavy metal content of urban wastewaters. Wastewater treatment plants (WWTPs) treating municipal sewage are not specifically designed to remove heavy metals. However, metals can be significantly displaced from the final effluents, as the result of the partitioning to the solid phase of the treatment systems: the sludge retains a great part of the metal content entering the WWTPs (Cantinho et al., 2016). The optimization of conventional treatment processes or the implementation of advanced treatment technologies (Hargreaves et al., 2018) may be required to be consistent with the current environmental regulation that imposes improved quality of both end-products of wastewater treatment (i.e., effluent and sludge). Land application of treated sewage sludge, worldwide considered as an economically and environmentally sustainable solution for sludge management (Cantinho et al., 2016), can be compromised by the high level of metals often retained in the excess sludge. If compared to many conventional treatment systems (e.g. chemical precipitation, ion exchange, electrochemical removal, membrane technology;

Wang et al., 2018) affected by significant disadvantages (e.g., incomplete removal, high-energy requirements and production of toxic sludge), biosorption represents a highly cost-effective alternative for the treatment of heavy metal-contaminated effluents, thanks to the low operational costs, high efficiency and comparatively less sludge production (Kratochvil and Volesky, 1998; L. Wang et al., 2018). Typical biosorbents can be recovered from non-living biomass (e.g., shrimp, krill, squid, crab shell, etc.), algal biomass, and microbial biomass (e.g., bacteria, fungi, and yeast) (Apiratikul and Pavasant, 2008) . EPS extracted from sewage sludge could pave the way towards resource recovery-oriented solutions in the field of the heavy metal biosorption. Indeed, excess sludge is the main waste product in WWTPs and its processing cost account for nearly half of the total operational capital (de Valk et al., 2019): the EPS extraction/recovery would reduce the mass of waste sludge to be treated/disposed concurrently with the production of a value-added biomaterial that could be valorized for its ability in binding heavy metals.

Many documents in literature investigate the anammox EPS-heavy metal interaction and binding mechanisms. Li et al. (2020) proposes a detailed description of the anammox EPS-Cu^{2+} interaction at molecular level, observing that functional groups in EPS exchange and coordinate with Cu^{2+} to form inner sphere complexes, through an endothermic and entropy-increasing process. Zhang et al. (2015) studied the behavior, distribution, and form dynamics of overloaded Cu^{2+} in anammox granular sludge reactors, disclosing that the Cu distribution migrated from the EPS-bound to the cell-associated Cu and the Cu forms shifted from the weakly bound to strongly bound fractions over time. These pioneering studies highlighted the potentiality of using anammox EPS for metal remediation purposes, at least in the case of Cu. However, further research effort is demanded to evaluate the feasibility of exploiting EPS from waste anammox granular sludge as biosorbent for the treatment of heavy metal-contaminated effluents.

In this perspective, the present work explores the potential recovery and valorization of EPS from waste AmxGS as biosorbent for the removal of some heavy metals commonly found in wastewaters both of municipal and industrial origins (lead, copper, nickel, zinc). Batch equilibrium biosorption

tests were carried out by treating single- and multi-metal aqueous solutions with the AmxGS-recovered EPS. The biosorption properties of the extracted EPS were then compared to those of pristine granules to shed light on the adsorption mechanisms of extracted EPS and non-extracted EPS in the biomass. The biosorption mechanisms were investigated combining a series of spectroscopic techniques. The main goal of this work is therefore to provide proof-of-principle of the feasible conversion of EPS from waste anammox granular sludge into value-added biomaterials suitable for the treatment of heavy metal-contaminated effluents. In addition, based on a comprehensive analysis of the anammox EPS adsorption properties, some outlines on their potential industrial application are suggested. Particularly, proof-of-principle studies on the development of anammox EPS-based sorbent media (e.g., in combination with activated carbon) were presented, thus shedding light on potential resource recovery-oriented solutions able to enhance the sustainability of the overall wastewater treatment chain and promote a more circular economy-based water sector.

2. Materials and methods

2.1 EPS extraction and characterization

EPS were extracted from waste anammox granular sludge originating from a full-scale reactor in Rotterdam (Dokhaven-Sluisijesdijk WWTP, van der Star et al., 2007). The pH-based chemical extraction method developed by Lotti et al. (2019a) was applied with some modifications to obtain concentrated EPS dispersions, directly suitable for single- and multi-metal equilibrium biosorption studies. Particularly, with respect to the original protocol, the final acidic concentration step was not performed, and the EPS extracts were dialyzed (3.5 kDa molecular weight cut-off, MWCO) against ultrapure water (3 sequences of dialysis of about 8 hours each) right after the alkaline extraction phase (4 hours of granule incubation in 0.1 M NaOH aqueous solution, pH 12). The average EPS extraction yield was calculated based on the volatile solid content of the starting biomass ($mgTS_{EPS}/gVS_{granules}$) according to the method described in *Appendix* (**Figure A.1**).

For the evaluation of Total Solids (TS, g), anammox EPS/granules were kept in oven (105 °C) for about 24/48 h and then weighted on a digital balance. The ash content (Ash, g) was determined by placing the dried EPS/granules in muffle-furnace (560 °C) for 2 h and then weighting the samples. The Volatile Solids (VS, g) were calculated as the weight difference between TS and Ash. The measurements were carried out in triplicate and the results (in terms of VS/TS ratio, g/g) are expressed as average values ± standard deviation. The granule particle size distribution was determined by an image analysis procedure adapted from Tijhuis et al. (1994) and using the software Image ProPlus®. Both extracted anammox EPS and granule were also analyzed in triplicate by a Varian 720-ES Inductively Coupled Plasma - Atomic Emission Spectrometer (ICP-AES) equipped with a pneumatic nebulizer and a cyclonic spray chamber.

2.2 Equilibrium biosorption studies

The biosorption properties of the extracted anammox EPS were assessed through equilibrium single-metal biosorption studies carried out at laboratory scale by treating synthetic aqueous solutions each containing one of the selected heavy metal ions M^{2+}: Pb^{2+}, Cu^{2+}, Ni^{2+}, Zn^{2+}. The heavy metal-contaminated aqueous systems to be treated were therefore prepared dissolving $Pb(NO_3)_2$, $CuCl_2 \cdot 2H_2O$, $NiCl_2 \cdot 6H_2O$ and $ZnCl_2$ in ultrapure water with concentrations ranging between 10 and 1000 mgM^{2+}/L (pH=4.41, 4.59, 4.51 and 4.44 for Pb^{2+}, Cu^{2+}, Ni^{2+} and Zn^{2+} aqueous solutions, respectively, at 1000 mgM^{2+}/L). $Pb(NO_3)_2$ (purity ≥ 99.0%), $CuCl_2 \cdot 2H_2O$ (purity ≥ 99.0%), $NiCl_2 \cdot 6H_2O$ (purity ≥ 99.9%) and $ZnCl_2$ (purity ≥ 98.0%) were purchased by Sigma-Aldrich. For the preparation of all samples, ultrapure water was used after filtration through a Milli-Q system (Millipore).

To evaluate the effect of the initial heavy metal concentration (C_0, mg/L) on biosorption, heavy metal solutions (4 mL) with concentrations ranging between 10 and 1000 mgM^{2+}/L were mixed with anammox EPS dispersions (4 mL, 12.95 ± 1.65 gTS_{EPS}/L) in separate flasks and kept in contact under stirred conditions (120 rpm) at a temperature of 20 ± 0.5 °C for 6 hours. Based on the information

available in literature (Liu et al., 2015; Wei et al., 2016; Sajjad et al., 2017) and on preliminary kinetic studies (**Figure A.2** in *Appendix*), a contact time of 6 hours was considered as sufficient to attain sorption equilibrium. The pH of the mixed EPS-heavy metal aqueous systems was adjusted to 5.0 (for Pb^{2+} and Cu^{2+}) - 6.0 (for Zn^{2+} and Ni^{2+}) by adding 0.1 M HCl and NaOH aqueous solutions in order to avoid precipitation of metal salts. The selected range of C_0 reflected the metal content of various types of industrial effluents (e.g., galvanic wastewater, electroplating wastewater, metal plating wastewater); even if heavy metals are normally present in lower concentrations in municipal wastewaters, the level of contamination by heavy metals could increase in the case of discharges of industrial effluents in municipal sewers. Hence, the tested C_0 would allow to assess the capability of the extracted EPS in treating effluents of various origins with different levels of pollution by heavy metals.

Multi-metal biosorption studies were performed under conditions similar to those described for single-metal biosorption tests: an aqueous solution containing all the selected heavy metal ions simultaneously (4 mL, 80 mgM^{2+}/L each) was mixed with an anammox EPS dispersion (4 mL, 15.22 gTS_{EPS}/L), providing a contact time of 8 hours under stirring (120 rpm) at a temperature of 20 ± 0.5 °C. Since the lower initial metal concentrations, these tests were carried out at pH 6.0 (by adjusting the original pH of the EPS-metal aqueous system with 0.1 M HCl/NaOH), avoiding metal precipitation.

After 6 - 8 hours of contact time (i.e., once the biosorption processes reasonably achieved the equilibrium), the EPS-M^{2+} aqueous dispersions were dialyzed (3.5 kDa molecular weight cut-off) against ultrapure water. The measure of the residual metal concentrations at equilibrium (C_e, mg/L) was performed in triplicate by a Varian 720-ES Inductively Coupled Plasma - Atomic Emission Spectrometer (ICP-AES) on the aqueous bulk after EPS-M^{2+} dialysis. The biosorption performance were evaluated in terms of removal efficiencies [%] and adsorption capacities Q_e [mg/g] as follows (Eqs. 1 and 2, respectively):

$$Removal\ effiency = \frac{C_0 - C_e}{C_0} \cdot 100 \quad (1)$$

$$Q_e = \frac{C_0 - C_e}{m} \cdot V \quad (2)$$

where V [L] is the volume of the aqueous system and m [g] is the sorbent mass.

The metal-binding ability of the extracted anammox EPS was than compared to that of pristine granules mainly to shed light on the adsorption mechanisms of extracted EPS and non-extracted EPS in the native biomass. Anammox granules were pre-treated to overcome their pH buffer capacity, which produced a progressive alkalizing effect in the aqueous medium, due to variable mineral and/or organic fractions present in the biomass. To this aim, anammox granules were subjected to consecutive washing cycles with 0.45 % (w/v) NaCl (aqueous solutions in demineralized water, pH 5) until reaching a stable pH 5 in the liquid bulk. The described pre-treatment method was time-consuming but also slightly invasive for the biomass: lower pH values might speed up the desorption processes, but also compromise the granular matrix and promote cell lysis phenomena. In addition, the use of buffer solution (e.g., containing phosphate) could promote competitions with the heavy metal cations to be adsorbed on the same binding sites. The pre-treated granules were drained by using a metal sieve (200 µm pore size): their VS/TS ratio (g/g) was determined and compared to that of the untreated biomass; the conversion factor between granule wet weight (WW, g) and dry weight (TS, g) was also evaluated (i.e., WW/TS, g/g). The effect of increasing C_0 on the biosorption performance (at equilibrium) extended by pristine biomass (after pre-treatment) was assessed. A series of each metal ion solution with concentrations ranging between 5 and 500 mg/L were mixed with anammox granules (1.69 ± 0.20 $gTS_{granules}/L$) in separate flasks at pH 5.0 (for Pb^{2+} and Cu^{2+}) - 6.0 (for Zn^{2+} and Ni^{2+}) and kept under stirring (≃ 120 rpm) for 6 hours at a temperature of 20 ± 0.5 °C. Each sample was then filtered through 0.45 µm filter paper and analyzed by ICP-AES for the measurement of the residual heavy metal concentrations at equilibrium (C_e, mg/L). Adsorption capacities and percentage removal efficiencies were calculated according to Eqs. 1 and 2.

The experimental adsorption isotherm curves, describing the relationship between adsorption capacity (Q_e, mg/g) and residual metal concentration (C_e, mg/L) at equilibrium, were therefore determined. Langmuir and Freundlich adsorption isotherm models (Eqs. 3 and 4, respectively) were applied to interpret the observed profiles:

$$Qe = \frac{b \cdot Qm \cdot Ce}{1 + b \cdot Ce} \quad (3)$$

$$Qe = K_f \cdot Ce^{1/n} \quad (4)$$

where Q_m [mg/g] is the theoretical maximum adsorption capacity, b [L/mg)] is the Langmuir constant related to adsorption energy, K_f [L/g] is the energy binding constant reflecting the affinity of the sorbent for the sorbate and n [-] is the Freundlich constant. The equilibrium parameter R_L, a dimensionless constant related to the separation factor (Balarak et al., 2017), was inferred from the Langmuir equation and determined as follows (Eq. 5):

$$R_L = \frac{1}{1 + b \cdot C_0^*} \quad (5)$$

where C_0^* [mg/L] is the highest tested initial metal concentration. The value of R_L identifies the type of isotherm: irreversible ($R_L = 0$), favorable ($0 < R_L < 1$), linear ($R_L = 1$) or unfavorable ($R_L > 1$).

2.3 Biosorption mechanisms

A detailed description of the EPS-heavy metal interaction at molecular level was provided combining a series of analytical techniques, thus proposing a mechanistic hypothesis for metal biosorption.

The occurrence of ion exchange mechanisms associated to the heavy metal uptake was assessed measuring the concentration of alkali and alkaline earth metal ions (e.g., Ca^{2+}, K^{+}, Mg^{2+} and Na^{+}) released in solution simultaneously with the heavy metal uptake via ICP-AES.

Hydrodynamic diameter and Z-potential of EPS dispersions (0.01% w/v) in contact with increasing concentrations of the selected heavy metal ions (0.001-1 mM) were detected by Dynamic Light

Scattering (DLS) at 90° and Phase Analysis Light Scattering, respectively (90Plus PALS, Brookhaven Instruments Corporation, USA). EPS samples treating highly concentrated heavy metal-contaminated aqueous solutions (C_0=500 mg/L) were also observed with a scanning electron microscope (SEM Zeiss Evo MA15; sample coating with gold) and analyzed with energy dispersive X-ray spectrometry (EDS Oxford Inca 250) to determine their elemental compositions.

To address the main EPS functional groups acting as metal-binding sites, Fourier Transform-Infrared (FT-IR) spectra of EPS samples before and after heavy metal biosorption were obtained in the transmission mode using a BioRad FTS-40 spectrometer (4 cm^{-1} resolution, 64 scans, spectral range 2000 – 400 cm^{-1}, DTGS detector).

2.4 Composite EPS-activated carbon sorbent media

The metal-binding properties of AmxGS-derived EPS were exploited in proof-of-concept preliminary tests to develop efficient sorbent media in combination with granular activated carbon (GAC).

2.4.1 GAC functionalization with AmxGS-derived EPS

For the preparation of the composite medium, GAC was preliminarily washed with abundant distilled water to remove fines and dried in oven at 60 °C (48 hours). GAC-filled sorption columns (ca. 11 cm height, 1 cm diameter, 2 g_{GAC} as dry weight) were therefore prepared into laboratory burettes and then functionalized by eluting repeatedly (n. 24 elution cycles) 20 mL of 1% (w/v) AmxGS-derived EPS dispersion (pH 8.5, EPS/GAC = 0.1 g/g). At each passage, an aliquot of the corresponding eluate was collected to evaluate the amount of non-adsorbed EPS via UV-vis spectroscopy, according to the method shown in *Appendix* (**Figure A.1)**. The composite medium was then washed by filtering abundant ultrapure water to avoid releases of EPS during the metal sorption studies. The functionalization efficiency over the consecutive elution cycles was evaluated as percentage fraction of EPS adsorbed on GAC as follows (Eq. 6):

$$Functionalization\ efficiency\ = {(EPS_0\ -\ EPS_i)}/{EPS_0} \cdot 100\% \quad (7)$$

where EPS_0 [mg] is the initial mass of EPS in the aqueous dispersion, while EPS_i [mg] is the mass of EPS not adsorbed (i.e., remained in the aqueous dispersion) after i = 1,…, 24 elution cycles on the the GAC-filled sorption colums.

2.4.2 Metal adsorption studies

Multi- and single-metal sorption tests were performed by eluting 25 mL of synthetic aqueous solutions containing the selected heavy metal ions M^{2+} (C_0 = 80 mgM^{2+}/L each) on the composite GAC-EPS medium with a downward flow, ensuring a contact time of 10 minutes at 41.7 L/h contaminated water flow. All the adsorption tests were carried at a temperature of 20 ± 0.5 °C and pH 6.5. The sorption behavior of the composite systems was compared with that shown by equivalent sorption columns filled with GAC only. To estimate the maximum potential sorption performance, the metal-contaminated aqueous solutions were recirculated many times (n. 8 elution cycles) on the composite medium simulating a batch recirculation system. At each passage of elution, an aliquot of the corresponding eluate was collected and analyzed by Inductively Coupled Plasma-Optical Emission Spectroscopy (ICP-AES) to determine the amount of non-adsorbed metal cations. The removal efficiencies [%] were calculated as follows (Eq. 7):

$$Removal\ efficiency\ = {(C_0 - C_i)}/{C_0} \cdot 100\% \quad (7)$$

where C_0 [mg/L] is the initial M^{2+} concentration and C_i [mg/L] is the M^{2+} concentration remained in solution (i.e., non-removed) after i = 1,…, 8 elution cycles.

During the first elution cyle, the expeted sorption rates [mg/(g · h)] were also estimated as follows (Eq. 8):

$$Sorption\ rate = {(C_0 - C) \cdot V}/{m \cdot t} \quad (8)$$

where V [L] is the volume of the eluted M^{2+} aqueous solution, m [g] is the mass of the sorbent medium and t [h] is the contact time.

3. Results and discussion

3.1 EPS extraction and characterization

The particle size distribution of anammox granules is given in *Appendix* (**Figure A.3**): the characteristic diameters D10, D50 and D90 were 180.9, 317.0 and 871.2 µm, respectively. The average VS/TS ratio of anammox granules was 0.909 ± 0.002 g/g, while the granule wet weight on dry weight ratio was 11.54 ± 0.98 g/g. The alkaline extraction yielded an average amount of EPS of 355.24 ± 4.48 $mgTS_{EPS}/gVS_{granules}$, in agreement with literature data (Lotti et al., 2019a). The VS/TS ratio of the extracted anammox EPS was 0.809 ± 0.020 g/g.

The presence of alkali, alkaline earth and heavy metals was detected both in anammox granules and extracted EPS (**Table 1**). To explain this evidence, it is necessary to consider the origin of the used biomass. The tested granular sludge came from a full-scale reactor treating the reject water of a waste activated sludge anaerobic digester. Sewage sludge retains large part of the metal content entering the WWTP, as result of the of the partitioning from the liquid to the solid phase of the treatment systems. Some metals (e.g., Fe, Ni, Cu, Zn) were mostly present in the EPS (i.e., adsorbed by granules via extracellular uptake) and do not solubilize in the extraction process: considering an average EPS content in granules of about 36 wt%, metal concentrations (in terms of $mg/kgTS_{EPS}$) in the extracted EPS can increase up to 2.8 times with respect to pristine granules. Other metals are mainly present in the cells (e.g., adsorbed by granules via intracellular accumulation and/or cell wall sorption) and/or as metal precipitates within the granular biomass: their concentration in the extracted EPS was therefore expected to be lower than in the original granules and eventually close to zero; this might be the case of Al, Co, Cr, Mo, V, Pb.

The applied granule pre-treatment allowed overcoming the biomass pH buffer capacity: a stable pH 5 was achieved in the aqueous medium via consecutive washing cycles of granules by means of 0.45% w/v NaCl at pH 5 (at least 3 changes of the liquid bulk), ensuring a total contact time (in 0.45% w/v NaCl, pH 5) in the range of 100 - 400 hours dependent on the granule concentration (**Figure A.4** in

Appendix). The pre-treatment permitted to maintain constant pH conditions during the metal sorption tests, thus avoiding uncontrolled formation of metal precipitates due to the increase of pH observed in preliminary sorption studies using untreated granules (data not shown). The alkalizing effect of the untreated granules under the conditions applied during the heavy metal biosorption experiments (pH 5 - 6) was likely due to the dissolution of carbonate-precipitates formed within the granular biomass during the operations in the parent full-scale reactor (operational pH > 7) (Lin et al., 2013). A meaningful variation of VS/TS ratio was not detected after granule pre-treatment (VS/TS = 0.888 ± 0.007 g/g for pre-treated granules).

Table 1 – Content of alkali, alkaline earth and heavy metals of pre-treated anammox granules (0.45% w/v NaCl, pH 5), untreated anammox granules and extracted EPS determined by Inductively Coupled Plasma-Optical Emission Spectroscopy (ICP-AES).

	Al [mg/kg]	Co [mg/kg]	Cr [mg/kg]	Fe [mg/kg]	Mn [mg/kg]	Mo [mg/kg]	Ni [mg/kg]	Mg[1] [mg/kg]
Pre-treated granules	63	< 2.4	6.2	1730	16.3	23.1	12.3	-
Untreated granules	44	10.1	4.4	1950	66	27.1	6.9	-
Extracted EPS	5	-	-	2530	40	-	10	870
	Pb [mg/kg]	Cu [mg/kg]	V [mg/kg]	Zn [mg/kg]	Ca [mg/kg]	K [mg/kg]	Na [mg/kg]	Sr [mg/kg]
Pre-treated granules	4.9	33.8	4.1	88	< 2400	< 2400	29000	< 240
Untreated granules	3.35	32.3	3.6	127	7500	17400	29000	< 240
Extracted EPS	-	80	-	320	7050	220	11600	70

[1] The anammox-based reactor was again inoculated in the period between the two sampling campaigns. Consequently, AmxGS used in the biosorption tests could have different properties (e.g., in terms of metal content) compared to pristine granules used as raw material for the EPS extraction: this might explain the absence of Mg in the treated/untreated granules applied as metal sorbent media compared to biomass for EPS extraction.

3.2 Effect of the initial metal concentration on the biosorption effectiveness

The adsorption capacities [mg/g] and removal efficiencies [%] were determined as a function of the initial metal concentration (C_0, mg/L). Single-metal biosorption tests evidenced increasing heavy metal adsorption capacities at equilibrium (Q_e, mg/g) upon increasing C_0, both for extracted EPS and pristine granules (**Figures 1a** and **1c**). C_0 provided an important driving force to overcome the mass transfer resistances of the metal between the aqueous and solid phase (Aksu and Akpinar, 2000), thus promoting adsorption phenomena. At the same time, with increasing C_0, the heavy metal ion competition for the available binding sites increased (Zheng et al., 2008), thus reducing the percentage removal efficiency (**Figures 1b** and **1d**). The highest EPS adsorption capacities obtained under the tested conditions were 84.9, 52.8, 21.7 and 7.4 mg/gTS_{EPS} for Pb^{2+}, Cu^{2+}, Ni^{2+} and Zn^{2+} respectively (C_0 = 500 mg/L). Free Pb^{2+} was found in the treated solution above the detection limits of ICP-AES (in the order of µg/L) only for C_0 > 40 mg/L, thus highlighting its large affinity towards EPS; a significant removal (about 93.9%) was detected also for the highest tested concentration (C_0=500 mg/L). Cu^{2+} and Ni^{2+} removals decreased from 90.8 and 60.9% to 62.2 and 28.3%, respectively, with increasing C_0 from 5 to 500 mg/L; lower removal efficiencies were obtained for Zn^{2+} (15.9 and 10.2% for C_0 equal to 5 and 500 mg/L, respectively). Concerning anammox granules, the highest observed metal uptakes at equilibrium were 103.7, 36.1, 48.2 and 49.8 mg/g$TS_{granules}$ for Pb^{2+}, Cu^{2+}, Ni^{2+} and Zn^{2+} respectively (C_0=500 mg/L). At the lowest C_0 of 5 mg/L, anammox granules were able to remove most of the metal content of the treated solutions (98.5, 97.4, 98.6 and 95.1% of Pb^{2+}, Cu^{2+}, Ni^{2+} and Zn^{2+}, respectively), while the removal efficiencies significantly decreased increasing C_0 up to 500 mg/L (33.5, 12.6, 15.5 and 14.2% for Pb^{2+}, Cu^{2+}, Ni^{2+} and Zn^{2+}, respectively), consistently with the results obtained for the recovered EPS. The increase of the adsorption capacities of both extracted EPS and pristine anammox granules upon increasing C_0 can be exploited in potential applications for the pre-treatment of wastewater containing high concentrations of M^{2+}.

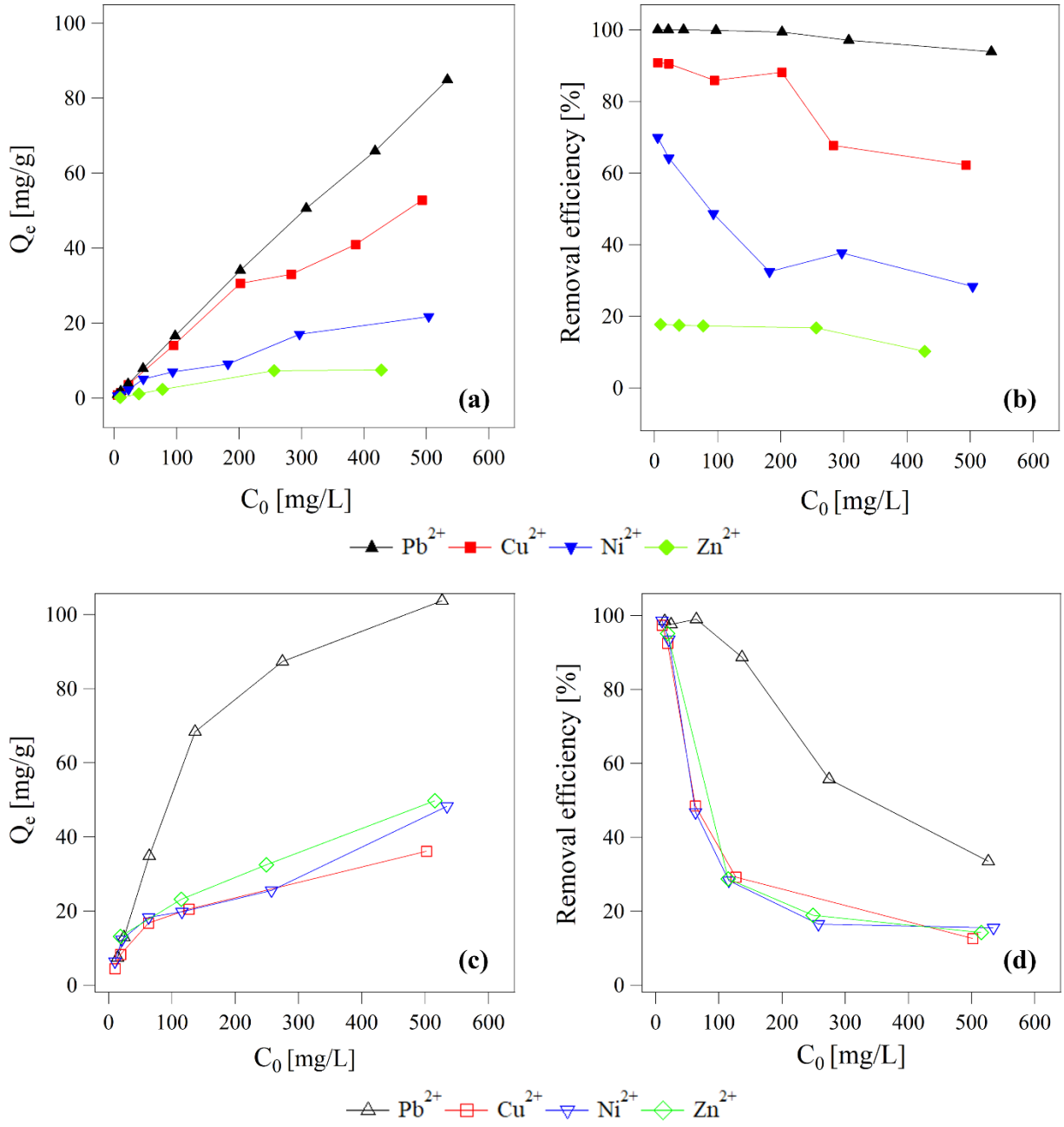

Figure 1 – Adsorption capacities (Q_e, mg/g) and removal efficiencies (%) observed for anammox EPS (**a**, **b**, respectively) and pristine granules (**c**, **d**, respectively) at increasing initial heavy metal concentrations (C_0 = 5-500 mg/L).

3.3 Comparison between extracted EPS and pristine anammox granules

Both extracted EPS and pristine anammox granules exhibited metal-binding capacities equivalent or higher than other conventional and/or unconventional sorbent media, like activated carbons (Kongsuwan et al., 2009), clay minerals (Bertagnolli et al., 2011), magnetic sorbents (Lan et al., 2013) and various biomaterials such as fungal biomass (Bhainsa and D'Souza, 2008) and macroalgae

(Pavasant et al., 2006). A more detailed literature survey of adsorbents and biosorbents for the copper removal is reported in **Table A.1** in *Appendix*.

The comparison between extracted EPS and pristine anammox granules in terms of equilibrium adsorption capacities Q_e [mg/g] is highlighted in **Figure 2**. As clearly noticeable, AmxGS-extracted EPS featured lower metal-binding capacities towards Pb^{2+}, Ni^{2+} and Zn^{2+} for all the studied range of initial concentrations C_0, but they appeared more performing in removing high concentrations of Cu^{2+} with respect to native biomass.

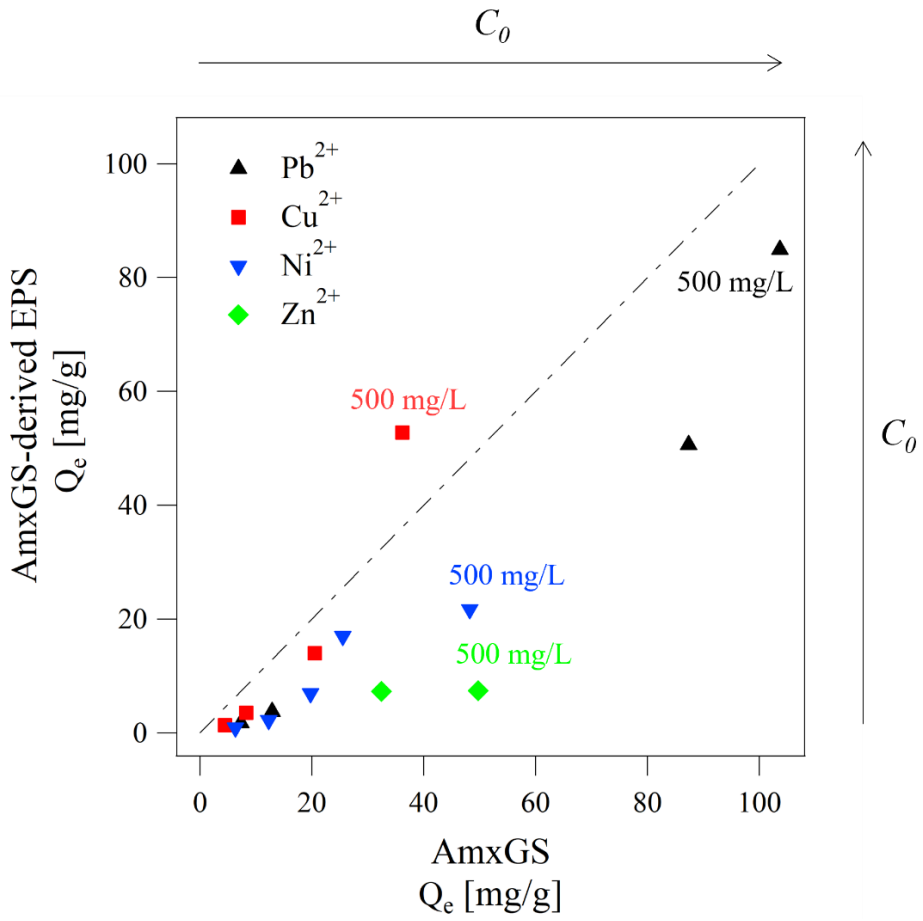

Figure 2 – Adsorption capacities (Q_e, mg/g) of extracted EPS (Y-axis) and pristine anammox granules (X-axis) at increasing initial metal concentration C_0. From bottom to top for AmxGS-derived EPS (and left to right for native AGS) Q_e values reported refer to $Pb_0 \simeq$ 12, 23, 290, 500 mg/L, $Cu_0 \simeq$ 10, 23, 100, 500 mg/L, $Ni_0 \simeq$ 11, 23, 100, 270, 500 mg/L, $Zn_0 \simeq$ 250, 500 mg/L,

These differences in terms of metal-binding ability observed for extracted EPS and pristine anammox granules might be ascribed to three main reasons:

i. multiple mechanisms participating in the heavy metal biosorption by native granules, in addition to the heavy metal uptake by EPS;
ii. EPS chemical modifications induced by the extraction method applied;
iii. different polymer chain mobility and binding site availability of extracted EPS in aqueous dispersions and non-extracted EPS in pristine granules.

Describing granules as dense microbial aggregates, comprising metabolically active microbial cells embedded in an EPS matrix (Liu and Tay, 2004), it is expected that the heavy metal uptake by EPS present within the biomass plays a crucial role in the biosorption phenomena. Indeed, EPS are rich in ionizable functional groups (e.g., carboxyl and hydroxyl groups) able to interact with cationic species in solution, thus representing potential metal-binding sites. Hypothesising that all the active metal-binding sites of anammox granules are localized on the EPS matrix, greater metal sorption capacities would be expected for the extracted EPS compared to pristine granules (up to 2.8 times higher in terms of mgM^{2+}/gTS, considering an average EPS content of about 36 wt% in the native biomass). However, other mechanisms might partecipate in the heavy metal sorpion promoted by anammox granules: cell wall adsorption and intracellular accumulation are usually common ways for biosorption (Vijayaraghavan and Yun, 2008). This could especially explain the lower zinc uptake exerted by the extracted EPS compared to pristine biomass: zinc is an essential co-factor for a large number of proteins, contributing to many structural and/or catalytic functions and hence bacteria are able to rapidly accumulate it on their cell walls as observed by Limcharoensuk et al. (2015). Furthermore, anammox granules presented adsorption capacities similar to other granular biomasses, like AGS and AnGS, as evidenced in **Table A.2** in *Appendix*. The microbial communities populating the above cited sludges are different, and therefore their EPS are expected to have different biochemical compositions. Therefore, regardless of these intrinsic differences among EPS at molecular level, the comparable adsorption capacities would suggest that there are also other driving factors that determine the mechanisms of M^{2+} biosorption, probably related to the 3D porous structure of granules, and relative EPS chain arrangement and biding site availability. In other words, given

the similar biosorption figures for different granular sludges, biosorption does not seem to be only dependent on the specific nature of the sludge/EPS considered, but also connected to structural aspects of the granules (e.g., high porous granular structure, polymer chain arrangement, binding site availability).

Despite the potential contribution in metal adsorption exerted by other components than EPS, it should be highlighted that the availability of binding sites of EPS themselves could be altered by the chemical extraction method applied. Some reports have shown that EPS extracted with chemical methods display meaningful differences in their ability to bind heavy metal ions, likely due to contamination of the recovered EPS with the chemicals used during the extraction (d'Abzac et al., 2010). The chemical extraction protocol here applied is based on the use of 0.1 M NaOH as alkaline agent to solubilize the EPS matrix. Although the extraction protocol included dialysis (3.5 kDa MWCO), the EPS extracts showed a relatively high content of Na^+ ions (11.6 mg/gTS_{EPS}, **Table 1**), which could compete with the heavy metal ions to be adsorbed on the availble binding sites. The extraction under alkaline conditions might also affect the conformation of EPS components through the loss of protein tertiary and/or quaternary stucture. This can promote specific interactions among proteins, resulting in more significant entanglement and progressive folding (i.e., association) of the peptidic chains, with subsequent reduction of the specific surface area and binding site availability.

Moreover, structural aspects of the sorbent medium can affect the performance in removing metal cations. While the highly porous structure of granules, with abundant and accesible sorption sites, promote the sequestration of contaminants upon diffusion into their deeper layers and channels (Liu et al., 2003), the use of the extracted EPS in the form of dispersions could result in weaker solute-sorbent interactions (or not strong enough to overcome the forces extended by the solvent). The relatively lower metal-binding capacities of the EPS dispersions compared to pristine granules in single-metal biosorption tests (especially in the case of Ni^{2+} and Zn^{2+} solutions) can be also attributed to the different impact that the EPS/metal complex formation has on the structural arrangement of EPS in suspension and on the EPS present within the native granules. Due to the higher mobility of

the EPS molecules dispersed in water, a potential explanation of the lower metal-binding capacity of the EPS dispersions could be that, when a M^{2+} is bound to EPS dispersed in water, the 3D conformation of the EPS molecules (free to move into the liquid aqueous phase) is strongly altered due to the arrangement of the EPS molecules around the M^{2+}. The experimental evidence of that was the increase of the hydrodynamic radius of EPS dispersed in water, observed upon loading M^{2+} (**Figure A.5** in *Appendix*). Instead, this effect is strongly inhibited for the EPS present within the granules due to their limited mobility. On the basis of this hypothesis, for dispersed EPS, with respect to EPS in granules, a higher number of EPS/M^{2+} bonds is expected in the EPS/M^{2+} complexes with a lower availability of binding sites for the formation of further bonds with other M^{2+} ions. This may results in a lower availability of binding sites for the formation of further bonds with other M^{2+} ions.

3.4 Langmuir and Freundlich adsorption isotherm models

The interpretation of the equilibrium biosorption data via Langmuir and Freundlich adsorption isotherm models (**Figure 3**) confirmed some differences in the sorption pathways followed by anammox EPS and granules. Firstly, it should be considered that in the tested range of C_0, the experimental isotherm curves (graphically representing the $Q_e - C_e$ relationship at increasing C_0) did not reach a plateau: to quantify the Q_e corresponding to the potential saturation point, C_0 should be hence increased above 500 mg/L (which is the maximum intial metal concentration here tested).

Based on the model statitistical indicators (**Table 2**), using anammox granules as biosorbent, a Zn^{2+} mono-layer biosorption was predicted due to the better statistical fitting via Langmuir model; Pb^{2+}, Cu^{2+} and Ni^{2+} biosorption data were better simulated by Freundlich model, thus suggesting a multi-layer biosorption on a heterogeneous surface. Using the EPS extracts as biosorbent, a Pb^{2+} multi-layer biosorption was predicted because of the better statistical fitting via Freundlich model; Langmuir model was more representative of Cu^{2+} and Zn^{2+} equilibrium biosorption data, thus implying an uniform and mono-layer adsorption on the EPS surface: the EPS-Cu^{2+}/Zn^{2+} interactions could be not strong enough to overcome the forces extended by the solvent except in the first layer, being both

solute and sorbent in a sol-like state. The slight differences in R^2 values observed for Ni^{2+} adsorption by anammox EPS, reflecting the simultaneously applicability of both theoretical models, suggested that mono- or multi-layer attachment, possibly with chemical interactions between EPS and metal ions, and also between the sorbate molecules, could explain the biosorption phenomena (Wang et al., 2018). Further information can be deducted from the model parameters (**Table 2**). The $0 < 1/n < 1$ values in Freundlich model (0.422 – 0.680 and 0.227 – 0.336 for extracted EPS and anammox granules, respectively) implied a favorable metal biosorption by anammox EPS and granules (Wang et al., 2018), consistent with the $0 < R_L < 1$ values (0.005 – 0.369 and 0.004 – 0.280 for extracted EPS and anammox granules, respectively) in Langmuir model. Similarly to the Langmuir constant *b*, the values of the energy binding constant K_f in Freundlich model reflected the metal binding affinity of the sorbent in the following orders: $Pb^{2+} > Cu^{2+} > Ni^{2+} > Zn^{2+}$ for extracted EPS and $Pb^{2+} > Zn^{2+} > Cu^{2+} > Ni^{2+}$ for anammox granules.

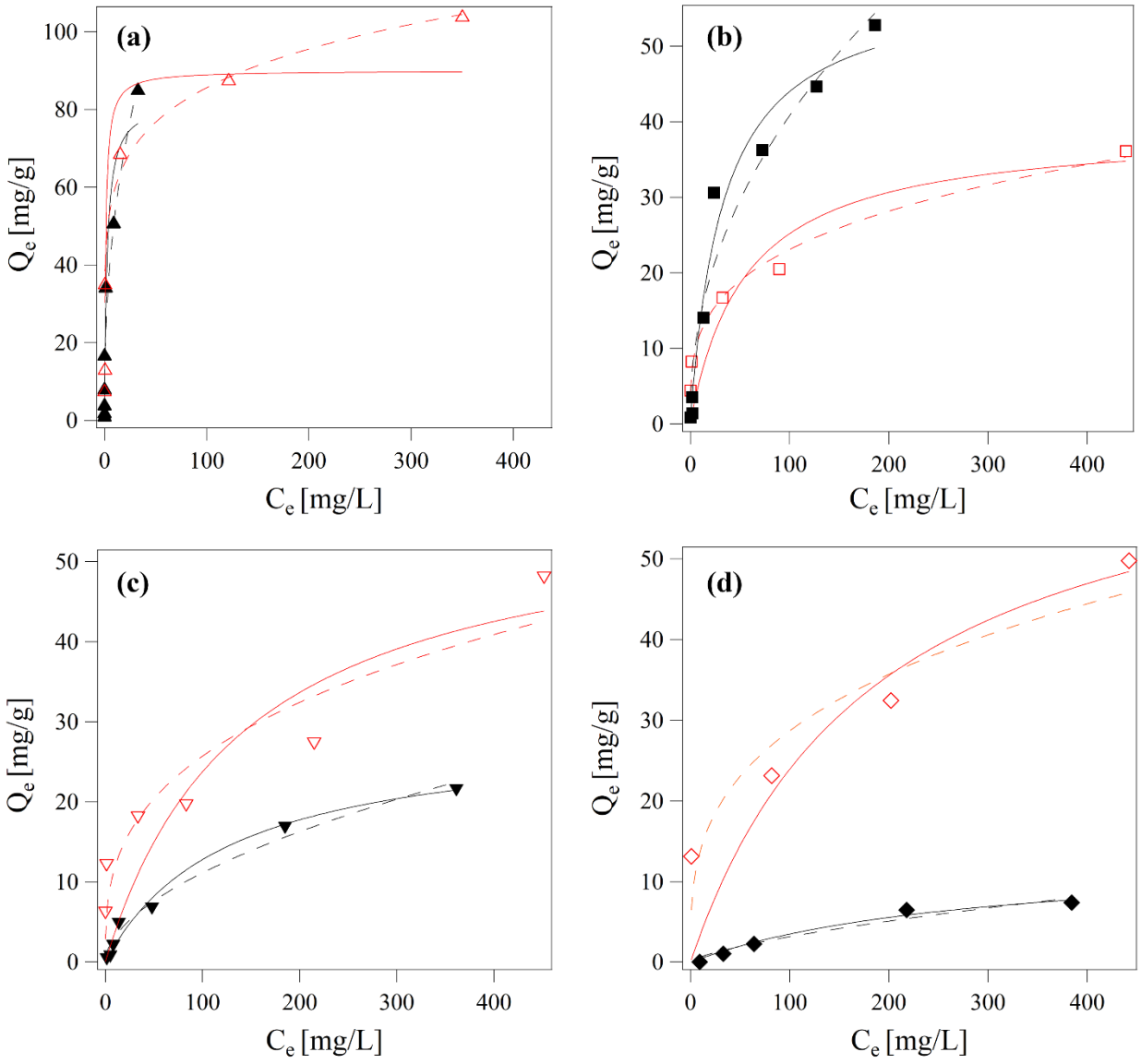

Figure 3 - Experimental adsorption isotherm curves and related fits via Langmuir and Freundlich models (in continuous and dotted lines, respectively) for anammox EPS (full markers, black lines) and pristine granules (empty markers, red lines) towards Pb^{2+} (**a**), Cu^{2+} (**b**), Ni^{2+} (**c**) and Zn^{2+} (**d**).

Table 2 - Model parameters and statistical indicators related to the fitting of anammox EPS and granule equilibrium sorption data via Langmuir and Freundlich adsorption isotherm models.

	Anammox EPS						
	Langmuir model				*Freundlich model*		
	Q_m [mg/g]	b [L/mg]	R_L [-]	R^2	K_f [L/g]	n [-]	R^2
Pb^{2+}	82.47	0.385	0.005	0.927	19.80	2.37	0.942
Cu^{2+}	58.73	0.030	0.063	0.974	4.83	2.16	0.953
Ni^{2+}	29.02	0.008	0.200	0.984	0.89	1.83	0.985

Zn^{2+}	13.40	0.004	0.369	0.986	0.14	1.47	0.958
				Anammox granules			
		Langmuir model			*Freundlich model*		
	Q_m [mg/g]	b [L/mg]	R_L [-]	R^2	K_f [L/g]	n [-]	R^2
Pb^{2+}	90.03	0.790	0.004	0.925	41.18	6.29	0.941
Cu^{2+}	39.18	0.018	0.100	0.948	6.15	3.48	0.990
Ni^{2+}	59.41	0.006	0.211	0.851	5.49	2.98	0.866
Zn^{2+}	69.07	0.005	0.280	0.938	6.70	3.17	0.903

3.5 Multi-metal biosorption studies

Similar metal-binding capacities were observed for the extracted EPS in multi- and single-metal biosorption experiments performed at the same initial concentration C_0 = 40 mgM^{2+}/L (**Table 3**): significant competitions among different heavy metal ions for the available EPS binding sites might be hence ruled out at least for Cu^{2+} and Zn^{2+}. Indeed, while no differences were detected for Cu^{2+}, the Ni^{2+} and Pb^{2+} adsorption capacities in multi-metal aqueous systems accounted for about 71 and 77% of those observed in single-metal biosorption studies, thus indicating that their binding sites were potentially contended by another cation. Conversely, the Zn^{2+} uptake was improved by a factor 2.3 when a multi-metal adsorption was promoted. Moreover, the total heavy metal uptake in the case of multi-metal systems (14.81 mg/gTS_{EPS}) was higher than the amount of each metal ion adsorbed in single-metal adsorption tests: this would indicate the capability of AmxGS-derived EPS in adsorbing multiple metal ions simultaneously (1.07 – 7.83 mg/gTS_{EPS}) and hence a synergic effect in multi-metal aqueous systems. Similar evidences were found by Sun et al. (2009) for Zn^{2+} and Co^{2+} binary sorption on EPS from aerobic granules, thus supporting the consistency of these considerations, regardless of the quality of EPS and original microbial aggregate. Many conventional techniques for the heavy metal removal (e.g., ion exchange resins, nanofiltration membranes) are often designed to target one contaminant at a time, thus making their use impractical for environmentally polluted

waters and/or wastewaters where several contaminants occur simultaneously (Bolisetty et al., 2019). Conversely, the sorption capability of extracted anammox EPS in multi-metal aqueous systems might be exploited in technologies for the treatment of effluents contaminated by several heavy metals.

Table 3 - Adsorption capacity of anammox EPS in single- and multi-metal biosorption tests (C_0=40 mgM^{2+}/L).

	Adsorption capacity [mg/gTS_{EPS}]	
	Multi-metal sorption	*Single-metal sorption*
Pb^{2+}	5.56	7.83
Cu^{2+}	4.45	4.35
Ni^{2+}	2.36	3.06
Zn^{2+}	2.43	1.07

3.6 Biosorption mechanisms

The process scale-up should be supported by a deeper molecular-level understanding of the biosorption processes, made challenging by the complexity of the mechanisms involved. This is hampered by the fact that the fine physic-chemical characterization of EPS recovered from biofilm-based engineered systems is still far from complete (Seviour et al., 2019). The investigation should start with the surface properties of the sorbent, representing a key element in all adsorption phenomena. The removal efficiencies of contaminants are strongly dependent on both their species and sorbent surface charge through mechanisms of electrostatic attraction. Modifications of the surface properties of the sorbent could be promoted by the pH of the medium, that not only affects the speciation of the solutes, but can also change the surface charge of the sorbent via protonation or deprotonation (Wang et al., 2018). The effect of pH on the Z-potential of aqueous solutions containing EPS extracted from AmxGS was recently reported in the literature (Lotti et al., 2019a). In brief, at pH $\leq$ 4, EPS surface is largely protonated and Z-potential is close to neutrality $|Z_{pot} \leq 10$ mV|: in these conditions H^+ ions compete with the heavy metal ions for the adsorption sites. For higher values of pH, deprotonation occurs and the EPS surface becomes negatively charged, thus increasing the ability

to interact with positively charged metals. In the tested sorption conditions (pH 5 – 6), anammox EPS were negatively charged ($Z_{pot} \leq -20$ mV, Lotti et al., 2019a) and could attract metal cations via electrostatic interactions as first step of biosorption, thus favouring further polymer-metal interactions (Wang et al., 2018). A detailed description on how biosorption proceeds is difficult: physic-chemical interactions between heavy metal cations and EPS (anionic) functional groups, based on ion exchange, surface complexation, redox reaction and micro-deposition, might be involved, individually or in combination (Wang et al., 2018). FT-IR spectroscopy suggested the involvement of multiple functional groups and components in the heavy metal biosorption provided by anammox EPS. The FT-IR spectra of the EPS samples presented some changes in terms of peak shifts after the interaction with the heavy metal ions (**Figure 4**). The highest shifts were observed for the peaks at 1547 cm^{-1} wavenumber (→ 1537, 1536, 1537 and 1535 cm^{-1} after Pb^{2+}, Cu^{2+}, Ni^{2+} and Zn^{2+} uptake, respectively), associated to C-N stretching and N-H bending of proteins (Amide II), and 1047 cm^{-1} (→ 1074, 1058, 1076 and 1074 cm^{-1} after Pb^{2+}, Cu^{2+}, Ni^{2+} and Zn^{2+} uptake, respectively) assigned to C-H in plane bending of polysaccharides (Lotti et al., 2019a; Niu et al., 2016). The metal-binding capability of AmxGS-extracted EPS might be therefore ascribed to both protein- and polysaccharide-like substances.

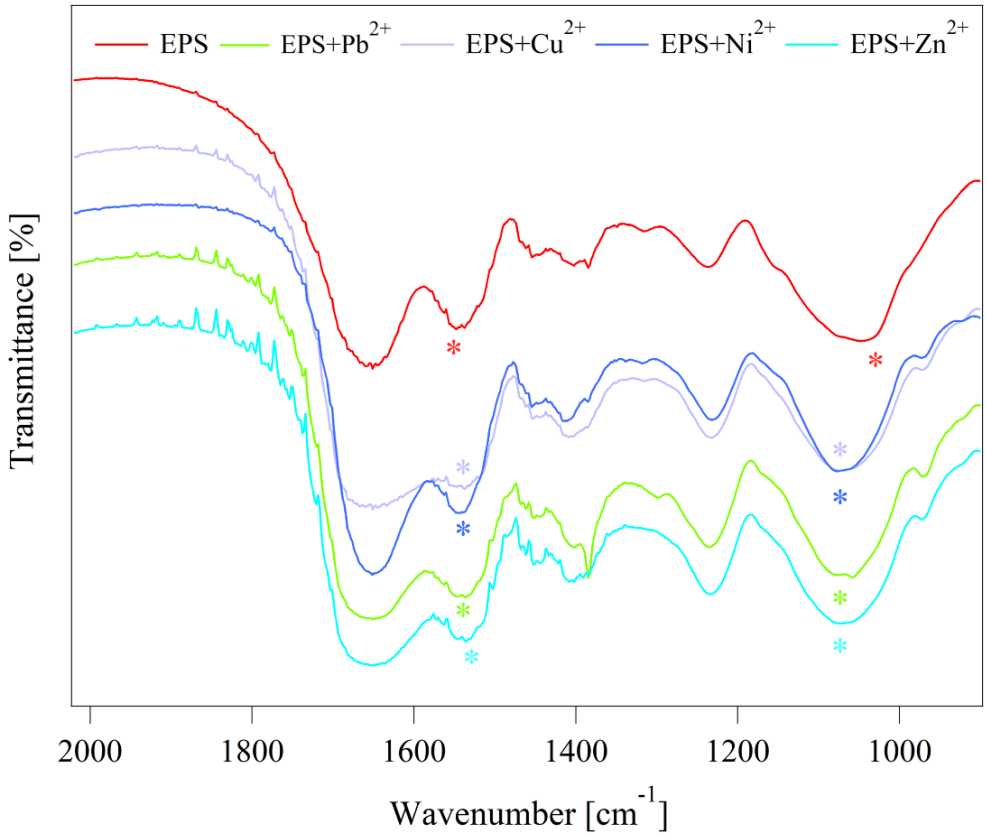

Figure 4 - FT-IR spectra of EPS samples before and after the heavy metal biosorption.

In agreement with literature data, which report the ion exchange as a common mechanism for the metal biosorption by EPS (Li and Yu, 2014) and/or biomass (Sajjad et al., 2017), the heavy metal uptake by extracted EPS and pristine anammox granules was associated to releases of alkali and alkaline earth metal ions (e.g., Ca^{2+}, Na^{+}, Mg^{2+} and K^{+}) in the bulk medium, resulting from a relatively lower affinity and competitiveness of the exchangeable cations to bind with the sorbent (Wang et al., 2010). **Figure 5 (a, b)** compares the amounts of Pb^{2+}, Cu^{2+}, Ni^{2+} and Zn^{2+} adsorbed by anammox EPS and granules with those of Ca^{2+}, K^{+}, Mg^{2+} and Na^{+} found in the aqueous medium after the heavy metal sorption tests (C_0 = 500 mg/L). It was noticed that the heavy metal adsorption by the extracted EPS was mainly associated to Ca^{2+} and Na^{+} releases, which accounted for 93.5, 93.4, 88.3 and 95.6% of the total amount of metal ions discarded by EPS following the Pb^{2+}, Cu^{2+}, Ni^{2+} and Zn^{2+} adsorption, respectively, whit a lower release of K^{+} and Mg^{2+} also detected (**Figure 5c**). Ion-exchange mechanisms were also observed for the pristine granules: Ca^{+} represented less than 1% of the total

release following the adsorption, while Na^+ ions were the most abundant (93.1, 94.2, 75.2 and 92.4% of the total metal ion release for Pb^{2+}, Cu^{2+}, Ni^{2+} and Zn^{2+} biosorption, respectively), with a lower amount of K^+ (5.7, 5.8, 24.1 and 6.7% of the total metal ion release for Pb^{2+}, Cu^{2+}, Ni^{2+} and Zn^{2+} biosorption, respectively) detected in the aqueous medium after biosorption (**Figure 5d**). A non-stoichiometric exchange (i.e., release/adsorption ratios < 1 meq/meq) was observed both for extracted EPS and pristine granules, suggesting that this process was not the only mechanism at play in biosorption. In addition to ion exchange, complexation and surface precipitation are considered as two of the major mechanisms responsible for the heavy metal-EPS/biomass interaction (Li and Yu, 2014). Depending on metal speciation in response to pH, directly affecting the metal solubility, many heavy metals can be also easily precipitated into EPS/biomass or onto the surface of some mineral fraction contained in EPS/biomass (Guibaud et al., 2009), thus greatly complicating the understanding of sorption processes. Particularly, at C_0 = 500 mg/L, ion exchange accounted for 46.4, 22.4, 26.1 and 32.6% of Pb^{2+}, Cu^{2+}, Ni^{2+} and Zn^{2+} biosorption, respectively, by extracted EPS and 88.6, 99.1 and 76.1% of the Cu^{2+}, Ni^{2+} and Zn^{2+} uptake, respectively, by pristine granules (data related to Pb^{2+} sorption were not clear, due to the release/sorption ratios > 1 meq/meq; unexpected releases not associated with the Pb^{2+} uptake seemed to be promoted).

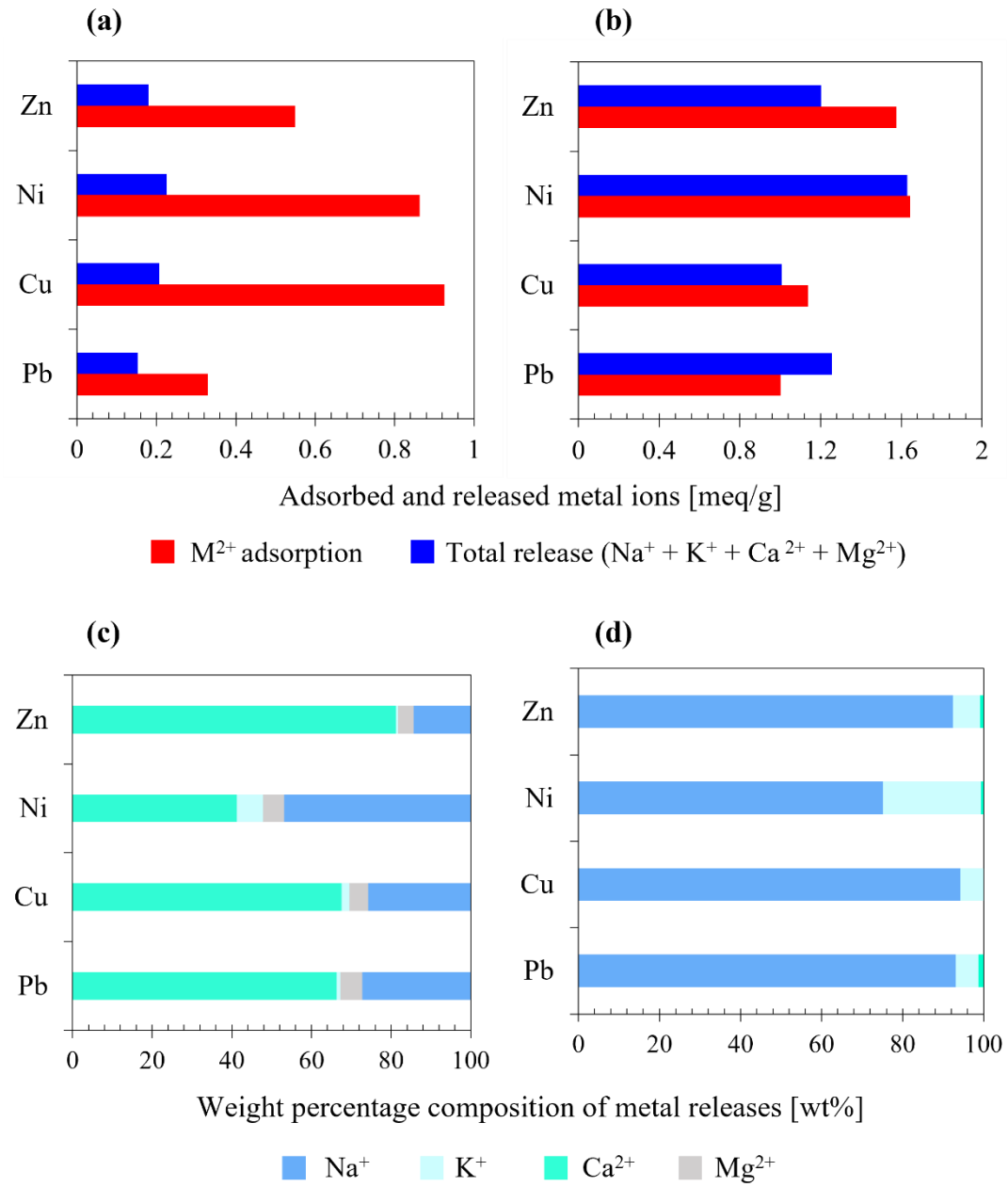

Figure 5 – Amount of metals adsorbed and released in the aqueous medium [meq/g] during the heavy metal uptake by extracted EPS **(a)** and pristine anammox granules **(b)** and relative weight percentage composition of the total release (Na^+, K^+, Ca^{2+}, Mg^{2+}) in the case of extracted EPS **(c)** and native biomass **(d)** as biosorbent.

It was observed that the ion exchange contribution to the heavy metal biosorption by anammox EPS increased by 45, 110, 157 and 88% in the case of Pb^{2+}, Cu^{2+}, Ni^{2+} and Zn^{2+} contaminated aqueous systems, respectively, upon decreasing C_0 from 500 to 200 mg/L. This evidence suggested a complex interplay of other adsorption mechanisms more active for the highest initial metal concentrations. Indeed, in single-metal biosorption tests treating C_0=500 mgM^{2+}/L, the Ni-EPS and Zn-EPS aqueous systems appeared slightly unstable (likely due to the potential formation of micro – and/or nano-

precipitates, not visually detectable), while the formation and subsequent precipitation of Pb-EPS and Cu-EPS composite aggregates was observed (aggregate size in the order of magnitude of millimetres, i.e., clearly visible). The Pb/Cu-EPS composite precipitates were observed with a scanning electron microscope (SEM) for the surface morphology investigation: the surface roughness indicated the presence of polymeric components, while regular crystalline structures expected for metal precipitates were not appreciated (**Figure 6**).

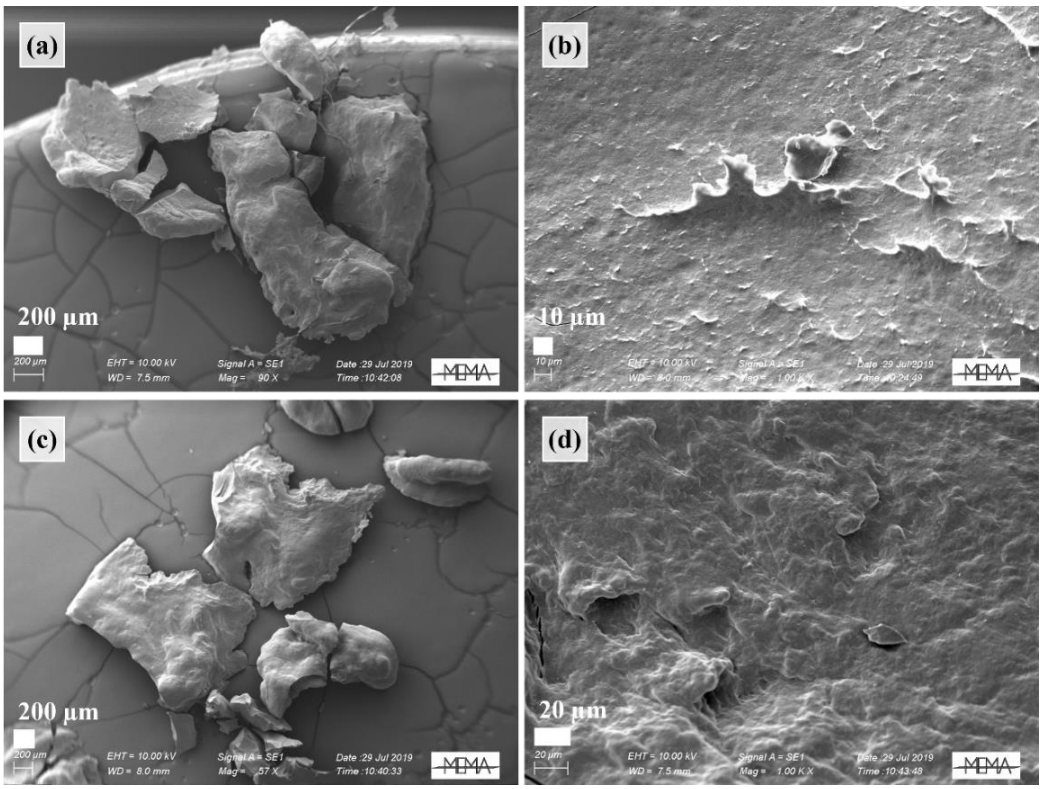

Figure 6 - EPS-Pb composite aggregates (**a**, **b**) and EPS-Cu composite aggregates (**c**, **d**) precipitated in single-metal biosorption tests treating C_0 = 500 mgM^{2+}/L observed through a scanning electron microscope (SEM Zeiss Evo MA15) at different magnifications.

Considering the molecular composition of AmxGS-extracted EPS reported in literature (i.e., $C_1H_{1.629}O_{0.503}N_{0.209}P_{0.009}$, 24.97 $gVS_{EPS}/C\text{-}mol_{EPS}$, Lotti et al., 2019a), the metal/EPS weight and atomic ratios of the composite aggregates were calculated based on their elemental analysis obtained through energy-dispersive X-ray spectroscopy (EDS) (**Table 4**). Details on the EDS analysis are reported in *Appendix* (**Figure A.6**). The EPS presence in the aggregates was confirmed by the O/C atomic ratios in agreement with those reported for pristine anammox EPS (Lotti et al., 2019a). As

emerged from EDS analysis, carbon, oxygen, and heavy metals (i.e., Pb and Cu, respectively) were prevalent (in terms of atomic% and weight%) in the aggregate composition, with weight and atomic ratios consistent with the polymer-heavy metal co-precipitation. To elucidate the contribution of precipitation (as composite EPS-M^{2+} aggregates) to the overall heavy metal removal, a mass balance should have been properly implemented: however, issues related to the separation of the observed precipitates made it difficult from a practical point of view.

Table 4 – Elemental analysis of EPS-Pb/Cu composite aggregates (precipitated in single-metal biosorption test at C_0=500 mg/L) detected by energy-dispersive X-ray spectrometry (EDS). Average values ± standard deviations (n. 4 and 3 points of analysis for composite EPS-Pb and EPS-Cu aggregates, respectively).

Composite EPS-Pb aggregates			**Composite EPS-Cu aggregates**		
C	40.51 ± 5.63	Weight%	**C**	53.55 ± 2.47	Weight%
	66.12 ± 7.38	Atomic%		63.90 ± 1.44	Atomic%
O	34.59 ± 4.79	Weight%	**O**	38.17 ± 0.04	Weight%
	30.80 ± 5.36	Atomic%		34.22 ± 0.85	Atomic%
Pb	9.85 ± 7.84	Weight%	**Cu**	8.28 ± 2.42	Weight%
	1.54 ± 0.63	Atomic%		1.88 ± 0.59	Atomic%
O/C	0.495 ± 0.104	mol/C-mol_{EPS}	**O/C**	0.536 ± 0.025	mol/C-mol_{EPS}
Pb/C	0.023 ± 0.007	mol/C-mol_{EPS}	**Cu/C**	0.029 ± 0.007	mol/C-mol_{EPS}
Pb/EPS	0.171 ± 0.056	g/gTS_{EPS}	**Cu/EPS**	0.068 ± 0.023	g/gTS_{EPS}

The EPS-heavy metal co-precipitation phenomena observed in biosorption tests treating highly concentrated heavy metal-contaminated aqueous solutions was probably not due to pH and/or ionic strength of the aqueous systems: the experiments were designed selecting operative conditions avoiding the precipitation of metal salts. The effect of ionic strength was not investigated in this study, but the applied experimental conditions (**Table A.3** in *Appendix*) would have allowed to overcome the competition with electrolyte cations, thus promoting the metal adsorption processes. More likely, increasing C_0, and therefore the amount of heavy metal ions adsorbed on the EPS binding sites, multiple-bridging complexation phenomena might be promoted. In line with this hypothesis, divalent

cations M^{2+} could act as bridges for different EPS units. This would result in a strong increase of EPS particle size, and in a reduction of the repulsive force among EPS units, thus leading to aggregation and finally to precipitation, as also suggested by preliminary Zeta-potential and Dynamic Light Scattering (DLS) measurements (**Figure A.7** in *Appendix*). This evidence agreed with what reported by Li et al. (2020), who observed a decreasing repulsive force between the EPS colloidal particles (i.e., a reduction of the absolute value of the Zeta-potential) upon increasing the Cu^{2+} concentration in contact with anammox EPS. Regardless of the mechanistic hypothesis, these findings would suggest that AmxGS-derived EPS might be applied as flocculant/complexing agent to pre-treat very concentrated heavy metal-contaminated wastewaters: EPS would concentrate heavy metals in the form of composite aggregates (i.e., metal concentration in the polymer-metal aggregates higher than those adsorbed by EPS in in aqueous dispersions), easily separable from the clarified effluent via sedimentation or filtration, thus greatly simplifying the post-treatment separation phase.

In summary, **Figure 7** proposes a schematic representation of the heavy metal biosorption mechanisms likely provided by the extracted EPS and pristine anammox granules.

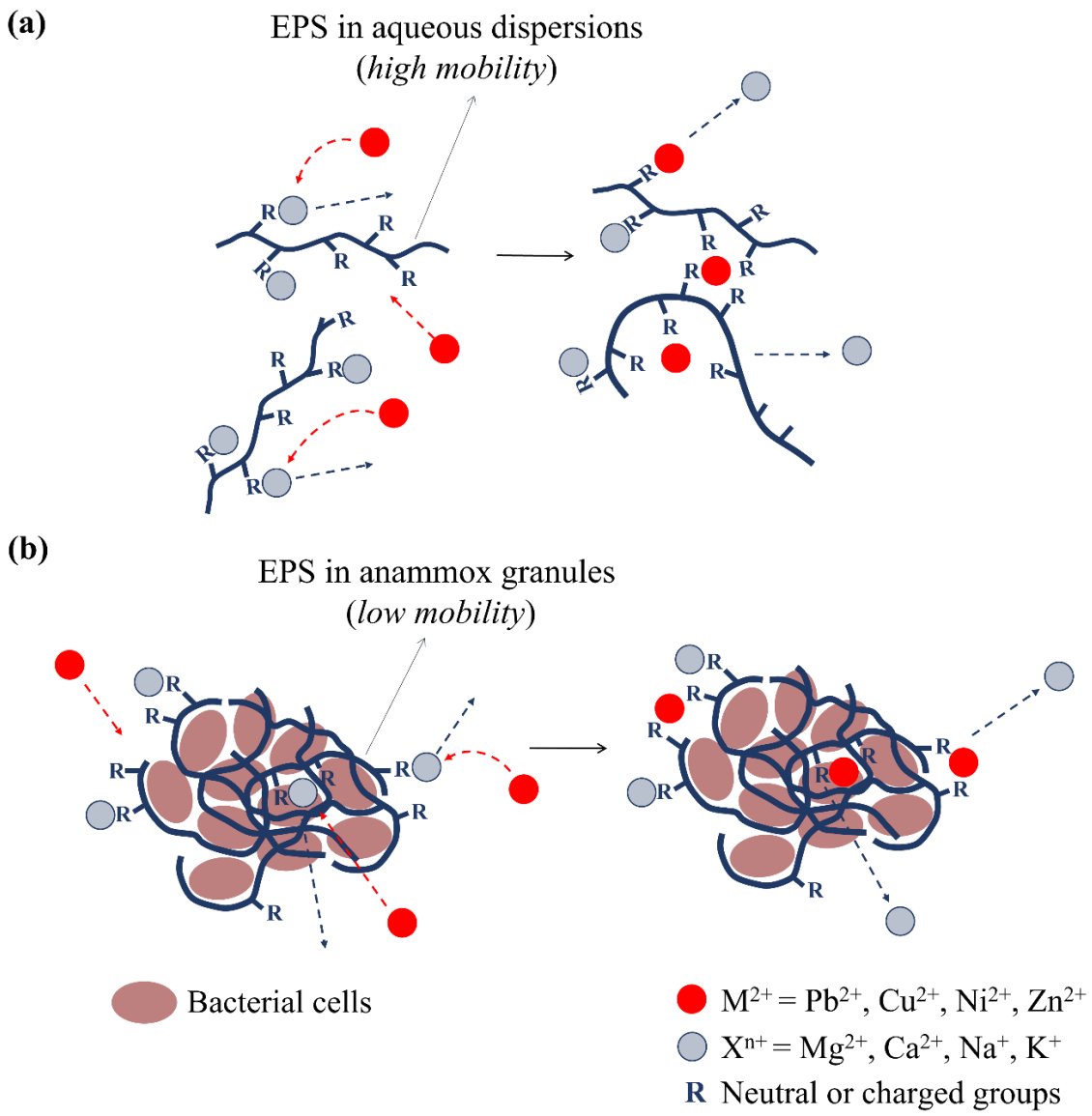

Figure 7 – Schematic representation of the adsorption mechanisms provided by the extracted anammox EPS and pristine granules. Heavy metal cations M^{2+} (Cu^{2+}; Ni^{2+}; Zn^{2+}; Pb^{2+}) form complexes with the functional groups R of EPS (i.e., neutral or charged acidic or alkaline groups) causing the partial substitution of the cations naturally bond to the EPS (i.e., Ca^{2+}; Mg^{2+}; Na^{+}; K^{+}) through ionic exchange processes. Due to the higher mobility of the EPS molecules dispersed in water, the 3D conformation of the EPS molecules could be strongly altered due to the arrangement of the EPS molecules around M^{2+}. With respect to EPS in granules, a higher number of EPS/M^{2+} bonds is hence expected in the EPS/M^{2+} complexes with a lower availability of binding sites for the formation of further bonds with other M^{2+}.

3.7 Composite EPS-activated carbon sorbent media

The use of the extracted EPS in the form of aqueous dispersions presents various disadvantages that could potentially limit the process scale-up (e.g., high transport costs, removal performance potentially decreased compared to solid-like media, etc.). The development of high-performance and

cost-effective EPS-based composite media has been therefore proposed in this study as appealing strategy to enhance the industrial applicability of AmxGS-derived EPS. The extracted EPS might be reasonably used to functionalize carrier materials (such as sorption columns, membranes, hydrogels, etc.) which would result more easily implementable on large-scale processes. Proof-of-principle of the feasible exploitation of AmxGS-derived EPS in composite media for the treatment of heavy metal-contaminated effluents was given through the functionalization of GAC-filled sorption columns. The GAC functionalization effectiveness over the consecutive EPS elution cycles is given in **Figure 8**. Large part of the EPS uptake by the GAC-filled columns took place during the first cycle (48.0 ± 3.1%); recirculating sequentially the EPS dispersion for n. 24 times the fraction of EPS adsorbed on GAC increased up to 71.5 ± 4.6%, corresponding to 71.5 ± 4.6 mg/g_{GAC}. EPS desorption phenomena were not observed by filtering abundant demineralized water, thus suggesting the strength nature of the EPS-GAC interaction and subsequent adsorption. The functionalization efficiency might enhance under acidic conditions: as previously highlighted, at pH ≤ 4 anammox EPS surface is largely protonated and Z-potential is close to neutrality, while EPS particle size increases up to aggregation/precipitation (Lotti et al., 2019a), thus potentially favoring the physisorption on GAC. This hypothesis was supported by preliminary studies performed with powder activated carbon (PAC) which evidenced an improvement of the functionalization efficiency from about 40 to 91 % upon decreasing pH from 8.5 to 4.0 (data not shown).

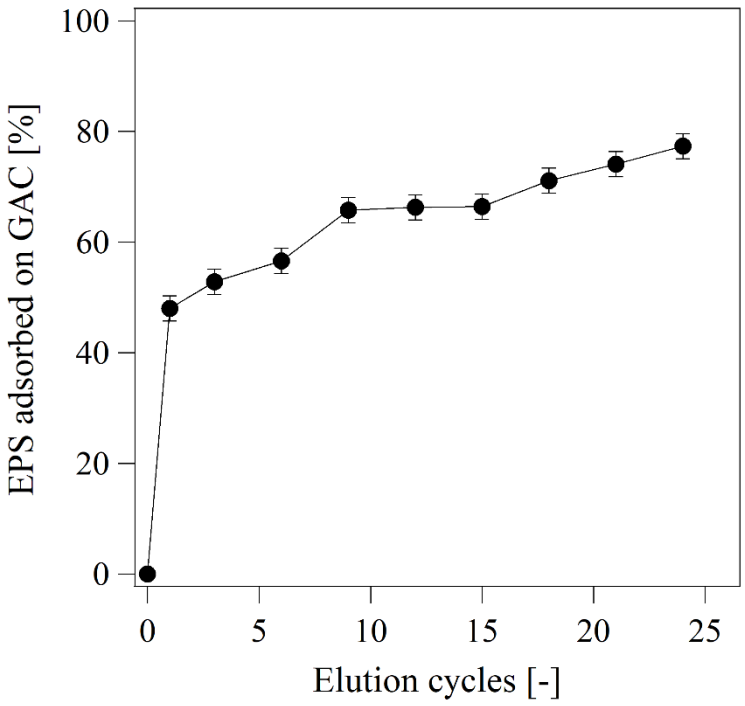

Figure 8 – Fraction of EPS adsorbed on GAC [%]. Average values ± standard deviation (n. 8 tests).

The surface morphology observation through scanning electron microscopy (SEM) revealed that EPS was mainly adsorbed on the GAC porosity as globular aggregates, whose tridimensional conformation was probably influenced by the drying procedure applied prior SEM analysis (**Figure 9**). Activated carbon (AC) is predominantly an amorphous solid with a large internal surface area and pore volume. The main characteristic common to all ACs is the presence of graphite-like plans, which show varying degrees of disorientation: the resulting space between these planes constitutes porosity. The ability of AC to adsorb molecules from both liquid and gaseous phases depends on the specific surface area or pore size distribution of the adsorbent as well as on the geometry and size of the adsorbate molecules (Benaddi et al., 2000). AC can be made from various raw materials that have a high carbonaceous content, like wood, charcoal, petroleum coke, sawdust, and coconut shells: the activation process (i.e., chemical, or physical methods) as well as AC origin can significantly affect the performance of the carbon, by altering the chemical, physical and functional properties of its surface. Particularly, the existence of surface functional groups (e.g., carboxyl, phenol, lactone, and acid anhydride) could affect the interaction of AC with polar and nonpolar adsorbates and hence

influence the selectivity towards certain molecules present in liquid phase (Park et al., 2003). The GAC surface chemistry can therefore favor the EPS adsorption upon diffusion into the GAC deeper layers and channels rich in active sites able to interact with the polymer functional groups.

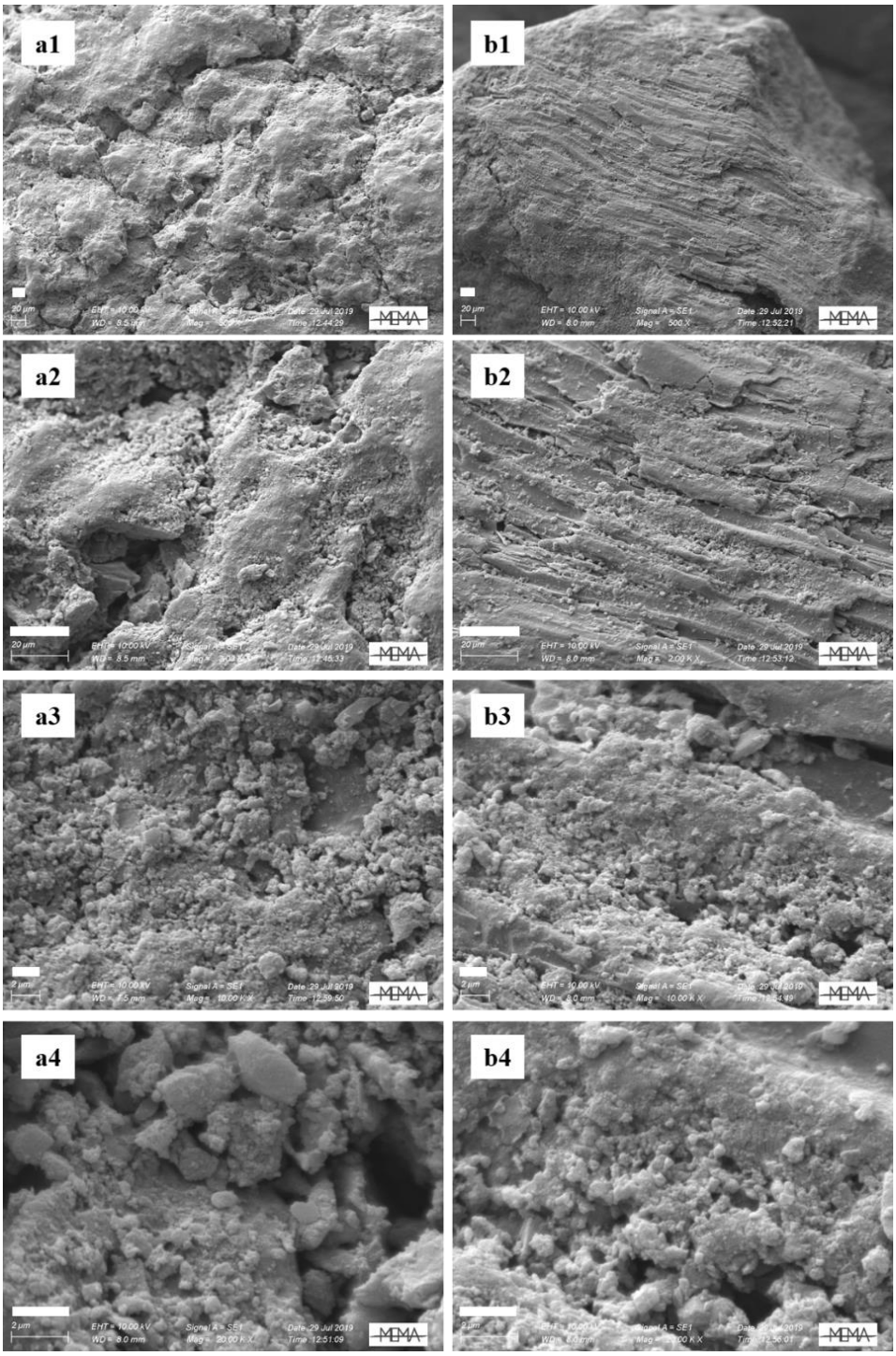

Figure 9 – SEM images related to two granules of functionalized GAC (**a**, **b**) at different magnifications: 500 X (**1**), 2000 X (**2**), 10000 X (**3**), 20000 X (**4**). Scale bar is 20 µm (**a1**/**b1**, **a2**/**b2**) and 2 µm (**a3**/**b3**, **a4**/**b4**).

Overall, the GAC functionalization protocol appeared highly performing, reproducible and easily implementable on larger scale, as schematically proposed in **Figure 10**. Compared to the lab-scale experimental set-up, the introduction of an automatized recirculation loop able to consecutively elute the EPS dispersion on the GAC-filled columns could enhance the effectiveness of the functionalization process by means of user-friendly operation units. The method robustness suggested its potential adaptation on carrier materials of various origins (e.g., sand, agriculture wastes and by-products, residues of food industry, etc.), thus expanding the opportunities of resource recovery-oriented solutions in the biosorption treatments.

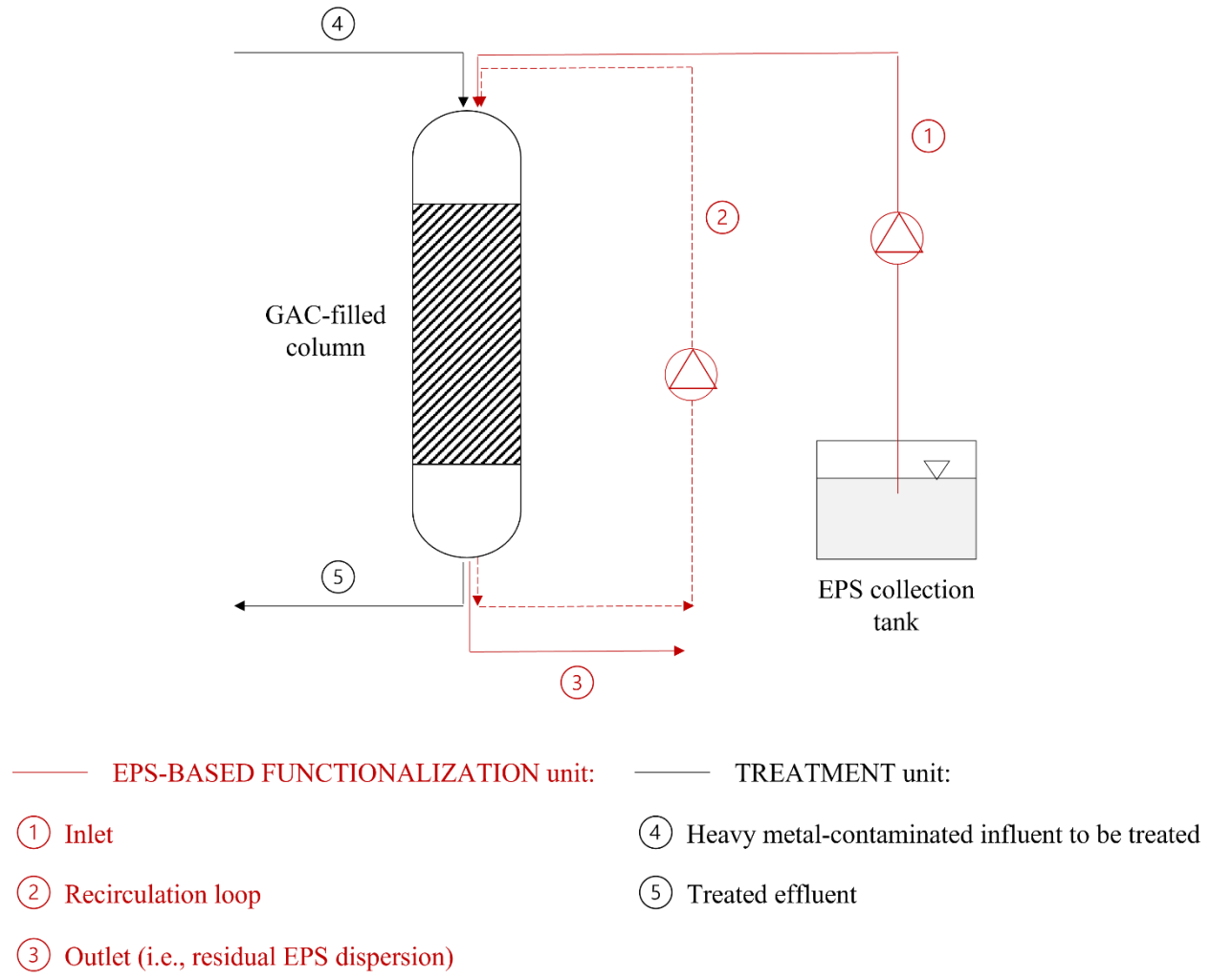

Figure 10 – Scheme of a potential configuration for the large-scale implementation of an EPS-driven functionalization unit of GAC-filled sorption columns treating heavy metal-contaminated wastewaters. The recovered EPS (in the form of aqueous dispersions) are pumped from the collection tank **(1)** towards the rector and consecutively eluted on the GAC-filled columns with a downward flow by providing a recirculation loop **(2)**. At the end of the elution cycles, whose number is strictly dependent on the GAC surface covering effectivneess and it is therefore defined in the design phase, the outlet cosisting of the residual EPS dispersion

is collected and moved away from the reactor **(3)**. The EPS-GAC composite medium is therefore used to treat the heavy metal-contaminated influent.

If compared to sorption columns filled with GAC only, the composite GAC-EPS sorption media featured greater performance in treating heavy metal-contaminated waters (**Tables 5** and **6**). Thanks to the functionalization by AmxGS-derived EPS, the removal efficiencies achieved through a single cycle of filtration were enhanced by 3.7, 35.1, 77.2 and 99.5% for Pb^{2+}, Cu^{2+}, Ni^{2+}, Zn^{2+}, respectively, in single-metal sorption tests and by 18.3, 21.4, 30.2 and 26.7% for Pb^{2+}, Cu^{2+}, Ni^{2+}, Zn^{2+}, respectively, in multi-metal sorption studies. An improvement of the sorption rates was also detected (4.3, 30.9, 91.7 and 86.4% for Pb^{2+}, Cu^{2+}, Ni^{2+} and Zn^{2+}, respectively, in single-metal sorption tests and by 36.4, 40.4, 52.2 and 48.4% for Pb^{2+}, Cu^{2+}, Ni^{2+}, Zn^{2+}, respectively, in multi-metal sorption studies). Overall, the GAC sorption performance were improved upon functionalization especially towards Ni^{2+} and Zn^{2+}, even if AmxGS-derived EPS in the form of aqueous dispersions appeared low performing towards these cations. This would suggest that the polymer three-dimensional conformation (and particularly the polymer chain arrangement and mobility and resulting metal-binding site availability) played a significant role in the adsorption phenomena, in agreement with the speculative conclusions drawn from the comparison between extracted EPS and pristine anammox granules. In line with the results obtained with AmxGS-derived EPS in a sol-like state, the performance stability in presence of distinct metal ions was confirmed. Interestingly, the Cu^{2+} uptake by GAC and GAC-EPS sorbents was improved by 77.6 and 49.9%, respectively, in multi-metal aqueous systems with respect to single-metal sorption studies, while the Pb^{2+} removals appeared comparable (slightly lower for pristine GAC in multi-metal systems). Conversely, the Ni^{2+} and Zn^{2+} adsorption decreased in presence of multiple metal ions for the composite GAC-EPS sorbent (but appeared comparable for pristine GAC) with respect to single-metal systems. This would highlight the lower affinity of AmxGS-derived EPS towards Ni^{2+} and Zn^{2+} ions, which could result in potential competitions for the available binding sites, especially considering the short time of the experiments.

Table 5 – (Percentage) removal efficiencies and sorption rates of composite GAC-EPS and GAC sorption columns achieved through a single cycle of filtration of single-metal aqueous solutions (C_0 = 80 mg/L). The results are expressed as average values ± standard deviation (n. 3 test replications).

	Single-metal sorption			
	GAC-EPS system		*GAC system*	
	Removal efficiency [%]	Sorption rate [mg/g · h]	Removal efficiency [%]	Sorption rate [mg/g · h]
Pb^{2+}	89.5 ± 4.3	8.8 ± 0.5	86.3 ± 4.7	8.5 ± 0.4
Cu^{2+}	48.9 ± 1.7	4.9 ± 0.2	36.2 ± 0.9	3.7 ± 0.2
Ni^{2+}	65.9 ± 2.9	6.2 ± 0.3	37.2 ± 3.2	3.2 ± 0.2
Zn^{2+}	74.0 ± 5.1	5.6 ± 0.3	37.1 ± 2.4	3.0 ± 0.2

Table 6 – (Percentage) removal efficiencies and sorption rates of composite GAC-EPS and GAC sorption columns achieved through a single cycle of filtration of multi-metal aqueous solutions (C_0 = 80 mg/L). The results are expressed as average values ± standard deviation (n. 3 test replications).

	Multi-metal sorption			
	GAC-EPS system		*GAC system*	
	Removal efficiency [%]	Sorption rate [mg/g · h]	Removal efficiency [%]	Sorption rate [mg/g · h]
Pb^{2+}	91.9 ± 5.7	9.0 ± 0.4	77.7 ± 4.2	6.6 ± 0.3
Cu^{2+}	86.8 ± 3.8	8.0 ± 0.4	71.5 ± 1.9	5.7 ± 0.3
Ni^{2+}	41.0 ± 1.5	3.5 ± 0.2	31.5 ± 1.4	2.3 ± 0.2
Zn^{2+}	51.2 ± 2.5	4.6 ± 0.2	40.4 ± 2.0	3.1 ± 0.1

The metal removal performance achieved simulating a batch recirculation system on both GAC and composite GAC-EPS sorbent media are given in **Figure 11**. In the case of single-metal aqueous systems, most part of the metal uptake by the composite GAC-EPS sorption columns occurred through a single passage of elution: an increase in the number of filtration cycles did not significantly improve the removal efficiency. Conversely, except for Pb^{2+}, upon increasing the number of treatment cycles (n. 8), the GAC sorption performance were considerably enhanced compared to the first passage of elution, achieving values comparable to those observed for the composite GAC-EPS

systems. This evidence would suggest that the presence of EPS mainly favoured higher sorption kinetics with respect to pristine GAC. In the case of multi-metal aqueous systems, the EPS contribution on the GAC sorption effectiveness has been more greatly highlighted upon increasing the number of elution cycles, especially in the case Ni^{2+} and Zn^{2+}. Indeed, the Ni^{2+} and Zn^{2+}adsorption efficiency of pristine GAC achieved simulating a batch recirculation system (n. 5 elution cycles) was enhanced by 42.0 and 29.7%, respectively, upon GAC functionalization with AmxGS-derived EPS. This evidence would suggest that the presence of EPS improved the GAC stability performance in presence of multiple metal ions. This effect was less emphasized in the case of Pb^{2+} and Cu^{2+} that could be efficiently removed by pristine GAC upon increasing the number of treatment cycles. Particularly, the higher affinity of GAC towards Pb^{2+} both in single- and multi-metal systems, which led to a greater adsorption with respect to Cu^{2+}, has been confirmed by literature data (Kongsuwan et al., 2009).

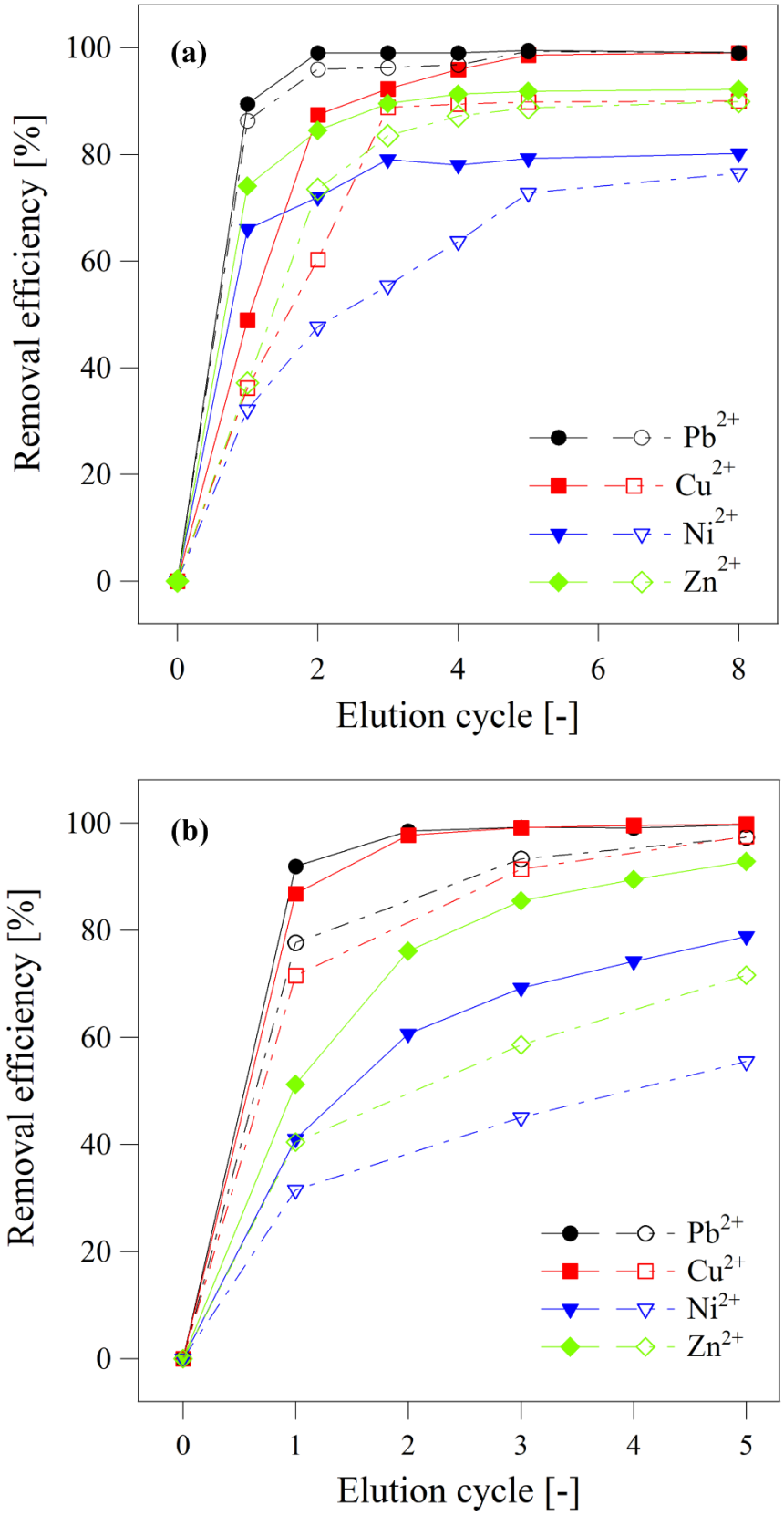

Figure 11 – Average removal efficiencies achieved by composite GAC-EPS (full markers, continuous lines) and GAC sorption columns (empty markers, dotted lines) over the consecutive treatment cycles in single-metal **(a)** and multi-metal **(b)** sorption studies.

Based on the results described above, the development of EPS-based composite media might help to progress towards more sustainable technologies for the treatment of heavy metal-contaminated wastewater; however, their design requires further investigations to ensure a successful large-scale implementation. In this perspective, it should be pointed out that these preliminary studies were mainly aimed to give insights on the proof-of-principle exploitation of AmxGS-derived EPS as functionalization agent to enhance the sorption properties of inert and/or low-performing solid media. Further technical considerations, which were not the object of the present dissertation, should be considered in follow up research. According to the results/speculations emerged from the comparison between extracted EPS and native biomass in terms of biosorption effectiveness, the reduced polymer chain mobility of EPS adsorbed on carrier materials could improve their sorption ability, thus leading to highly performing treatment units. This enhancement was not significantly appreciated for EPS-GAC composite media likely because activated carbon featured a certain sorption capacity itself under the tested conditions. Moreover, the effectiveness of the functionalization process remains to be clarified and so optimized: for instance, the selectivity of GAC in binding EPS on specific active sites might lead to an inhomogeneous surface covering that could result in preferential flows during the influent filtration and therefore to decreased treatment performance.

3.8 Outlook and perspectives

Both waste anammox granular sludge and extracted EPS proved to be highly performing in removing heavy metals from contaminated aqueous systems, thus suggesting distinct resource recovery-oriented solutions able to contribute to a more circular economy-based wastewater sector. However, the quality of the waste AmxGS, strictly dependent on the type of wastewater treated, should be pivotal in the evaluation of the most efficient and cost-effective management strategy. In this sense, the EPS extraction/recovery as well as the application of the sludge itself as metal biosorbent should carefully assessed in terms of both environmental and economic impacts. For example, in the case of sludges containing high levels of heavy metals (and/or other inorganic pollutants), whose valorization

in agriculture is unfeasible due to the high qualitative standard imposed, the use of pristine biomass and/or extracted EPS for the treatment of heavy metal-contaminated wastewater might be a viable alternative.

If compared to conventional suspended microbial flocs, granular biomasses feature the advantages of compact structure and superior settleability, which can facilitate the post-separation (Adav et al., 2009) in water and/or wastewater treatment systems. After the heavy metal biosorption (i.e., transfer of the heavy metals from liquid to solid phase), granules could be easily separated from treated water by gravity/sieving reaching concentrations up to 100 KgTS/m^3; eventually after further concentration (e.g., centrifuge, belt presses), the granular sludge could be then subjected to incineration, thus concentrating the metals in the ashes, or anyway disposed similarly to pristine biomass.

Compared to the direct application of pristine granules, the recovery and conversion of EPS into value-added products could pave the way towards interesting scenarios in the treatment of heavy metal-contaminated effluents. It should be noticed that the biosorption effectiveness largely depends on wide range of factors (e.g., pH, temperature, conductivity, EPS-pollutant contact area, etc.) which have to be considered to enhance the potential of AmxGS-derived EPS in this kind of environment-related applications. Moreover, the performance stability and selectivity in presence of organic pollutants and/or other compounds with different charges (positive) should be investigated to shed light on potential competitions among different substances eventually leading to unexpected desorption phenomena. In this study, the feasibility of exploiting the extracted anammox EPS in the treatment of aqueous systems contaminated by multiple heavy metals was suggested (i.e., significant competitions among different metal ions for the EPS binding sites were not appreciated): however, further work is required to understand the EPS sorption behaviour in presence of various (organic and/or inorganic) substances which are reasonably present in both municipal and industrial wastewaters.

A practical concern to be addressed is related to the AmxGS-derived EPS productivity and resulting potential in terms of heavy metal removal. With this regard, it could be observed that, even

considering the low growth yield of anammox bacteria (0.11 gVS/gNH_4-N, Lotti et al., 2014), significant removal potentials might be anticipated by using AmxGS-derived EPS (**Figure 12**) especially in treating highly concentrated heavy metal-contaminated effluents (up to 3.57, 2.22, 0.91 and 0.31 grams of Pb^{2+}, Cu^{2+}, Ni^{2+} and Zn^{2+}, respectively, per kilogram of NH_4-N removed from wastewater during the AmxGS-based biological process). The metal-binding capability of AmxGS-derived EPS could be therefore exploited for designing technologies able to target large part of the metal content of concentrated wastewaters. A dedicated treatment might be useful also in the case of low concentrated influents (e.g., municipal wastewaters): for instance, integrating a biosorption unit exploiting the metal-binding capacity of AmxGS-derived EPS (produced *in situ* or coming from another WWTP) before the biological processes, the accumulation of heavy metals into the produced excess sludge could be avoided (or significantly reduced), thus enhancing its qualitative properties in view of further valorization solutions and/or final disposal.

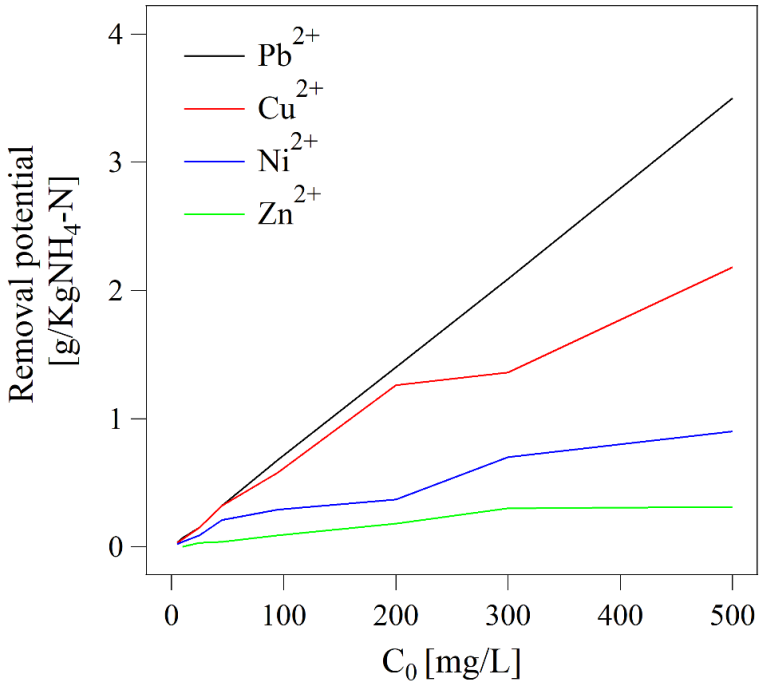

Figure 12 – Removal potential estimated for AmxGS-derived EPS as a function of the initial heavy metal concentration (C_0, mg/L) of the treated effluent.

Further research effort is demanded to progress towards the actual implementation of AmxGS-extracted EPS as high-performance and cost-effective biosorbent media in WWTPs and/or in other

industrial sectors: future work is expected to be dedicated on the optimization of the overall process of EPS production and on the assessment of the economic, technical, and environmental sustainability of the whole chain of EPS recovery/valorization. As emphasized in **Chapter 2** for AGS, another aspect which remains to be investigated is the digestibility and dewaterability of the residual (i.e., non-extracted) AmxGS, that could be enhanced by the alkaline treatment involved in the EPS extraction process, as suggested by Lotti et al. (2019a): in this way, the efficiency of the excess sludge treatment via aerobic/anaerobic digestion would be improved, and its mass to be handled reduced, thus contributing to the economic and environmental sustainability of the overall treatment chain.

Based on the results described above, an interesting route to engineer the metal-binding ability of AmxGS-derived EPS might be their application as flocculant/complexing agent to pre-treat very concentrated heavy metal-contaminated effluents (e.g., galvanic and mining wastewaters). Conceiving the treatment unit in this way, technological limitations due to the use of EPS in the form of aqueous dispersions would be avoided, in addition to the advantage of using waste-derived biomaterials in substitution to chemicals usually applied in this type of processes. Moreover, the amount of heavy metal-contaminated sludge to be disposed after this kind of pre-treatment could be significantly lower compared to the application of pristine biomass, as demonstrated by their adsorption potentialities: 171 mg Pb/gTS_{EPS} and 68 mgCu/gTS_{EPS} (**Table 4**) for EPS acting as flocculant agent versus 103.7 mgPb/$gTS_{granules}$ and 36.1 mgCu/$gTS_{granules}$ for native granules (**Figure 1**) at $C_0 \simeq 500$ mg/L. In the case of effluents contaminated by a single heavy metal (condition that can be relevant for many kinds of industrial wastewaters, Bolisetty and Mezzenga, 2016), the use of AmxGS-derived EPS as flocculant/biosorbent media might also provide a feasible option for metal recovery strategies. For example, the amyloid fibrils present in anammox EPS (Lotti et al., 2019b) could be able to reduce metal ions into metal nanoparticles via a bio-mineralization processes as reported for synthetically formed amyloid fibrils by Bolisetty and Mezzenga (2016), thus enabling the recovery of expensive metal ions (Bolisetty et al., 2011; Bolisetty and Mezzenga, 2016).

It has been suggested that industrial applicability of AmxGS-extracted EPS might be enhanced through the development of composite materials in which EPS act as functionalizing agent able to improve the biosorption effectiveness. Indeed, the search for high-performing and cost-effective sorbent media has been intensified in the last decades: the urge for renewable feedstock for material synthesis has been emphasized as result of the growing environmental awareness forcing scientific community to embrace "*green*" thinking. In this perspective, EPS could be used in combination with a broad range of waste-derived products, thus leading to integrated resource recovery-oriented solutions able to improve the environmental and economical sustainability of the water/wastewater treatment sector. For instance, activated carbon-like materials can be produced from many waste-derived sources (e.g., fly ash, lignite, coal, petroleum pitch, coconut shell, rise husk, etc.), thus combining low costs and high-quality properties compared to other available sorbents. Particularly, lignocellulosic-based activated carbon is gaining increasingly attention given that lignocellulosic biomass can be obtained from a wide range of agricultural products and by-products (Kosheleva et al., 2019).

Overall, further work is expected to guide future research: particularly, the effectiveness in using waste AGS or extracted EPS should be addressed, taking into account the environmental and economic impacts of the overall process of EPS recovery/valorization and technological implementation with respect to pristine biomass.

4. Conclusions

This chapter proposed a comprehensive overview of the biosorption properties towards heavy metals of EPS extracted from waste anammox granular sludge, thus suggesting resource recovery-oriented solutions able to progress towards a more circular economy-based water sector. Thanks to the high metal-binding capacities evidenced both in single- and multi-metal contaminated aqueous systems, AmxGS-derived EPS proved to be value-added biomaterials with outstanding properties in the treatment of heavy metal-contaminated wastewaters. With the aim of shedding light on the metal-

binding mechanisms of extracted and non-extracted EPS in the native biomass, the comparison with pristine anammox granules was added. Different biosorption capacities were observed for extracted EPS (84.9, 52.8, 21.7 and 7.4 mg/gTS_{EPS}) and pristine anammox granules (103.7, 36.1, 48.2 and 49.8 mg/g$TS_{granules}$) towards Pb^{2+}, Cu^{2+}, Ni^{2+} and Zn^{2+}, respectively (C_0=500 mgM^{2+}/L) and distinct metal-binding pathways were postulated based on the interpretation of the experimental data through theoretical models. Despite the potential metal uptake exerted by other components than EPS in pristine granules (e.g., cell surface adsorption, intracellular accumulation, etc.), the metal-binding capability of EPS could be altered by chemical modifications induced by the extraction protocol applied and by the spatial re-arrangement allowed by the much higher mobility of EPS in aqueous dispersion compared to EPS in native granules. A molecular-level analysis, supported by various techniques, disclosed a multifaceted adsorption mechanism, involving a combination of electrostatic interaction, ion-exchange, complexation, and precipitation. Particularly, it was found that AmxGS-derived EPS behaved like flocculant/complexing agents in presence of high-concentrated heavy metal-contaminated aqueous systems, leading to the spontaneous precipitation of EPS-metal composite aggregates.

The development of composite sorbent media was reasonably proposed as strategy to enhance the AmxGS-derived EPS industrial applicability. With this regard, the extracted EPS were used to functionalize GAC-filled sorption columns, thus giving proof-of-principle of the potential development of EPS-based composite media as appealing route to progress towards more sustainable technologies for the treatment of heavy metal-contaminated wastewater.

Appendix

A.1. Evaluation of anammox EPS concentration (weight%) in aqueous systems via UV-vis spectroscopy

The concentration of AmxGS-derived EPS in aqueous systems was evaluated via UV-vis spectroscopy (UV-visible spectrophotometer Cary 100 Bio), according to the method here described. An aliquot of the EPS extract was frieze-dried and weighted in order to measure its EPS (weight) concentration. The remaining EPS extract was then used to prepare EPS dispersions with lower concentrations via subsequent dilutions with ultrapure water. The UV-vis spectra in 350 – 600 nm wavelength range were collected for all the obtained EPS samples (**Figure A.1a**). The intensity of the characteristic absorbance peak of anammox EPS at about 408 nm wavelength increased linearly with the EPS concentration: the absorbance/concentration calibration curve (**Figure A.1b**) was thus obtained plotting the EPS concentration-absorbance data and fitting them via linear regression (experimental data reported as average values ± standard deviation, n. 3 replications).

For the determination of the EPS extraction yields ($mgTS_{EPS}/gVS_{granules}$; TS: total solids, VS: volatile solids) all the EPS extracts were analyzed via UV-Vis spectroscopy, evaluating the absorbance peak at 408 nm wavelength (attributed to the presence of cytochrome-c, Cirpus et al., 2005), and their concentration was determined using the absorbance/concentration calibration curve. Known concentration and volume of the EPS extracts, the EPS extraction yield was therefore calculated as ratio between the amounts of extracted EPS (TS_{EPS}, mg) and pristine granules ($VS_{granules}$, g).

This method was also adapted to estimate the residual anammox EPS concentration in aqueous dispersion upon consecutive elution cycles on GAC-filled sorption columns.

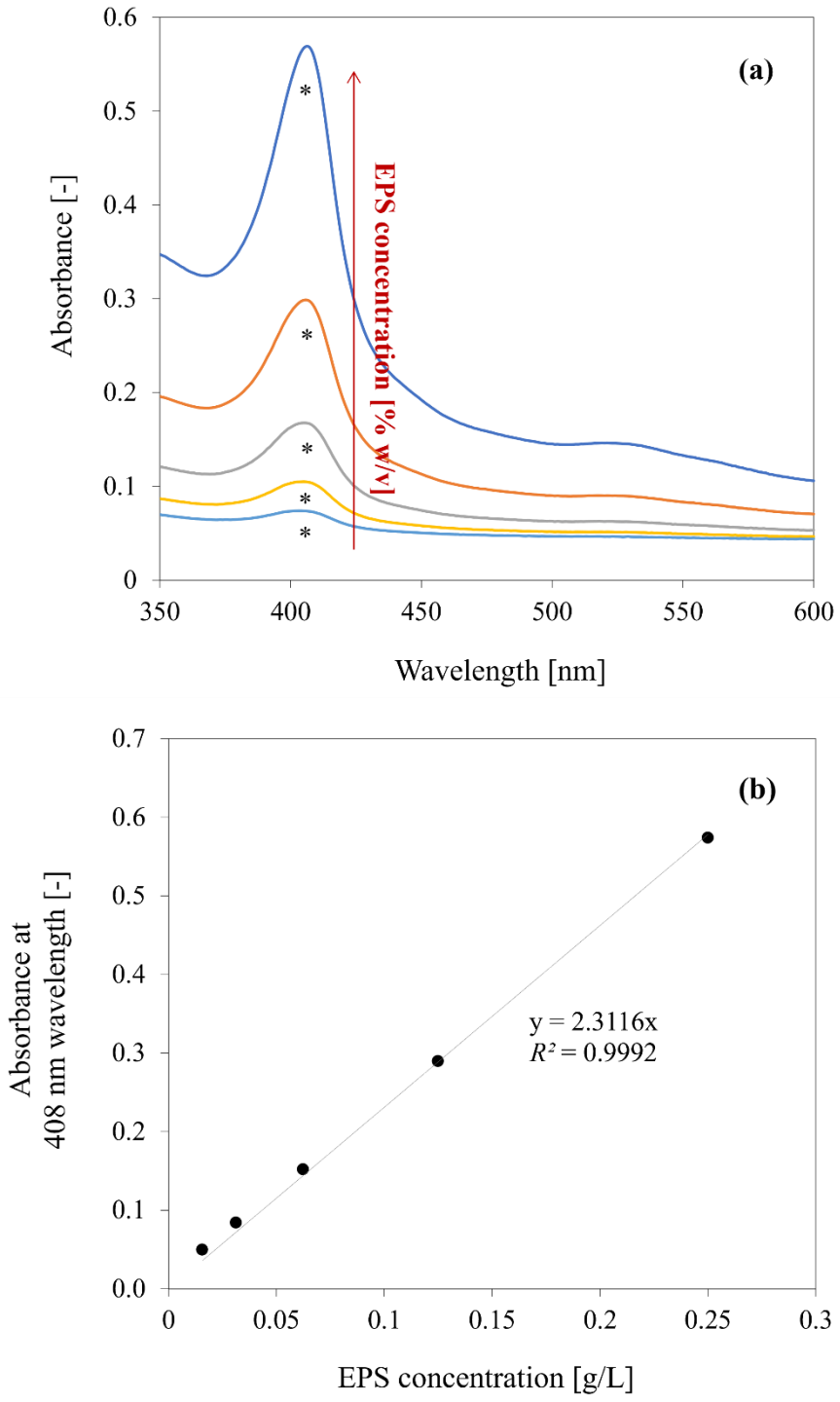

Figure A.1 - Evaluation of anammox EPS concentration (weight%) in aqueous systems via UV-vis spectroscopy.

A.2. Heavy metal biosorption kinetics

The preliminary biosorption kinetic studies were carried out by treating synthetic aqueous solutions containing the studied heavy metal cations M^{2+} (C_0 = 40 mg M^{2+}/L) with the recovered anammox EPS (2.82 ± 0.05 % (w/v) as EPS dry weight) at pH 6.38 ± 0.12 and room temperature. The biosorption performance were evaluated over time (0 - 24 h) after centrifugation (10000xg, 15 min, room temperature) and the experimental data were correlated by a first order kinetic model (Eq. A.1):

$$C_{M^{2+}}(t) = A \cdot e^{-\frac{t}{\iota}} + A_0 \quad \text{(A.1)}$$

where $C_{M^{2+}}(t)$ (%) is the heavy metal content remained in solution (i.e., not adsorbed) at time t; ι (%) is the relaxation time, correlated to the process velocity and time required to reach the curve plateau (i.e., sorption equilibrium); A and A_0 (%) are the pre-exponential term and the asymptotic value of heavy metal content remained in solution, i.e., not adsorbed, at equilibrium, respectively.

Although the Pb^{2+} and Cu^{2+} biosorption by anammox EPS was faster than the Ni^{2+} and Zn^{2+} uptake, all the biosorption processes achieved the equilibrium within 6 hours of contact (**Figure A.2**).

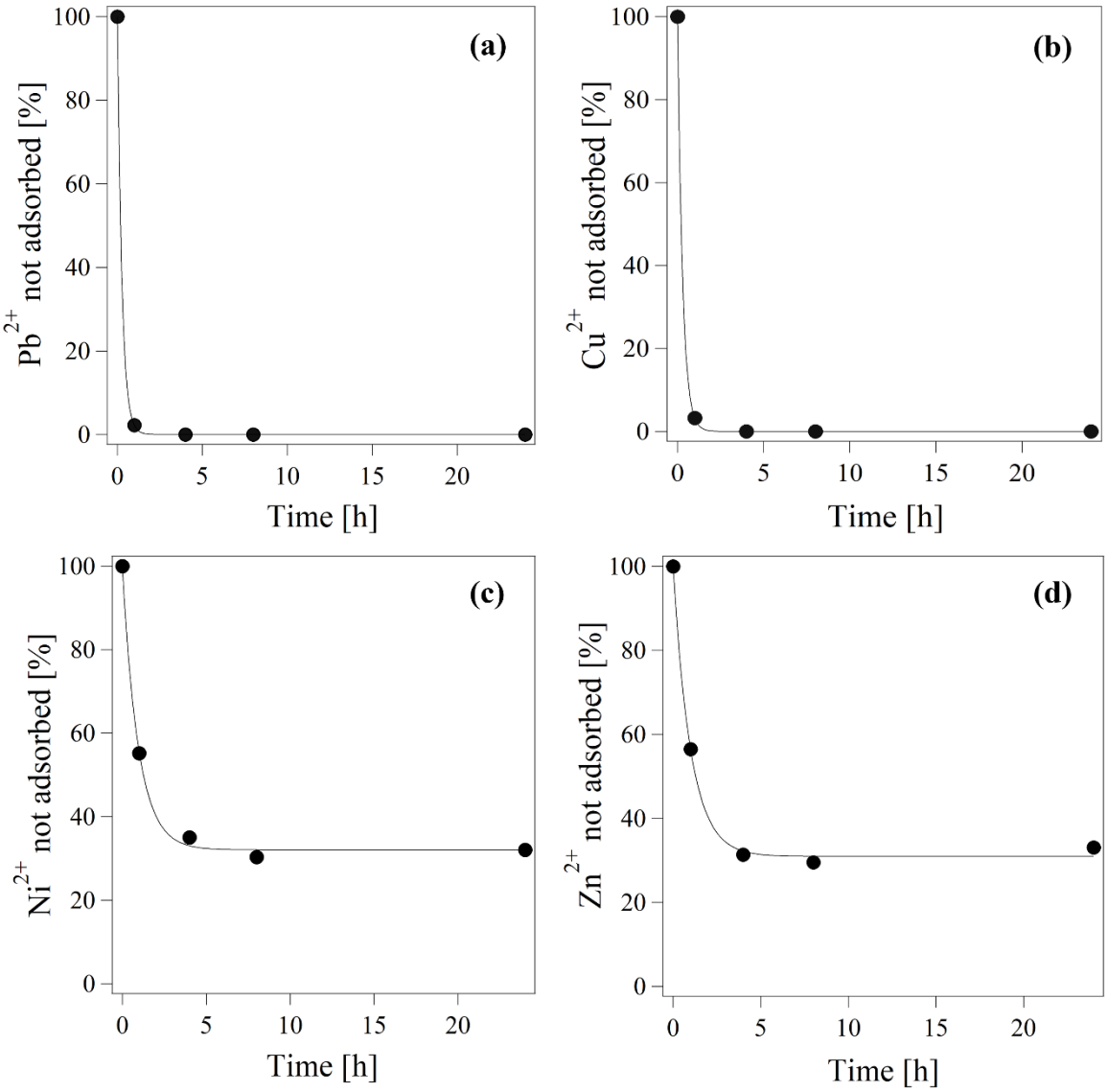

Figure A.2 - Biosorption kinetics of Pb^{2+} (**a**), Cu^{2+} (**b**), Ni^{2+} (**c**) and Zn^{2+} (**d**) on the recovered anammox EPS (i.e., percentage heavy metal content remained in solution, and thus not adsorbed, over time) and related fits through a first order kinetic model.

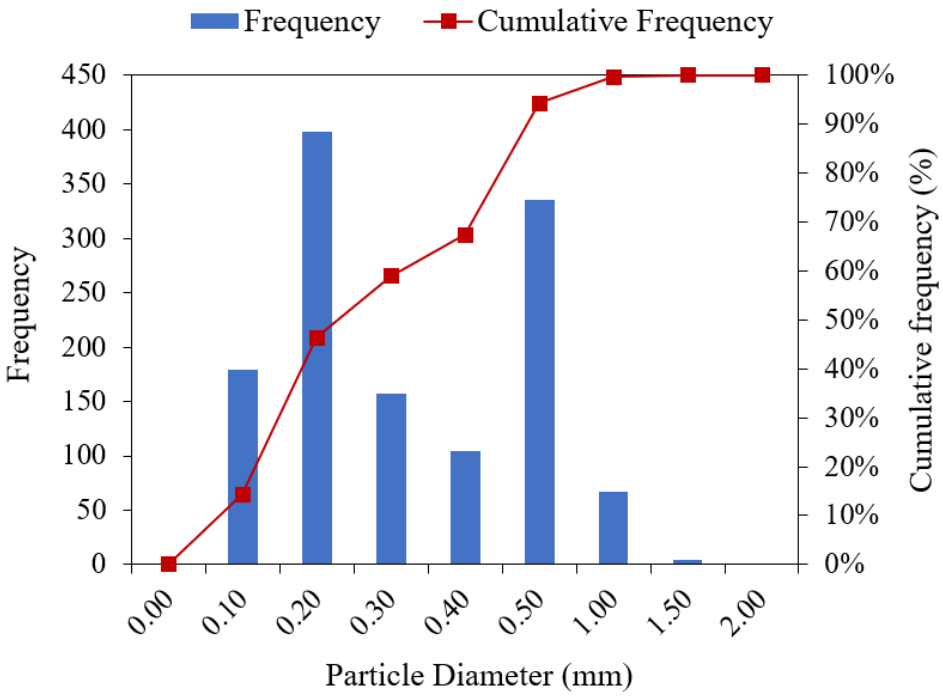

Figure A.3 – Particle size distribution of anammox granules.

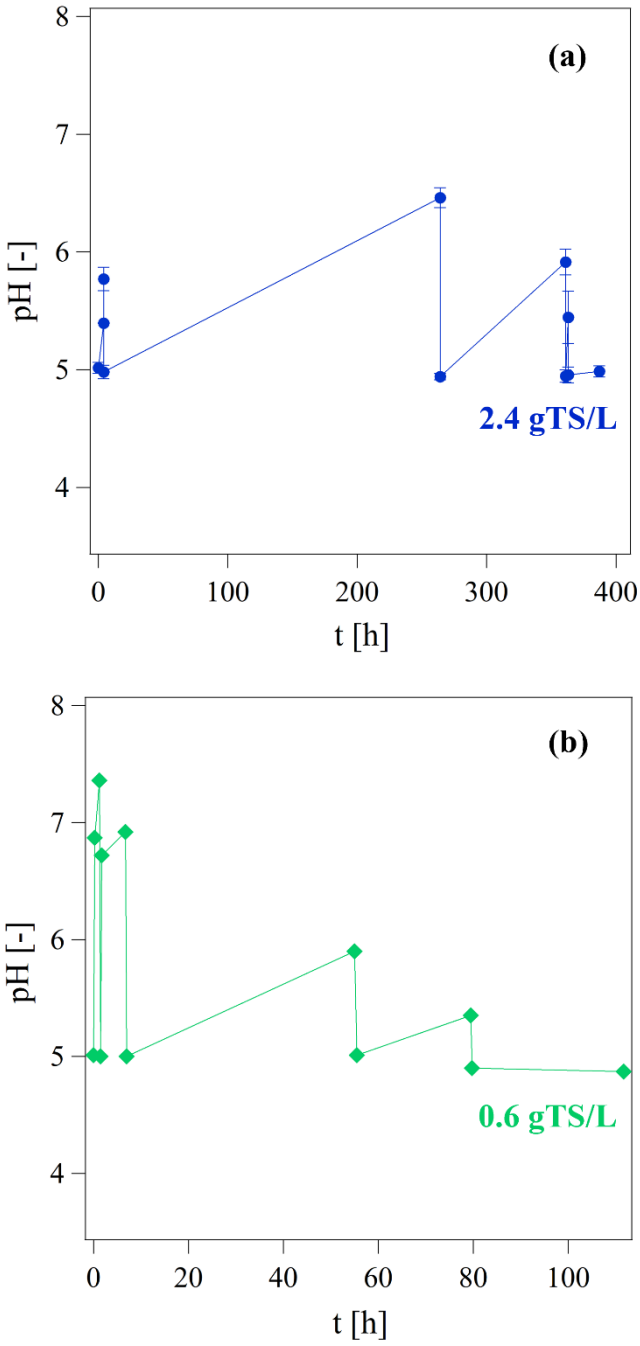

Figure A.4 – pH monitoring during the granule pre-treatment aimed at overcoming their pH buffer capacity, which produced a progressive alkalizing effect in the aqueous medium.

Table A.1 – Literature survey of sorbent and biosorbent media used for copper removal.

	pH (-)	C_0 (mg/L)	Q_e (mg/g)	References
Clay				
Bentonite clay (after calcification 400 °C)	5	90	11.89	Bertagnolli et al., 2011
Bofe bentonite calcinated clay	4.5	100	19.06	de Almeida Neto et al., 2014
Magnetic adsorbents				
Sulfonated graphene oxide composite	4.68	73.71	63.73	Hu et al., 2013
Pectin-coated iron oxide magnetic nanocomposite	-		48.99	Gong et al., 2012
Hyaluronic acid-supported magnetic microspheres	6.8	50	12.2	Lan et al., 2013
Alumina				
γ-alumina nanoparticles	5	200	31.3	Fouladgar et al., 2015
3 new alumina adsorbents of acidic, neutral, and basic nature	7	1	27.96, 28.58, 28.59	Mahmoud et al., 2010
Aminated/protonated mesoporous alumina	-	20	7.92, 14.53	Rengaraj et al., 2004
Fungal biomass				
Chlorella sp. and Chlamydomonas sp.	7	5	33.4	Wan Maznah et al., 2012
Rhizopus oryazae filamentous fungus	6	200	19.4	Bhainsa and D'Souza, 2008
Aspergillus niger biomass	5	100	20.62	Mukhopadhyay et al., 2007
Algal biomass				
Macroalga, Sargassum muticum	4.5	190	71	Herrero et al., 2011
Dried micro-algal/bacterial biomass	4	1000	31	Loutseti et al., 2009
Codium vermilara	5	150	16.52	Romera et al., 2007
Yeast biomass				
Saccharomyces cerevisiae biomass	5	200	2.59	Cojocaru et al., 2009
ETDAD-modified biomass of baker's yeast	6	100	65	Yu et al., 2008
Bacteria				
Escherichia coli	5	64	10.36	Ravikumar et al., 2011
Lactobacillus sp. (DSM 20057)	6	39.8	0.046	Schut et al., 2011
Pseudomonas stutzeri	5	100	36.2	Hassan et al., 2009

Table A.2 – Literature survey of granular biomasses (AGS: aerobic granular sludge; AnGS: anaerobic granular sludge; AmxGS: anammox granular sludge) used as biosorbent media for the heavy metal removal. Q_{max} values (mg/g) are related to the theoretical maximum adsorption capacities interfered by Langmuir adsorption isotherm model.

Biosorbent	Heavy metals	pH	Q_{max} (mg/g)	References
AGS	Copper	5	36.72	Gai et al., 2008
AGS	Zinc	5	64.44	Wei et al., 2016
AGS	Nickel	7	28.00	Xu et al., 2006
AGS; AnGS	Nickel	4	65.77 (AGS) 54.18 (AnGs)	Li et al., 2017
AmxGS [1]	Lead, Copper, Nickel, Zinc	5 - 6	103.7, 36.1, 48.2, 48.9	Present study

[1] Q_{max} values (mg/g) related to the maximum adsorption capacities obtained under the tested experimental conditions (C_0=500 mg/L), given that the equilibrium sorption data were not well correlated by Langmuir model.

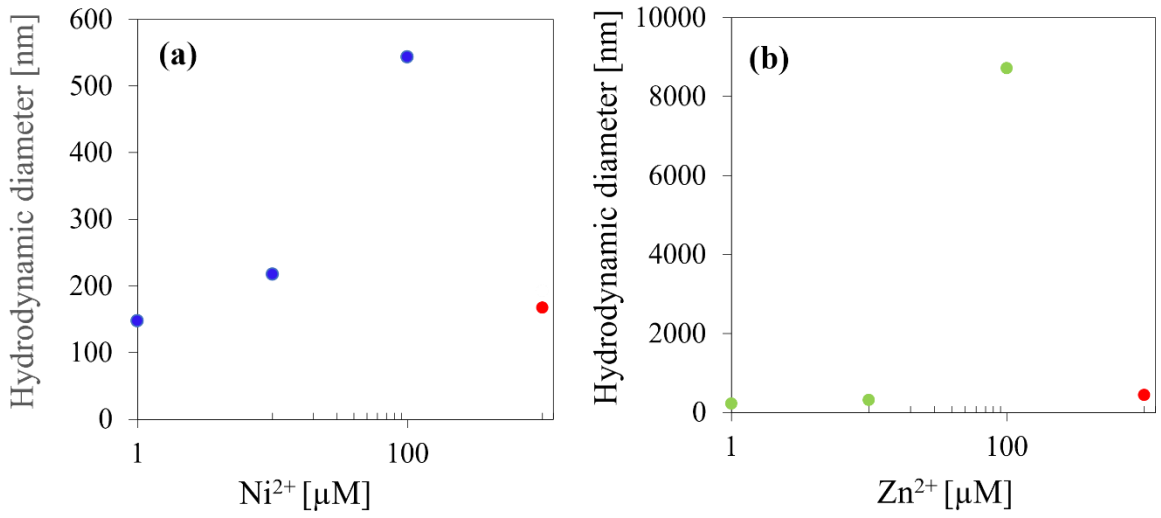

Figure A.5 - Hydrodynamic diameter of anammox EPS (0.01% w/v) in aqueous dispersions (pH 8) containing increasing concentrations of Ni^{2+} (**a**) and Zn3n h^{2+} (**b**). The increase of Ni^{2+}/Zn^{2+} content resulted in a strong increase of EPS particle size, and in a reduction of the repulsive force among EPS units, thus leading to aggregation. Precipitation was observed increasing the metal content up to 1000 mM, as confirmed by the significative drop of the hydrodynamic diameter (red markers).

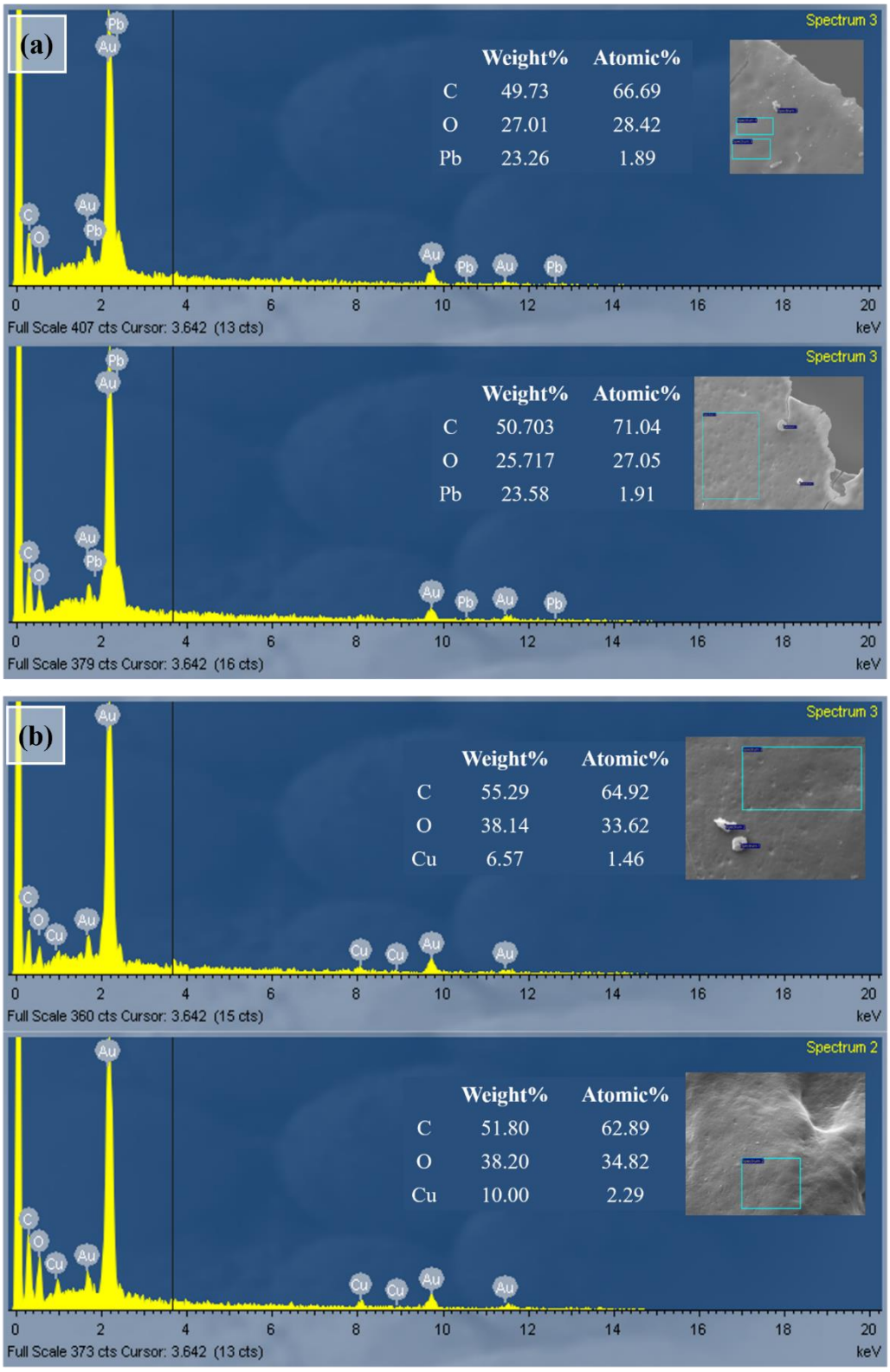

Figure A.6 – Elemental analysis of composite EPS-Pb aggregates **(a)** and EPS-Cu aggregates **(b)** (precipitated in single-metal sorption tests at C_0=500 mg/L) detected by energy-dispersive X-ray spectrometry (EDS Oxford Inca 250) in two points of analysis reported as example. The Au peaks are due to the sample coating with gold prior to SEM-EDS analysis.

Table A.3 – Ionic strength (μ, mM) of EPS-M^{2+} mixed aqueous systems (M^{2+}=Pb^{2+}, Cu^{2+}, Ni^{2+} and Zn^{2+}, respectively) in single-sorbate sorption tests performed with increasing initial metal concentration ([M^{2+}], mM). pH of the polymer-metal aqueous dispersions was adjusted to 5-6 adding 0.1 NaOH/1M HCl.

EPS-Pb aqueous systems (pH 5)		**EPS-Cu aqueous systems** (pH 5)	
[M^{2+}] (mM)	μ (mM)	[M^{2+}] (mM)	μ (mM)
0.02	16.50	0.08	25.24
0.05	20.22	0.17	28.29
0.11	20.40	0.36	28.86
0.22	20.75	1.49	22.42
0.47	26.23	3.18	22.27
0.98	23.00	4.46	22.72
2.02	21.25	6.09	27.59
2.58	21.70	7.76	30.63
EPS-Ni aqueous systems (pH 6)		**EPS-Zn aqueous systems** (pH 6)	
[M^{2+}] (mM)	μ (mM)	[M^{2+}] (mM)	μ (mM)
0.09	7.39	0.07	13.11
0.19	7.68	0.15	10.86
0.39	8.29	0.31	23.54
0.80	9.51	0.61	14.71
1.59	11.90	1.19	15.46
3.11	16.44	2.60	20.67
5.06	22.29	3.92	19.69
8.59	32.88	6.55	29.81

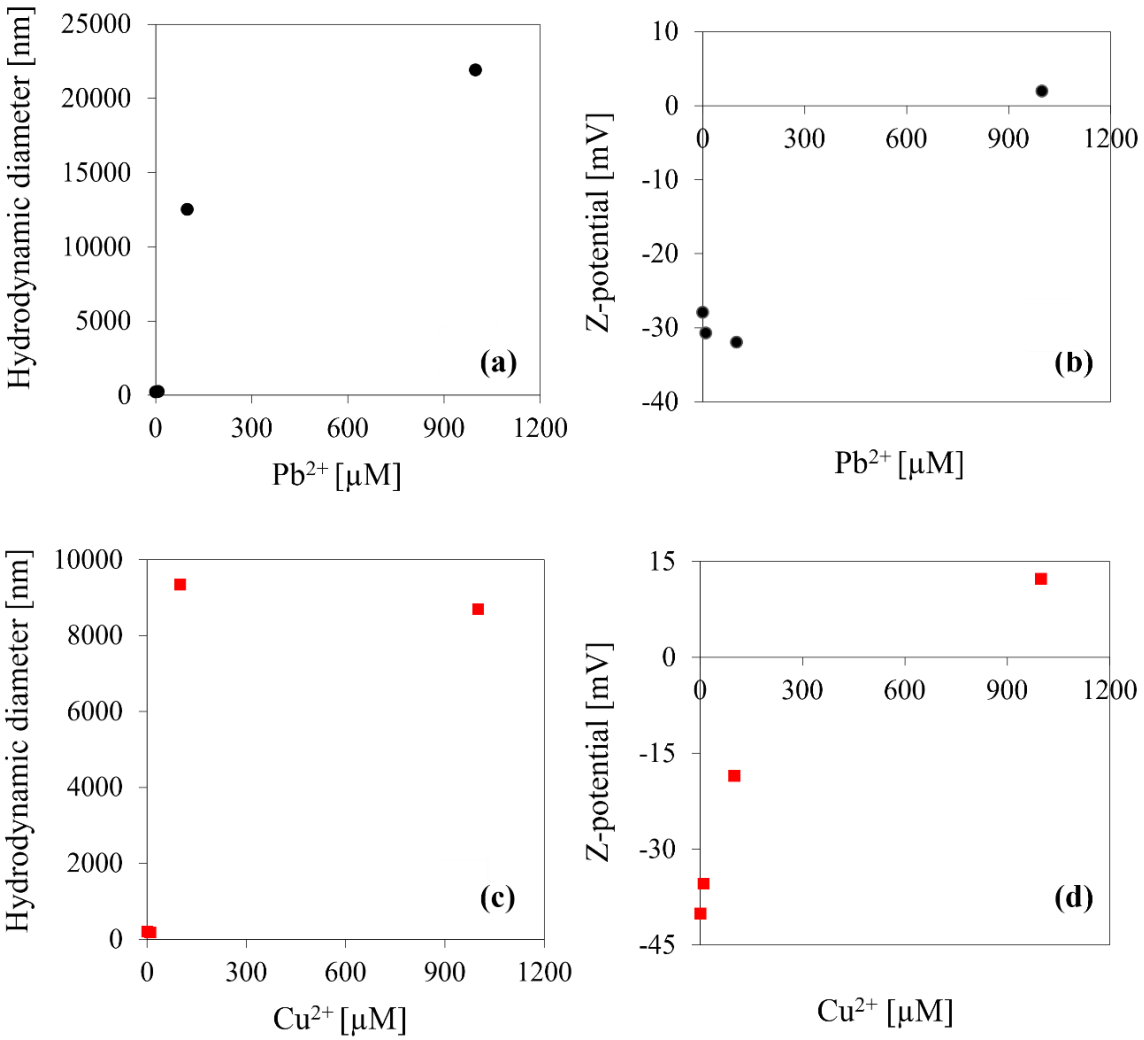

Figure A.7 - Hydrodynamic diameter and Zeta-potential of anammox EPS (0.01% w/v) in aqueous dispersions (pH 8) containing increasing concentrations of Pb^{2+} (**a**, **b**, respectively) and Cu^{2+} (**c**, **d**, respectively). The increase of Pb^{2+}/Cu^{2+} content resulted in a strong increase of EPS particle size, and in a reduction of the repulsive force among EPS units, thus leading to aggregation.

Chapter 5

Conclusions and future perspectives

The urge for more sustainable wastewater treatment solutions based on the well-established concept of "*circular economy*" has been emphasized in the last decades, thus progressively shifting the research attention towards new resource recovery-oriented technologies. Particularly, strategies for the efficient management of waste sludge are demanded with the aim to improve the economics and sustainability of the overall treatment chain. Granular sludge (GS)-based technologies have been recognized as high-performance and cost-effective alternative to conventional activated sludge systems able to hold the promise of a more circular economy-based water sector by means of enhanced potentials in terms of resource recovery. Granular sludge consists of a self-aggregated biofilm (without the presence of carrier materials) in which microrganisms are embedded in a matrix of hydrated Extracellular Polymeric Substances (EPS) secreted by bacterial consortia during cell metabolism (Flemming and Wingender, 2010; Seviour et al., 2019, 2012). EPS are a complex mixture of proteins (PN), polysaccharides (PS), uronic acids, lipids, nucleic acids, humic-like substances, etc. and are mainly associated with the structural integrity, rheological behaviour, physic-chemical properties, and functional stability of granules on one hand and with the protection from predation and harsh environmental conditions, nutrients/exoenzymes reservoir, and homeostasis functions of the microbial communities inhabiting/forming the granules on the other hand (Seviour et al., 2019).

The recovery of EPS from waste GS and consequent conversion into value-added biomaterials appears pivotal in driving the paradigm shift from wastewater treatment plants (WWTPs) towards resource recovery facilities (WRRFs). The versatile properties of GS-derived EPS can be successful exploited in multiple industrial/environmental solutions that could represent an eco-friendly alternative to synthetic polymer-related applications able to contribute to a less fossil-fuel dependent manufacturing sector. However, the implementation of EPS recovery-oriented solutions is currently hampered by many bottlenecks which can be mainly identified in a still incomplete understanding of

the EPS chemical and functional properties as well as in the poor regulation of the EPS production depending on the specific applicative goals. The high-diversity and complexity of the EPS matrix makes challenging its fine characterization, thus pushing the research efforts towards more dedicated approaches and methodologies able to lead to a deeper awareness of the EPS potential in the resource recovery framework. The general criteria applied for the EPS extraction should be updated based on the distinct research purposes to move towards the sustainable production of high-quality EPS-based biomaterials in line with the standard imposed by the targeted industrial sector.

The present thesis has been developed starting from the described holdups with the aim to progress towards the feasible conversion of GS-derived EPS into value-added biomaterials to be applied in multiple industrial and/or environmental solutions. The thesis mainly aimed to shed light on the recovery, characterization, and valorization of EPS from granular sludge of different origin (particularly, aerobic and anammox GS). Distinct resource recovery-oriented scenarios have been addressed based on the nature of the studied microbial aggregates: the high-diversity of the EPS physic-chemical and functional properties has been therefore valorized to expand the EPS potential in terms of resource recovery. Particular emphasis has been dedicated to the development of consistent approaches to engineer the outstanding features of these waste-derived biopolymers, evaluating the impact of the overall recovery process on the EPS valorization effectiveness.

Biopolymer-based hydrogels are gaining increasingly commercial interest for environmental-related applications thanks to their excellent properties of water-holding ability, biocompatibility, softness, etc. The hydrogel-forming ability of AGS-derived structural EPS (i.e., portion of total EPS considered as strongly involved in the structural integrity of granules, Felz et al., 2016) might be therefore engineered in sustainable industrial solutions with great market supply potential. The successful implementation of EPS-based hydrogels appears subordinated to a better understanding of their physic-chemical and mechanical properties: a key aspect emphasized in the framework of this thesis is how these features can be tuned by the modification of the extraction/recovery methods. With this

regard, **Chapter 2** proposes a comprehensive analysis of the AGS-derived sEPS hydrogel-forming properties and post-gelling mechanics able to progress towards a deeper understanding of this class of waste-derived biopolymers. The capability of sEPS to form ionically cross-linked hydrogels in presence of divalent metal ions has been therefore deeply investigated and the methodologic aspects have been intensively emphasized along the entire research line. Particularly, the synergy between the sample production processes (i.e., sEPS extraction and hydrogel-formation) and following characterization studies has been demonstrated as key tool to improve the robustness of the analytical investigation. Recognizing rheometry as eligible technique to shed light on the mechanics of sEPS-based hydrogels, the hydrogel-forming protocols have been hence optimized to ensure high-resolution measurements based on the following criteria: (i) minimization of the polymer consumption for the analytical investigation and (ii) optimization of the hydrogel geometry and homogeneity. The design of supports forcing the sol-gel transition into pre-selected geometries as well as the use of dialysis to control the gelling kinetics have been demonstrated as successful tools to improve the post-gelling homogeneity and experimental reproducibility. By means of simple practices in the design phase, sEPS-based hydrogels can be therefore prepared into a wide range of distinct products (in terms of geometry, uniformity, and strength) as a function of the specific research goals. Another methodologic concern highlighted in **Chapter 2** is related to the high complexity of sEPS that makes challenging their fine characterization: the implementation of a comparative study with well-known biopolymers (i.e., alginate and k-/ι-carrageenan), whose hydrogel-formation was driven by distinct mechanisms and functional components, was hence demonstrated as a robust approach to strengthen the outcome of the mechanical analysis. Particularly, the study of sensitive parameters extrapolated from the mechanical profiles observed under both compression (e.g., Young's modulus, E) and shear stress conditions (e.g., storage modulus, G', loss modulus, G'', complex viscosity, η^*) was found to be useful not only to elucidate the mechanics of the studied systems but also to gather information (at speculative level) on the gelling processes. Looking at the

results of the mechanical tests under compression conditions according to a comparative approach, the main findings can be summarized as follows.

i. The higher polymer and (ionic) cross-linker concentrations needed to enable the sEPS hydrogel-formation with respect to the studied reference polymers gave a proof-of-principle of the greater complexity and diversity of the sEPS matrix (likely involving also compounds not really contributing to the gelling processes and resulting post-gelling mechanics).

ii. Distinct mechanical responses to consecutive compression-decompression cycles were observed among the studied biopolymer-based hydrogels, thus pointing out that the polymer chemical and functional properties at molecular-level strongly affected the post-gelling mechanics. Interestingly, sEPS and ι-carrageenan hydrogels behaved similarly under mechanical stresses (i.e., consecutive compression-decompression cycles): their linear elastic behaviour was preserved along the subsequent loading-unloading cycles, but lower levels of stiffness were achieved compared to alginate and k-carrageenan-based systems.

iii. For all the studied biopolymers, the post-gelling stiffness varied significantly over the applied hydrogel-forming conditions, even if the overall mechanical response remained almost unchanged: *E* increased upon increasing the polymer and (ionic) cross-linker concentrations and varied based on the (divalent) metal cation used as cross-linking agent. The distinct dependence of the post-gelling stiffness on the nature of the metal cation used in the gelling processes could be explained by the different functional groups involved in the hydrogel-formation of the studied biopolymers.

The oscillatory shear measurements confirmed that sEPS were able to form (ionically cross-linked) hydrogels with solid-like mechanical properties and high-water content (up to 99 wt%): particularly, the minimum sEPS (weight percentage, wt%, $g_{sEPS}/g_{Hydrogel}$) concentration enabling the formation of an extended cross-linked polymeric network has been recognized in the range 2.5 – 5 wt% (for sEPS concentrations lower than 2.5 wt% only weakly interconnected polymeric clusters were

probably present). In agreement with the trend observed for the Young's modulus *E*, the storage modulus *G'* significantly increased upon increasing the sEPS concentration (wt%): the relationship has been satisfactorily simulated by a power-low function whose exponential coefficient ($n \simeq 2$) suggested that a percolation site process could drive the sEPS hydrogel-formation.

From an applicative point of view, the feasibility of forming AGS-derived sEPS-based hydrogels with mechanical properties comparable to other biopolymer-based systems currently applied for commercial purposes has been demonstrated, thus suggesting potential resource recovery-oriented solutions able to progress towards a less fossil fuel-dependent manufacturing sector.

However, the mechanical characterization cannot be sufficient to gain a comprehensive overview of the great potential of sEPS-based hydrogels as value-added biomaterials. In the framework of this thesis, an integrated and synergic assessment of multiple application-related properties, taking into account the impact of the overall process of the EPS extraction/recovery on the valorization effectiveness, has been presented. This strategy has been hence proposed to progress towards a more consistent regulation of the EPS production and application, thus defining integrated targets to address existing and potential industrial and/or environmental solutions. Particularly, these aspects define the outlines of **Chapter 3** in which the AGS-derived sEPS hydrogel-forming properties have been engineered based on the high qualitative standards imposed by the agronomic sector. Indeed, biopolymer-based systems have been recognized within the scientific community as key actors able to drive more sustainable agriculture-related technologies and practices thanks to their outstanding features (e.g., biodegradability, biocompatibility, cost-effectiveness, etc.). A great market potential demand might be therefore anticipated for the AGS-recovered sEPS that can be established as feasible alternative to synthetic polymer-derived materials. In this perspective, the overall process of extraction/recovery has been optimized to improve the agronomic potential of the extractable sEPS (e.g., in terms of high nutrient content and low quantity of phytotoxic elements). Particularly, sEPS and derived biomaterials (i.e., hydrogels) with agronomy-oriented characteristics have been

obtained by the use of chemicals not containing sodium and chlorine (which are considered phytotoxic in large quantities) without significantly altering the sEPS extraction yield, macromolecule nature (e.g., in terms of PN and PS content) and overall hydrogel-forming ability. Both sEPS and derived hydrogels hence appeared within the maximum limits in terms of contaminant levels (e.g., heavy metals, to be verified values related to Cr(VI)) imposed by the environmental legislation in matter of soil improvers and fertilizing products (Regulation EU 1009/2019).

The encouraging potential of sEPS-based biomaterials (e.g., hydrogels) in sustainable agro-practices upon optimization of the extraction/recovery processes has been hence demonstrated. The behaviour as superabsorbent polymers (SAPs) suggested by the great water-holding capacity could make sEPS-based hydrogels a viable eco-friendly alternative to synthetic polymers (e.g., polyacrylate-based SAPs) for soil conditioning-related applications. Moreover, the feasibility of forming nutrient-loaded sEPS hydrogels (e.g., upon swelling in nutrient-enriched aqueous solutions) has been observed, giving a proof-of-principle of their nutrient release ability. Overall, these findings might pave the way towards further resource recovery-oriented solutions in agriculture such as controlled-release systems of agrochemicals in soil.

Being aware of the key role of the biodegradability assessment in agriculture-oriented solutions, respirometric techniques have been implemented taking advantage of time-saving and well-established experimental protocols able to emphasize the impact of the whole extraction/valorization process on the biodegradation of both sEPS and derived hydrogels. It has been demonstrated that sEPS and derived hydrogels can be utilized as substrates from the microbial communities inhabiting the activated sludge, but the chemicals applied in the extraction and gelling processes strongly influenced the organic matter biodegradation. Moreover, it has been found that the overall sEPS biodegradation was differently kinetically characterized upon hydrogel-formation: the establishment of an extended 3D polymeric network in which the sEPS macromolecules are more confined likely result in a decreased substrate accessibility, thus requiring further hydrolytic reactions before their

microbial utilization. Overall, the outcome of respirometry might be useful to lead towards a more aware design of the experiments of biodegradation in soil which should be necessarily integrated to address the conformity of the developed sEPS-based biomaterials with the above-mentioned European directive in matter of soil improvers and bio-stimulants.

Reasonably, the approach described in this chapter to enhance the sEPS valorization effectiveness can be easily extend to other industrial solutions: based on the target sector, distinct high-priority macro-classes of properties can be identified and the overall process of sEPS extraction/recovery can be consequently optimized, thus leading to further resource recovery-oriented scenarios able to actively support and promote a more bio-based economy.

Together with the AGS full-scale installations, anammox granular sludge (AmxGS)-based technologies have been established in the last decades. Strategies for the efficient waste AmxGS management might be therefore found in the EPS recovery as value-added biomaterials. With this regard, **Chapter 4** proposes the valorization of AmxGS-derived EPS in environment-related applications for the heavy metal removal. This resource recovery-oriented strategy meets the increasingly legislative pressure concerning the heavy metal pollution of aquatic environments: indeed, heavy metals became an issue of great concern due to their toxicity, non-biodegradability, and potential to bioaccumulate in human body and food chain, thus driving the research efforts towards new advance and sustainable solutions that can be reasonably found in the biosorption processes. The feasibility of exploiting AmxGS-derived EPS in high-performance and cost-effective technologies for the treatment of heavy metal-contaminated wastewater has been therefore comprehensively addressed. Metal-binding capacities equivalent or higher than conventional and/or unconventional sorbent media have been found in single- and multi-metal biosorption studies, thus suggesting AmxGS-derived EPS as promising value-added biomaterials able to progress towards a more circular economy-based water sector. The comparison with pristine anammox granules in terms of biosorption effectiveness and processes has been added mainly to shed light on the metal-

binding mechanisms of extracted and non-extracted EPS in the native biomass. Distinct sorption pathways have been observed as result of the different polymer chain arrangement and binding site availability, likely affected by the EPS chemical extraction method applied. The impact of the overall process of EPS extraction/recovery has been therefore emphasized, thus highlighting the urge for more application-oriented extraction methods able to enhance the industrial applicability of the derived EPS-based biomaterials. Mechanistic hypothesis on metal biosorption have been proposed by means of a detail molecular-level analysis which revealed a multifaceted mechanism based on a combination of electrostatic interaction, ion exchange, complexation, and precipitation. Particularly, it has been found that AmxGS-derived EPS behaved like flocculant/complexing agents in presence of high-concentrated heavy metal-contaminated aqueous systems, leading to the spontaneous precipitation of EPS-metal composite aggregates. Overall, these findings might support the development EPS-based technologies for metal biosorption, thus helping the process scale-up in the design phase.

Furthermore, it has been reasonably proposed that the industrial applicability of AmxGS-derived EPS could be enhanced through the development of composite sorbent media. With this regard, proof-of-principle of the promising application of EPS in combination with granular activated carbon (GAC) has been given. Integrated resource recovery-oriented solutions can be therefore designed providing the EPS-based functionalization of waste-derived adsorbent materials (e.g., biochar, agro-derived residues, industrial by-products, etc.) which could be able to enhance the biosorption effectiveness of the pristine media.

In summary, the outstanding potential of both AGS- and AmxGS-derived EPS in environment-related applications has been demonstrated in the present thesis, thus shedding light on recourse recovery-oriented strategies able to hold the promise of a more circular economy-based water sector. Overall, the outcome of the presented analysis reenforced the growing environmental awareness which leads

scientific community to embrace "*green*" thinking in implementing eco-friendly technologies and industrial solutions.

A more consistent regulation of the overall EPS production/valorization process has been emphasized as crucial in developing cost-effective and high-performance EPS-based bioproducts in line with the high qualitative standard imposed by the various applicative sectors. New integrated targets have been defined to assess existing and potential industrial/environmental solutions for the recoverable EPS (for instance by means of application-related extraction processes), thus helping to change the critical status of waste sludge management in WWTPs. The methodologic contribution of this thesis to the research in matter of GS-derived EPS might be hence found in multiple aspects: (i) the regulation of the EPS extraction/recovery (and gelling) methods depending on the specific research and/or applicative goals (e.g., development of hydrogel-forming protocols ensuring low polymer consumption and high-accuracy rheological measurements, optimization of the extraction/gelling processes based on the nature of the selected environment- and/or industry-related application playing with the chemicals applied); (ii) the implementation of multidisciplinary and comparative approaches able to overcome the limitations due to the high-complexity and diversity of the treated matrices and (iii) the integrated and synergic assessments of multiple application-related properties by means of dedicated techniques.

Looking at the effective implementation of GS-extracted EPS in sustainable technologies, many considerations concerning the distinct applicability of AGS- and AmxGS-derived EPS should be done. Particularly, the choice of the targeted sector for AGS- and AmxGS-derived EPS should be firstly driven by their distinct properties that could be (or not) in line with the standard imposed by specific industrial and/or environmental solution. For instance, AGS-derived sEPS can form hydrogel (upon ionic cross-linking) at much lower concentrations (and with higher mechanical properties) with respect to AmxGS-derived EPS, and hence they might be more effectively implemented in hydrogel-related applications (e.g., agriculture). On the other side, from a process point of view, the mass

production of waste AGS is expected to be much higher compared to that of waste AmxGS due to higher biomass yield and much higher loads to be treated. Indeed, AGS is applied in the water line of both municipal and industrial WWTPs of any size (high organic loads potentially treated), while AmxGS processes are currently used only in the side-stream of large installations of both municipal and industrial nature. Hence, the sector where to apply GS-derived EPS would be also dependent on the mass flows required: high for AGS-derived EPS (e.g., agronomy-oriented processes) and less for AmxGS-derived EPS (e.g., treatment of heavy metal-contaminated wastewaters).

Overall, all the above-described methodologies and findings would represent a tool to progress in this complex and comprehensive research area, but further work is expected to drive the effective implementation of EPS-based technologies. Follow up research should deal with the following aspects:

i. **Effective regulation of the overall EPS extraction/valorization processes** in order to enhance the industrial applicability of the GS-derived EPS-based biomaterials.

   Integrated standards should be considered to optimize the extraction processes based on the research purposes. The method effectiveness should be hence addressed based on general criteria such as high efficiency, cost-effectiveness, user-friendly operation and reduced chemical additives (Feng et al., 2021). Particularly, the effect of the recovery method on the quality/quantity of the extractable EPS macromolecules and on the properties of the resulting biomaterials should be comprehensively investigated in follow up research. Furthermore, more dedicated approaches and integrated methodologies (Raman spectroscopy, FTIR, MS, MRI and CLSM imaging techniques, metagenomic sequencing, NMR spectroscopy, etc., Seviour et al., 2019) able to shed light on the GS-derived EPS composition, structural properties and multiple functionalities could potentially pave the way towards new potential industrial applications able to sustain and promote a more bio-based economy.

Another key point to be addressed in implementing EPS recovery/valorization technologies in WWTPs should concern the stability of the EPS characteristics upon GS process fluctuations (e.g., load, performance, environmental conditions due to the seasonality, etc.). Reasonably, the GS cultivation conditions could influence the quality/quantity of the extractable EPS macromolecules and resulting properties, thus generating a potential constrain for the EPS valorization in standardized industrial solutions. For instance, in the case of GS-derived EPS as viscosity-modifying agents in the textile industry, targeted compositions and properties might be demanded and the feasibility of keeping them unchanged upon variations of the EPS production process conditions could be crucial. Conversely, lower constrains might be involved in agriculture-related applications where GS-derived EPS-based biomaterials (e.g., hydrogels) are applied as soil conditioners and/or as coating agents for fertilizing products to control the nutrient release kinetics. The EPS stability should be therefore properly addressed depending on the specific applicative goals. To be noticed that the integration of EPS recovery processes in WWTPs treating certain kinds of industrial influents characterized by higher stability due to non-seasonal production processes (e.g., paper mill, brewery, semiconductor industry, etc.) might reduce the limits described above.

ii. **Enhancement of the GS-derived EPS potential in environment-related applications.** The present thesis proposed distinct resource recovery-oriented solutions able to exploit the outstanding properties of both AGS- and AmxGS-derived EPS such as agriculture-related practices and biosorption technologies. Further research effort is expected be dedicated on the technological development of these processes towards higher TRLs (Technology Readiness Level). Follow up research should address the effective feasibility of exploiting sEPS-based hydrogels as soil improvers (to enhance the soil water-retention ability) and/or as carrier systems for the delivery/controlled-release of agrochemicals. With this regard, the

phytotoxicity and biodegradability assessment appears pivotal to be consistent with the increasingly pressure in matter of environmental protection. With reference to various European directives (e.g., UNI EN 16086-1, UNI EN 16086-2), the phytotoxicity of EPS-derived biomaterials (e.g., hydrogels) can be addressed by measuring the decrease (or absence) of seed germination and root growth after seed exposure to the studied substrates. This evaluation could drive further industrial applications: the absence of phytotoxic macromolecules together with the high qualitative properties achievable controlling the production processes (**Chapter 3**) could make AGS-derived sEPS-biomaterials (e.g., weakly cross-linked hydrogels) eligible substrates for cutting cultivation and/or micropropagation in flower and horticulture nursery sector. Polymer biodegradation in soil is a very comprehensive and recent area of research; however, many regulations in matter of microbial soil respiration (e.g., UNI EN ISO 16072:2002) might be adapted on the here studied substrates (i.e., EPS and/or derived hydrogels) as detailed in **Chapter 3** to define suitable experimental setup. Biodegradation of SAPs in soil is influenced by multiple factors (e.g., soil type, polymer nature, temperature range, cross-linking density, etc.) thus making difficult to draw general conclusions on their overall biodegradability. The assessment should hence start with the definition of a target soil and the identification of the *optimum* in terms EPS-based biomaterial production to then extend the emerged outcome to a wide range of experimental conditions. A further bottleneck in the application of EPS-based biomaterials in soil (e.g., controlled-release systems of agrochemicals) might be found in combining long-term functionality with reasonable biodegradation rates under the mild conditions of agricultural fields. Further research effort should be therefore dedicated to improve the chemical and biological stability of the designed EPS-based products without compromising their biodegradability. Other environment-related applications might be proposed for the GS-extracted EPS. As suggested in **Chapter 4**, the industrial applicability of AmxGS-derived EPS in the treatment of heavy metal-contaminated wastewaters may be enhanced through the development of EPS-based

composite media. In this perspective, a wide range of waste-derived materials (e.g., agro-residues, industrial by-products, biochar, etc.) can be tested. The performance stability in presence of organic pollutants and/or other inorganic compounds with different charges should be comprehensively addressed before designing the process scale-up.

iii. **Integration of the EPS extraction/recovery processes with an efficient management of the residual (i.e., non-extracted) waste GS.**

To enhance the potential of WWTPs as WRRFs and improve the sustainability of the whole treatment chain, multiple resource recovery-oriented solutions might be combined such as EPS recovery as value-added biomaterials and anaerobic digestion (AD) of the sludge residues for biomethane production. With this regard, the effect of the EPS extraction (including the chemicals applied) on the digestibility and dewaterability of the residual waste GS should be carefully addressed.

iv. **Evaluation of the whole process of EPS recovery and valorization in terms of environmental and economic impacts** (for instance by means of life cycle assessments). Further work is expected to be focused on the actual implementation of GS-derived EPS as value-added biomaterials: particularly, the entire production/valorization chain should be optimized (e.g., through application-related extraction methods) to enhance the industrial applicability of these waste-derived biopolymers. The process scale-up should accurately consider the capital equipment costs and operational expenses, largely dependent on production scale and extraction process (Feng et al., 2021), and should be driven by the existence of a considerable market demand potential for the designed EPS-based products.

References

Afridi, S., Sikandar, M.A., Waseem, M., Nasir, H., Naseer, A., 2019. Chemical durability of superabsorbent polymer (SAP) based geopolymer mortars (GPMs). Constr. Build. Mater. 217, 530–542. https://doi.org/10.1016/j.conbuildmat.2019.05.101

Ahearne, M., Siamantouras, E., Yang, Y., Liu, K.K., 2009. Mechanical characterization of biomimetic membranes by micro-shaft poking. J. R. Soc. Interface 6, 471–478. https://doi.org/10.1098/rsif.2008.0317

Aksu, Z., Akpinar, D., 2000. Modelling of simultaneous biosorption of phenol and nickel(II) onto dried aerobic activated sludge. Sep. Purif. Technol. 21, 87–99. https://doi.org/10.1016/S1383-5866(00)00194-5

Almdal, K., Dyre, J., Hvidt, S., & Kramer, O. Towards a phenomenological definition of the term 'gel.'. Polymer Gels and Networks, 1993, 1(1), 5–17. https://doi.org/10.1016/0966-7822(93)90020-I

Alvarez, J., Amutio, M., Lopez, G., Bilbao, J., Olazar, M., 2015. Fast co-pyrolysis of sewage sludge and lignocellulosic biomass in a conical spouted bed reactor. Fuel 159, 810–818. https://doi.org/10.1016/j.fuel.2015.07.039

American Public Health Association (APHA), 2005. Standard Methods for the Examination of Water and Wastewater, twenty-first ed.

Apiratikul, R., Pavasant, P., 2008. Batch and column studies of biosorption of heavy metals by Caulerpa lentillifera. Bioresour. Technol. 99, 2766–2777. https://doi.org/10.1016/j.biortech.2007.06.036

Bailey, S.E., Olin, T.J., Bricka, R.M., Adrian, D.D., 1999. A review of potentially low-cost sorbents for heavy metals. Water Res. 33, 2469–2479. https://doi.org/10.1016/S0043-1354(98)00475-8

Banerjee, A., Ganguly, S., 2019. Mechanical behaviour of alginate film with embedded voids under compression-decompression cycles. Sci. Rep. 9, 1–12. https://doi.org/10.1038/s41598-019-49589-w

Barnes, H. A. (2000). A handbook of elementary rheology (Vol. 1). Aberystwyth: University of Wales, Institute of Non-Newtonian Fluid Mechanics.

Beck, M.B., Jiang, F., Shi, F., Villarroel Walker, R., 2008. Technology, Sustainability, and Business: Cities as Forces for Good in the Environment. Integr. Urban Water Manag. Temp. Clim.

Benaddi, H., Bandosz, T.J., Jagiello, J., Schwarz, J.A., Rouzaud, J.N., Legras, D., Béguin, F., 2000. Surface functionality and porosity of activated carbons obtained from chemical activation of wood. Carbon N. Y. 38, 669–674. https://doi.org/10.1016/S0008-6223(99)00134-7

Bengtsson, S., de Blois, M., Wilén, B.M., Gustavsson, D., 2018. Treatment of municipal wastewater with aerobic granular sludge. Crit. Rev. Environ. Sci. Technol. 48, 119–166. https://doi.org/10.1080/10643389.2018.1439653

Bertagnolli, C., Kleinübing, S.J., da Silva, M.G.C., 2011. Preparation and characterization of a Brazilian bentonite clay for removal of copper in porous beds. Appl. Clay Sci. 53, 73–79. https://doi.org/10.1016/j.clay.2011.05.002

Bessaies-Bey, H., Khayat, K.H., Palacios, M., Schmidt, W., Roussel, N., 2022. Viscosity modifying agents: Key components of advanced cement-based materials with adapted rheology. Cem. Concr. Res. 152, 106646. https://doi.org/10.1016/j.cemconres.2021.106646

Bhainsa, K.C., D'Souza, S.F., 2008. Removal of copper ions by the filamentous fungus, Rhizopus oryzae from aqueous solution. Bioresour. Technol. 99, 3829–3835. https://doi.org/10.1016/j.biortech.2007.07.032

Boleij, M., Kleikamp, H., Pabst, M., Neu, T.R., van Loosdrecht, M.C.M., Lin, Y., 2020. Decorating the Anammox House: Sialic Acids and Sulfated Glycosaminoglycans in the Extracellular Polymeric Substances of Anammox Granular Sludge. Environ. Sci. Technol. 54, 5218–5226. https://doi.org/10.1021/acs.est.9b07207

Boleij, M., Pabst, M., Neu, T.R., Van Loosdrecht, M.C.M., Lin, Y., 2018. Identification of Glycoproteins Isolated from Extracellular Polymeric Substances of Full-Scale Anammox Granular Sludge. Environ. Sci. Technol. 52, 13127–13135. https://doi.org/10.1021/acs.est.8b03180

Boleij, M., Seviour, T., Wong, L.L., van Loosdrecht, M.C.M., Lin, Y., 2019. Solubilization and characterization of extracellular proteins from anammox granular sludge. Water Res. 164, 114952. https://doi.org/10.1016/j.watres.2019.114952

Bolisetty, S., Peydayesh, M., Mezzenga, R., 2019. Sustainable technologies for water purification from heavy metals: review and analysis. Chem. Soc. Rev. 48, 463–487. https://doi.org/10.1039/c8cs00493e

Borzooei, S., Simonetti, M., Scibilia, G., Zanetti, M.C., 2021. Critical evaluation of respirometric and physicochemical methods for characterization of municipal wastewater during wet-weather events. J. Environ. Chem. Eng. 9, 105238. https://doi.org/10.1016/j.jece.2021.105238

Breckle, S.W., 1991. Growth under stress - Heavy metals. In: Waisel, A., Eshel, A., Kafkafi, U. (eds.). Plant roots: The hidden half. Marcel Dakker. New York., 351 - 373.

Campo, R., Sguanci, S., Caffaz, S., Mazzoli, L., Ramazzotti, M., Lubello, C., Lotti, T., 2020. Efficient carbon, nitrogen and phosphorus removal from low C/N real domestic wastewater with aerobic granular sludge. Bioresour. Technol. 305, 122961. https://doi.org/10.1016/j.biortech.2020.122961

Cannazza, G., Cataldo, A., de Benedetto, E., Demitri, C., Madaghiele, M., Sannino, A., 2014. Experimental assessment of the use of a novel superabsorbent polymer (SAP) for the optimization of water consumption in agricultural irrigation process. Water (Switzerland) 6, 2056–2069. https://doi.org/10.3390/w6072056

Cantinho, P., Matos, M., Trancoso, M.A., dos Santos, M.M.C., 2016. Behaviour and fate of metals in urban wastewater treatment plants: a review. Int. J. Environ. Sci. Technol. 13, 359–386. https://doi.org/10.1007/s13762-015-0887-x

Cao, L., Lu, W., Mata, A., Nishinari, K., Fang, Y., 2020. Egg-box model-based gelation of alginate and pectin: A review. Carbohydr. Polym. 242, 116389. https://doi.org/10.1016/j.carbpol.2020.116389

Chen, H., Zhou, S., Li, T., 2010. Impact of extracellular polymeric substances on the settlement ability of aerobic granular sludge. Environ. Technol. 31, 1601–1612. https://doi.org/10.1080/09593330.2010.482146

Christensen, B.E., Indergaard, M., Smidsrød, O., 1990. Polysaccharide research in Trondheim. Carbohydr. Polym. 13, 239–255. https://doi.org/10.1016/0144-8617(90)90057-Y

Chróst, R.J., 1991. Environmental Control of the Synthesis and Activity of Aquatic Microbial Ectoenzymes 29–59. https://doi.org/10.1007/978-1-4612-3090-8_3

Cirik, K., Dursun, N., Sahinkaya, E., Çinar, Ö., 2013. Effect of electron donor source on the treatment of Cr(VI)-containing textile wastewater using sulfate-reducing fluidized bed reactors (FBRs). Bioresour. Technol. 133, 414–420. https://doi.org/10.1016/j.biortech.2013.01.064

Cirpus, I.E.Y., De Been, M., Op Den Camp, H.J.M., Strous, M., Le Paslier, D., Kuenen, G.J., Jetten, M.S.M., 2005. A new soluble 10 kDa monoheme cytochrome c-552 from the anammox bacterium Candidatus “Kuenenia stuttgartiensis.” FEMS Microbiol. Lett. 252, 273–278. https://doi.org/10.1016/j.femsle.2005.09.007

Cojocaru, C., Diaconu, M., Cretescu, I., Savić, J., Vasić, V., 2009. Biosorption of copper(II) ions from aqua solutions using dried yeast biomass. Colloids Surfaces A Physicochem. Eng. Asp. 335, 181–188. https://doi.org/10.1016/j.colsurfa.2008.11.003

Corominas, L., Rieger, L., Takács, I., Ekama, G., Hauduc, H., Vanrolleghem, P.A., Oehmen, A., Gernaey, K. V., Van Loosdrecht, M.C.M., Comeau, Y., 2010. New framework for standardized notation in wastewater treatment modelling. Water Sci. Technol. 61, 841–857. https://doi.org/10.2166/wst.2010.912

d'Abzac, P., Bordas, F., van Hullebusch, E., Lens, P.N.L., Guibaud, G., 2010. Effects of extraction procedures on metal binding properties of extracellular polymeric substances (EPS) from anaerobic granular sludges. Colloids Surfaces B Biointerfaces 80, 161–168. https://doi.org/10.1016/j.colsurfb.2010.05.043

D'Abzac, P., Bordas, F., Van Hullebusch, E., Lens, P.N.L., Guibaud, G., 2010. Extraction of extracellular polymeric substances (EPS) from anaerobic granular sludges: Comparison of chemical and physical extraction protocols. Appl. Microbiol. Biotechnol. 85, 1589–1599. https://doi.org/10.1007/s00253-009-2288-x

Daigger, G.T., 2009. Evolving Urban Water and Residuals Management Paradigms: Water Reclamation and Reuse, Decentralization, and Resource Recovery. Water Environ. Res. 81, 809–823. https://doi.org/10.2175/106143009x425898

Dandurand, J., Samouillan, V., Lacoste-Ferre, M.H., Lacabanne, C., B.Bochicchio, Pepe, A., 2014. Conformational and thermal characterization of a synthetic peptidic fragment inspired from human tropoelastin: Signature of the amyloid fibers. Pathol. Biol. 62, 100–107. https://doi.org/10.1016/j.patbio.2014.02.001

Davidovich-Pinhas, M., Bianco-Peled, H., 2009. A quantitative analysis of alginate swelling. Carbohydr. Polym. 79, 1020–1027. https://doi.org/10.1016/j.carbpol.2009.10.036

de Almeida Neto, A.F., Vieira, M.G.A., da Silva, M.G.C., 2014. Adsorption and desorption processes for copper removal from water using different eluents and calcined clay as adsorbent. J. Water Process Eng. 3, 90–97. https://doi.org/10.1016/j.jwpe.2014.05.014

de Gennes, P. G., 1976. On a relation between percolation theory and the elasticity of gels. J. Phys. Lett. 37, 1–2.

de Graaff, D.R., Felz, S., Neu, T.R., Pronk, M., van Loosdrecht, M.C.M., Lin, Y., 2019. Sialic acids in the extracellular polymeric substances of seawater-adapted aerobic granular sludge. Water Res. 155, 343–351. https://doi.org/10.1016/j.watres.2019.02.040

de Kreuk, M.K., Picioreanu, C., Hosseini, M., Xavier, J.B., Van Loosdrecht, M.C.M., 2007. Kinetic model of a granular sludge SBR: Influences on nutrient removal. Biotechnol. Bioeng. 97, 801–815. https://doi.org/10.1002/bit.21196

de Sousa, T.A.T., do Monte, F.P., do Nascimento Silva, J.V., Lopes, W.S., Leite, V.D., van Lier, J.B., de Sousa, J.T., 2021. Alkaline and acid solubilisation of waste activated sludge. Water Sci. Technol. 83, 2980–2996. https://doi.org/10.2166/wst.2021.179

de Valk, S., Feng, C., Khadem, A.F., van Lier, J.B., de Kreuk, M.K., 2019. Elucidating the microbial community associated with the protein preference of sludge-degrading worms. Environ. Technol. (United Kingdom) 40, 192–201. https://doi.org/10.1080/09593330.2017.1384071

Dignac, M.F., Urbain, V., Rybacki, D., Bruchet, A., Snidaro, D., Scribe, P., 1998. Chemical description of extracellular polymers: Implication on activated sludge floc structure. Water Sci. Technol. 38, 45–53. https://doi.org/10.1016/S0273-1223(98)00676-3

Donati, I., Mørch, Y.A., Strand, B.L., Skjåk-Braek, G., Paoletti, S., 2009. Effect of elongation of alternating sequences on swelling behavior and large deformation properties of natural alginate gels. J. Phys. Chem. B 113, 12916–12922. https://doi.org/10.1021/jp905488u

Draget, K.I., Skjåk Bræk, G., Smidsrød, O., 1994. Alginic acid gels: the effect of alginate chemical composition and molecular weight. Carbohydr. Polym. 25, 31–38. https://doi.org/10.1016/0144-8617(94)90159-7

Dreywood, R., 1946. Qualitative Test for Carbohydrate Material. Ind. Eng. Chem. - Anal. Ed. https://doi.org/10.1021/i560156a015

Dubé, C.D., Guiot, S.R., 2019. Characterization of the protein fraction of the extracellular polymeric substances of three anaerobic granular sludges. AMB Express 9, 1–11. https://doi.org/10.1186/s13568-019-0746-0

Ekama, G.A., Dold, P.L., Marais, G.v.R., 1896. Procedures for determining influent cod fractions and the maximum specific growth rate of heterotrophs in activated sludge systems. Wat. Sci. Tech. 18, 91–114.

Felz, S., Al-Zuhairy, S., Aarstad, O.A., van Loosdrecht, M.C.M., Lin, Y.M., 2016. Extraction of structural extracellular polymeric substances from aerobic granular sludge. J. Vis. Exp. 2016, 1–8. https://doi.org/10.3791/54534

Felz, S., Kleikamp, H., Zlopasa, J., van Loosdrecht, M.C.M., Lin, Y., 2020a. Impact of metal ions on structural EPS hydrogels from aerobic granular sludge. Biofilm 2, 100011. https://doi.org/10.1016/j.bioflm.2019.100011

Felz, S., Neu, T.R., van Loosdrecht, M.C.M., Lin, Y., 2020b. Aerobic granular sludge contains Hyaluronic acid-like and sulfated glycosaminoglycans-like polymers. Water Res. 169, 115291. https://doi.org/10.1016/j.watres.2019.115291

Felz, S., Vermeulen, P., van Loosdrecht, M.C.M., Lin, Y.M., 2019a. Chemical characterization methods for the analysis of structural extracellular polymeric substances (EPS). Water Res. 157, 201–208. https://doi.org/10.1016/j.watres.2019.03.068

Felz, S., Vermeulen, P., van Loosdrecht, M.C.M., Lin, Y.M., 2019b. Chemical characterization methods for the analysis of structural extracellular polymeric substances (EPS). Water Res. 157, 201–208. https://doi.org/10.1016/j.watres.2019.03.068

Feng, C., Lotti, T., Canziani, R., Lin, Y., Tagliabue, C., Malpei, F., 2021. Extracellular biopolymers recovered as raw biomaterials from waste granular sludge and potential applications: A critical review. Sci. Total Environ. 753, 142051. https://doi.org/10.1016/j.scitotenv.2020.142051

Feng, C., Lotti, T., Lin, Y., Malpei, F., 2019. Extracellular polymeric substances extraction and recovery from anammox granules: Evaluation of methods and protocol development. Chem. Eng. J. 374, 112–122. https://doi.org/10.1016/j.cej.2019.05.127

Feng, C., Welles, L., Zhang, X., Pronk, M., de Graaff, D., van Loosdrecht, M., 2020. Stress-induced assays for polyphosphate quantification by uncoupling acetic acid uptake and anaerobic phosphorus release. Water Res. 169. https://doi.org/10.1016/j.watres.2019.115228

Feng, D., Bai, B., Wang, H., Suo, Y., 2016. Enhanced mechanical stability and sensitive swelling performance of chitosan/yeast hybrid hydrogel beads. New J. Chem. 40, 3350–3362. https://doi.org/10.1039/c5nj02404h

Fernández Farrés, I., Douaire, M., Norton, I.T., 2013. Rheology and tribological properties of Ca-alginate fluid gels produced by diffusion-controlled method. Food Hydrocoll. 32, 115–122. https://doi.org/10.1016/j.foodhyd.2012.12.009

Flemming, H., Wingender, J., 2010. The biofilm matrix. Nat. Publ. Gr. 8, 623–633. https://doi.org/10.1038/nrmicro2415

Flemming, H.C., Neu, T.R., Wozniak, D.J., 2007. The EPS matrix: The “House of Biofilm Cells.” J. Bacteriol. 189, 7945–7947. https://doi.org/10.1128/JB.00858-07

Flemming, H.C., Wingender, J., 2010. The biofilm matrix. Nat. Rev. Microbiol. 8, 623–633. https://doi.org/10.1038/nrmicro2415

Fouladgar, M., Beheshti, M., Sabzyan, H., 2015. Single and binary adsorption of nickel and copper from aqueous solutions by γ-alumina nanoparticles: Equilibrium and kinetic modeling. J. Mol. Liq. 211, 1060–1073. https://doi.org/10.1016/j.molliq.2015.08.029

Frolund, B., Griebe, T., Nielsen, P.H., 1995. Enzymatic activity in the activated-sludge floc matrix. Appl. Microbiol. Biotechnol. 43, 755–761. https://doi.org/10.1007/BF00164784

Funami, T., Fang, Y., Noda, S., Ishihara, S., Nakauma, M., Draget, K.I., Nishinari, K., Phillips, G.O., 2009. Rheological properties of sodium alginate in an aqueous system during gelation in relation to supermolecular structures and Ca2+ binding. Food Hydrocoll. 23, 1746–1755. https://doi.org/10.1016/j.foodhyd.2009.02.014

Gagliano, M.C., Sudmalis, D., Pei, R., Temmink, H., Plugge, C.M., 2020. Microbial Community Drivers in Anaerobic Granulation at High Salinity. Front. Microbiol. 11, 1–15. https://doi.org/10.3389/fmicb.2020.00235

Gehr, R., Henry, J.G., 1983. Removal of extracellular material techniques and pitfalls. Water Res. 17, 1743–1748. https://doi.org/10.1016/0043-1354(83)90195-1

Gong, J.L., Wang, X.Y., Zeng, G.M., Chen, L., Deng, J.H., Zhang, X.R., Niu, Q.Y., 2012. Copper (II) removal by pectin-iron oxide magnetic nanocomposite adsorbent. Chem. Eng. J. 185–186, 100–107. https://doi.org/10.1016/j.cej.2012.01.050

Goodwin, J.W., Huges, R.W., 2000. Rheology for chemists. The Royal Society of Chemistry: Cambridge, 98–145.

Gottlieb, M., Macosko, C.W., Benjamin, G.S., Meyers, K.O., Merrill, E.W., 1981. Equilibrium Modulus of Model Poly(dimethylsiloxane) Networks. Macromolecules 14, 1039–1046. https://doi.org/10.1021/ma50005a028

Guenet, J.M., 2000. Structure versus rheological properties in fibrillar thermoreversible gels from polymers and biopolymers. J. Rheol. 44, 947–960. https://doi.org/10.1122/1.551121

Guest, J.S., Skerlos, S.J., Barnard, J.L., Beck, M.B., Daigger, G.T., Hilger, H., Jackson, S.J., Karvazy, K., Kelly, L., Macpherson, L., Mihelcic, J.R., Pramanik, A., Raskin, L., Van Loosdrecht, M.C.M., Yeh, D., Love, N.G., 2009. A new planning and design paradigm to achieve sustainable resource recovery from wastewater. Environ. Sci. Technol. 43, 6126–6130. https://doi.org/10.1021/es9010515

Guibaud, G., Bhatia, D., d'Abzac, P., Bourven, I., Bordas, F., van Hullebusch, E.D., Lens, P.N.L., 2012. Cd(II) and Pb(II) sorption by extracellular polymeric substances (EPS) extracted from anaerobic granular biofilms: Evidence of a pH sorption-edge. J. Taiwan Inst. Chem. Eng. 43, 444–449. https://doi.org/10.1016/j.jtice.2011.12.007

Guibaud, G., van Hullebusch, E., Bordas, F., d'Abzac, P., Joussein, E., 2009. Sorption of Cd(II) and Pb(II) by exopolymeric substances (EPS) extracted from activated sludges and pure bacterial strains: Modeling of the metal/ligand ratio effect and role of the mineral fraction. Bioresour. Technol. 100, 2959–2968. https://doi.org/10.1016/j.biortech.2009.01.040

Guo, H., Felz, S., Lin, Y., van Lier, J.B., de Kreuk, M., 2020. Structural extracellular polymeric substances determine the difference in digestibility between waste activated sludge and aerobic granules. Water Res. 181, 115924. https://doi.org/10.1016/j.watres.2020.115924

Hamoda, M.F., Al-Attar, I.M.S., 1995. Effects of high sodium chloride concentrations on activated sludge treatment. Water Sci. Technol. 31, 61–72. https://doi.org/10.1016/0273-1223(95)00407-E

Hargreaves, A.J., Vale, P., Whelan, J., Alibardi, L., Constantino, C., Dotro, G., Cartmell, E., Campo, P., 2018. Impacts of coagulation-flocculation treatment on the size distribution and bioavailability of trace metals (Cu, Pb, Ni, Zn) in municipal wastewater. Water Res. 128, 120–128. https://doi.org/10.1016/j.watres.2017.10.050

Hassan, S.H.A., Kim, S.J., Jung, A.Y., Joo, J.H., Oh, S.E., Yang, J.E., 2009. Biosorptive capacity of Cd(II) and Cu(II) by lyophilized cells of Pseudomonas stutzeri. J. Gen. Appl. Microbiol. 55, 27–34. https://doi.org/10.2323/jgam.55.27

Hay, I.D., Rehman, Z.U., Moradali, M.F., Wang, Y., Rehm, B.H.A., 2013. Microbial alginate production, modification and its applications. Microb. Biotechnol. 6, 637–650. https://doi.org/10.1111/1751-7915.12076

He, J., Chen, J.P., 2014. A comprehensive review on biosorption of heavy metals by algal biomass: Materials, performances, chemistry, and modeling simulation tools. Bioresour. Technol. 160, 67–78. https://doi.org/10.1016/j.biortech.2014.01.068

Heidmann, I., Calmano, W., 2010. Removal of Ni, Cu and Cr from a galvanic wastewater in an electrocoagulation system with Fe- and Al-electrodes. Sep. Purif. Technol. 71, 308–314. https://doi.org/10.1016/j.seppur.2009.12.016

Henze, M., 1992. Characterization of wastewater for modelling of activated sludge processes. Water Sci. Technol. 25, 1–15. https://doi.org/10.2166/wst.1992.0110

Henze, M., Gujer, W., Mino, T., Van Loosdrecht, M.C.M. Activated Sludge Models ASM1, ASM2, ASM2d and ASM3: Scientific and Technical Report No. 9. IWA Task Group on Mathematical Modelling for Design and Operation of Biological Wastewater Treatment, IWA Publishing, London, 2000.

Hernández, R., Sacristán, J., Mijangos, C., 2010. Sol/gel transition of aqueous alginate solutions induced by Fe2+ cationsa. Macromol. Chem. Phys. 211, 1254–1260. https://doi.org/10.1002/macp.200900691

Herrero, R., Lodeiro, P., García-Casal, L.J., Vilariño, T., Rey-Castro, C., David, C., Rodríguez, P., 2011. Full description of copper uptake by algal biomass combining an equilibrium NICA model with a kinetic intraparticle diffusion driving force approach. Bioresour. Technol. 102, 2990–2997. https://doi.org/10.1016/j.biortech.2010.10.007

Hu, X.J., Liu, Y.G., Wang, H., Chen, A.W., Zeng, G.M., Liu, S.M., Guo, Y.M., Hu, X., Li, T.T., Wang, Y.Q., Zhou, L., Liu, S.H., 2013. Removal of Cu(II) ions from aqueous solution using sulfonated magnetic graphene oxide composite. Sep. Purif. Technol. 108, 189–195. https://doi.org/10.1016/j.seppur.2013.02.011

Hu, Z., Chandran, K., Smets, B.F., Grasso, D., 2002. Evaluation of a rapid physical-chemical method for the determination of extant soluble COD. Water Res. 36, 617–624. https://doi.org/10.1016/S0043-1354(01)00273-1

Hu, Z., Lotti, T., de Kreuk, M., Kleerebezem, R., van Loosdrecht, M., Kruit, J., Jetten, M.S.M., Kartal, B., 2013. Nitrogen removal by a nitritation-anammox bioreactor at low temperature. Appl. Environ. Microbiol. 79, 2807–2812. https://doi.org/10.1128/AEM.03987-12

Hulshoff Pol, L.W., De Castro Lopes, S.I., Lettinga, G., Lens, P.N.L., 2004. Anaerobic sludge granulation. Water Res. 38, 1376–1389. https://doi.org/10.1016/j.watres.2003.12.002

Jiang, L., Zhou, W., Liu, D., Liu, T., Wang, Z., 2017. Biosorption isotherm study of Cd2 +, Pb2 + and Zn2 + biosorption onto marine bacterium Pseudoalteromonas sp. SCSE709-6 in multiple systems. J. Mol. Liq. 247, 230–237. https://doi.org/10.1016/j.molliq.2017.09.117

Jones, J.L. and Marque`s, C.M., 1990. Rigid polymer network models, J. Phys. 51, 1113–1127.

Kajjumba, G.W., Emik, S., Öngen, A., Kurtulus Özcan, H., Aydın, S., 2019. Modelling of Adsorption Kinetic Processes—Errors, Theory and Application. Adv. Sorption Process Appl. 1–19. https://doi.org/10.5772/intechopen.80495

Kalinoski, R.M., Shi, J., 2019. Hydrogels derived from lignocellulosic compounds: Evaluation of the compositional, structural, mechanical and antimicrobial properties. Ind. Crops Prod. 128, 323–330. https://doi.org/10.1016/j.indcrop.2018.11.002

Karakas, I., Sam, S.B., Cetin, E., Dulekgurgen, E., Yilmaz, G., 2020. Resource recovery from an aerobic granular sludge process treating domestic wastewater. J. Water Process Eng. 34, 101148. https://doi.org/10.1016/j.jwpe.2020.101148

Kehrein, P., Van Loosdrecht, M., Osseweijer, P., Garfí, M., Dewulf, J., Posada, J., 2020. A critical review of resource recovery from municipal wastewater treatment plants-market supply potentials, technologies and bottlenecks. Environ. Sci. Water Res. Technol. 6, 877–910. https://doi.org/10.1039/c9ew00905a

Kim, N.K., Mao, N., Lin, R., Bhattacharyya, D., van Loosdrecht, M.C.M., Lin, Y., 2020. Flame retardant property of flax fabrics coated by extracellular polymeric substances recovered from both activated sludge and aerobic granular sludge. Water Res. 170. https://doi.org/10.1016/j.watres.2019.115344

Kongsuwan, A., Patnukao, P., Pavasant, P., 2009. Binary component sorption of Cu(II) and Pb(II) with activated carbon from Eucalyptus camaldulensis Dehn bark. J. Ind. Eng. Chem. 15, 465–470. https://doi.org/10.1016/j.jiec.2009.02.002

Kosheleva, R.I., Mitropoulos, A.C., Kyzas, G.Z., 2019. Synthesis of activated carbon from food waste. Environ. Chem. Lett. 17, 429–438. https://doi.org/10.1007/s10311-018-0817-5

Kotaś, J., Stasicka, Z., 2000. Chromium occurrence in the environment and methods of its speciation. Environ. Pollut. 107, 263–283. https://doi.org/10.1016/S0269-7491(99)00168-2

Kozlowska, J., Pauter, K., Sionkowska, A., 2018. Carrageenan-based hydrogels: Effect of sorbitol and glycerin on the stability, swelling and mechanical properties. Polym. Test. 67, 7–11. https://doi.org/10.1016/j.polymertesting.2018.02.016

Kratochvil, D., Volesky, B., 1998. Advances in the biosorption of heavy metals. Trends Biotechnol. 16, 291–300. https://doi.org/10.1016/S0167-7799(98)01218-9

Kreyenschulte, D., Krull, R., Margaritis, A., 2014. Recent advances in microbial biopolymer production and purification. Crit. Rev. Biotechnol. 34, 1–15. https://doi.org/10.3109/07388551.2012.743501

Kuo, C.K., Ma, P.X., 2001. Ionically crosslinked alginate hydrogels as scaffolds for tissue engineering: Part 1. Structure, gelation rate and mechanical properties. Biomaterials 22, 511–521. https://doi.org/10.1016/S0142-9612(00)00201-5

Lackner, S., Gilbert, E.M., Vlaeminck, S.E., Joss, A., Horn, H., van Loosdrecht, M.C.M., 2014. Full-scale partial nitritation/anammox experiences - An application survey. Water Res. 55, 292–303. https://doi.org/10.1016/j.watres.2014.02.032

Lan, S., Wu, X., Li, L., Li, M., Guo, F., Gan, S., 2013. Synthesis and characterization of hyaluronic acid-supported magnetic microspheres for copper ions removal. Colloids Surfaces A Physicochem. Eng. Asp. 425, 42–50. https://doi.org/10.1016/j.colsurfa.2013.02.059

Latimer, G.W., 2016. Official Methods of Analysis of AOAC International. AOAC International, Gaithersburg, MD, USA.

Layer, M., Adler, A., Reynaert, E., Hernandez, A., Pagni, M., Morgenroth, E., Holliger, C., & Derlon, N. (2019). Organic substrate diffusibility governs microbial community composition, nutrient removal performance and kinetics of granulation of aerobic granular sludge. Water Research X, 4, 100033. https://doi.org/10.1016/j.wroa.2019.100033

Lee, K.Y., Mooney, D.J., 2012. Alginate: Properties and biomedical applications. Prog. Polym. Sci. 37, 106–126. https://doi.org/10.1016/j.progpolymsci.2011.06.003

Lee, K.Y., Yuk, S.H., 2007. Polymeric protein delivery systems. Prog. Polym. Sci. 32, 669–697. https://doi.org/10.1016/j.progpolymsci.2007.04.001

Li, D., Chen, L., Yi, X., Zhang, X., Ye, N., 2010. Pyrolytic characteristics and kinetics of two brown algae and sodium alginate. Bioresour. Technol. 101, 7131–7136. https://doi.org/10.1016/j.biortech.2010.03.145

Li, G.F., Ma, W.J., Cheng, Y.F., Li, S.T., Zhao, J.W., Li, J.P., Liu, Q., Fan, N.S., Huang, B.C., Jin, R.C., 2020. A spectra metrology insight into the binding characteristics of Cu2+ onto anammox extracellular polymeric substances. Chem. Eng. J. 393, 124800. https://doi.org/10.1016/j.cej.2020.124800

Li, N., Wei, D., Wang, S., Hu, L., Xu, W., Du, B., Wei, Q., 2017a. Comparative study of the role of extracellular polymeric substances in biosorption of Ni(II) onto aerobic/anaerobic granular sludge. J. Colloid Interface Sci. 490, 754–761. https://doi.org/10.1016/j.jcis.2016.12.006

Li, N., Wei, D., Wang, S., Hu, L., Xu, W., Du, B., Wei, Q., 2017b. Comparative study of the role of extracellular polymeric substances in biosorption of Ni(II) onto aerobic/anaerobic granular sludge. J. Colloid Interface Sci. 490, 754–761. https://doi.org/10.1016/j.jcis.2016.12.006

Li, W.W., Yu, H.Q., 2014. Insight into the roles of microbial extracellular polymer substances in metal biosorption. Bioresour. Technol. 160, 15–23. https://doi.org/10.1016/j.biortech.2013.11.074

Li, X., Lin, S., Hao, T., Khanal, S.K., Chen, G., 2019. Elucidating pyrolysis behaviour of activated sludge in granular and flocculent form: Reaction kinetics and mechanism. Water Res. 162, 409–419. https://doi.org/10.1016/j.watres.2019.06.074

Li, Y., Yang, S.F., Zhang, J.J., Li, X.Y., 2014. Formation of artificial granules for proving gelation as the main mechanism of aerobic granulation in biological wastewater treatment. Water Sci. Technol. 70, 548–554. https://doi.org/10.2166/wst.2014.260

Li, Z., Xu, X., Shao, B., Zhang, S.S., Yang, F.L., 2014. Anammox granules formation and performance in a submerged anaerobic membrane bioreactor. Chem. Eng. J. 254, 9–16. https://doi.org/10.1016/j.cej.2014.04.068

Liang, H., DeMeester, K.E., Hou, C.W., Parent, M.A., Caplan, J.L., Grimes, C.L., 2017. Metabolic labelling of the carbohydrate core in bacterial peptidoglycan and its applications. Nat. Commun. 8, 15015. https://doi.org/10.1038/ncomms15015

Lim, S.J., Kim, T.H., 2014. Applicability and trends of anaerobic granular sludge treatment processes. Biomass and Bioenergy 60, 189–202. https://doi.org/10.1016/j.biombioe.2013.11.011

Lima-Tenório, M.K., Tenório-Neto, E.T., Guilherme, M.R., Garcia, F.P., Nakamura, C. V., Pineda, E.A.G., Rubira, A.F., 2015. Water transport properties through starch-based hydrogel nanocomposites responding to both pH and a remote magnetic field. Chem. Eng. J. 259, 620–629. https://doi.org/10.1016/j.cej.2014.08.045

Limcharoensuk, T., Sooksawat, N., Sumarnrote, A., Awutpet, T., Kruatrachue, M., Pokethitiyook, P., Auesukaree, C., 2015. Bioaccumulation and biosorption of Cd2+ and Zn2+ by bacteria isolated from a zinc mine in Thailand. Ecotoxicol. Environ. Saf. 122, 322–330. https://doi.org/10.1016/j.ecoenv.2015.08.013

Lin, Y., de Kreuk, M., van Loosdrecht, M.C.M., Adin, A., 2010. Characterization of alginate-like exopolysaccharides isolated from aerobic granular sludge in pilot-plant. Water Res. 44, 3355–3364. https://doi.org/10.1016/j.watres.2010.03.019

Lin, Y., Reino, C., Carrera, J., Pérez, J., van Loosdrecht, M.C.M., 2018. Glycosylated amyloid-like proteins in the structural extracellular polymers of aerobic granular sludge enriched with ammonium-oxidizing bacteria. Microbiologyopen 7, 1–13. https://doi.org/10.1002/mbo3.616

Lin, Y.M., Lotti, T., Sharma, P.K., van Loosdrecht, M.C.M., 2013. Apatite accumulation enhances the mechanical property of anammox granules. Water Res. 47, 4556–4566. https://doi.org/10.1016/j.watres.2013.04.061

Lin, Y.M., Nierop, K.G.J., Girbal-Neuhauser, E., Adriaanse, M., van Loosdrecht, M.C.M., 2015. Sustainable polysaccharide-based biomaterial recovered from waste aerobic granular sludge as a surface coating material. Sustain. Mater. Technol. 4, 24–29. https://doi.org/10.1016/j.susmat.2015.06.002

Liu, H., Fang, H.H.P., 2002. Extraction of extracellular polymeric substances (EPS) of sludges. J. Biotechnol. 95, 249–256. https://doi.org/10.1016/S0168-1656(02)00025-1

Liu, L., Yang, J.P., Ju, X.J., Xie, R., Liu, Y.M., Wang, W., Zhang, J.J., Niu, C.H., Chu, L.Y., 2011. Monodisperse core-shell chitosan microcapsules for pH-responsive burst release of hydrophobic drugs. Soft Matter 7, 4821–4827. https://doi.org/10.1039/c0sm01393e

Liu, W., Zhang, J., Jin, Y., Zhao, X., Cai, Z., 2015. Adsorption of Pb(II), Cd(II) and Zn(II) by extracellular polymeric substances extracted from aerobic granular sludge: Efficiency of protein. J. Environ. Chem. Eng. 3, 1223–1232. https://doi.org/10.1016/j.jece.2015.04.009

Liu, Y., Tay, J.H., 2004. State of the art of biogranulation technology for wastewater treatment. Biotechnol. Adv. 22, 533–563. https://doi.org/10.1016/j.biotechadv.2004.05.001

Liu, Y., Yang, S.F., Xu, H., Woon, K.H., Lin, Y.M., Tay, J.H., 2003. Biosorption kinetics of cadmium(II) on aerobic granular sludge. Process Biochem. 38, 997–1001. https://doi.org/10.1016/S0032-9592(02)00225-X

Lotti, T., Carretti, E., Berti, D., Martina, M.R., Lubello, C., Malpei, F., 2019a. Extraction, recovery and characterization of structural extracellular polymeric substances from anammox granular sludge. J. Environ. Manage. 236, 649–656. https://doi.org/10.1016/j.jenvman.2019.01.054

Lotti, T., Carretti, E., Berti, D., Montis, C., Del Buffa, S., Lubello, C., Feng, C., Malpei, F., 2019b. Hydrogels formed by anammox extracellular polymeric substances: Structural and mechanical insights. Sci. Rep. 9, 1–9. https://doi.org/10.1038/s41598-019-47987-8

Lotti, T., Kleerebezem, R., Lubello, C., van Loosdrecht, M.C.M., 2014. Physiological and kinetic characterization of a suspended cell anammox culture. Water Res. 60, 1–14. https://doi.org/10.1016/j.watres.2014.04.017

Loutseti, S., Danielidis, D.B., Economou-Amilli, A., Katsaros, C., Santas, R., Santas, P., 2009. The application of a micro-algal/bacterial biofilter for the detoxification of copper and cadmium metal wastes. Bioresour. Technol. 100, 2099–2105. https://doi.org/10.1016/j.biortech.2008.11.019

Ma, J., Wang, Z., Xu, Y., Wang, Q., Wu, Z., Grasmick, A., 2013. Organic matter recovery from municipal wastewater by using dynamic membrane separation process. Chem. Eng. J. 219, 190–199. https://doi.org/10.1016/j.cej.2012.12.085

Mackintosh, F.C., Kas, J., Janmey, P.A., 1995. Elasticity of Semi-flexible polymer networks. Phys. Rev. Lett. 75, 4425.

Macosko C.W., 1994. Rheology: Principles, measurements and applications. New York: Wiley VCH.

Mahmoud, M.E., Osman, M.M., Hafez, O.F., Elmelegy, E., 2010. Removal and preconcentration of lead (II), copper (II), chromium (III) and iron (III) from wastewaters by surface developed alumina adsorbents with immobilized 1-nitroso-2-naphthol. J. Hazard. Mater. 173, 349–357. https://doi.org/10.1016/j.jhazmat.2009.08.089

Mainardis, M., Buttazzoni, M., Cottes, M., Moretti, A., Goi, D., 2021. Respirometry tests in wastewater treatment: Why and how? A critical review. Sci. Total Environ. 793, 148607. https://doi.org/10.1016/j.scitotenv.2021.148607

McSwain, B.S., Irvine, R.L., Hausner, M., Wilderer, P.A., 2005. Composition and distribution of extracellular polymeric substances in aerobic flocs and granular sludge. Appl. Environ. Microbiol. 71, 1051–1057. https://doi.org/10.1128/AEM.71.2.1051-1057.2005

Milani, P., França, D., Balieiro, A.G., Faez, R., 2017. Polymers and its applications in agriculture. Polimeros 27, 256–266. https://doi.org/10.1590/0104-1428.09316

Mirdarikvande, S., Sadeghi, H., Godarzi, A., Alahyari, M., Shasavari, H., Khani, F., 2014. Effect of pH, and salinity onto swelling properties of hydrogels based on H-alginate-g-poly(AMPS). Biosci. Biotechnol. Res. Asia 11, 205–209. https://doi.org/10.13005/bbra/1256

Morales, A., Labidi, J., Gullón, P., Astray, G., 2021. Synthesis of advanced biobased green materials from renewable biopolymers. Curr. Opin. Green Sustain. Chem. 29. https://doi.org/10.1016/j.cogsc.2020.100436

More, T.T., Yadav, J.S.S., Yan, S., Tyagi, R.D., Surampalli, R.Y., 2014a. Extracellular polymeric substances of bacteria and their potential environmental applications. J. Environ. Manage. 144, 1–25. https://doi.org/10.1016/j.jenvman.2014.05.010

More, T.T., Yadav, J.S.S., Yan, S., Tyagi, R.D., Surampalli, R.Y., 2014b. Extracellular polymeric substances of bacteria and their potential environmental applications. J. Environ. Manage. 144, 1–25. https://doi.org/10.1016/j.jenvman.2014.05.010

More, T.T., Yan, S., Hoang, N. V., Tyagi, R.D., Surampalli, R.Y., 2012. Bacterial polymer production using pre-treated sludge as raw material and its flocculation and dewatering potential. Bioresour. Technol. 121, 425–431. https://doi.org/10.1016/j.biortech.2012.06.075

Morgenroth, E., Kommedal, R., Harremoës, P., 2002. Processes and modeling of hydrolysis of particulate organic matter in aerobic wastewater treatment - A review. Water Sci. Technol. 45, 25–40. https://doi.org/10.2166/wst.2002.0091

Morra et al 1997 M.J., Fendorf, S.E., Brown, P.D., 1997. Speciation of sulfur in humic and fulvic acids using X-ray absorption near-edge structure (XANES) spectroscopy. Geochim. Cosmochim. Acta. https://doi.org/10.1016/S0016-7037(97)00003-3

Mukhopadhyay, M., Noronha, S.B., Suraishkumar, G.K., 2007. Kinetic modeling for the biosorption of copper by pretreated Aspergillus niger biomass. Bioresour. Technol. 98, 1781–1787. https://doi.org/10.1016/j.biortech.2006.06.025

Muniz, M.A.P., Dos Santos, M.N.F., Da Costa, C.E.F., Morais, L., Lamarão, M.L.N., Ribeiro-Costa, R.M., Silva-Júnior, J.O.C., 2015. Physicochemical characterization, fatty acid composition, and thermal analysis of Bertholletia excelsa HBK oil. Pharmacogn. Mag. 11, 147–151. https://doi.org/10.4103/0973-1296.149730

Murasnige, T., and Skooga., F., 1962. Revised Medium for Rapid Growth and Bio Agsays with Tohaoco Tissue Cultures. Physiol. Plant. 15, 473–497.

Nakajima, H., Dijkstra, P., Loos, K., 2017. The recent developments in biobased polymers toward general and engineering applications: Polymers that are upgraded from biodegradable polymers, analogous to petroleum-derived polymers, and newly developed. Polymers (Basel). 9, 1–26. https://doi.org/10.3390/polym9100523

Nancharaiah, Y. V., Kiran Kumar Reddy, G., 2018. Aerobic granular sludge technology: Mechanisms of granulation and biotechnological applications. Bioresour. Technol. 247, 1128–1143. https://doi.org/10.1016/j.biortech.2017.09.131

Neu, T.R., Lawrence, J.R., 2014. In: Donelli, G. (Ed.), Microbial Biofilms: Methods and Protocols. Springer New York, New York, NY, 43 – 64.

Ni, B., Liu, M., Lü, S., Xie, L., Wang, Y., 2010. Multifunctional slow-release organic-inorganic compound fertilizer. J. Agric. Food Chem. 58, 12373–12378. https://doi.org/10.1021/jf1029306

Ni, B.J., Hu, B.L., Fang, F., Xie, W.M., Kartal, B., Liu, X.W., Sheng, G.P., Jetten, M., Zheng, P., Yu, H.Q., 2010. Microbial and physicochemical characteristics of compact anaerobic ammonium-oxidizing granules in an upflow anaerobic sludge blanket reactor. Appl. Environ. Microbiol. 76, 2652–2656. https://doi.org/10.1128/AEM.02271-09

Niu, Z., Zhang, Z., Liu, S., Miyoshi, T., Matsuyama, H., Ni, J., 2016. Discrepant membrane fouling of partial nitrification and anammox membrane bioreactor operated at the same nitrogen loading rate. Bioresour. Technol. 214, 729–736. https://doi.org/10.1016/j.biortech.2016.05.022

Nu, T., Viet, T., 2019. Structure , Rheological Properties and Connectivity of Gels Formed by Carrageenan Extracted from Different Red Algae Species Tran Nu Thanh Viet Bui To cite this version : HAL Id : tel-02077051 « Tran Nu Thanh Viet BUI » « Structure , Rheological Propertie.

Oleszczuk, P., 2008. Phytotoxicity of municipal sewage sludge composts related to physico-chemical properties , PAHs and heavy metals 69, 496–505. https://doi.org/10.1016/j.ecoenv.2007.04.006

Orts, W.J., Sojka, R.E., Glenn, G.M., 2000. Biopolymer additives to reduce erosion-induced soil losses during irrigation. Ind. Crops Prod. 11, 19–29. https://doi.org/10.1016/S0926-6690(99)00030-8

Ouwerx, C., Velings, N., Mestdagh, M.M., Axelos, M.A.V., 1998. Physico-chemical properties and rheology of alginate gel beads formed with various divalent cations. Polym. Gels Networks 6, 393–408. https://doi.org/10.1016/S0966-7822(98)00035-5

Oyen, M.L., 2014. Mechanical characterisation of hydrogel materials. Int. Mater. Rev. 59, 44–59. https://doi.org/10.1179/1743280413Y.0000000022

Pagliaccia, B., Carretti, E., Severi, M., Berti, D., Lubello, C., Lotti, T., 2021. Heavy metal biosorption by Extracellular Polymeric Substances (EPS) recovered from anammox granular sludge. J. Hazard. Mater. 424, 126661. https://doi.org/10.1016/j.jhazmat.2021.126661

Park, S.J., Jang, Y.S., Shim, J.W., Ryu, S.K., 2003. Studies on pore structures and surface functional groups of pitch-based activated carbon fibers. J. Colloid Interface Sci. 260, 259–264. https://doi.org/10.1016/S0021-9797(02)00081-4

Passauer, L., Hallas, T., Ba, E., Ciesielski, G., Lebioda, S., Hamer, U., 2015. Biodegradation of Hydrogels from Oxyethylated Lignins in Model Soils. https://doi.org/10.1021/acssuschemeng.5b00139

Pavasant, P., Apiratikul, R., Sungkhum, V., Suthiparinyanont, P., Wattanachira, S., Marhaba, T.F., 2006. Biosorption of Cu2+, Cd2+, Pb2+, and Zn2+ using dried marine green macroalga Caulerpa lentillifera. Bioresour. Technol. 97, 2321–2329. https://doi.org/10.1016/j.biortech.2005.10.032

Payne, J., McKeown, P., Jones, M.D., 2019. A circular economy approach to plastic waste. Polym. Degrad. Stab. 165, 170–181. https://doi.org/10.1016/j.polymdegradstab.2019.05.014

Pernetti, M., Di Palma, L., 2005. Experimental evaluation of inhibition effects of saline wastewater on activated sludge. Environ. Technol. 26, 695–704. https://doi.org/10.1080/09593330.2001.9619509

Pronk, M., de Kreuk, M.K., de Bruin, B., Kamminga, P., Kleerebezem, R., van Loosdrecht, M.C.M., 2015. Full scale performance of the aerobic granular sludge process for sewage treatment. Water Res. 84, 207–217. https://doi.org/10.1016/j.watres.2015.07.011

Pronk, M., Neu, T.R., van Loosdrecht, M.C.M., Lin, Y.M., 2017. The acid soluble extracellular polymeric substance of aerobic granular sludge dominated by Defluviicoccus sp. Water Res. 122, 148–158. https://doi.org/10.1016/j.watres.2017.05.068

Rabnawaz, M., Wyman, I., Auras, R., Cheng, S., 2017. A roadmap towards green packaging: The current status and future outlook for polyesters in the packaging industry. Green Chem. 19, 4737–4753. https://doi.org/10.1039/c7gc02521a

Raszka, A., Chorvatova, M., Wanner, J., 2006. The role and significance of extracellular polymers in activated sludge. Part I: Literature review. Acta Hydrochim. Hydrobiol. 34, 411–424. https://doi.org/10.1002/aheh.200500640

Ravikumar, S., Yoo, I.K., Lee, S.Y., Hong, S.H., 2011. Construction of copper removing bacteria through the integration of two-component system and cell surface display. Appl. Biochem. Biotechnol. 165, 1674–1681. https://doi.org/10.1007/s12010-011-9386-9

Reguieg, F., Ricci, L., Bouyacoub, N., Belbachir, M., Bertoldo, M., 2020. Thermal characterization by DSC and TGA analyses of PVA hydrogels with organic and sodium MMT. Polym. Bull. 77, 929–948. https://doi.org/10.1007/s00289-019-02782-3

Rengaraj, S., Kim, Y., Joo, C.K., Yi, J., 2004. Removal of copper from aqueous solution by aminated and protonated mesoporous aluminas: Kinetics and equilibrium. J. Colloid Interface Sci. 273, 14–21. https://doi.org/10.1016/j.jcis.2004.01.007

Rochas, C., Rinaudo, M., 1982. Calorimetric determination of the conformational transition of kappa carrageenan. Carbohydr. Res. 105, 227–236. https://doi.org/10.1016/S0008-6215(00)84970-8

Romera, E., González, F., Ballester, A., Blázquez, M.L., Muñoz, J.A., 2007. Comparative study of biosorption of heavy metals using different types of algae. Bioresour. Technol. 98, 3344–3353. https://doi.org/10.1016/j.biortech.2006.09.026

Rondel, C., Marcato-Romain, C.E., Girbal-Neuhauser, E., 2013. Development and validation of a colorimetric assay for simultaneous quantification of neutral and uronic sugars. Water Res. 47, 2901–2908. https://doi.org/10.1016/j.watres.2013.03.010

Sajjad, M., Aziz, A., Kim, K.S., 2017. Biosorption and Binding Mechanisms of Ni2+ and Cd2+ with Aerobic Granules Cultivated in Different Synthetic Media. Chem. Eng. Technol. 40, 2179–2187. https://doi.org/10.1002/ceat.201600419

Sam, S.B., Dulekgurgen, E., 2016. Characterization of exopolysaccharides from floccular and aerobic granular activated sludge as alginate-like-exoPS. Desalin. Water Treat. 57, 2534–2545. https://doi.org/10.1080/19443994.2015.1052567

Scarlat, N., Dallemand, J.F., Fahl, F., 2018. Biogas: Developments and perspectives in Europe. Renew. Energy 129, 457–472. https://doi.org/10.1016/j.renene.2018.03.006

Schambeck, C.M., Girbal-Neuhauser, E., Böni, L., Fischer, P., Bessière, Y., Paul, E., da Costa, R.H.R., Derlon, N., 2020. Chemical and physical properties of alginate-like exopolymers of aerobic granules and flocs produced from different wastewaters. Bioresour. Technol. 312, 123632. https://doi.org/10.1016/j.biortech.2020.123632

Schut, S., Zauner, S., Hampel, G., König, H., Claus, H., 2011. Biosorption of copper by wine-relevant lactobacilli. Int. J. Food Microbiol. 145, 126–131. https://doi.org/10.1016/j.ijfoodmicro.2010.11.039

Sesay, M.L., Özcengiz, G., Dilek Sanin, F., 2006. Enzymatic extraction of activated sludge extracellular polymers and implications on bioflocculation. Water Res. 40, 1359–1366. https://doi.org/10.1016/j.watres.2006.01.045

Seviour, T., Derlon, N., Dueholm, M.S., Flemming, H.C., Girbal-Neuhauser, E., Horn, H., Kjelleberg, S., van Loosdrecht, M.C.M., Lotti, T., Malpei, M.F., Nerenberg, R., Neu, T.R., Paul, E., Yu, H., Lin, Y., 2019. Extracellular polymeric substances of biofilms: Suffering from an identity crisis. Water Res. 151, 1–7. https://doi.org/10.1016/j.watres.2018.11.020

Seviour, T., Donose, B.C., Pijuan, M., Yuan, Z., 2010. Purification and conformational analysis of a key exopolysaccharide component of mixed culture aerobic sludge granules. Environ. Sci. Technol. 44, 4729–4734. https://doi.org/10.1021/es100362b

Seviour, T., Pijuan, M., Nicholson, T., Keller, J., Yuan, Z., 2009a. Understanding the properties of aerobic sludge granules as hydrogels. Biotechnol. Bioeng. 102, 1483–1493. https://doi.org/10.1002/bit.22164

Seviour, T., Pijuan, M., Nicholson, T., Keller, J., Yuan, Z., 2009b. Gel-forming exopolysaccharides explain basic differences between structures of aerobic sludge granules and floccular sludges. Water Res. 43, 4469–4478. https://doi.org/10.1016/j.watres.2009.07.018

Seviour, T., Yuan, Z., van Loosdrecht, M.C.M., Lin, Y., 2012. Aerobic sludge granulation: A tale of two polysaccharides? Water Res. 46, 4803–4813. https://doi.org/10.1016/j.watres.2012.06.018

Sharma, D., Chaudhari, P.K., Prajapati, A.K., 2020. Removal of chromium (VI) and lead from electroplating effluent using electrocoagulation. Sep. Sci. Technol. 55, 321–331. https://doi.org/10.1080/01496395.2018.1563157

Sheng, G.P., Yu, H.Q., Li, X.Y., 2010. Extracellular polymeric substances (EPS) of microbial aggregates in biological wastewater treatment systems: A review. Biotechnol. Adv. 28, 882–894. https://doi.org/10.1016/j.biotechadv.2010.08.001

Smith, P.K., Krohn, R.I., Hermanson, G.T., Mallia, A.K., Gartner, F.H., Provenzano, M.D., Fujimoto, E.K., Goeke, N.M., Olson, B.J., Klenk, D.C., 1985. Measurement of protein using bicinchoninic acid. Anal. Biochem. 150, 76–85. https://doi.org/10.1016/0003-2697(85)90442-7

Spérandio, M., Paul, E., 2000. Estimation of wastewater biodegradable cod fractions by combining respirometric experiments in various So/Xo ratios. Wat. Res. 34, 4, 1233 – 1246.

Stahl, J.D., Cameron, M.D., Haselbach, J., Aust, S.D., 2000. Biodegradation of superabsorbent polymers in soil. Environ. Sci. Pollut. Res. 7, 83–88. https://doi.org/10.1065/espr199912.014

Stanchev, P., Vasilaki, V., Dosta, J., Katsou, E., 2017. Measuring the circular economy of water sector three-fold linkage of water, energy and materials.

Stauffer, D., 1976. Gelation in concentrated critically branched polymer solutions. J. Chem. Soc., Faraday Trans. 2 72, 1354–1362.

Stauffer, D., 1985. Introduction to Percolation Theory. Taylor and Francis, London.

Su, X., Tian, Y., Li, H., Wang, C., 2013. New insights into membrane fouling based on characterization of cake sludge and bulk sludge: An especial attention to sludge aggregation. Bioresour. Technol. 128, 586–592. https://doi.org/10.1016/j.biortech.2012.11.005

Sudmalis, D., Mubita, T.M., Gagliano, M.C., Dinis, E., Zeeman, G., Rijnaarts, H.H.M., Temmink, H., 2020. Cation exchange membrane behaviour of extracellular polymeric substances (EPS) in salt adapted granular sludge. Water Res. 178, 115855. https://doi.org/10.1016/j.watres.2020.115855

Sun, X.F., Wang, S.G., Zhang, X.M., Paul Chen, J., Li, X.M., Gao, B.Y., Ma, Y., 2009. Spectroscopic study of Zn2+ and Co2+ binding to extracellular polymeric substances (EPS) from aerobic granules. J. Colloid Interface Sci. 335, 11–17. https://doi.org/10.1016/j.jcis.2009.03.088

Tang, C.J., Duan, C.S., Yu, C., Song, Y.X., Chai, L.Y., Xiao, R., Wei, Z., Min, X.B., 2017. Removal of nitrogen from wastewaters by anaerobic ammonium oxidation (ANAMMOX) using granules in upflow reactors. Environ. Chem. Lett. 15, 311–328. https://doi.org/10.1007/s10311-017-0607-5

Thomas, M., Kozik, V., Bąk, A., Barbusiński, K., Jazowiecka-rakus, J., Jampilek, J., 2021. Removal of heavy metal ions from wastewaters: An application of sodium trithiocarbonate and

wastewater toxicity assessment. Materials (Basel). 14, 1–18. https://doi.org/10.3390/ma14030655

Thrimawithana, T.R., Young, S., Dunstan, D.E., Alany, R.G., 2010. Texture and rheological characterization of kappa and iota carrageenan in the presence of counter ions. Carbohydr. Polym. 82, 69–77. https://doi.org/10.1016/j.carbpol.2010.04.024

Ueno, K., Hata, K., Katakabe, T., Kondoh, M., Watanabe, M., 2008. Nanocomposite ion gels based on silica nanoparticles and an ionic liquid: Ionic transport, viscoelastic properties, and microstructure. J. Phys. Chem. B 112, 9013–9019. https://doi.org/10.1021/jp8029117

Ullah, F., Othman, M.B.H., Javed, F., Ahmad, Z., Akil, H.M., 2015. Classification, processing and application of hydrogels: A review. Mater. Sci. Eng. C 57, 414–433. https://doi.org/10.1016/j.msec.2015.07.053

UNI EN 16086-1:2012 – Soil improvers and growing media – Determination of plant response – Part 1: Pot growth test with Chinese cabbage

UNI EN 16086-2:2012 – Soil improvers and growing media – Determination of plant response –Part 2: Petri dish test using cress

UNI EN ISO 16072:2002 – Soil Quality − Laboratory Methods for Determination of Microbial Soil Respiration

Van Der Hoek, J.P., De Fooij, H., Struker, A., 2016. Wastewater as a resource: Strategies to recover resources from Amsterdam's wastewater. Resour. Conserv. Recycl. 113, 53–64. https://doi.org/10.1016/j.resconrec.2016.05.012

van der Star, W.R.L., Abma, W.R., Blommers, D., Mulder, J.W., Tokutomi, T., Strous, M., Picioreanu, C., van Loosdrecht, M.C.M., 2007. Startup of reactors for anoxic ammonium

oxidation: Experiences from the first full-scale anammox reactor in Rotterdam. Water Res. 41, 4149–4163. https://doi.org/10.1016/j.watres.2007.03.044

van Leeuwen, K., de Vries, E., Koop, S., Roest, K., 2018. The Energy & Raw Materials Factory: Role and Potential Contribution to the Circular Economy of the Netherlands. Environ. Manage. 61, 786–795. https://doi.org/10.1007/s00267-018-0995-8

Van Loosdrecht, M.C.M., Brdjanovic, D., 2014. Anticipating the next century of wastewater treatment. Science (80-.). 344, 1452–1453. https://doi.org/10.1126/science.1255183

Vanrolleghem, P., Insel, G., Petersen, B., Pauw, D., Nopens, I., Dovermann, H., Weijers, S., Gernaey, K., 2003. A Comprehensive Model Calibration Procedure for Activated Sludge Models. Proc. Water Environ. Fed. WEFTEC 2003 210–237.

Verma, A., Shalu, Singh, A., Bishnoi, N.R., Gupta, A., 2013. Biosorption of Cu (II) using free and immobilized biomass of Penicillium citrinum. Ecol. Eng. 61, 486–490. https://doi.org/10.1016/j.ecoleng.2013.10.008

Vieira, T., Artifon, S.E.S., Cesco, C.T., Vilela, P.B., Becegato, V.A., Paulino, A.T., 2020. Chitosan-based hydrogels for the sorption of metals and dyes in water: isothermal, kinetic, and thermodynamic evaluations. Colloid Polym. Sci. 299, 649–662. https://doi.org/10.1007/s00396-020-04786-2

Vijayaraghavan, K., Yun, Y.S., 2008. Bacterial biosorbents and biosorption. Biotechnol. Adv. 26, 266–291. https://doi.org/10.1016/j.biotechadv.2008.02.002

Wagner, M., Ivleva, N.P., Haisch, C., Niessner, R., Horn, H., 2009. Combined use of confocal laser scanning microscopy (CLSM) and Raman microscopy (RM): Investigations on EPS - Matrix. Water Res. 43, 63–76. https://doi.org/10.1016/j.watres.2008.10.034

Wan Maznah, W.O., Al-Fawwaz, A.T., Surif, M., 2012. Biosorption of copper and zinc by immobilised and free algal biomass, and the effects of metal biosorption on the growth and cellular structure of Chlorella sp. and Chlamydomonas sp. isolated from rivers in Penang, Malaysia. J. Environ. Sci. (China) 24, 1386–1393. https://doi.org/10.1016/S1001-0742(11)60931-5

Wang, B., Gao, B., Zimmerman, A.R., Zheng, Y., Lyu, H., 2018. Novel biochar-impregnated calcium alginate beads with improved water holding and nutrient retention properties. J. Environ. Manage. 209, 105–111. https://doi.org/10.1016/j.jenvman.2017.12.041

Wang, L., Liu, X., Lee, D.J., Tay, J.H., Zhang, Y., Wan, C.L., Chen, X.F., 2018. Recent advances on biosorption by aerobic granular sludge. J. Hazard. Mater. 357, 253–270. https://doi.org/10.1016/j.jhazmat.2018.06.010

Wang, X.H., Song, R.H., Teng, S.X., Gao, M.M., Ni, J.Y., Liu, F.F., Wang, S.G., Gao, B.Y., 2010. Characteristics and mechanisms of Cu(II) biosorption by disintegrated aerobic granules. J. Hazard. Mater. 179, 431–437. https://doi.org/10.1016/j.jhazmat.2010.03.022

Warren, R.A.J., 1996. Microbial hydrolysis of polysaccharides. Annu. Rev. Microbiol. 50, 183–212. https://doi.org/10.1146/annurev.micro.50.1.183

Watase, M., Nishinari, K., 1987. Effect of sulfate content. Macromol. Chem. 188, 2213–2221.

Wei, D., Li, M., Wang, X., Han, F., Li, L., Guo, J., Ai, L., Fang, L., Liu, L., Du, B., Wei, Q., 2016. Extracellular polymeric substances for Zn (II) binding during its sorption process onto aerobic granular sludge. J. Hazard. Mater. 301, 407–415. https://doi.org/10.1016/j.jhazmat.2015.09.018

Wei, D., Wang, B., Ngo, H.H., Guo, W., Han, F., Wang, X., Du, B., Wei, Q., 2015. Role of extracellular polymeric substances in biosorption of dye wastewater using aerobic granular sludge. Bioresour. Technol. 185, 14–20. https://doi.org/10.1016/j.biortech.2015.02.084

Wei, L., Li, J., Xue, M., Wang, S., Li, Q., Qin, K., Jiang, J., Ding, J., Zhao, Q., 2019. Adsorption behaviors of Cu2+, Zn2+ and Cd2+ onto proteins, humic acid, and polysaccharides extracted from sludge EPS: Sorption properties and mechanisms. Bioresour. Technol. 291, 121868. https://doi.org/10.1016/j.biortech.2019.121868

Wilske, B., Bai, M., Lindenstruth, B., Bach, M., Rezaie, Z., Frede, H.G., Breuer, L., 2014. Biodegradability of a polyacrylate superabsorbent in agricultural soil. Environ. Sci. Pollut. Res. 21, 9453–9460. https://doi.org/10.1007/s11356-013-2103-1

Yilmaz, G., Lemaire, R., Keller, J., Yuan, Z., 2008. Simultaneous nitrification, denitrification, and phosphorus removal from nutrient-rich industrial wastewater using granular sludge. Biotechnol. Bioeng. 100, 529–541. https://doi.org/10.1002/bit.21774

Yu, J., Tong, M., Sun, X., Li, B., 2008. Enhanced and selective adsorption of Pb2+ and Cu2+ by EDTAD-modified biomass of baker's yeast. Bioresour. Technol. 99, 2588–2593. https://doi.org/10.1016/j.biortech.2007.04.038

Zallen, R., 1983. In: The Physics of Amorphous Solids. Wiley, New York, 1983, Chapter 4.

Zhang, P., Shen, Y., Guo, J.S., Li, C., Wang, H., Chen, Y.P., Yan, P., Yang, J.X., Fang, F., 2015. Extracellular protein analysis of activated sludge and their functions in wastewater treatment plant by shotgun proteomics. Sci. Rep. 5, 1–11. https://doi.org/10.1038/srep12041

Zhang, X., Bishop, P.L., 2003. Biodegradability of biofilm extracellular polymeric substances 50, 63–69.

Zhang, Z.Z., Deng, R., Cheng, Y.F., Zhou, Y.H., Buayi, X., Zhang, X., Wang, H.Z., Jin, R.C., 2015. Behavior and fate of copper ions in an anammox granular sludge reactor and strategies for remediation. J. Hazard. Mater. 300, 838–846. https://doi.org/10.1016/j.jhazmat.2015.08.024

Zheng, Y., Fang, X., Ye, Z., Li, Y., Cai, W., 2008. Biosorption of Cu(II) on extracellular polymers from Bacillus sp. F19. J. Environ. Sci. 20, 1288–1293. https://doi.org/10.1016/S1001-0742(08)62223-8

Zhou, C., Wu, Q., Lei, T., Negulescu, I.I., 2014. Adsorption kinetic and equilibrium studies for methylene blue dye by partially hydrolyzed polyacrylamide/cellulose nanocrystal nanocomposite hydrogels. Chem. Eng. J. 251, 17–24. https://doi.org/10.1016/j.cej.2014.04.034

Zhu, L., Zhou, J., Lv, M., Yu, H., Zhao, H., Xu, X., 2015. Specific component comparison of extracellular polymeric substances (EPS) in flocs and granular sludge using EEM and SDS-PAGE. Chemosphere 121, 26–32. https://doi.org/10.1016/j.chemosphere.2014.10.053

Zhu, Y., Romain, C., Williams, C.K., 2016. Sustainable polymers from renewable resources. Nature 540, 354–362. https://doi.org/10.1038/nature21001

Ziglio, G., Andreottola, G., Foladori, P., Ragazzi, M., 2001. Experimental validation of a single-OUR method for wastewater RBCOD characterisation. Water Sci. Technol. 43, 119–126. https://doi.org/10.2166/wst.2001.0674

Zohuriaan-Mehr, M.J., Omidian, H., Doroudiani, S., Kabiri, K., 2010. Advances in non-hygienic applications of superabsorbent hydrogel materials. J. Mater. Sci. 45, 5711–5735. https://doi.org/10.1007/s10853-010-4780-1

Zumstein, M.T., Schintlmeister, A., Nelson, T.F., Baumgartner, R., Woebken, D., Wagner, M., Kohler, H.P.E., McNeill, K., Sander, M., 2018. Biodegradation of synthetic polymers in soils: Tracking carbon into CO_2 and microbial biomass. Sci. Adv. 4, 1–8.

Acknowledgements

I would like to really thank all the people who made possible this thesis. Since the beginning I was very enthusiastic to deal with this interesting and challenging subject and I am still very motivated to continue the route I have taken. It was a pleasure to have had the opportunity to do my PhD in a really emphasized international dimension, working with people who have been for me continuous source of inspiration and growth.

Firstly, I need to thank my tutors, Claudio Lubello and Etienne Paul, and my co-tutors, Tommaso Lotti and Yolaine Bessiere, who firstly made it possible. They were always very encouraging and passionate, supporting me constantly in my research. I am really grateful to all of you!

I thank all the DICEA (Florence) and TBI (Toulouse) teams, always ready to help me. Special thanks to my colleagues Gemma Mannarino, Riccardo Campo, Letizia Macellaro La Franca, Sidonie Durieux and Abdo Bou-Sarkis for the constant support in these years.

I would like to thank people from CSGI consortium and Department of Chemistry – University of Florence (Emiliano Carretti, Debora Berti, Mirko Severi) for the support in many analyses (e.g., rheology, ICP-AES, DLS, etc.) and particularly Emiliano who helped me to approach this complex subject through a multidisciplinary vision. I thank people from MEMA – University of Florence for the support in the SEM/EDS analyses and the team of San Colombano WWTP (Publiacqua S.p.A.) where I carried out part of the experimental activities.

Finally, I would like to thank my family and friends who made this journey easier with their constant encouragement and support.